N O T I C E

THIS DOCUMENT HAS BEEN REPRODUCED FROM MICROFICHE. ALTHOUGH IT IS RECOGNIZED THAT CERTAIN PORTIONS ARE ILLEGIBLE, IT IS BEING RELEASED IN THE INTEREST OF MAKING AVAILABLE AS MUCH INFORMATION AS POSSIBLE

"Made available under NASA sponsorship in the interest of early and wide dissemination of Earth Resources Survey Program information and without liability for any use made thereof."

8.0 - 1 0.0.8 4
TM-80550

NASA

Technical Memorandum 80550

EARTH SURVEY APPLICATIONS DIVISION RESEARCH REPORT

(E80-10084) [EARTH SURVEY APPLICATIONS DIVISION: RESEARCH LEADING TO THE EFFECTIVE USE OF SPACE TECHNOLOGY IN APPLICATIONS RELATING TO THE EARTH'S SURFACE AND INTERIOR] (NASA) 298 p HC A13/MF A01

N80-20722

Unclas

G3/43 00084

NOVEMBER 1979

National Aeronautics and
Space Administration

Goddard Space Flight Center
Greenbelt, Maryland 20771

RECEIVED

EARTH SURVEY
APPLICATIONS DIVISION
RESEARCH REPORT

November 1979

GODDARD SPACE FLIGHT CENTER
Greenbelt, Maryland

CONTENTS

CONTENTS (continued)

CONTENTS (continued)

CONTENTS (continued)

ILLUSTRATIONS

CONTENTS (continued)

ILLUSTRATIONS (continued)

CONTENTS (continued)

ILLUSTRATIONS (continued)

CONTENTS (continued)

ILLUSTRATIONS (continued)

CONTENTS (continued)

ILLUSTRATIONS (continued)

CONTENTS (continued)

ILLUSTRATIONS (continued)

CONTENTS (continued)

TABLES

CONTENTS (continued)

TABLES (continued)

EARTH SURVEY APPLICATIONS DIVISION

CODE 920

LIST OF RESEARCHERS

Louis S. Walter, Chief

Ph.D., 1960, Penn. State U.
Geochemistry

(Betty Wilson, Secretary)

GEODYNAMICS BRANCH

Code 921

David Smith, Branch Head
Ph.D., 1966, University of London
Mathematics

(Beatrice Boccucci, Secretary)

Lloyd Carpenter, *B.S., 1951, U. of Missouri, Mathematics*
Robert Cheney, *M.S., 1974, U. of Rhode Island, Oceanography*
Stephen Cohen, *Ph.D., 1973, U. of Maryland, Physics*
Theodore Felsentreger, *M.A., 1961, U. of Maryland, Mathematics*
Michael Graber, *Ph.D., 1970, Princeton U., Physics*
Werner Kahn, *M.S., 1955, U. of Illinois, Mathematics*
Ronald Kolenkiewicz, *M.S., 1965, Catholic U., Space Science and Applied Physics*
Francis Lerch, *M.S., 1950, U. of Delaware, Mathematics*
Han-Shou Liu, *Ph.D., 1963, Cornell U., Physics*
James Marsh, *M.S., 1963, West Virginia U., Physics*
Patrick McClain, *M.S., 1959, Howard U., Mathematics*
Barbara Putney, *B.S., 1960, Brooklyn College, Mathematics*
David Rubincam, *Ph.D., 1973, U. of Maryland, Physics*
Braulio Sanchez, *Ph.D., 1975, U. of Texas, Aerospace Engineering*
Frederick Schamann, *B.S., 1967, City College of New York, Mathematics*
Carl Wagner, *M.S., 1960, Columbia, U., Engineering Mechanics*
George Wyatt, *B.S., 1962, North Carolina State College, Mathematics*

GEOPHYSICS BRANCH

CODE 922

Gilbert Mead, Branch Head
Ph.D., 1962, U. of California, Berkeley, Physics

Barbara Luders, Secretary

Richard J. Allenby, *Ph.D., 1952, U. Toronto, Geophysics*
Herbert Frey, *Ph.D., 1977, U. of Maryland, Astronomy*
Robert Langel, *Ph.D., 1973, U. of Maryland, Physics*
Paul D. Lowman, Jr., *Ph.D., 1963, U. of Colorado, Geology*
Chopo Ma, *Ph.D., 1978, U. of Maryland, Physics*
James Ryan, *M.S., 1968, George Washington U., Mathematics*
Patrick T. Taylor, *Ph.D., 1965, Stanford U., Geophysics*
Herman H. Thomas, *Ph.D., 1973, U. of Pennsylvania, Geochemistry*
William J. Webster, Jr., *Ph.D., 1970, Case Western Reserve U., Astronomy*

EARTH RESOURCES BRANCH

CODE 923

Charles Schnetzler, Branch Head
Ph.D., 1962, MIT, Geochemistry

Karen Doyle, Secretary

Arthur Anderson, *B.S., 1961, City U. of New York, Geology*
John Barker, *Ph.D., 1967, Chicago U., Nuclear Chemistry*
Emmett Chappelle, *M.S., 1954, U. of Washington, Biochemistry*
Jerrold Christenson, *M.S., 1975, San Diego State U., Geography*
Donald Deering, *Ph.D., 1978, Texas A. & M. U., Range Sciences*
Brent Holben, *M.S., 1975, Colorado State U., Agricultural Sciences*
James Irons, *M.S., 1978, Penn State U., Agronomy*
George Jacobs, *Ph.D., 1955, U. of Mississippi, Biology*
Daniel Kimes, *Ph.D., 1979, Colorado State U., Natural Resources*
Charles W. Louns, *M.S., 1966, George Washington U., Geology*
Mark Labovitz, *Ph.D., 1978, Penn State U., Geostatistics*
Brian Markham, *M.S., 1978, Cornell U., Civil Engineering*
Kenneth Meehan, *Ph.D., 1978, Idaho U., Geology*
John Schutt, *Ph.D., 1954, Rochester U., Physical Chemistry*
David Toll, *M.S., 1978, Colorado State U., Natural Resources*
Compton J. Tucker, *Ph.D., 1975, Colorado State U., Remote Sensing*
Jean Welker, *B.A., 1975, Hofstra College, Physics*
Steven Wharton, *M.S., 1979, Penn State U., Forestry/Computer Sciences*
Darrell Williams, *M.S., 1975, Penn State U., Forestry*
Frank Wood, *Technician*

Postdoctoral Associates

Christopher Justice, *Ph.D., 1978, U. of Reading, England, Geography*
James Uhl, *Associate Professor, on sabbatical leave from Penn State U.*

INTRODUCTION

The function of the Earth Survey Applications Division is to perform research leading to the effective use of space technology in applications relating to the Earth's surface and interior. The interests and expertise of the Division thus focus on disciplines spanning geodesy, geophysics, and land resources. The purpose of this document is to report on the progress, status, activities, and future directions of the research being carried out in the Division. The individual reports which generally were prepared and updated in mid-1979 represent the status as of that date. Annual publication of this report will permit continued assessment of progress and will provide a basis for evaluation of future research objectives.

CHAPTER 1

GEOLOGIC INVESTICATIONS

OVERVIEW

The overall objective of the geology research effort within the Earth Survey Applications Division is the development and evaluation of the application of satellite data in solving geological problems. In conforming with this objective and the mission and research plans of NASA, substantial effort is being applied to the development of new digital image processing and statistical analysis techniques for use with satellite and aircraft derived data. These techniques will extract relevant geologic data to assist in the design and improvement of future orbital sensor systems with increased geologic potential.

To meet the goals and directions of NASA within the framework of nonrenewable resources, efforts in geological remote sensing at GSFC have been divided into four primary research areas. These include a texture analysis effort headed by Dr. Kenneth T. Meehan, a rock discrimination effort directed jointly by Drs. Charles C. Schnetzler and Kenneth T. Meehan, a geological/geophysical multisource data analysis effort led by Dr. Kenneth T. Meehan and a geobotanical exploration program led by Dr. Charles C. Schnetzler. The work described in sections 1, 3 and 4 of this chapter will be expanded in the future.

In the overall plan for the extracting of relevant data from remote sensors to aid in the interpretation of often complex geologic problems, spatial analysis techniques will be developed to analyze multisource data. Statistical evaluation will then be developed to ascertain original data characteristics and usefulness in more sophisticated stochastic processes and modeling. These analyses serve to define the limitations of exisiting data and thus provide criteria for the design of new sensor systems with increased geologic information capabilities.

TEXTURAL ANALYSIS

OBJECTIVES

The textural analysis research effort includes investigating the ability of textural analysis of various satellite and ground data types (e.g., spectral, magnetic, gravity and altimetry) to correlate with and provide indications of the primary stress regimes related to a major intraplate, tectonic feature and its associated mineral deposits. Definition of the primary stress regimes or tectonic provinces will provide a framework within which to correlate known mineral deposits and further to extrapolate areas with the potential for mineralization. Statistical analyses will be used to perform this tectonic definition and elucidate those variables responsible for the model that are most clearly in accordance with the features' characteristics.

BACKGROUND

Texture can be defined as the spatical distribution of tone. Spatially derived texture will consist of recognition of patterns of linear gradients within registered multisource data sets. These patterns vary according to the crustal stress regime in which they are found. Selective recognition of a specific arrangement (distribution) of grid cells comprising these patterns may, if properly defined, aid in identifying magnetic, gravitational, or fracture induced lineaments. The Rio Grande Rift through central New Mexico and Colorado was selected for study because linear patterns apparent in spectral and geophysical data may aid in defining its structural components and extent. In addition, juxtaposed contrasting tectonic regimes lie on either side of the rift thereby presenting contrasting patterns within similar data. The arrangement or pattern of intersecting lineaments has been shown to help define the stress orientations which predominate within the rift and can differentiate them from other stress regimes which prevail in adjacent areas.

RECENT ACCOMPLISHMENTS

Several textural extraction algorithms have been investigated and implemented on the IBM 360/91 for testing and evaluation. One of these incorporates a variable size moving window within which textural parameters are calculated. A supervised, stepwise linear discriminant classifier (parametric) and an empirical discriminant classifier (nonparametric) have also been implemented to categorize spatially a multivariate data set into its textural components.

SIGNIFICANCE

The ability to define, extract, and classify terrain according to its textural character will provide insight to those areas more likely to be mineralized or be related to geothermal potential.

FUTURE EMPHASIS

As our model for tectonic regimes becomes more sophisticated and more data become available (e.g., via Magsat, Gravsat, Thermosat, SWIR/MLA/MRS), additional work will be conducted on the statistical basis required for advanced spatial analyses of such varied data types. Further, emphasis will be placed on extracting more refined and meaningful textural parameters for tectonic definition. Methods of preclassification will be developed. Procedures for classification in the spatial domain and modeling tectonic regimes will be refined to indicate areas of economic resource potential.

REFERENCES AND PUBLICATIONS:

Meehan, K., "Spatial Classification of Multisource Data Types for Lithologic Mapping in Southwestern Idaho," paper presented at the Symposium on Remote Sensing of Natural Resources, University of Idaho, Moscow, Idaho, September 10-14, 1979.

ROCK DISCRIMINATION

OBJECTIVE

T. objective of the rock discrimination project was to analyze spec data from a wide range of rock types by multivariate statist cal techniques to determine the optimum combination of wavelength intervals for rock discrimination.

BACKGROUND

From seven geologically diverse test sites in Utah, radiance measures were collected by the Bendix Multispectral Scanner and Data System (MSDS) mounted in a NC-130B aircraft. The instrument simultaneously viewed 15 bands in the range between 0.34 and 4.75 μm. Statistical analyses were performed on these bands as well as on simulations of the bands present on the Multispectral Scanner (MSS) and those projected for the Thematic Mapper (TM).

RECENT ACCOMPLISHMENTS

Using stepwise discriminant analysis, the ability of the aircraft scanner to discriminate diverse rock types was determined as greatest in the interval 1.18 to 1.30 μm and in the combination of intervals (in order of importance) 1.18 to 1.30, 4.50 to 4.75, 0.46 to 0.50, 1.52 to 1.73 and 2.10 to 2.36 μm. This optimum set achieved a higher classification accuracy of the rock types than either the simulated MSS or TM data sets. These results are presented in Table 1-1 by test site and simulated scanner type.

SIGNIFICANCE

The wavelength interval from approximately 1.18 to 1.30 μm should be examined by a number of disciplines for possible inclusion on future satellite sensors.

FUTURE EMPHASIS

Future research in the area of rock discrimination will consist of three major areas as follows:

- Inclusion of ratioed individual spectral channels into the stepwise linear discriminant procedure for improved lithologic discrimination and incorporate orthogonal transformations of these data to both reduce data volume and enhance the accuracy of thematic classification by colinearity reduction.

- Utilize our Geographical Information System (GIS) to quantitatively assess classification errors by category and evaluate improvements in calssification accuracy.

- Refine the classificatory procedure using the above in conjunction with textural analyses to incorporate lithologic maps in the tectonic/structural analysis of the Rio Grande Rift, in relation to its associated mineral deposits.

REFERENCES AND PUBLICATIONS

Blodget, H., F. Gunther, "Discrimination of Rock-Classes and Alternation Products in Southwestern Saudi Arabia with Computer-Enhanced Landsat Data," *Proceedings of the Forty-fourth Annual Convention of the American Society of Photogrammetry,* March 1978.

Podwysocki, M., and F. Gunther, H. Blodget, and A. Anderson, "A Comparison of Rock-Discrimination Capabilities Based on Present and Future Landsat Satellite Sensor Systems," Fifth Symposium, International Association on the Genesis of Ore Deposits, August 1978.

Watson, A. T. and C. C. Schnetzler, "Application of Classification Analysis to Rock Discrimination Using Remotely Sensed Data," paper presented at the ASP-ACSM Convention, Washington, D.C., March 1979.

Watson, A. T., and C. C. Schnetzler, "Optimum Bands for Rock Discrimination Using Remotely Sensed Data," manuscript submitted to *Photogrammetric Engineering and Remote Sensing,* 1979.

Table 1-1
Spectral Analysis of Rock Types
Showing Optimum Range

Test Site Location	MSDS Band Rank (Band Midpoint, μm)					Classification Accuracy		
	1	2	3	4	5	Optimum MSDS	Simulated MSS	Simulated TM
Confusion Range	1.24	4.62	0.48	0.66	2.23	63%	45%	62%
White Mountain	1.24	0.48	2.23	3.77	1.62	96%	86%	90%
Star Mountain	1.24	4.62	1.01	0.84	1.62	72%	60%	68%
Marysvale	1.24	4.62	2.23	1.62	1.01	81%	72%	75%
Monroe	0.37	1.24	0.66	0.48	1.01	96%	88%	98%
Waterpocket Fold	0.48	4.62	1.24	1.01	1.62	61%	24%	27%
Lisbon Valley	1.24	0.37	0.60	0.66	4.62	96%	53%	52%
Optimum	1.24	4.62	0.48	1.62	2.23			

GEOLOGICAL/GEOPHYSICAL RESOURCE ASSESSMENT

OBJECTIVE

This effort will investigate the ability of satellite derived data to identify primary tectonic provinces associated with major intraplate structural features and correlate these with known mineral deposits and volcanic activity throughout the feature. Analysis techniques and procedures specific to this effort will be developed to: (1) Spatially and statistically delineate the structural feature; (2) compile multisource data, including spectral, topographic, geophysical and vectorial into an easily manageable data structure; (3) illuminate variables/data types most clearly responsible for explanation of the structure and its deformational characteristics, as well as its relationship to surrounding provinces; (4) explain reliably recognized mineralization and establish a relationship between these (mineralization), fractures (appearing as lineaments) and strain patterns throughout the rift, and (5) determine the relationships of such measurable geophysical quantities as gravity magnetism and altimetry to variations in strain patterns and occurrences of mineralization and volcanism. The area of study selected for the first phase of this project is the Rio Grande Rift in Colorado, New Mexico, and the western part of Texas.

BACKGROUND

Large quantities of data from the Rio Grande Rift are available, and for the most part have been qualitatively interpreted. Systematic organization of these data into a workable structure (data base) that can be readily managed, quantitatively analyzed, and interpreted will greatly improve tectonic and mineral implacement models to be developed through stochastic processes. These intricate models will be applied to the Rio Grande Rift, a complex structural/tectonic feature. New techniques in pattern recognition, spatial analysis, and image processing will greatly aid this effort.

RECENT ACCOMPLISHMENTS

Preliminary work by researchers at numerous universities and governmental agencies has indicated that multisource spatial data analysis can significantly improve model development in the geologic sciences. This current effort relies on that foundation and while just beginning, should yield improved mineralization and tectonic models near its completion.

SIGNIFICANCE

Effective use of multisource data types in a complex spatial analysis will demonstrate the ability of quantitative techniques to refine subjectively determined structural models. Thorough evaluation of this major intraplate suture (Rio Grande Rift) and the mineral deposits that are intermittently located along its flanks should allow comparison with similar rifts in other plates and perhaps those on other planets. The Rio Grande Rift has been extensively studied and much data have been generated. Accordingly, this type of area lends itself especially well to thorough quantitative analysis. Such an analysis is profitable in view of the possible relationship of the rift to conduits for mineralization and emplacement of upper crustal geothermal sources.

FUTURE EMPHASIS

Future emphasis will be placed on utilization of the multisource data in an increasingly meaningful and effective manner to derive more sophisticated models. Results will be extended to other rifts. Statistical analysis will be perfected to determine optimally those data types contributing most to model development for use on future spacecraft.

REFERENCES AND PUBLICATIONS

Meehan, K., "Spatial Classification of Multisource Data Types for Lithologic Mapping in Southwestern Idaho," paper presented at the Symposium on Remote Sensing of Natural Resources, University of Idaho, Moscow, Idaho, Septemper 10-14, 1979.

GEOBOTANICAL EXPLORATION

OBJECTIVES

The objectives of our geobotanical research are to investigate the utility of remote sensing of geobotanical indicators for mineral and petroleum exploration, and to develop new remote-sensing geobotanical exploration techniques and systems.

BACKGROUND

The use of the type or vigor of vegetation as a guide to subsurface mineral or petroleum deposits has been an accepted exploration tool for centuries. However, the possibility of using remote-sensing techniques to detect the changes in vegetation caused by nearby mineralization has just recently received attention. Satellite remote sensing enables investigators to analyze large segments of the Earth's surface repeatedly at different seasons and under different conditions, and an increasing awareness of potential mineral and energy shortages has stimulated the development of new exploration techniques. Since over two-thirds of the Earth's land surface is covered with vegetation, the need to establish a research program for the development and evaluation of geobotanical exploration techniques is essential.

During CY '78, a longrange research effort in geobotanical exploration was initiated. The effort during 1978 was designed to: (1) Survey the state-of-the-art and prepare a five-year research plan which could be used by NASA and the research community as a guide to future work; (2) foster communication between researchers in this field which hopefully would lead to cooperative, complementary efforts; and (3) start a pilot test study on several known geobotanical anomalies.

RECENT ACCOMPLISHMENTS

A one-day meeting was held in April which brought together researchers who were or had been engaged in geobotanical research. The objectives of this meeting were to initiate communications between people in the field, to review past work, and to discuss the most significant directions for future research. A summary of this meeting was produced and sent to all participants. A five-year geobotanical research plan was produced and sent to the Earth Observations Division of NASA Headquarters and interested researchers.

Dr. William Collins, an NRC/NASA post-doctoral fellow, was supported in 1978 to perform geobotanical research. He flew a Very High Resolution Spectrometer (VHRS) over several known geobotanical sites in the U.S., and developed new computer techniques for the analysis of the data. To date, only data from one site have been analyzed: the Cotter Basin area in Montana. Certain spectral features, which seem to be associated with retarded pigment system development, correlate well with the location and strike of the vein system and also with the available geochemical data. This can be seen in figure 1-1 (Collins, et. al. 1979). The ratio of 10 nanometer wide bands, centered at 745 and 785 nm, is plotted against position along the flight path. The mineralized zone is located between positions 60 and 100, and it can be seen that ratios of about 1.04 are found outside of the mineralized area and ratios of about 1.0 are obtained within (the large peak at position 85 is a nonvegetated area).

SIGNIFICANCE

The information of the association of the certain spectral shifts in the spectra of geochemically stressed vegetation would provide a means, via satellite remote sensing, of surveying vast tracks of heavily vegetated areas which are not readily studied by other means. The Cotter Basin results should be confirmed and the technique extended to other sites before the significance can be evaluated.

FUTURE EMPHASIS

Analysis of the aircraft data will continue including data of a second year's flight of the Cotter Basin and data from several other sites will be accumulated. Work will be initiated on an automated geographic data base for each site, so that ground, aircraft and satellite data can be correlated and statistically analyzed. This work will be done in conjunction with the U.S. Geological Survey (USGS) and Columbia University. A second meeting of geobotanical investigations is being planned for late spring at GSFC.

REFERENCES AND PUBLICATIONS

Collins, W.E., G.L. Raines, and F.C. Canney, "Airborne Spectrometer Discrimination of Vegetation Anomalies Over Sulfide Mineralization On Remote Sensing Technique," paper presented at the Geological Society of America Meeting, October 1978.

Collins, W.E., G.L. Raines and F.C. Canney, "Airborne Spectroradiometer Discrimination of Vegetation Anomalies Over Sulfide Mineralization in the Cotter Basin Area, Lewis and Clark County, Montana," submitted to *Photogrammetric Engineering and Remote Sensing*, 1979.

"Definition of Geobotanical Research Needs," prepared by the General Electric Co., Space Division for NASA/GSFC, *1, 2,* July 1978.

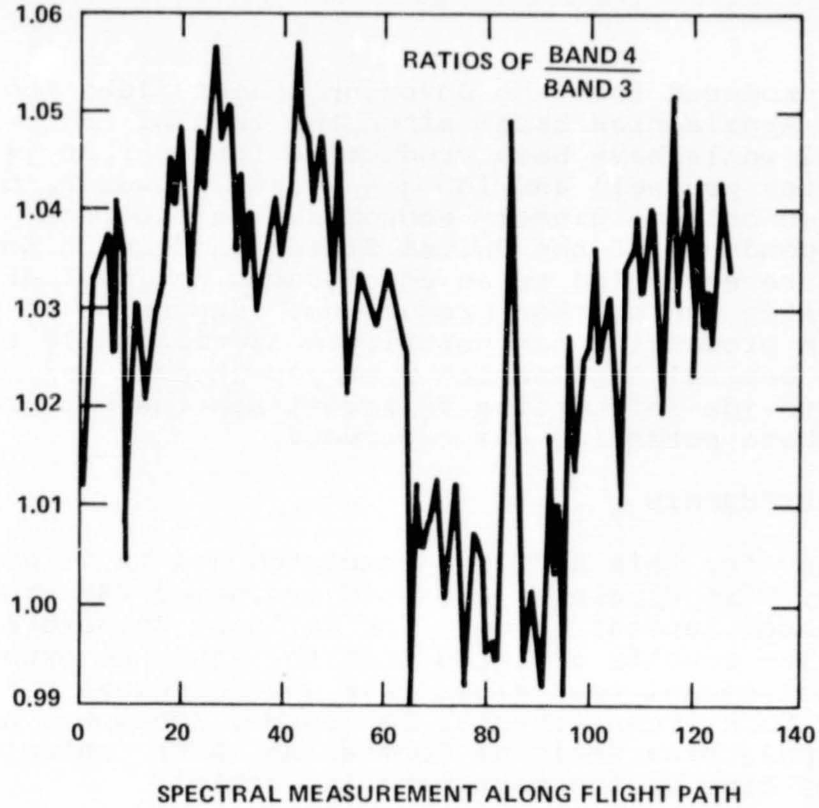

Figure 1-1. Analysis of Geobotanical Data Obtained from Cotter Basin, Montana

APPALACHIAN LINEAMENT APPLICATIONS SYSTEMS VERIFICATIONS TEST

OBJECTIVE

The objectives of the Appalachian lineaments Applications Systems Verifications Test (ASVT) are to demonstrate and transfer the application of Landsat-derived lineament information and mapping techniques to state geological and planning institutions, and to identify those structural lineaments on enhanced Landsat imagery that define zones of increased permeability in Devonian shale formations, and thus indicate areas prospective for gas production.

BACKGROUND

Gas has been produced from the Devonian shales along the western margin of the Appalachian basin since the turn of the century, and individual wells have been productive for over 30 years. Low production rates per well and low gas prices, however, have made this production only marginally economical in the past. The increasing dependence of the United States on foreign sources of petroleum has recently led to an accelerated national effort to increase domestic hydrocarbon production. Expansion of the Devonian shale production can contribute significantly to relieving local central Appalachian energy problems, and Landsat imagery can provide information to facilitate the exploration process for those potential gas reserves.

RECENT ACCOMPLISHMENTS

The pilot study for this ASVT was completed and in it geologists from Kentucky, West Virginia, and Ohio evaluated GSFC-generated, computer-enhanced Landsat imagery for defining structure-related lineaments. The results dictated that the study be expanded to include two additional test sites that would include parts of the states of New York, Pennsylvania, Tennessee, Kentucky, and Virginia. Appalachian Regional Commission (ARC) contracts have been signed by five of the participating states.

A variety of image contrast and edge enhancements were applied to Landsat MSS data for the two new test areas using GSFC inhouse computer (VICAR/SMIPS) capabilities. These images were used for the preliminary evaluation of lineament-enhanced products at the second short course/workshop (May 10-12, 1978), which was attended by twenty-two state participants.

The contract to provide standard commercially-enhanced imagery for state user evaluation, and then to later assess specific user requirements and capabilities, was awarded to the GE Corporation on Septembet 27, 1978. Preliminary image processing for the two northern sites was initiated by year end.

SIGNIFICANCE

Successful correlation of Landsat lineaments with fracture-related porosity in Devonian shale gas fields will provide a powerful tool for locating additional gas prospects.

FUTURE EMPHASIS

Future experiment efforts will be directed toward refinement and extension of the technology transferred in the pilot test site (an area of known Devonian shale gas production) to geologically similar areas where gas production has not yet been exploited. Using digital Landsat data for a wide range of disciplines will provide broader, better-informed satellite data users.

REFERENCES AND PUBLICATIONS

Anderson, A.T., "Preliminary Results of the NASA/ARC Study to Relate Satellite-Defined Lineaments to Devonian Shale Gas Production," *Proceedings of the D.O.E.-sponsored Second Eastern Gas Shale Symposium*, held in Morgantown, Pennsylvania, October 16-18, 1978.

Onash, C., "Appalachian Lineament Analysis Task, Final Report," Computer Sciences Corporation Task 20700, 1978.

CHAPTER 2

CRUSTAL MODELS

OVERVIEW

The basic goal of the crustal modeling program is to use space-derived data to increase our understanding of the structure, composition, and evolution of the Earth's crust. The primary data types are satellite-derived magnetic and gravity data (described in the sections on Crustal Modeling and Magnetic Field Studies) and solar system data obtained under NASA's lunar and planetary program (described in the section on Comparative Planetology/ Crustal Evolution).

The space-derived potential field data is of necessity limited in resolution to wavelengths roughly comparable to the altitude of the satellite from which the data was derived. In the magnetic field studies program, global measurements of the Earth's scalar magnetic field were taken at altitudes of 400-1000 km with the three Pogo satellites from 1965 to 1972. These data have been used to derive magnetic anomaly maps over the entire globe with resolution approaching 200 km. In October 1979 the Magsat satellite will be launched to make measurements of the vector field at altitudes of 300 to 500 km, which will significantly improve the resolution obtainable in the anomaly maps. In addition, the vector data is expected to help resolve certain ambiguities in the interpretation of the anomaly maps.

Satellite gravity data is currently limited to resolutions of about 500 to 1000 km. When data from a Gravsat satellite is available (perhaps in the mid-80's) much higher resolutions are expected. Until such time, however, satellite-derived gravity anomaly maps can only be used to study very broad-scale features of the Earth's crust.

The objective of the comparative planetology studies is to use comparative planetary data from the Moon and terrestrial planets to help define models of the earliest nature and evolution of the Earth's continental crust. Events that took place on the Earth over a billion years ago have largely been masked by subsequent subsidence, sedimentation, erosion, mountain-building and continental drift. However, clues to this early history can be obtained from studies of other bodies, such as the Moon and Mars, whose surface has changed far less than the Earth's over the past several aeons.

Contributors to this chapter include Richard Allenby, Herbert Frey, Robert Langel, Paul Lowman, Gilbert Mead, and Herman Thomas.

CRUSTAL MODELING

OBJECTIVES

The objectives of crustal modeling are to develop methods for using satellite magnetic and gravity data to investigate regions of nonrenewable resource potential by constructing geophysical/geological models of subsurface structure and composition, to gather correlative data and utilize it to refine crustal geological and geophysical models based on Magsat data and to compile available data in a Geophysical Atlas consisting of geophysical data in individual maps on a common Van der Grinten Grid. Correlative data will include laboratory measurements of rock magnetic properties, aeromagnetic, heat flow and seismology data.

BACKGROUND

Models derived from satellite magnetometer data can be mapped as magnetization contrast or magnetic anomalies. Interpretation of these maps requires two main inputs: a temperature-depth profile and an upper and lower boundary for a "near surface" magnetic layer as well as data on the magnetic properties of rocks within the layer. Direct measurements of rock magnetic properties can be made on samples brought to the Earth's surface rapidly enough so as not to re-equilibrate to the new surficial P-T-fo_2 conditions. Estimates of the pressure (and thus depth), and temperature environment where the rocks are formed are obtained from laboratory phase equilibria studies.

In those regions where the sampling of rocks from depth is inadequate, indirect methods may suffice. Gravity anomalies, as an indicator of rock density, will frequently agree in sense and magnitude with magnetic anomalies; in cases where there is a lack of agreement, petrologic and physical conditions must be modelled so as to explain them. Seismology offers another indirect means of estimating rock composition at depth, but is, by itself, unable to accurately delineate rock type due to the many rock types which have similar seismic velocities. Heat flow models are unconstrained as to depth of heat production sources and thermal conductivity of intervening rock types, so unambiguous models are obtained infrequently. The aforementioned data sets can often jointly constrain models so as to improve the odds for a unique solution.

Tectonic style, to the degree that associated rocks have nearly the same composition, may serve as a basis for interpreting magnetization models. Rifts, sutures, subduction zones, etc., produce characteristic rock types and thus are expected, with minor modifications for individual cases, to form a foundation for a comprehensive global model. Conversely, the models may aid in locating hidden structures with their contained mineral resources.

Surface geology and drill cores to crystalline basement can, in many cases, give clues to the lithology of inaccessible levels in the Earth's crust.

Inasmuch as the Mohorovičić Discontinuity (Moho) is a chemical discontinuity, it would be expected to have a pronounced effect on a magnetic profile with depth. To the extent that the Moho has relatively constant chemistry globally, it could provide a calibration point at variable depths in various regions from which lithospheric magnetization can be estimated. An obvious need therefore exists for global depth to the Moho models.

RECENT ACCOMPLISHMENTS

Completed magnetization models include: the United States, Australia, and Canada. Figure 2-1 shows an apparent magnetization contrast model for the United States. Units are emu/cc x 10^4. Areas such as Kentucky appear to require more intensive investigation. A comprehensive model, with seismic and heat flow correlative data, has been completed for the western United States (Mayhew 1979).

Results from a comprehensive study of the Bangui magnetic anomaly and a correlative gravity anomaly show that the anomalies do not correspond to surficial features, but they are crustal in origin. An interpretation consistent with available data is that the anomalies are the result of an intrusion into the crustal rocks of the region (see figure 2-2 and Regan and Marsh 1979).

Magnetic data for mantle-derived periodotitic and eclogitic xenoliths show the samples to be insignificantly magnetic at room temperature. Petrologic and magnetic field modeling data support this finding that the Earth's mantle is nonmagnetic (Wasilewski, Thomas, and Mayhew 1979).

A revised basement map of the interior of the United States has been prepared. This map is based on all data available prior to 1977. A preliminary basement rock lithologic map of the eastern midcontinent has been prepared based on qualitative correlations of rock type with small scale Bouguer anomalies (Lidiak 1978).

A correlation study of near surface gravity and magnetic data over the Great Lakes region of North America has been completed. The study shows that rock density and rock magnetization do not agree on a one-to-one basis (Purdue University group).

Global correlations between free-air gravity and magnetic anomalies have been examined using data contained in the Geophysical Atlas (Lowman and Frey 1979). There is evidence of geographical coincidence(Frey 1978).

Two tectonic maps of the rift systems and sutures of the world from the Archean to the present have been completed. These data will be invaluable in potential field modeling inasmuch as both regimes have nearly constant mineralogy and they serve as indicators of present and past plate boundaries and regions of magnetic and gravity anomalies. The global rift map (figure 2-3) shows continental rifts, which are extensional ruptures penetrating a substantial thickness of lithosphere. Oceanic rifts and spreading centers are not shown, as they are very well documented in other published maps (SUNY at Albany Group).

A survey has been completed of all available seismic refraction lines penetrating the upper mantle in the conterminous United States and the border areas of Canada and Mexico. From this data, a contour map of the top of the mantle-depth to the Moho (figure 2-4) has been constructed (Allenby 1979).

A global atlas of geophysical data has been compiled and is expected to facilitate correlations of satellite gravity and magnetic data with surface and lithospheric features. The beauty of the atlas lies in the common Van der Grinten projection for all of the maps which allows instant comparison of several geophysical data sets (figures 2-5 and 2-6) over a given region of the Earth (Lowman and Frey 1979).

Maps of global tectonic and volcanic activity have been completed covering the central global region and the two polar regions as part of a synthesis of satellite geophysical data (see figures 2-7, 2-8, and 2-9). These maps, which are the first of their sort, show major geologic features which are active now or have been active within the past million years. The central map was drawn as an overlay on the National Geographic Society's "The Physical World" map, with the addition of data from other sources, including Landsat mosaics and a computer plot of seismic epicenters.

Five major types of geologic features are shown. Zones in which new crust is being created are the active oceanic spreading centers and their continental extensions. The complementary zones of crustal destruction are subduction zones, or in some areas, continental overthrusts such as the front of the Himalayas. Shear zones such as the San Andreas, in which one plate is moving past another, are major active faults. Tensional features include grabens, rifts, and individual normal faults. The criterion for recency (i.e., activity within the past million years) in all these is either seismic activity or geomorphic evidence of youth. Volcanos are similarly included on the basis of reported activity or physiography.

One of the completed maps intended for inclusion in the Geophysical Atlas shows distribution of recent major volcanism, i.e., the centers of volcanic activity of the Earth during the past 1,000,000 years (figure 2-10). These data were compiled from the published literature and Landsat imagery. Most of this activity is associated with the present active plate margins. In some areas, such as the interiors of Africa, the Western United States, or China, this relationship is not clear, and the volcanism may be associated with incipient plate boundaries (rift zones) or earlier plates already subducted under continental masses.

Although the maps are chiefly a compilation of previously available information, they have some interesting tectonic implications. In particular, they illustrate the fact discussed in papers by McKenzie and Atwater, i.e., that continental crust is much more deformable than oceanic crust, and that plate boundaries may be extremely broad, or "diffuse" in Atwater's term. The area of active faulting in central Asia, for example, is bigger than several recognized plates. When considered in the light of McKenzie's work, the maps suggest that orthodox plate tectonic theory, based on movement of rigid plates, is not applicable to large parts of the continental crust. A specific implication of this for GSFC projects is that space-related geodetic techniques, such as VLBI and laser ranging, must be carefully planned to allow for diffuse plate boundaries and intra-plate deformation.

There is no further updating planned for the map showing volcanic activity of the past 1,000,000 years (figure 2-10), but a separate publication on the three tectonic activity maps will also be prepared.

FUTURE EMPHASIS

In the future, magnetization modeling will: produce final maps and models based on processed vector data; develop structural and thermal models based on these results; and interpret the models in terms of temperature and composition in the crust, and the implications for resource distribution.

Future laboratory work in rock magnetism will include the following:

- Analysis of rocks characteristic of the Earth's crust and modeling of the magnetic mineralogy properties of the lower crust and the upper crust.
- Investigation of the role of serpentinization in local and regional crustal magnetization.
- Development of a body of rock magnetic property data for rocks characteristic of tectonic style, e.g., rifts, sutures, etc.
- Development of comprehensive models delineating temperature, magnetization and magnetic mineralogy for selected areas.

Crystalline basement research will include petrologic and geochronologic work on drill cores as well as updating maps of basement lithology.

Additional work in tectonic style investigations will include mapping the world's "hot spots" and mapping unusual topography. Research correlating magnetic and gravity anomalies globally will be extended to include fits with structure and tectonics.

The polar regions will be added to magnetic and gravity maps in the Geophysical Atlas (Lowman and Frey 1978).

REFERENCES AND PUBLICATIONS

Allenby, R.J., "United States Crustal Thickness," in preparation, 1979.

Bowman, P.L., L.W. Braile, V.W. Chandler, W.J. Hinze, A.J. Luca, and R.R.B. von Frese, "Magnetic and Gravity Anomaly Correlations and its Application to Satellite Data, Final Report," NASA contract NAS 5-22816, 1978.

Frey, H., "Global Geophysics: Correlations of Satellite Derived Magnetic and Gravity Anomalies," *E@S, Trans. Am. Geophys. Un.*, *59*, 1204 (abstract), 1978.

Hinze, W.J., N.R. Richardson, L.W. Braile and E.G. Lidiak, "Ring Magnetic Anomalies in the Central Midcontinent," AGU Midwest Meeting (abstract), 1978.

Lidiak, E.G., "Rifting in the Midcontinent, U.S.A.," International Symposium on The Rio Grande Rift (abstract), 1978.

Lowman, P.D. and H.V. Frey, "A Global Geophysical Atlas of Satellite and Surface Data," *E@S, Trans. Am. Geophys. Un.*, *59*, 1204 (abstract), 1978.

Lowman, Paul D., Jr., and Herbert V. Frey, "A Geophysical Atlas for Interpretation of Satellite-Derived Data," NASA TM 79722, February, 1979.

Mayhew, M.A., "A Computer Program for Reduction of Pogo Satellite Magnetic Anomaly Data to Common Elevation and to the Pole, Interim Report," NASA contract NAS 5-25047, 1978.

Mayhew, M.A., "Regional Crustal Magnetization Variation in the Western United States," presented at Fall 1978 AGU Meeting and in abstract, 1978.

Mayhew, M.A., "Inversion of Satellite Magnetic Anomaly Data," *Journal of Geophysics*, *45*, 119-128, 1979.

Mayhew, M.A., "Magnetic Anomalies at Satellite Elevations Over the United States," in preparation 1979.

Mayhew, M.A., "Magnetic Field Studies, Final Report," in preparation, to be published under NASA contract NAS5-25047.

Mayhew, M.A., B.D. Johnson and R.A. Langel, "Magnetic Anomalies at Satellite Elevations Over Australia," in preparation, to be published under NASA contract NAS5-25047.

Mayhew, M.A., and H.H. Thomas, "Anomalous Crustal Structure in Eastern Kentucky and Tennessee," presented at the Midwest A.G.U. Meeting, Columbus, Ohio, September 13, 1979.

Regan, R.D., and B. Marsh, "The Bangui Anomaly," *Geophysics*, in press.

Thomas, H.H., P.J. Wasilewski, and M.A. Mayhew, "Magnetization of a Cross section of the Continental Crust: Evidence from the Ivrea-Verbano and Strona-Cenari Zones," to be presented at the AGU Meeting, San Francisco, California, December 3-7, 1979.

Wasilewski, P.M., H.H. Thomas, and M.A. Mayhew, "The Moho as a Magnetization Boundary," *Geoph. Res. Lett.*, *6*, 541-544, 1979.

EQUIVALENT BULK MAGNETIZATION DERIVED FROM POGO SATELLITE DATA ASSUMING A CONSTANT THICKNESS MAGNETIC CRUST OF 40 KM. UNITS ARE EMU/CC x 10^4.

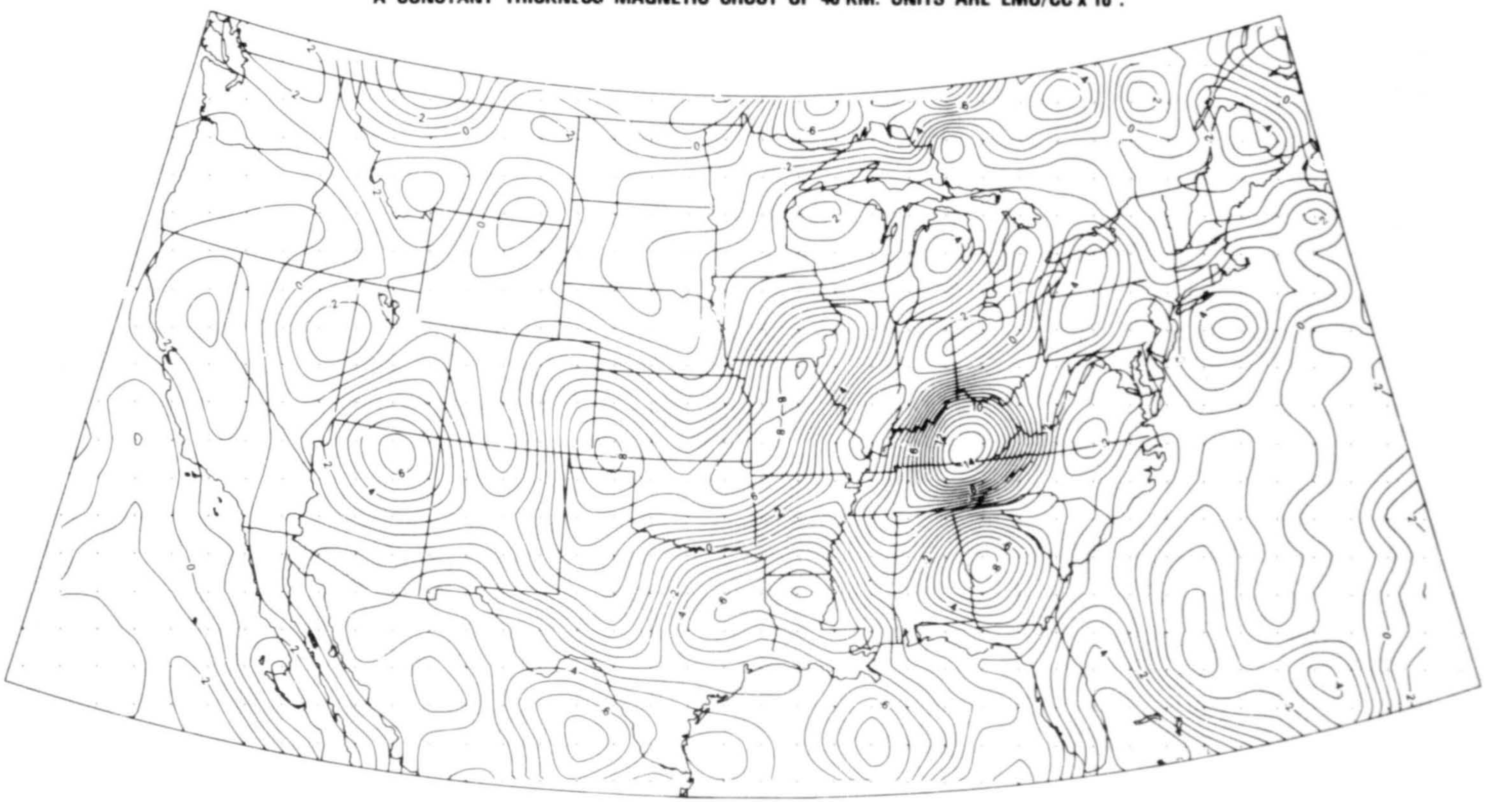

Figure 2-1. An Apparent Magnetization Contrast Model for the United States

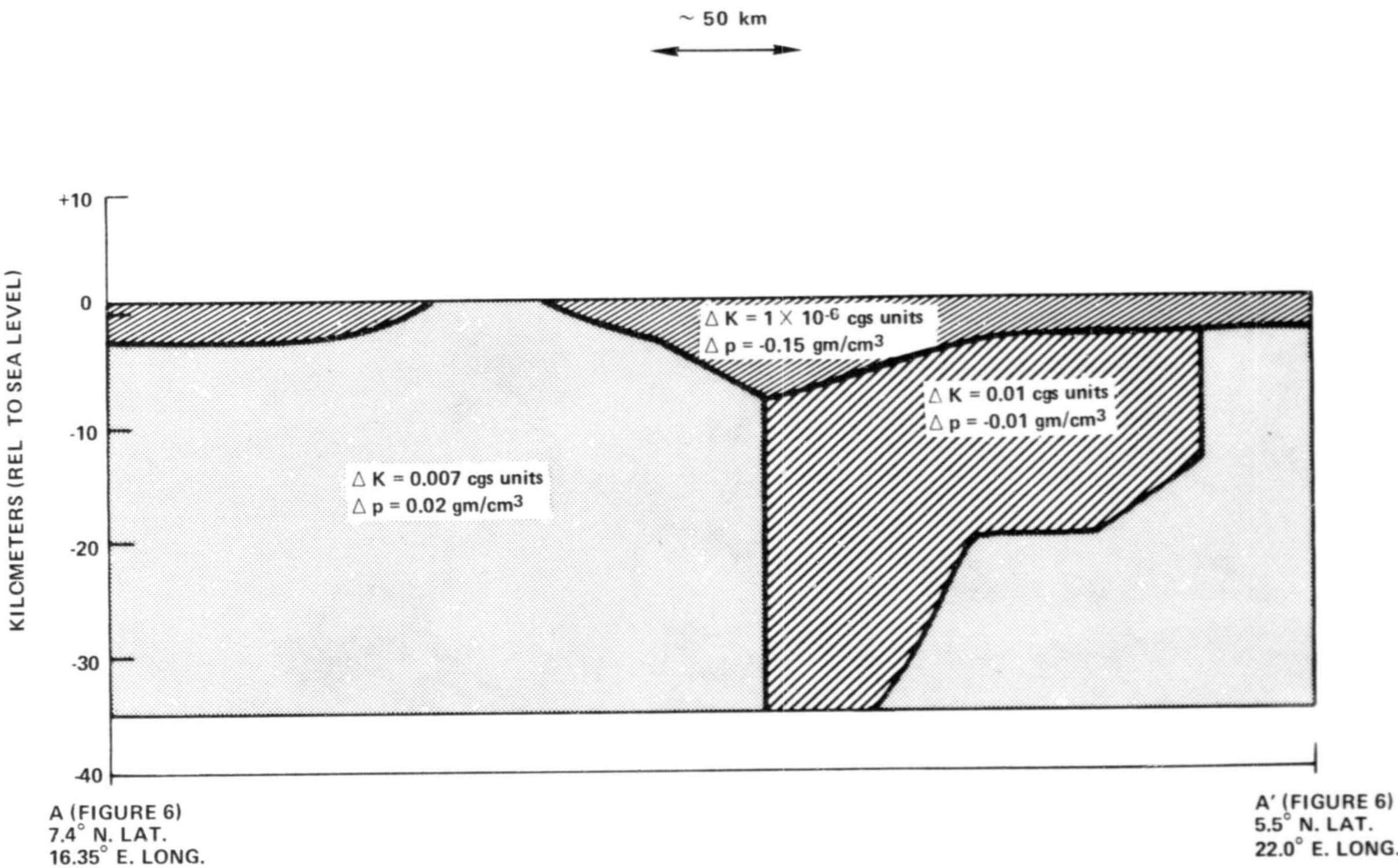

Figure 2-2. Interpretation of the Bangui Magnetic Anomaly and a Correlative Gravity Anomaly

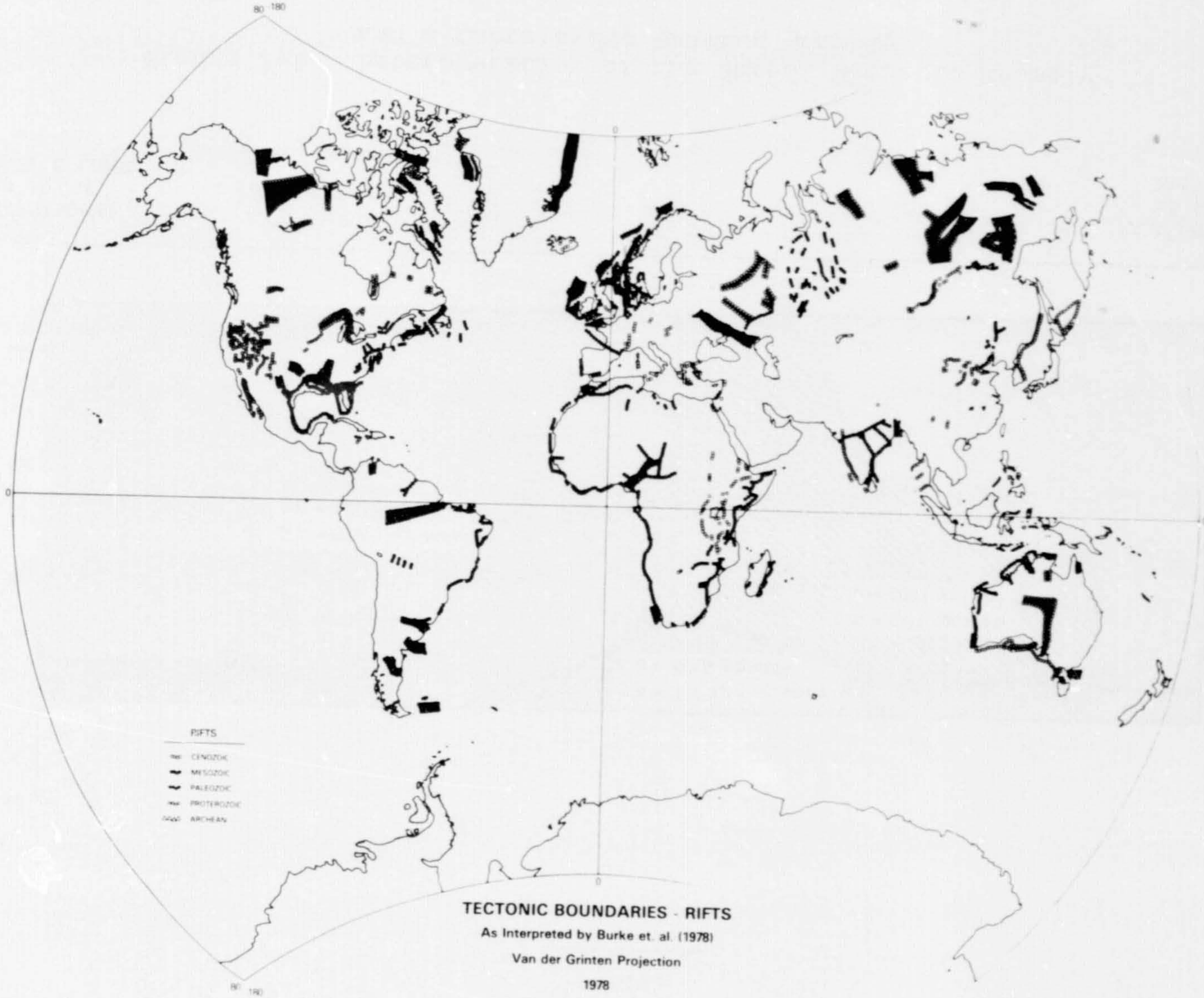

Figure 2-3. Global Rift Map

2-10
23

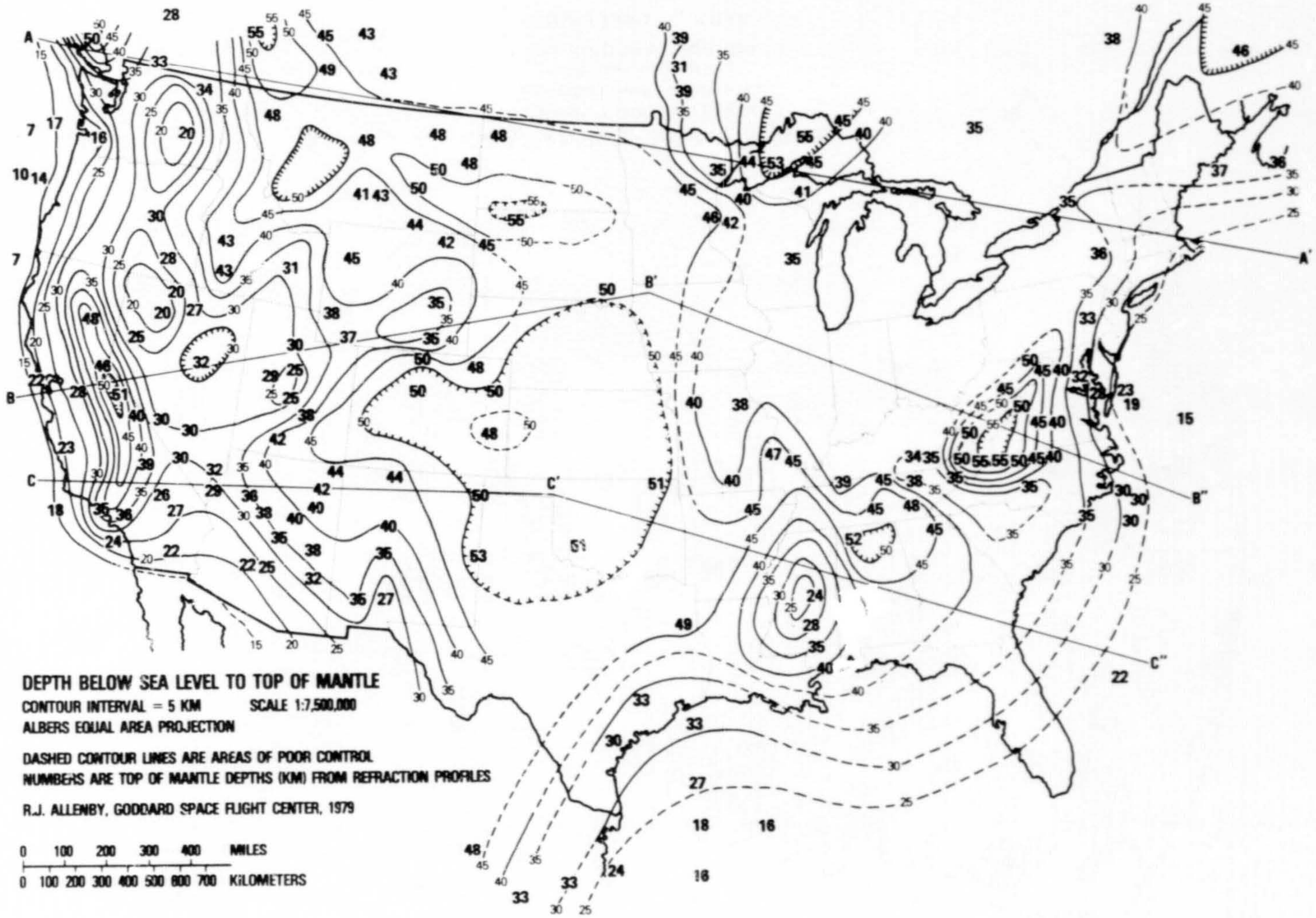

Figure 2-4. Contour Map of the Top of the Mantle-depth to the Moho

2-12
25

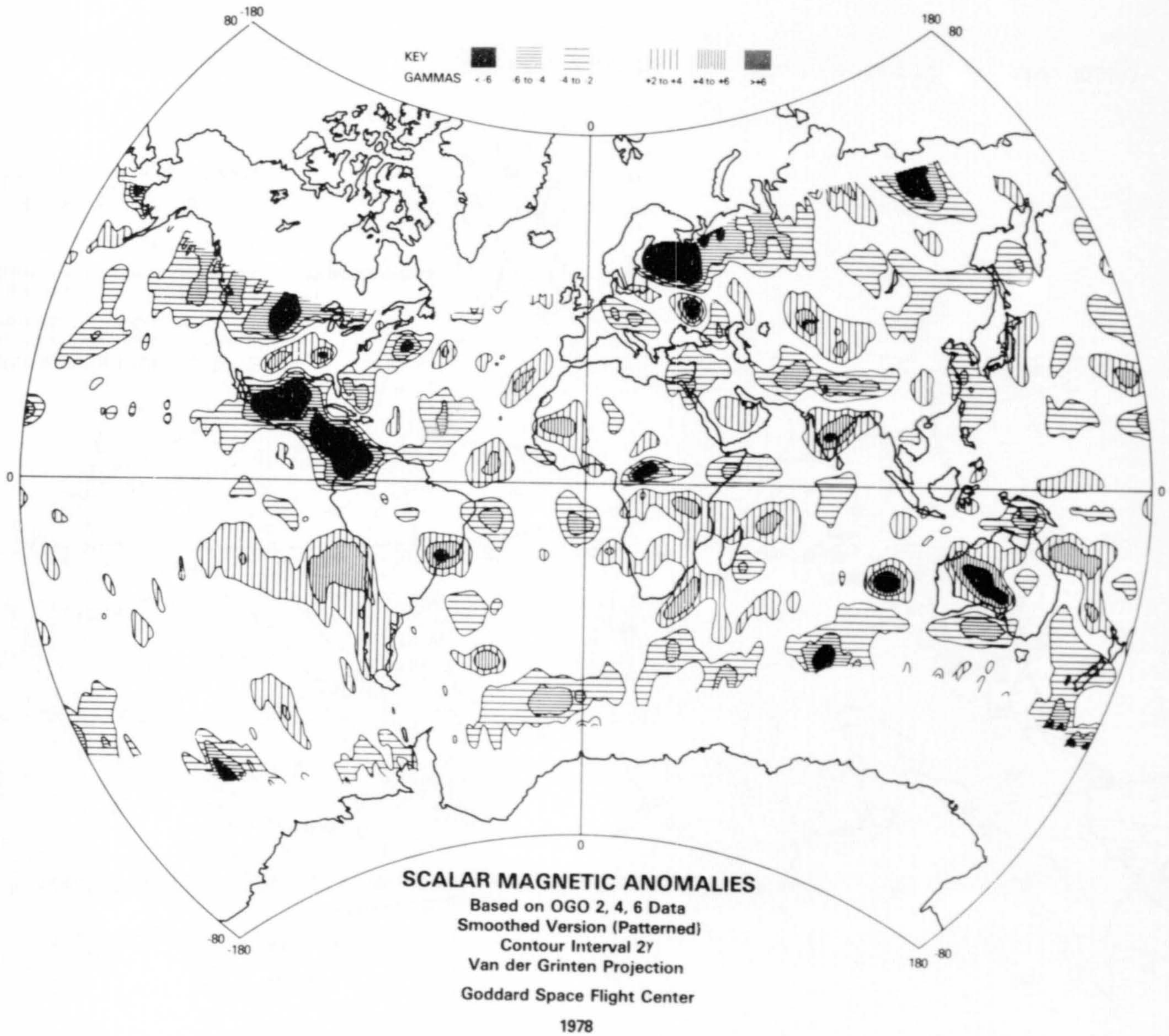

Figure 2-5. Global Geophysical Atlas Showing Scalar Magnetic Anomalies

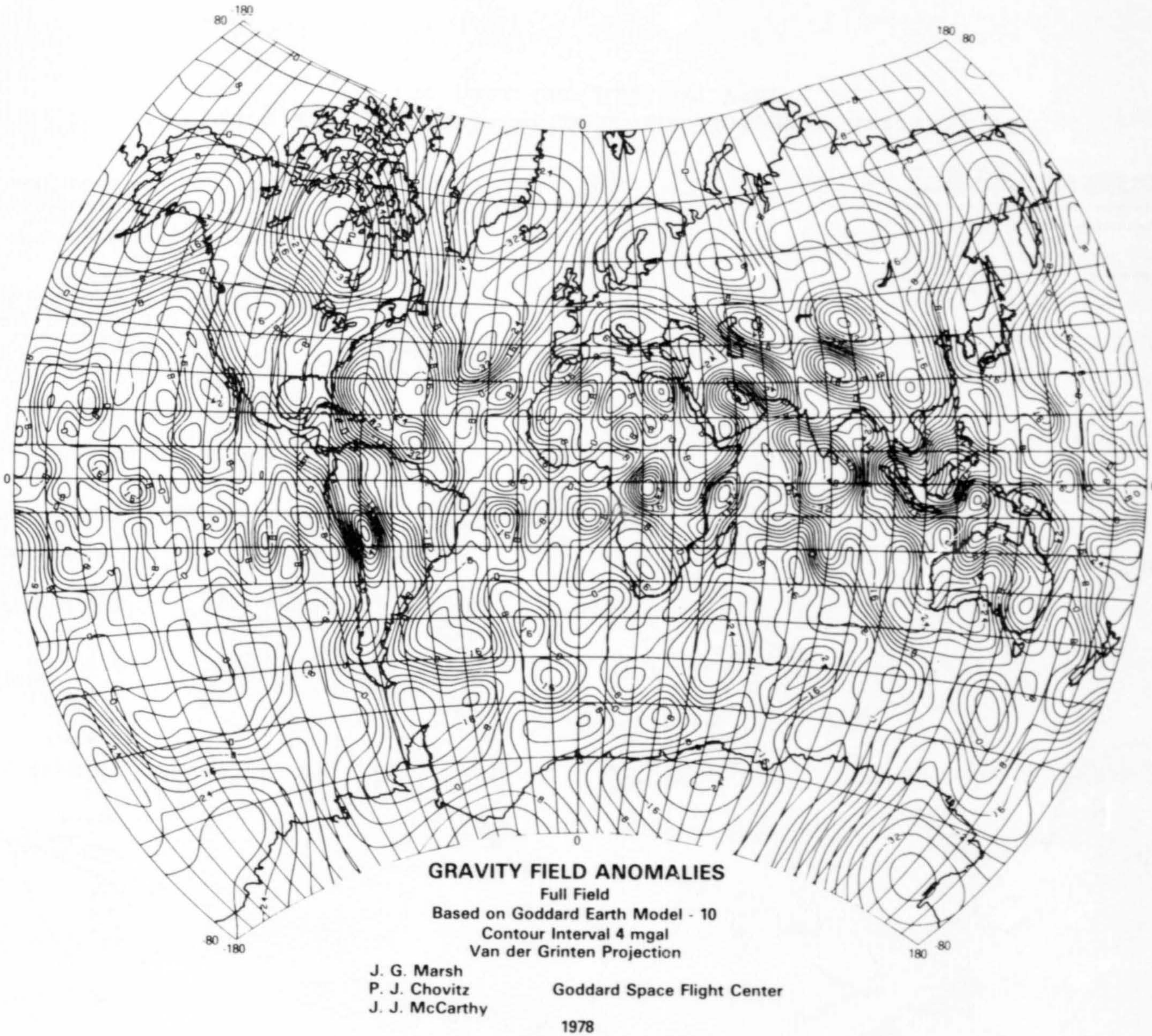

Figure 2-6. Global Geophysical Atlas Showing Gravity Field Anomalies

2-13
26

REPRODUCIBILITY OF THE ORIGINAL PAGE IS POOR

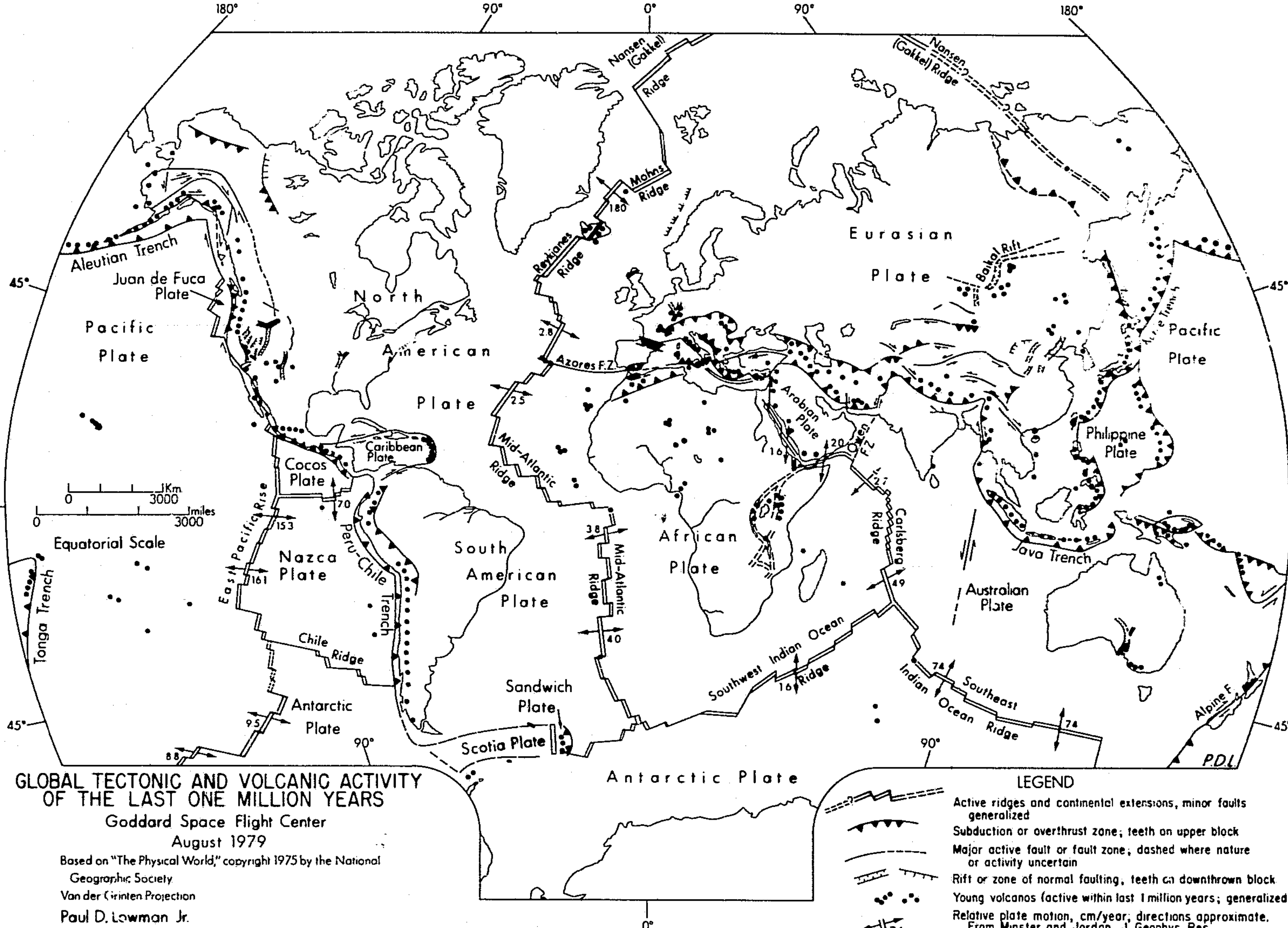

Figure 2-7. Global Tectonic and Volcanic Activity of the Last One Million Years

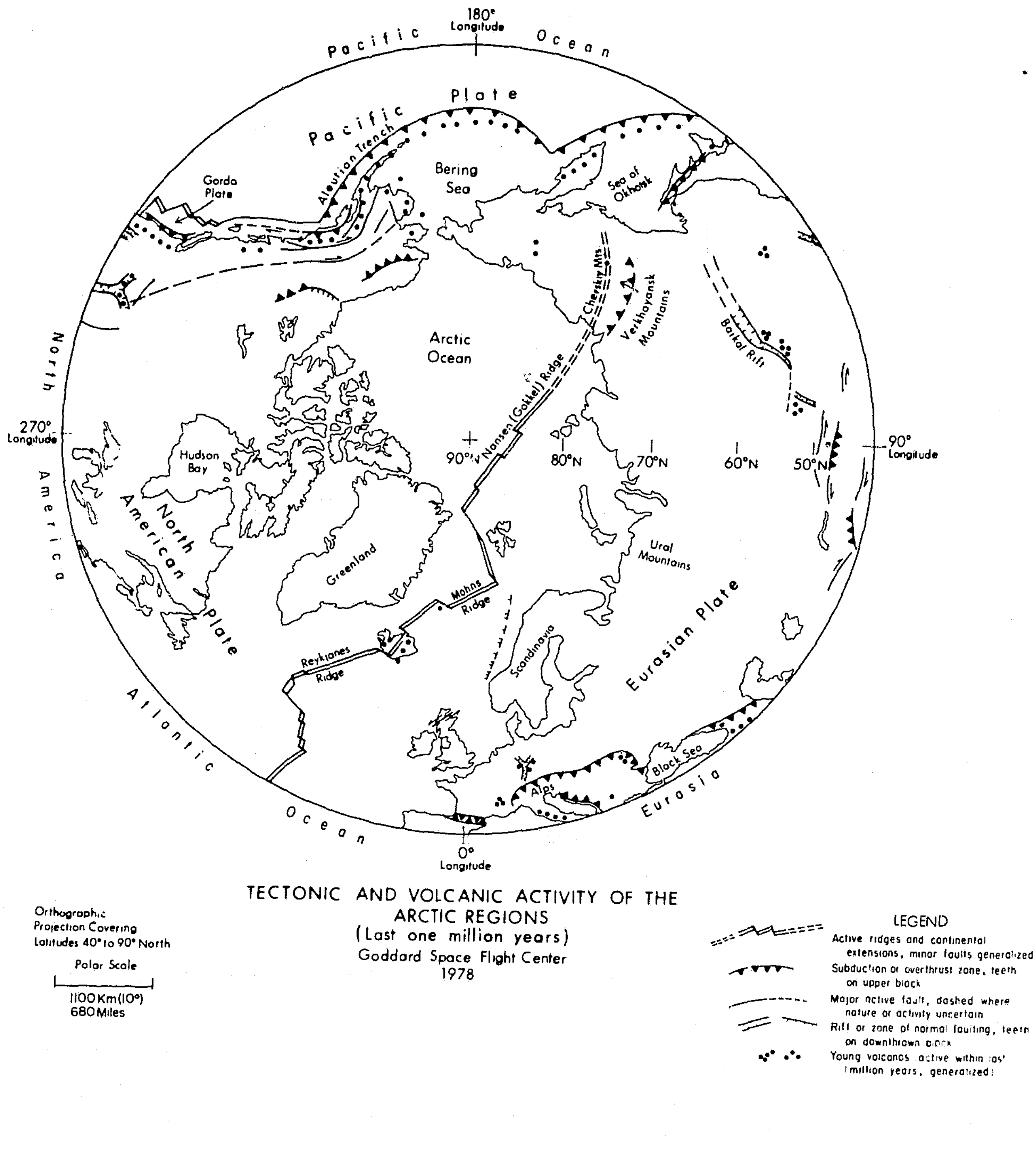

Figure 2-8. Tectonic and Volcanic Activity of the Arctic Regions (Last One Million Years)

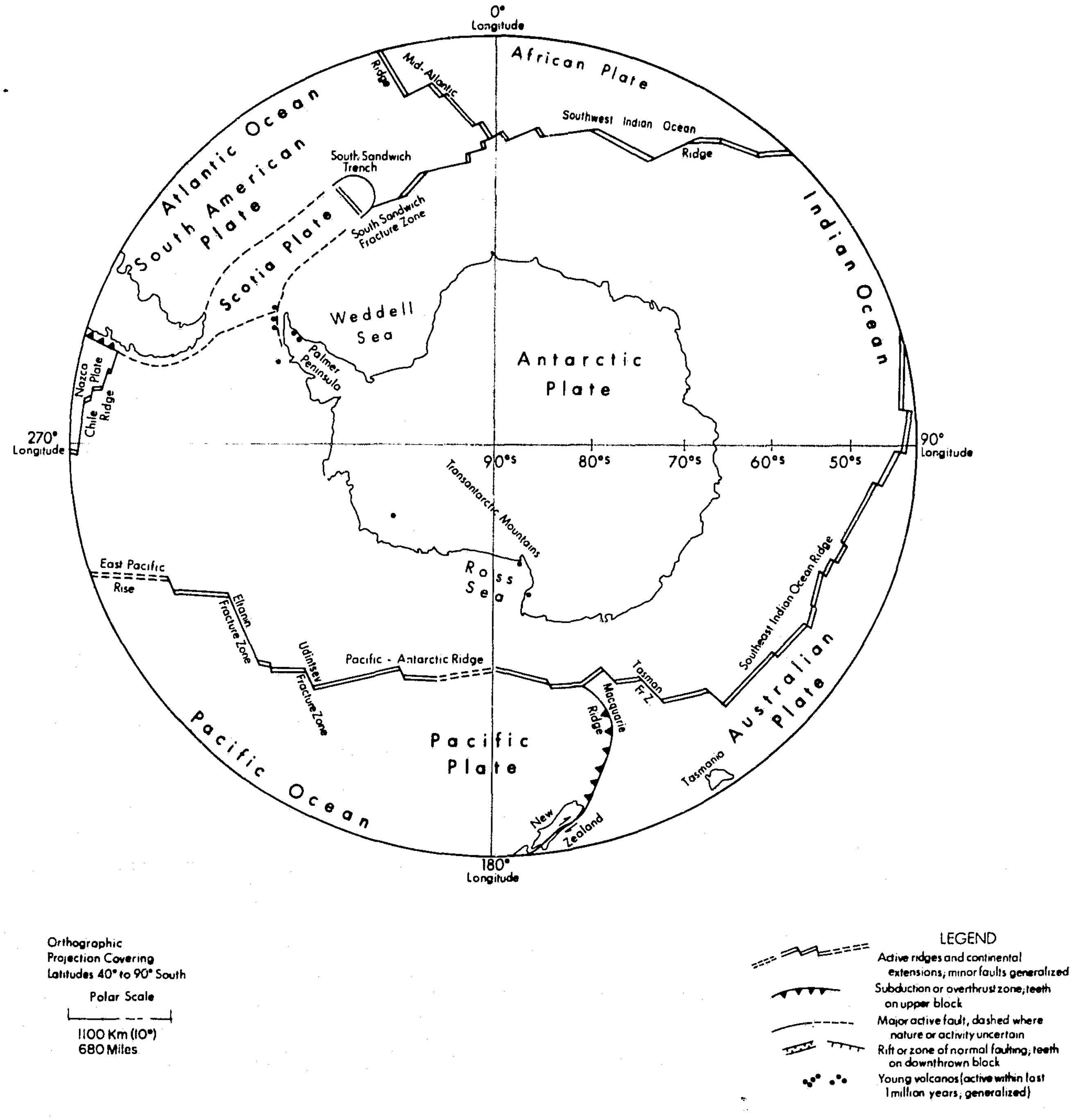

Figure 2-9. Tectonic and Volcanic Activity of the Antarctic Regions (Last One Million Years)

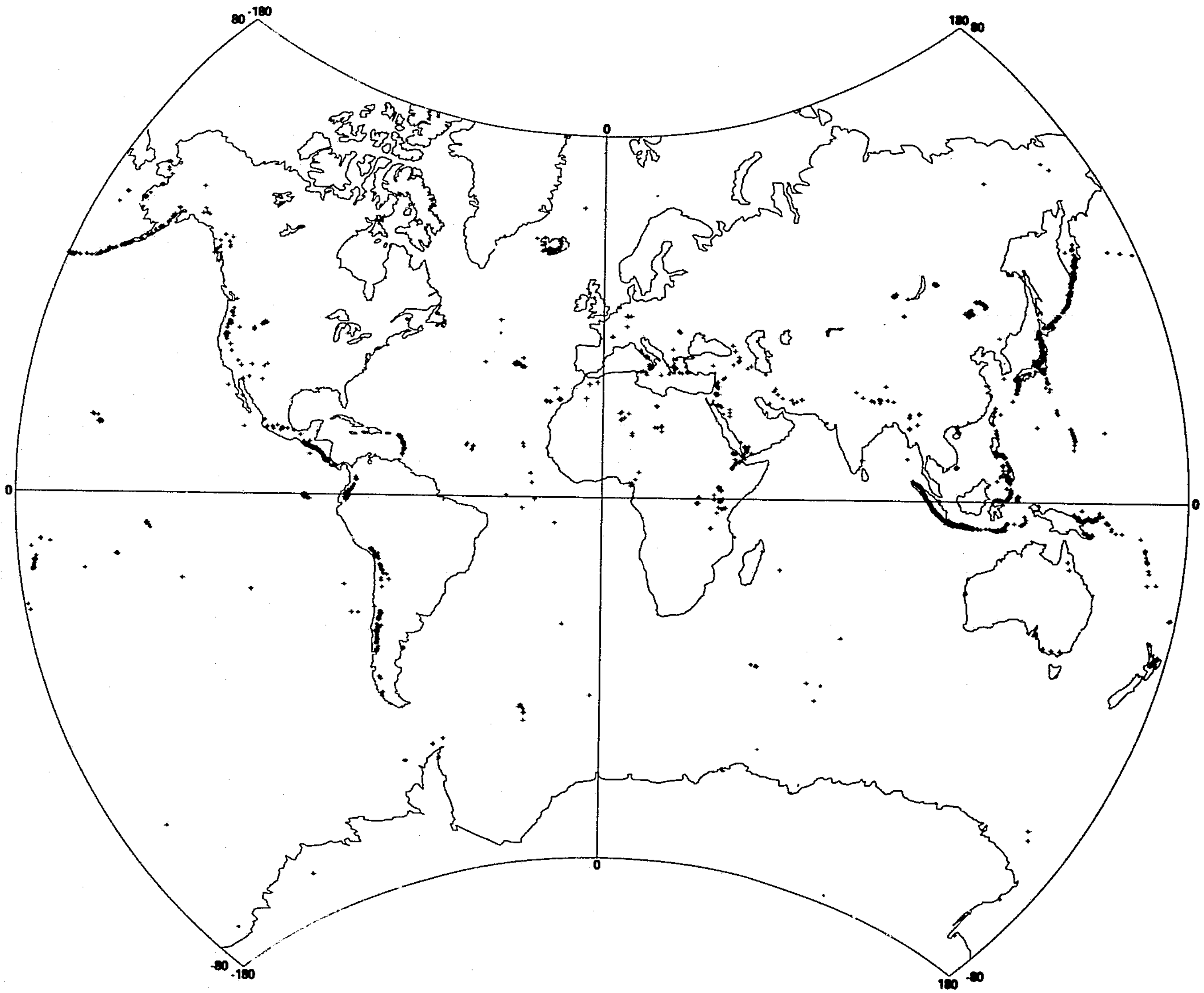

Figure 2-10. Recent Volcanic Activity (1,000,000 Years Ago to Present)

MAGNETIC FIELD STUDIES

OBJECTIVES

The objective of the magnetic field studies program is to develop models of the Earth's core field, secular variation, and crustal field from satellite data. Models of the crustal field are useful for probing beneath the surface to increase our knowledge of the structure and composition of the Earth's crust.

BACKGROUND

Until Magsat is launched in October 1979, our basic data set is from the Pogo satellite. This is supplemented in varying degrees by data from other satellites (Triad, Kosmos-49, Kosmos-321), by aeromagnetic and shipborne magnetic data, and by observatory and repeat station data. Representations of the internal (core) field of the Earth are via the traditional spherical harmonic analyses. Representations of the crustal, or anomaly, field are in terms of suitable maps and of equivalent source models. The first global scale crustal anomaly map from satellite data was published in 1975. Since that time, various refinements have been developed. Some have been published (Mayhew 1976, 1977) and some are in progress.

RECENT ACCOMPLISHMENTS

Models of the Internal Field

During the past year three efforts have been underway:

- An evaluation was prepared of the relative merits of secular variation models.
- A determination and recommendation was made concerning the value of observatory and repeat station data in support of the Magsat project.
- An effort to prepare software for derivation of spherical harmonic models utilizing Magsat was begun. Already completed are the incorporation of an ability to solve for angular biases in the spacecraft coordinate system, an evaluation (with negative results) of the value of prediction error filtering to secular variation modeling, optimization of inversion code, inclusion of cubic time terms for representation of secular variation, and selection of suitable OGO-6 data for use in future modeling.

Separation of the Measured Field Into its Various Sources

This effort is focussed on isolating the crustal anomaly fields from the core and external fields. External fields are particularly a problem at high latitudes. By visual data selection we have obtained an anomaly map over western Canada which is in good agreement with aeromagnetic data (see figure 2-11). This confirms our ability to adequately accomplish the separation of anomaly fields from external fields for scalar data.

Representations of the crustal anomaly field are obtained to first order by subtracting a field computed from a spherical harmonic analysis from the measured data and then removing a field with mathematical form equivalent to that expected from sources deep in the magnetosphere. A more consistent separation is then achieved by removing a linear or quadratic trend from the field. A map was produced for the Geophysical Atlas and for publication in *EØS* utilizing this technique (see figure 2-12). The difficulty with this technique is that it undoubtedly is also removing some of the core field from the anomaly map. An alternate technique, consisting of two-dimensional filtering, was also applied to the data to produce the other map used in the Geophysical Atlas. Work in this area is continuing.

Representation of Anomaly Fields

Software was developed to derive equivalent source models from the Pogo data. These programs are now available for use and a report has been written. Results for the United States are shown in figure 2-13.

Correlation of Magnetic and Gravity Anomalies

Purdue University has developed a quantitative technique to measure various aspects of magnetic and gravity anomaly correlation. Based on Poisson's theorem, the technique identifies areas of high positive or negative correlation and estimates the quality $\Delta J/\Delta\sigma$, when ΔJ is magnetization contrast and $\Delta\sigma$ is density contrast. Interpretation of these results is in its infancy and is being carried out under crustal modeling.

FUTURE EMPHASIS

The main emphasis in internal field modeling will be investigating the best way to represent secular variation and incorporating the best possible methods of evaluating the accuracy of derived models. Also, effort will be expended to further optimize the existing software.

Application of techniques of separating anomaly fields from external fields to high latitude data is continuing. High latitude anomaly maps from Pogo are expected to be published during FY 79.

Further investigation of the longest wavelength component of the anomaly field is under way. In particular, researchers are evaluating the effect of inaccuracies in its representation on modeling efforts at the same time as they seek to find the best method of estimating its value.

Equivalent source models will be modified to incorporate vector data and to model vector magnetization. The existing equivalent source model will be utilized to derive a global anomaly map reduced to common elevation and inclination.

REFERENCES AND PUBLICATIONS

Bowman, P.L., L.W. Braile, V.W. Chandler, W.J. Hinze, A.J. Luca, R.B. von Frese, "Magnetic and Gravity Anomaly Correlation and its Application to Satellite Data," Contractor Report, August 1978.

Langel, R.A., E.B. Fabiano, and G.D. Mead, "The Utility of Surface Magnetic Field Measurements in the Magsat Program," NASA TM 79614, August 1978.

Langel, R.A., R.L. Coles, and M.A. Mayhew, "Comparisons of Magnetic Anomalies of Lithospheric Origin as Measured by Satellite and by Airborne Magnetometer over Western Canada," NASA TM 80568, September 1979.

Mayhew, M.A., "A Computer Program for Reduction of Pogo Satellite Magnetic Anomaly Data to Common Elevation and to the Pole, Interim Report," NASA contract NAS5-25047, 1978.

Mayhew, M.A., "A Method of Inversion of Satellite Magnetic Anomaly Data," NASA/GSFC X-922-77-269, October 1977, and *Jour. of Geophys.*, in press 1979.

Mayhew, M.A., B.D. Johnson, and R.A. Langel, "Magnetic Anomalies at Satellite Elevations over Australia," in preparation, to be published under NASA contract NAS5-25047.

Mead, G.D., "An Evaluation of Recent Internal Field Models," *Quantitative Modeling of Magnetospheric Processes, Geophysical Monograph Series, 21,* 110-117, edited by W.P. Olson, AGU, Washington, D.C., 1979.

2-21
34

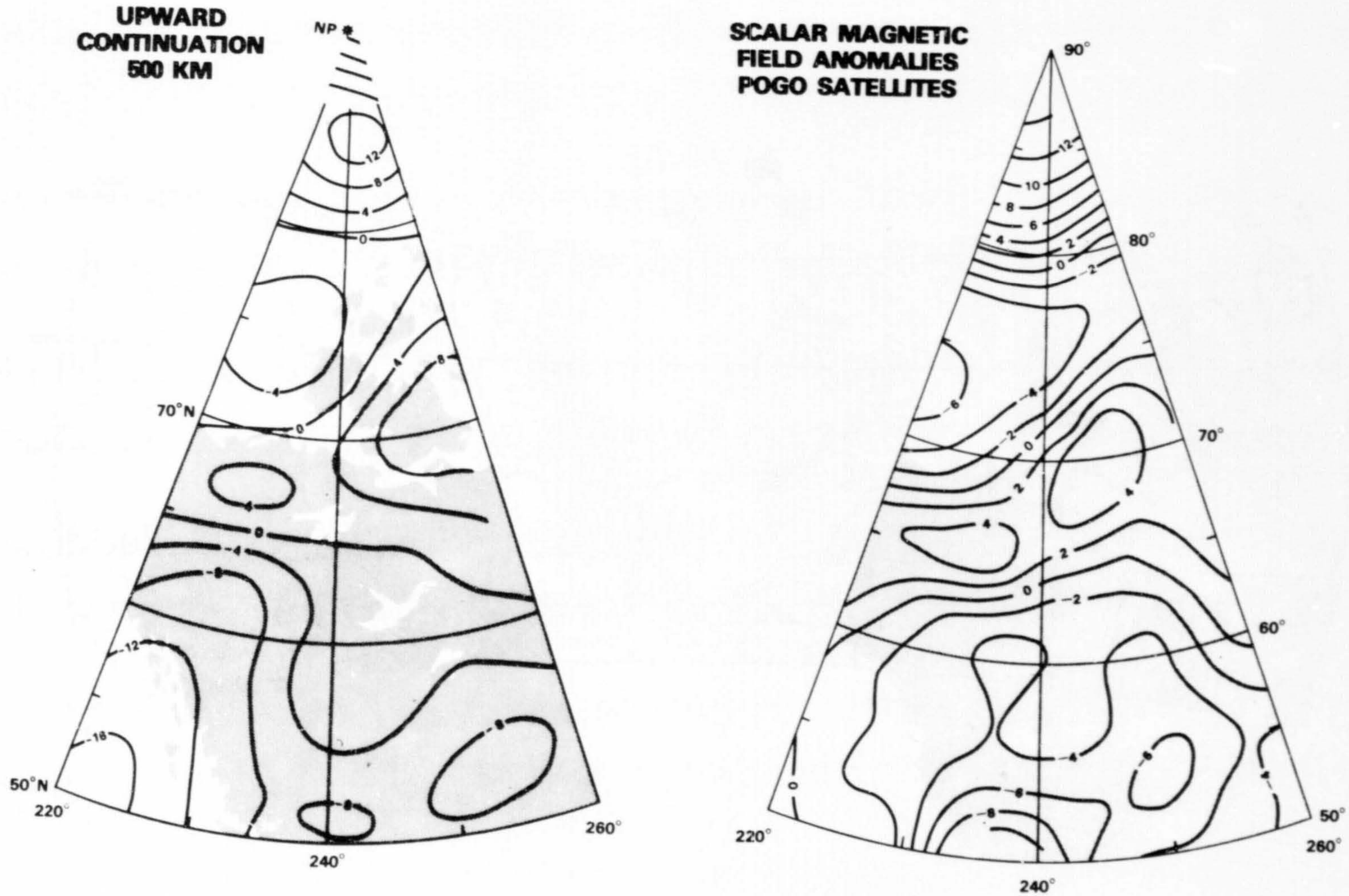

Figure 2-11. Comparison of Aeromagnetic and Satellite Anomaly Maps of Western Canada

2-22
33

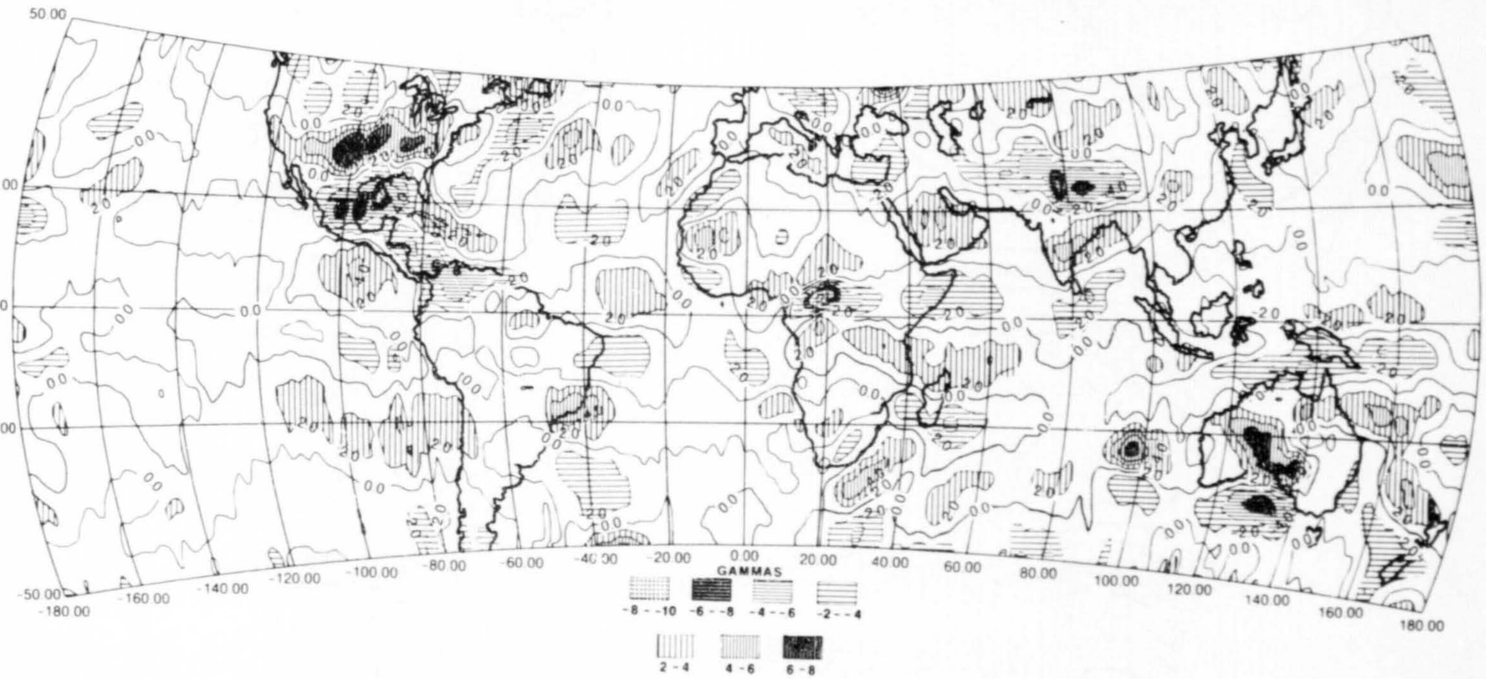

Figure 2-12. Global Map of Crustal Magnetic Anomalies

REPRODUCIBILITY OF THE
ORIGINAL PAGE IS POOR

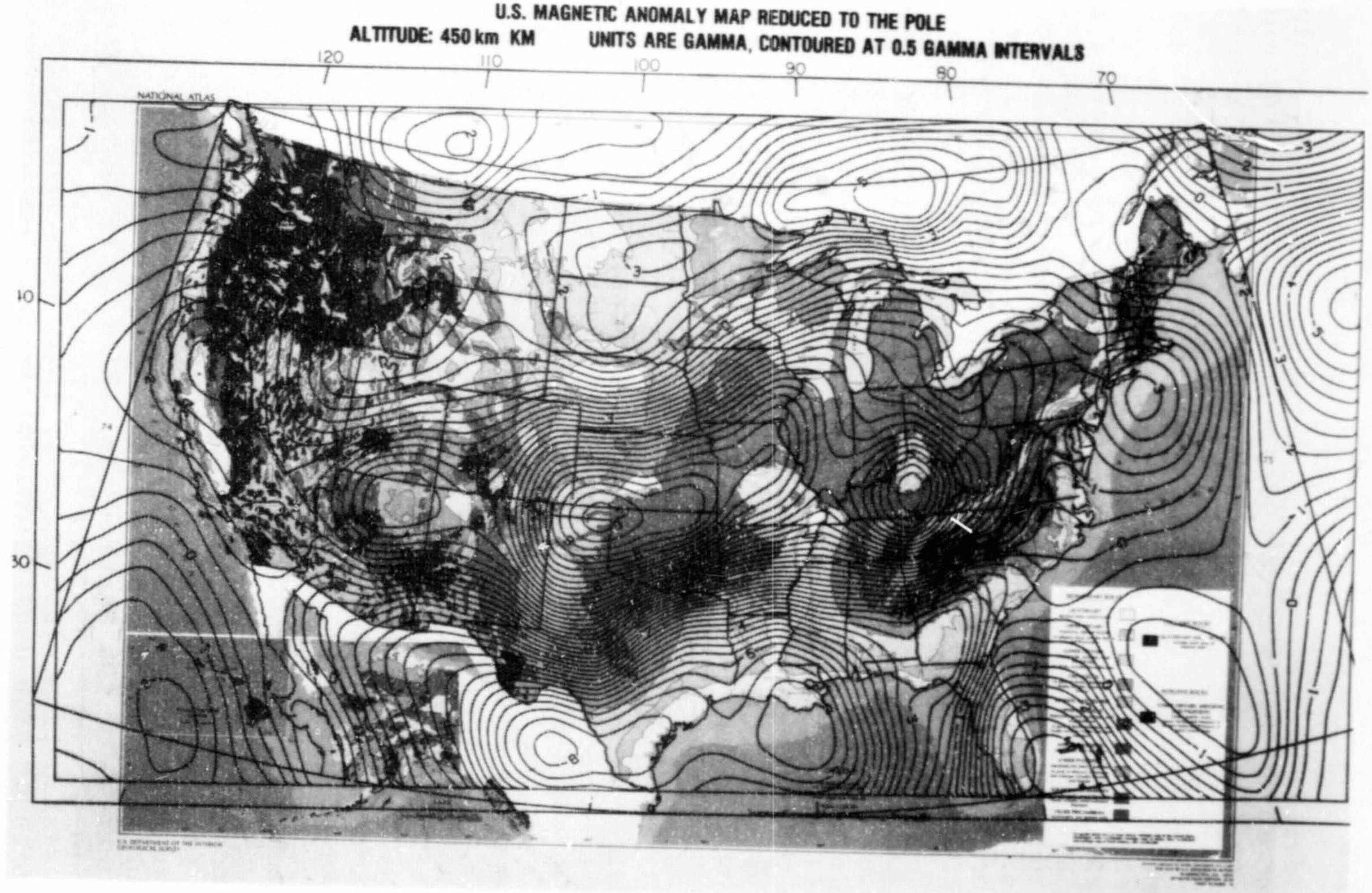

Figure 2-13. Map Showing United States Anomaly Field Derived From Pogo Data

COMPARATIVE PLANETOLOGY/CRUSTAL EVOLUTION

OBJECTIVE

The objective of comparative planetology and crustal evolution research is to use comparative planetary data to constrain models of the earliest nature and evolution of the Earth's continental crust.

BACKGROUND

The present-day structure and composition of the Earth's lithosphere and crust is a result of a long, complex history of volcanic and tectonic activity. Understanding that evolutionary process as well as the nature of the original crust is essential to a complete understanding of the present-day crust and how that crust is evolving.

There is almost no terrestrial data available that can constrain models of the earliest Earth. This is due to the scarcity of very old rocks, which are almost nonexistent from before about 3.5 billion years ago. Yet this is the very time when so many of the processes which continue today to change the Earth had their origin. Those processes have been so active for so long that they have literally destroyed the old rocks in the process of making new ones. It is very unlikely that the necessary data for understanding the early Earth will be found on the Earth.

The smaller terrestrial planets have had simpler, shorter and generally more sluggish evolutionary histories. They therefore preserve a greater percentage of their ancient, even primordial crusts. When allowance is made for differences in size and mass, bulk composition and position in the solar system (all of which can affect thermal histories, for example), the study of the crust and crustal evolution of these smaller planets can be used to constrain models of the early Earth. This results directly from the greater preservation of the effects of both external and internal processes which shaped those crusts 3 and 4 billion years ago.

One example is the effect of major, basin-forming impacts which occurred on all the terrestrial planets prior to 4 billion years ago. No trace of these immense impact structures remains on the Earth, yet these impacts were the dominant process affecting the structure and crust of the smaller terrestrial planets. Previous study has shown that these impacts may have had important consequences for the Earth (Frey, 1977a,b; 1979a,b). These include: (a) Conversion of some 50 percent of the Earth's original global sialic crust (Lowman 1976, 1978) into deep basins (b) concentration of high density basaltic crust ("oceanic crust") at the surface making subduction possible, and (c) steepening of the thermal gradients below the lithosphere, which may have triggered an early form of plate tectonics. The effects of major impacts are almost always ignored by those who construct models of the early Earth, yet these impacts may have been responsible for the most basic characteristic of the Earth's crustal structure: the dichotomy between low density continental crust and high density oceanic crust. Likewise the earliest oceans formed at this same time.

Precise calculation of the effects of these major impacts required knowledge about the number of such impacts, which was obtained by scaling from observed lunar impact basins. This was necessary because no direct trace of the impacts remains on the Earth. Likewise no evidence of the original uplift, rifting, and spreading that began plate tectonic motions remains on this planet, but Mars shows rift-like structures associated with crustal uplifts that suggest an early aborted form of "incipient plate tectonics" began on that planet. The origin of that process is much more clearly preserved on the much smaller world.

Therefore, the study of sialic crusts on the other terrestrial planets offers clues about the nature and occurrence of the original sialic crust of the Earth. Thermal history calculations for the terrestrial planets, combined with the knowledge obtained about surface features, can be used to model their early lithospheric evolution, which can then be extrapolated for the larger and hotter Earth. Variations in lithospheric thickness can be inferred from modeling the gravity fields of the smaller planets. This has important consequences for the deep structure of the Earth's lithosphere and crust, and the cause of the variations in that thickness. The occurrence and timing of volcanism on the smaller planets can be related to lithospheric thickness and thermal history models. These in turn may be useful in understanding the mode of emplacement of some volcanic materials on the present Earth, as well as the development of volcanic activity throughout Earth history. In short, the improved constraints on the nature and composition of the early crust of the Earth makes possible the construction of more plausible models of the Earth's crustal evolution than has been possible before.

RECENT ACCOMPLISHMENTS

The effects of major impacts on the earliest crust of the Earth have been studied in more detail during 1978. The question of the relative sizes of impact basins on the Earth and on the Moon when produced by identical impact bodies has been investigated, including the effects of gravity fields confining the crater dimensions. We have also explored the likelihood that basins larger than those which formed on the Moon may have formed on the Earth. This is quite likely, given that most populations of impacting bodies will produce a D^{-2} distribution in diameters. Previous estimates that at least 50 percent of an original crust would have been converted into large deep basins have been confirmed, but the uncertainties in that estimate can now be related to the various parameters that come into the calculation.

We have also attempted to obtain a better estimate of the nature of the impacting population by studies of large impact basins on Mercury and Mars. Comparison of the number/unit area versus size distributions for Mercury and the Moon shows that many proposed populations can probably be eliminated if both planets have been recording impacts for the same period of time (see figure 2-14). We have been able to relate our counts of major basins to the predicted numbers from dynamical and other studies, and find several candidate populations are more likely than most of the others suggested (see figure 2-15). This can now be related to the flux that should have impacted the Earth, making the Earth/Moon scaling more accurate in terms of the collective effects on the Earth's crust.

One of the effects of the major impacts was the reduction of sea level if, as some have proposed, the original crust of the Earth was covered by a global sea. The topography which resulted from the formation of the large impact basins was such that, by the time the bombardment was over 4 billion years ago, roughly half of the Earth's crust stood above sea level (see figure 2-16). Thus not only has the division of continental crust/oceanic crust been part of the Earth for most of its history, but likewise the separation of dry land and seas has been present for at least 4 billion years.

Studies of the rift valleys of Mars as they compare with the well-known rifts of East Africa have shown that both planets have a very similar distribution of rift lengths, when measured in units of the planetary radius (see figure 2-17). That is, compared with the size of the planet on which they formed, rifts of Mars have lengths comparable to those in East Africa. This suggests that the rifting mechanism is probably the same on both planets. The fact that rifts on Mars are wider than those on Earth reflects differences in crustal thickness; the Martian crust and lithosphere were undoubtedly thicker than the African crust and lithosphere at the time of rifting (see figure 2-18). This is important for understanding the extent and timing of thermal evolution on both planets.

We also find that the rifting pattern is more simple on Mars, and that two major periods of crustal uplift were significant in producing the observed Martian structures. The simple pattern on Mars compares with a very complex pattern of faults on the Earth, which is due to the complex tectonic history of the Earth's crust prior to the present episode of rifting (see figure 2-19). Thus the extensional features we observe on Mars are likely to be the first major breakup of that surface due to tectonic processes. Therefore, the continued study of the Martian rifts offers a chance to better understand how the rifting process was related to early mantle convection. When compared with thermal history calculations, it should be possible to relate mantle processes with lithospheric responses on Mars, and thereby infer something of the nature of the original rifting and plate tectonic breakup of the thinner lithospere of the Earth.

The rifting process on Mars has not progressed as far as has that in East Africa. The late-forming features found in the Gregory Rift (including dense fault swarms and central volcanos) are not present in the Martian rifts. This is due to the greater thickness of the Martian crust, and can be a constraint on the thermal profile at the time of rifting. The thickness of the present lithosphere on Mars can be determined from studies and modeling of the gravity field. Combined with the above studies this offers a strong possibility of determining the rate of thickening of the Martian lithosphere and how that thickening has varied over the planet.

We have discovered a previously unreported volcanic landform on Mars, a small, dome-like structure similar to terrestrial phreatic eruption cones where hot lava comes into contact with water or water-logged ground. Such features are well known in Iceland, and their occurrence on Mars indicates the presence of subsurface ice. It also places constraints on the thickness of the lava flows there, which can be related to the rate of eruption or extrusion of lava, and hence to the thermal profiles in the lithosphere at the point of eruption. This constrains the general volcanic evolution of the surface of Mars, and can be related to the early occurrence of some types of volcanism likely on the Earth.

FUTURE EMPHASIS

Work will continue on the redifferentiating of the original andesitic crust of the Earth and its relation to the appearance of granitic rocks common on the Earth today. This in turn will be related to the problem of the evolution of the crust in earliest times, and to the likely connection of that evolution with an early microplate tectonic environment.

The group will continue to examine in more detail through the use of numerical modeling the thermal effects of major impacts and the resulting volcanic and convective patterns in the lithosphere and upper asthenosphere in the early Earth. We hope through such computer modeling to bridge the gap between the earliest crust and the more recent crust through studies of the onset of plate tectonic processes. We will construct early models of the lithosphere during the period of between 4 to 3 billion years ago in an attempt to understand the gradual shift in evolutionary style to large plate tectonics.

Study of the Martian rifts will attempt to determine the timing and sequence of uplift, rifting, and volcanism that have produced the observed structures. When the effects of erosive modification of the old rifts are removed it should be possible to work out the evolutionary development of this region, and then relate that to the internal processes which were responsible (convection). We hope to build numerical models of the rifting process which reproduced the sequence of events on Mars. Then, if successful, the same techniques can be applied to the earliest rifting on the Earth, taking into account the differences in thermal profiles, lithospheric structure and composition.

We will undertake a comparative gravitational field analysis for Mars and the Earth in order to determine the relative lithospheric thicknesses and rigidities, as well as to model the upper asthenospheres for possible comparison of convective states.

We want to map the distribution of phreatic eruption cones on Mars in order to determine the distribution of thin volcanic flows on that planet. This we hope will provide constraints on the extrusion history for Mars and its thermal evolution. We also intend to study the relationship of the major volcanic structures and centers to the major rifts in order to determine the relative sequence of events that disrupted the lithosphere.

As radar data from the Pioneer Venus mission becomes available, we intend to incorporate this into comparative crustal structure analysis. We expect numerous rift valleys on Venus; their size and structure will reflect lithospheric properties and sublithospheric dynamics. We know the surface of Venus retains some more ancient crust than does the Earth. Comparison with the surface of Mars and the Earth will help define the evolutionary pattern as a function of size and mass, which are related to the thermal profiles for these bodies.

REFERENCES AND PUBLICATIONS

Chase, S.A. and H.V. Frey, "Volcanic Landforms in Cydonia," *B.A.A.S., 10,* 571, (abstract) 1978.

Frey, H.V., "Thausmasia: A Fossilized, Early-Formed Tharsis Uplift," *J. of Geophys. Res., 84,* 1009-1023, 1979.

Frey, H.V., and P.D. Lowman, Jr., "Comparative Planetology: Significance for Terrestrial Geology," submitted to *E@S, Trans. Am. Geophys. Un.,* and published as NASA TM 78051, 1978.

Frey, H.V., "The Earth's First Oceans," *Astronomy,* August 1978.

Frey, H.V., "Mars: A planetary Paradox," *Astronomy,* November 1978.

REFERENCES (continued)

Frey, H.V., and B.L. Lowry, "Martian Rifts and African Analogs," *B.A.A.S., 10,* 570, (abstract) 1978.

Frey, H.V., "Emergence of The Continents," submitted to *Origins of Life,* NASA TM 79669, November 1978.

Frey, H.V., "Martian Canyons and African Rifts: Structural Comparisons and Implications," *Icarus, 37,* 142-155, 1979.

Frey, H.V., "Origins of the Earth's Ocean Basins: Implications for the Development of Extraterrestrial Life," *Comparative Planetology (the Proceedings of the Third College Park Colloquium on Chemical Evolution),* Academic Press N.Y. 79-101, 1979.

Frey, H.V., "Martian Rift Tectonics," Second International Colloquium on Mars, NASA Conference Publication 2072, 28pp (abstract) 1979.

Frey, H.V., "Crustal Evolution of the Early Earth: The Role of Major Impacts,: in press, *Precambrian Research,* and published as NASA TM 80251, March 1979.

Lowman, P.D., Jr., "Crustal Evolution in the Silicate Planets," *Naturwissenschaften, 65,* 117-124, 1978.

Lowman, P.D., Jr., "Comparative Planetology and the Origin of the Continents," *Comparative Planetology (The Proceedings of the Third College Park Colloquium on Chemical Evolution)* Academic Press, 79-101, 1979.

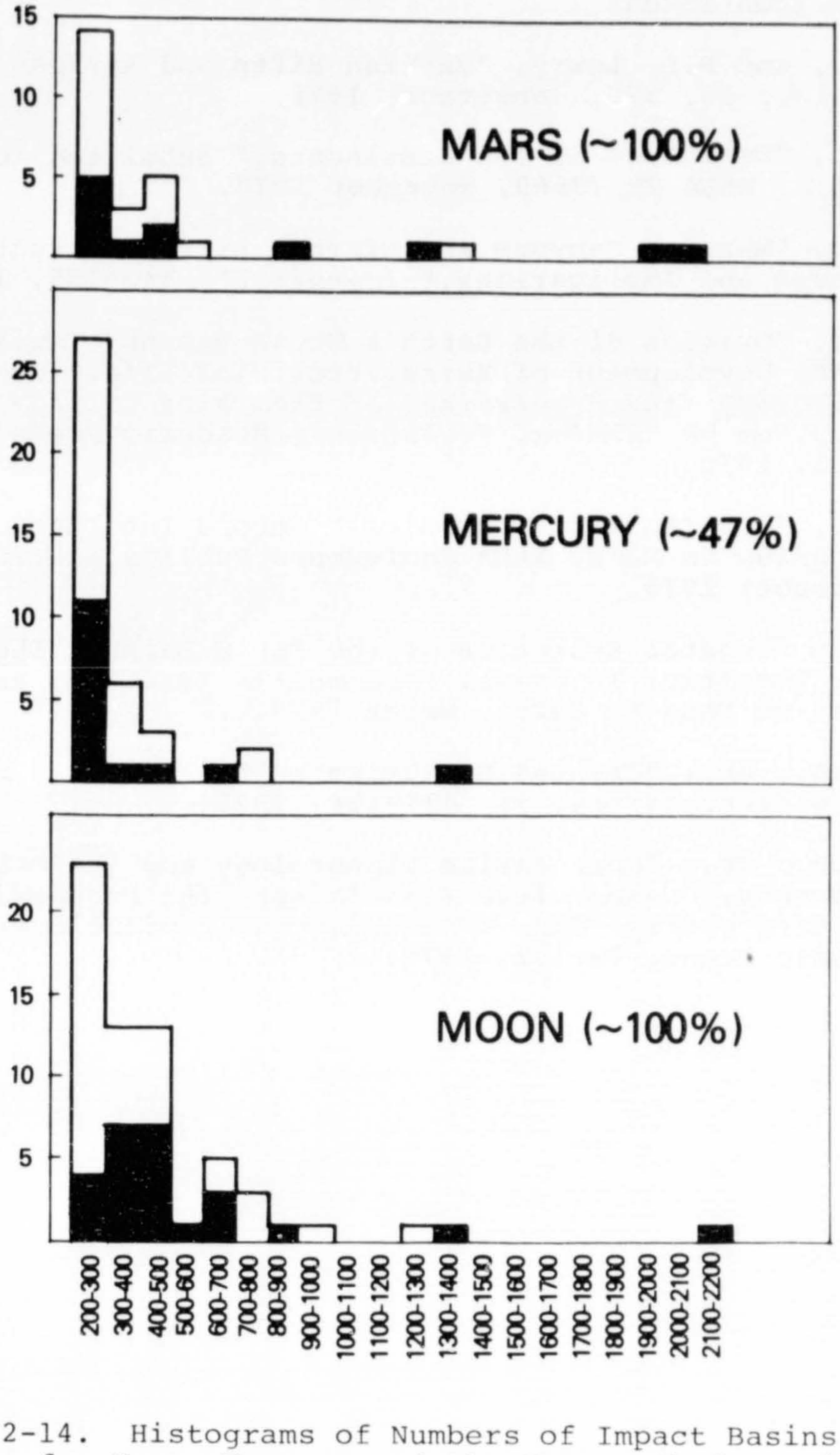

Figure 2-14. Histograms of Numbers of Impact Basins Versus Diameter for Mars, Mercury and the Moon. Shade regions indicate multiringed basins identified by Wood and Head (1976). Note that only 47% of Mercury has been photographed, while nearly 100% of Mars and the Moon has been observed.

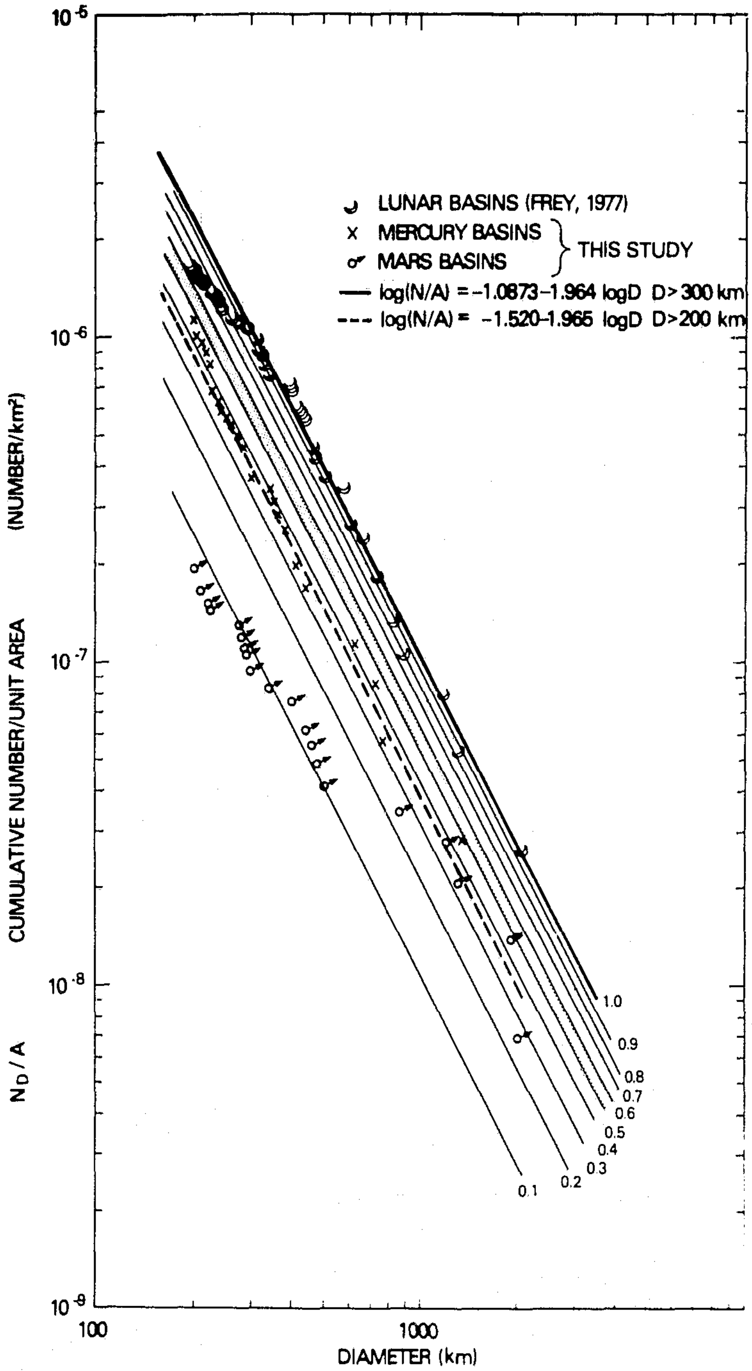

Figure 2-15. Cumulative Number Versus Diameter for the Impact Basins (shown in figure 2-14). Solid dark line indicates a least squares fit through the lunar data (for $D \geq 300$ km). Thin solid lines indicate .1, .2, .3, .4, ... of the lunar value. Dashed line shows least-squares fit through Mercury.

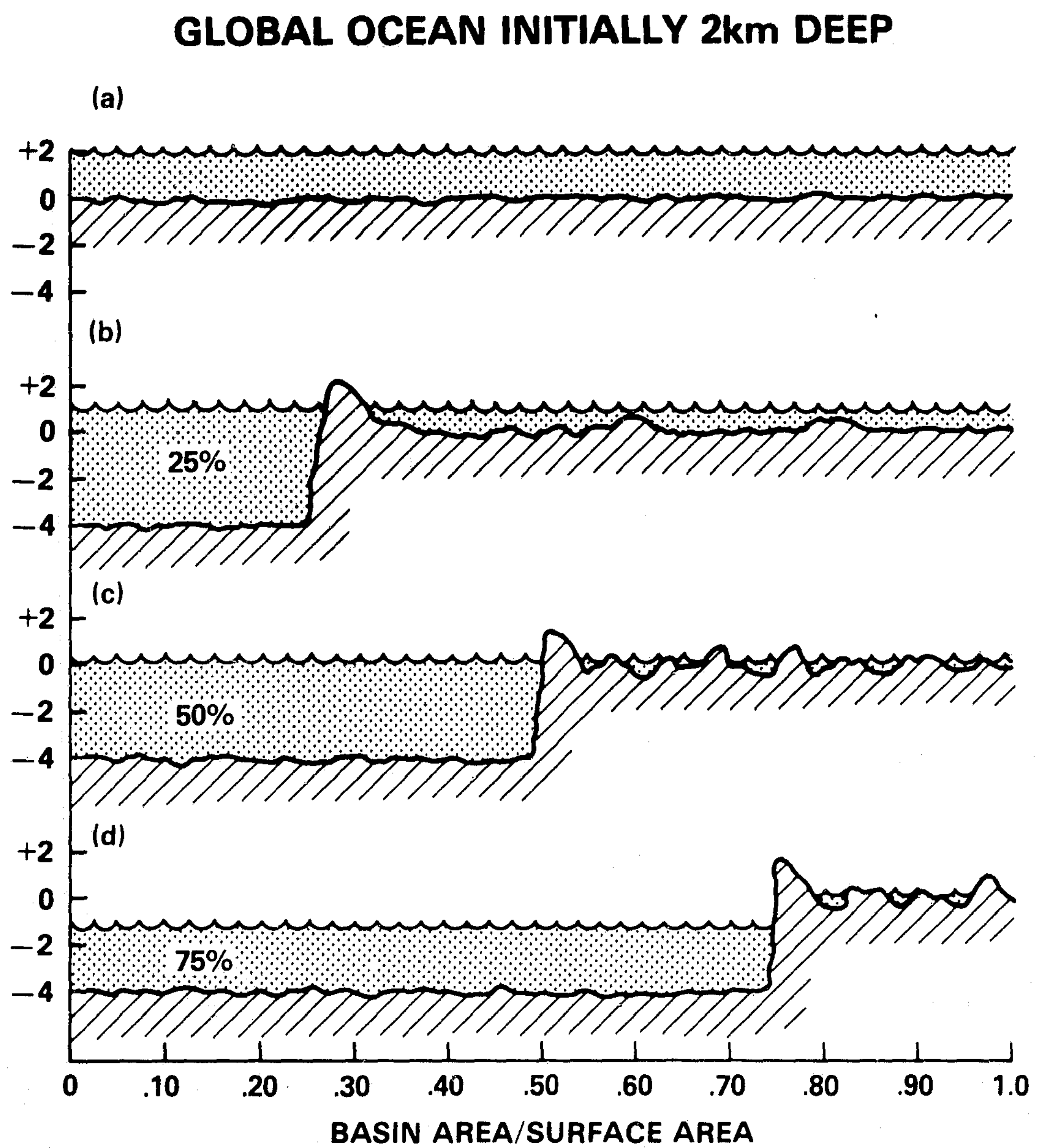

Figure 2-16. Effect of Formation of Large Impact Basins on Earth's Topography and Resultant Lowering of Sea Level. The large basins provide drains for the presumed global ocean, eventually exposing dry land.

MEASURED LENGTH AND LENGTH/RADIUS

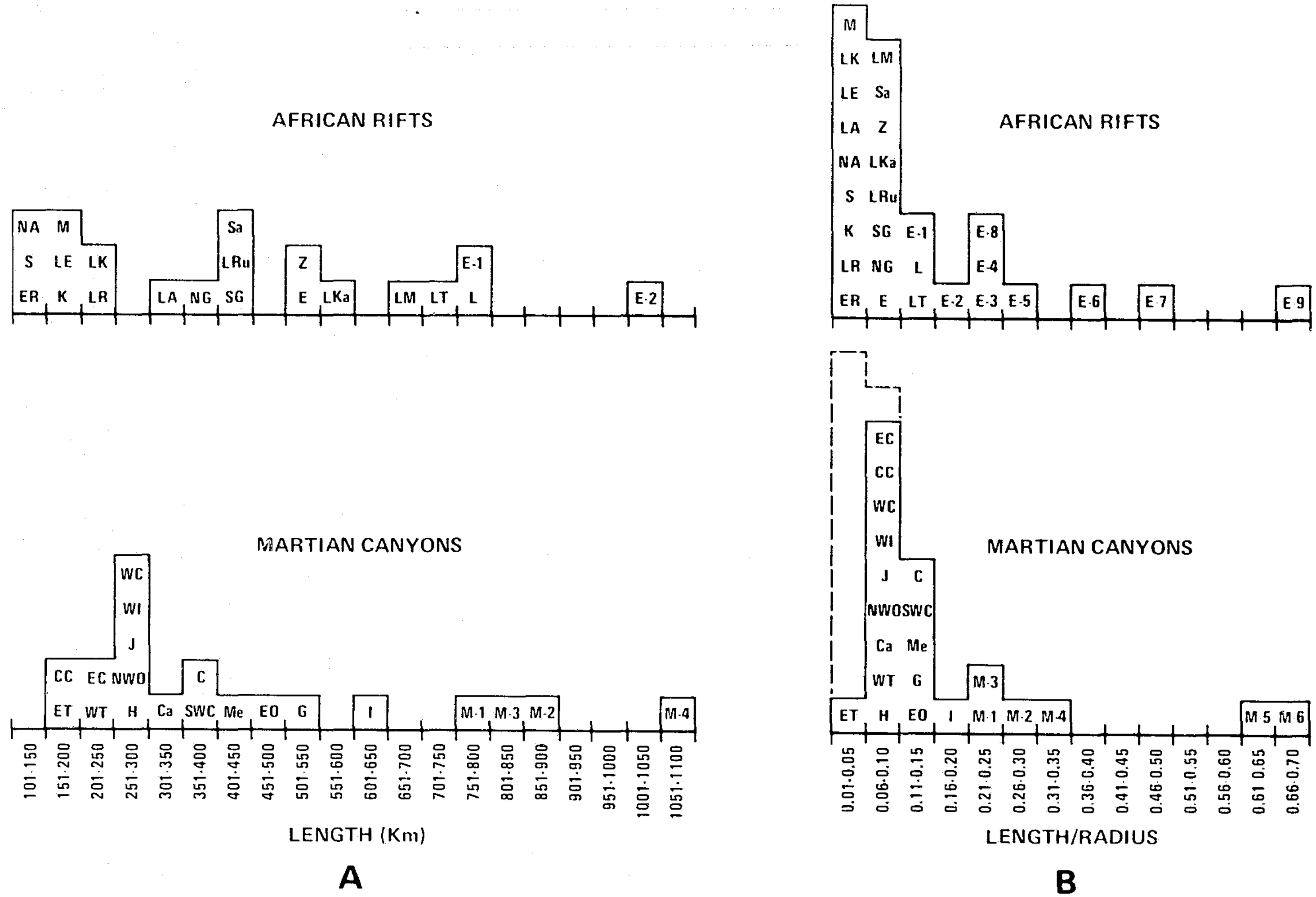

Figure 2-17. Comparison of Length and (Length/Planetary Radius) for African Rifts (Top) and Martian Canyons (Bottom). Both planets show a very similar distribution in rift length measured in units of planetary radius.

2-33
46

MEASURED WIDTH AND (WIDTH/RADIUS) x 10

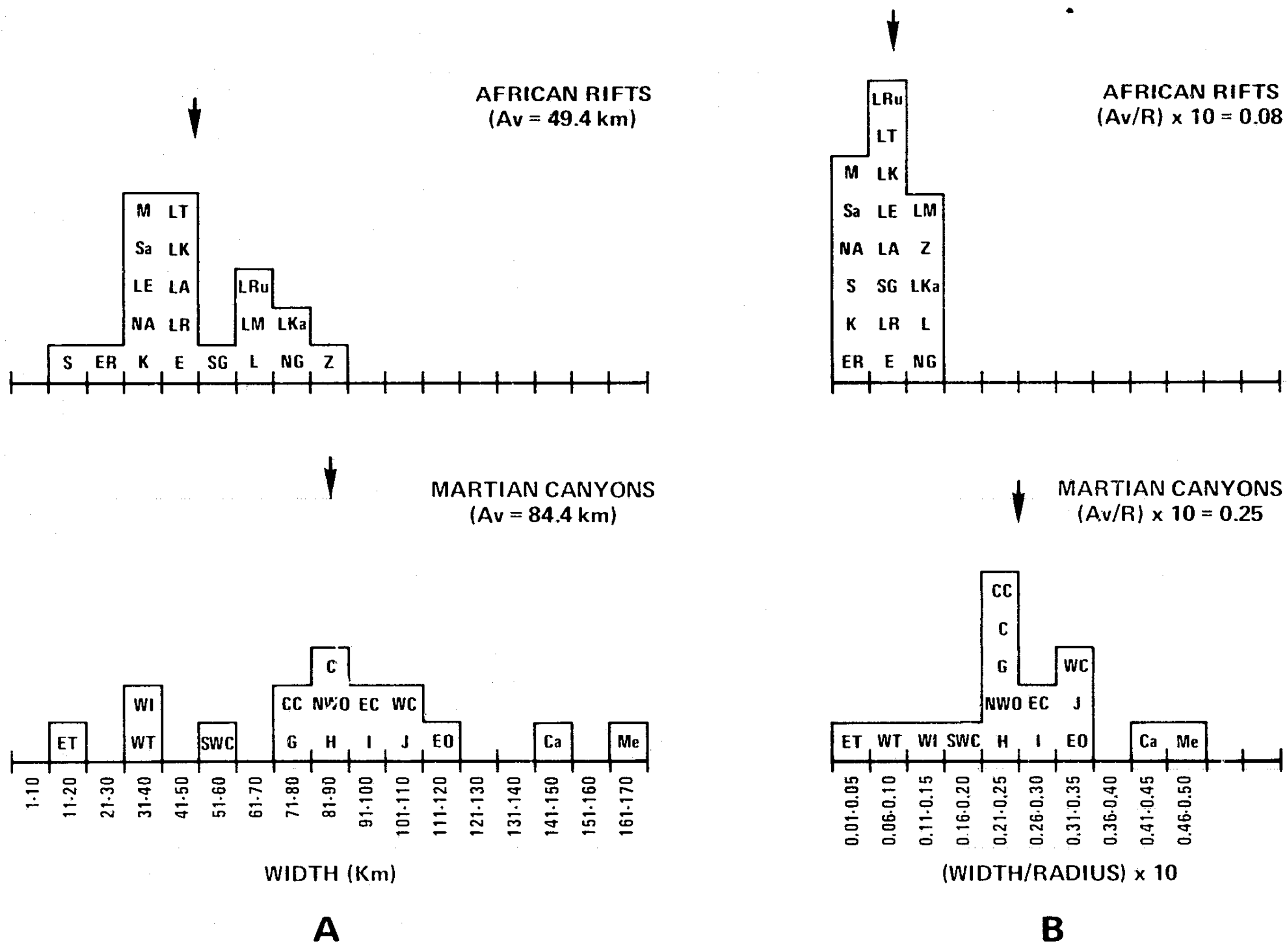

Figure 2-18. Comparison of Width and (Width/Planetary Radius) x 10 for African Rifts (Top) and Martian Canyons (Bottom). Martian Canyons are significantly wider than African rifts, in both sbsolute and relative units.

47

~~2-34~~

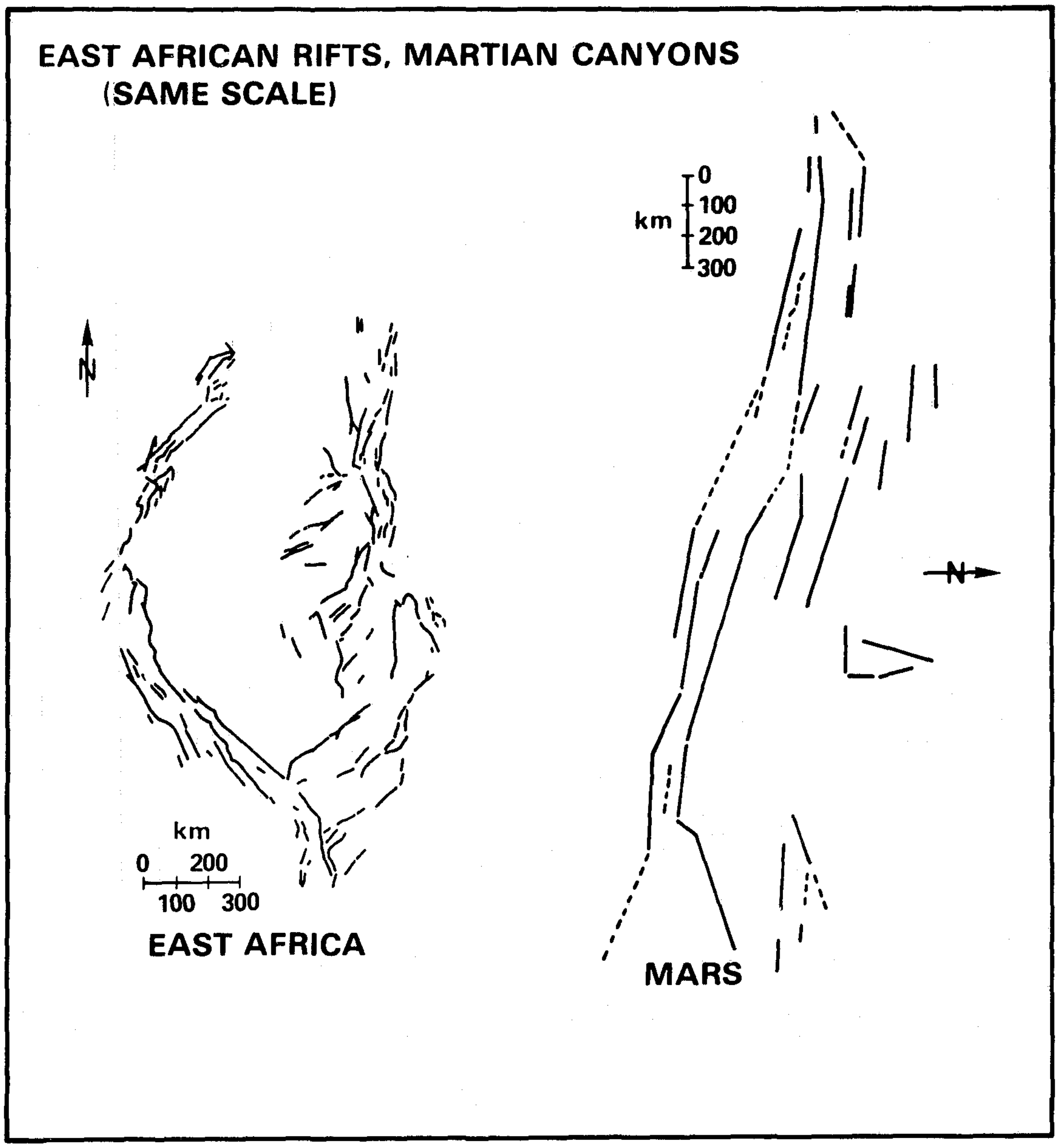

Figure 2-19. Comparison of Major Fault Patterns for East African Rifts and (Inferred) Faults Banding Martian Canyons, at the Same Absolute Scale. The Martian fault pattern is significantly simpler where the African Pattern shows great complexity.

CHAPTER 3

CRUSTAL DEFORMATION AND EARTHQUAKE MODELS

OVERVIEW

The goals of the crustal deformation and earthquake models program are to improve the current understanding of global and regional scale motions of the crust, to improve understanding of the driving mechanisms for earthquakes, and to provide measurements of crustal deformation and crustal motion of potential use in long-range earthquake forecasting.

NASA is currently developing a crustal dynamics and earthquake research program to conduct basic research and make precise geodetic measurements useful for understanding crustal movements and production of earthquakes. Several technologies (i.e., satellite Doppler, satellite laser ranging, lunar laser ranging, and Very Long Baseline Interferometry (VLBI) have been developed to the point at which geodetic measurements of geophysical significance are possible. Research programs are underway in the following areas to make measurements and help interpret the data:

- Laser ranging across the San Andreas Fault.
- Modeling earthquake mechanisms and crustal deformation in California.
- Transcontinental baseline measurements with VLBI.
- Geodetic stability of key laser and VLBI sites.
- Seismogenic models in China.
- Development of a seismic Data Collection Platform (DCP).
- Spaceborne laser ranging system concepts.
- Intercomparison of geodetic systems.

A description of these various programs is given in the following sections.

Contributors to this chapter include Richard Allenby, Steven Cohen, Werner Kahn, Ronald Kolenkiewicz, Han-Shou Liu, Paul Lowman, Chopo Ma, James Ryan, David Smith, and William Webster.

CRUSTAL MOTION MEASUREMENTS IN CALIFORNIA (SAFE)

OBJECTIVES

The objectives of the crustal motion measurements in California and the San Andreas Fault Experiment (SAFE) are to determine present-day crustal motion in the western United States, and to develop and demonstrate the method of laser ranging to satellites for high precision, long baseline geodesy.

BACKGROUND

Since 1972, an experiment has been in progress to measure the total present-day plate motion taking place across the San Andreas fault system in California. The SAFE experiment was initiated as both a test of the concept of using laser ranging to satellites for geodynamics and also to improve our large scale perspective of the strain accumulation in the western United States (and the frequency of very large earthquakes). The basis of the experiment is that the distances between points on opposite sides of the fault will change with time as the tectonic plates of North America and the Pacific slowly grind past each other. Consequently, the measurement of the change in distance between points on opposite sides of the fault can be used to infer the present-day plate velocity.

The geological history of western North America tells us that the San Andreas fault is predominantly right lateral strike-slip with an average motion of about 5 to 6 cm/year over the last several million years. Whether the motion along the fault varies over years or centuries and what the present-day motion is in California are basic questions of plate tectonics. The scientific objective of SAFE was to provide a first attempt at answering these questions.

RECENT ACCOMPLISHMENTS

The method that is being used in the experiment is laser ranging to satellites. The two primary locations for the experiment are Otay Mountain near San Diego and Quincy in Northern California. The stations are nearly 900 km apart, are on opposite sides of the main strike of the fault and the line between the stations makes an acute angle of about 25° with the general direction of the fault. In the fall of 1972, mobile laser stations were established at the San Diego and Quincy sites and each station tracked the Beacon Explorer 3 spacecraft, which is equipped with laser retroreflectors, on every pass simultaneously observable from stations (weather permitting). The laser tracking systems measure the distance from the ground to the satellite approximately once every second as the satellite passes near the station and from the analysis of the quasi-simultaneous data collected at each of the sites, the relative locations of the tracking stations can be determined.

In the fall of 1974, the mobile lasers returned to San Diego and Quincy and repeated the measurements of the relative locations of the two sites. At each location a permanent marker has been established to which all the measurements are referred. In the fall of 1976 the lasers returned a third time to San Diego and Quincy and a third laser was set up at Bear Lake in Utah. This third site is some 800 km east of Quincy across the basin and range province and was set up because the basin and range is believed to be undergoing extension at the rate of about 0.5 cm/year. From the 1976 tracking data the relative locations of all three lasers were determined. Beacon Explorer 3 was the primary spacecraft, but Lageos, launched in May 1976, was also tracked and provided an independent solution. In future occupations of these sites, Lageos is expected to be the prime spacecraft because of its greater altitude and better orbit stability.

The primary source of error in estimating the relative locations of the tracking stations is the Earth's gravity field. Model errors in the gravity field distort the orbit of the satellite and pollute the recovery of the station coordinates. The best gravity fields presently available are believed to be the GEM 9 and 10 models (Lerch, et al. 1977). The GEM 9 is based on satellite tracking data alone and is complete to degree and order 20 while GEM 10 uses satellite and surface gravity data and is complete to degree and order 22. Both of these fields have been used to analyze the laser tracking data and provide estimates of the relative station positions for each of the three observation periods (Smith, et al., 1977).

Figure 3-1 shows the San Diego-Quincy baselines and the Quincy heights obtained with GEMS 9 and 10. The baseline values suggest a decrease has occurred over the four years of the experiment of nearly 9 ± 3 cm/year (GEM 9). This value appears to be significantly larger than the geological average of 5 to 6 cm/year, but because of the large uncertaintly in the laser result it is too early to be sure that it is geophysically significant. The GEM 10 solution for the baseline also indicates a similar decrease in the baseline, but this solution is best used as an indication of the effect of changing the gravity model and suggests that the error bars shown in figure 3-1 for GEM 9 are probably optimistic.

Figure 3-1 also shows the height obtained for Quincy each year. The height at San Diego was adjusted but kept the same for the whole four-year period so that the Quincy height variations may more properly reflect a height variation between San Diego and Quincy. The indication from figure 3-1 is that the Quincy height probably did not change throughout this period. There is a slight suggestion of a height increase, but considering the magnitude of the error bars this is not significant.

SIGNIFICANCE

As a demonstration of the technique of using satellite laser ranging for measuring crustal motions the experiment has shown that the method is capable of providing consistent results to the level that the behavior of the baseline is geophysically understood. Geophysically, the experiment is tending to confirm the plate tectonics hypothesis about motion along the fault with the suggestion that the motion may be larger than the geological average. The rate of change of baseline is equivalent to a strain rate of 0.1 ± 0.03 micro-strain/year which is consistent with the results of Savage, et al. (1978) for southern California determined from local geodetic surveys of several areas. However, if the larger rate of motion across the fault system is finally demonstrated, it will imply that variations in plate motion do exist and that at the present time strain is accumulating at a higher rate.

FUTURE EMPHASIS

Further measurements from San Diego, Quincy, and Bear Lake are scheduled for early 1979 and should provide a fourth measurement between San Diego and Quincy and an equally important second set of measurements from Bear Lake to both San Diego and Quincy. Subsequently, it is hoped that the network will be expanded to include more sites in California in order to better understand the distribution of plate motion and strain accumulation across the San Andreas Fault system.

REFERENCES AND PUBLICATIONS

Lerch, F.J., S.M. Klosko, R.E. Laubscher, and C.A. Wagner, "Gravity Model Improvement Using GEOS-3 (GEM 9 & 10)," *J. Geophys. Res., 84,* 3897-3916, 1979.

Savage, J.C., W.H. Prescott, M. Lisowski, and N. King, "Strain in Southern California: Measured Uniaxial North-South Regional Contraction," *Science, 202,* November 24, 1978.

Smith, D.E., R. Kolenkiewicz, P.J. Dunn, and M.H. Torrence, "The Measurement of Fault Motion by Satellite Laser Ranging," presented at the International Symposium on Recent Crustal Movements, Standford University, Palo Alto, California, July 25-30, 1977, and published in *Tectonophysics, 52,* 59-67, 1979.

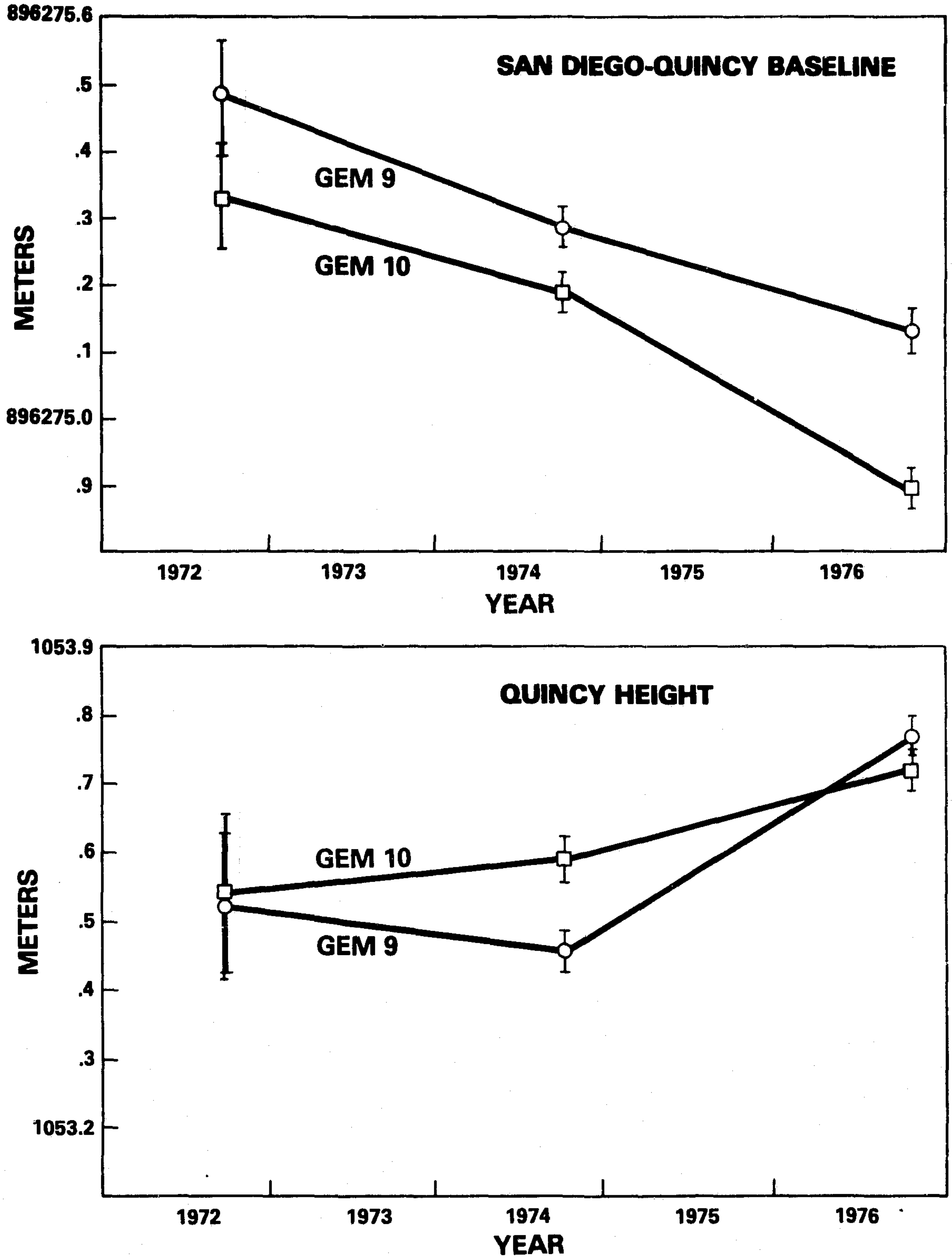

Figure 3-1. SAFE Results, Showing the San Diego-Quincy Baseline and Quincy Heights

MEASUREMENTS OF EARTH MOTIONS WITH VLBI

OBJECTIVES

The objectives of the recent Very Long Baseline Interferometer (VLBI) activities were threefold: (1) To make new observations as time and personnel permitted; (2) to analyze the data acquired prior to and during 1978, and (3) to upgrade the Mark III VLBI system software in order to improve the data analysis. These objectives are preparatory for the geophysical interpretation of the much better data expected in the next few years.

BACKGROUND

The VLBI activities are a continuation of efforts begun in 1974 under the proposed Pacific Plate Motion Experiment (PPME). The primary objective of PPME was the direct measurement of the motion of the Pacific plate relative to the North American plate in order to increase understanding of global tectonic plate motion. PPME is now a part of the Crustal Dynamics Project. Other objectives are to determine polar motion and variations in rotation rate in order to examine the relationship with major earthquakes and to study and improve models and experimental techniques through comparison with other high precision systems. To meet these objectives, new instrumentation and software (the Mark III system) with greater sensitivity, reliability and flexibility has been developed and is currently being deployed.

RECENT ACCOMPLISHMENTS

Observing sessions in January, February and May, 1978 were scheduled on the Haystack (HO)/Owens Valley (OVRO)/ Green Bank (NRAO) baselines. These were the last observations made using the 360-kHz bandwidth Mark I equipment which is now retired.

The entire set of HO/OVRO data has been processed. A graph of the baseline length as a function of time shows a weighted RMS scatter of 3.3 cm. The slope is 4mm±11mm per year. The associated polar motion and UT1 parameters are being analyzed and compared with lunar laser and satellite laser results. A preliminary comparison was presented at the International Astronomical Union (IAU) Symposium No. 82, on the rotation of the Earth. The complete data set was also used to derive values for source coordinates, the precession constant, and the Love numbers h and l. Older VLBI data now intergrated into the data base will improve these determinations.

The HO/OVRO data from January and February, 1978 were used in the validation and intercomparison of the Goddard/HO VLBI, JPL/Deep Space Network (DSN) VLBI, Lageos satellite laser and NGS Doppler systems. The comparison of baseline results was done by NGS at the request of Office of Space Tracking and Data Systems (OSTDS).

In order to present the best analysis possible, we used revised astronomical constants and new source coordinates based on earlier HO/OVRO data. The absence of phase calibration for the JPL data as well as weather and equipment problems with the OVRO laser made it impossible to achieve agreement at the desired level for all parameters. The GSFC and JPL VLBI results agreed to better than 10 cm in baseline length but disagreed by up to 90 cm in the baseline vector components. The source of the disagreement was traced to errors in the JPL data, and these errors were only uncovered when the JPL data was analyzed by the GSFC team. Of the three hardware systems participating in the intercomparison experiment, the GSFC/HO VLBI system had by far the fewest problems.

Several large software subsystems were upgraded to improve the flow of data and the precision of analysis. The data base handler was revised to increase the retrieval speed and to improve compatibility with other machines. A paper was presented at the Second Working Group on Oceanographic Data Systems on the structure and use of the data base. Material was supplied to Dr. G. Lohman at JPL, who is doing a study for NASA Headquarters on the data requirements for geodynamic research. An interactive scheduling program was written for the VLBI minicomputer. Several modules were coded for CALC, which is the program which calculates theoreticals and partial derivatives for parameter estimation. These new modules account for elastic corrections to astronomical models and provide for the impending change to epoch 2000.0 coordinates. SOLVE, which prepares and solves normal equations for parameter estimation, was modified to take advantage of arc-parameter elimination in analyzing large amounts of data. The design of a comprehensive data and software catalog/archive system was initiated and is largely implemented.

FUTURE EMPHASIS

Future work will be in two areas: New observations and refined analysis and interpretation.

The Mark III VLBI system is about to become operational. The hardware implementation schedule is appended. The first full test will be in April, 1979 on the HO/OVRO/NRAO baselines. Fort Davis, Texas should be ready by the end of 1979. Consequently, a large effort will be directed to testing the equipment and field software, making observations on a bimonthly basis, analyzing the data, and integrating the new observations into the data base. The field operating system which will automate data acquisition and equipment monitoring must be completed and debugged.

In the other direction, the exisiting data will be analyzed and interpreted. Since much of the software development has been finished, more emphasis will be placed on improving the models used and the analysis of data. Atmospheric calibration will be added to the 1969 through 1975 data. The effects of source structure and antenna flexure need to be included. A new version of

SOLVE with more flexible algorithms and interactive capabilities is being coded and should be operational by August, 1979. This version of SOLVE will also incorporate an expanded solution library.

The combination of better data, longer time base, and refined models should make it possible to examine several problems of geophysical and astronomical interest. The May American Geophysical Union (AGU) meeting and June meeting at MIT on radio interferometry techniques for geodesy will be appropriate forums for discussing the results.

A proposal was submitted under the Lageos Announcement of Opportunity (AO). If it is accepted, a considerable fraction of our activities will be devoted to analyzing and comparing VLBI and laser data at a level of detail which will validate the techniques against each other.

Over the longer term we expect to study several areas in more detail: (1) Interplate motion, (2) intraplate deformation, and (3) polar and rotation rate.

Through cooperation with several European VLBI groups we expect to make observations between the North American and Eurasian Plates. These measurements will be of use in determining whether interplate motion is continuous or episodic. A full international network of VLBI stations will contribute strongly to understanding of contemporary interplate motion on a global scale.

A network of VLBI stations is planned within the North American Plate. The probable sites are HO, NRAO, Fort Davis, Goldstone, and OVRO. The baselines between these stations will enable us to study the deformation within the North American Plate over such areas as the Basin and Range Province, where local deformation has been suggested.

The area of polar motion and rotation studies will be expanded, particularly by cooperation with the National Geodetic Survey (NGS) Polaris project. The high spatial and temporal resolution expected should enable us to examine the relationship between these parameters and such driving effects as major earthquakes, atmospheric distribution, and ocean circulation.

REFERENCES AND PUBLICATIONS

C. Ma, "Very Long Baseline Interferometry Applied to Polar Motion, Relativity, and Geodesy," NASA TM-79582, 1978.

Wittels, J.J., I.I. Shapiro, H.F. Hinteregger, C.A. Knight, A.E.E. Rogers, A.R. Whitney, T.A. Clark, C. Ma, L.K. Hutton, D.S. Robertson, B.O. Ronnang, O.E.H. Rydbeck, A.E. Niell, G.M. Resch, "A High Declination Search at 8 GHz for Compact Radio Sources," *Astron. J. 83*, 6, p.560, 1978.

REFERENCES AND PUBLICATIONS (continued)

J.W. Ryan, T.A. Clark, R. Coates, C. Ma, D.S. Robertson, B.E. Corey, C.C. Counselman, I.I. Shapiro, J.J. Wittels, H.F. Hinteregger, C.A. Knight, A.E.E. Rogers, A.R. Whitney, J.M. Moran. "Precision Surveying Using Radiointerferometry," *J. of the Surveying and Mapping Div. Amer. Soc. Civil Engineers, 104,* No. SU1, 25, 1978.

Ryan, J.W., and C. Ma, "A Small Data Base Handler for Scientific Applications," *Transactions of the Second Working Group on Oceanographic Data Systems,* April 1979.

Robertson, D.S., W.E. Carter, B.E. Corey, W.D. Cotton, C.C. Counselman, I.I. Shapiro, J.J. Wittels, H.F. Hinteregger, C.A. Knight, A.E.E. Rogers, A.R. Whitney, J.W. Ryan, T.A. Clark, R.J. Coates, C. Ma, and J.M. Moran. "Recent Results of Radio Interferometric Determinations of a Transcontinental Baseline, Polar Motion, and Earth Rotation," *Proceedings of the IAU Symposium,* No. 82, in press.

N.R. Vandenberg, T.A. Clark, L.N. Foster, C. Ma, J.W. Ryan, H.F. Hinteregger, C.A. Knight, E.F. Nesman, A.E.E. Rogers, A.R. Whitney, B. Rayhrer, R. Lacasse, and B.E. Corey, "The Mark III VLBI System," *B.A.A.S., 10,* p. 640 (abstract), 1978.

INTRAPLATE DEFORMATION AND VLBI RESULTS

OBJECTIVE

The purpose of this project is to interpret the intraplate deformation and VLBI data obtained by GSFC.

BACKGROUND

Very Long Baseline Interferometry (VLBI) experiments over the last 2 years between Owens Valley, CA and Haystack, and MA Radio Observatories suggest an upper limit of east-west crustal deformation between the two sites of well under 3 cm/year over a distance of almost 4,000 km. In view of the fact that the baseline between the two sites traverses most of the major geological provinces of the United States (figure 3-2), this relatively low ceiling on the rate of crustal deformation has direct relevance to intraplate crustal Tectonics. The most active region traversed by this baseline is the Basin and Range Province which has been estimated by various researchers to be expanding in an east-west direction at rates of .3 to 1.5 cm/year. The Colorado Plateau and Rocky Mountain system also appear to be expanding, but at somewhat lower rate. East of the Rocky Mountains, while the stress field is complex and not well understood, the predominant stress appears to be compressional, nearly horizontal, and east to northeast trending.

RECENT ACCOMPLISHMENTS

The experimenters have developed four possible explanations for the relatively low rate of change of distance between the two VLBI observatories are:

- The North American Plate, as required by continental drift theory, is perfectly rigid.
- The North American Plate is sufficently elastic to absorb intraplate regional tectonic motions but, overall, behaves as a nearly rigid plate.
- Intraplate crustal motions are episodic and this is a quiet period.
- Motions in the various geologic provinces counteract one another.

While the available data are not sufficient to resolve the above explanations, it is suggested that the last one is the most plausible explanation and that opposing motions between various geological provinces do exceed the 3-cm/year limit.

FUTURE EMPHASIS

In order to advance our understanding of an area as complex as the contiguous United States, continued observations over a significant time period (5 to 10 years) are required at a variety of sites. Continued analysis is planned utilizing NASA and ground-based geodynamic data as it becomes available.

REFERENCES AND PUBLICATIONS

Allenby, R.J., "Implications of Very Long Baseline Interferometry Measurements on North American Intra-Plate Crustal Deformation," *Tectonics*, in press 1979.

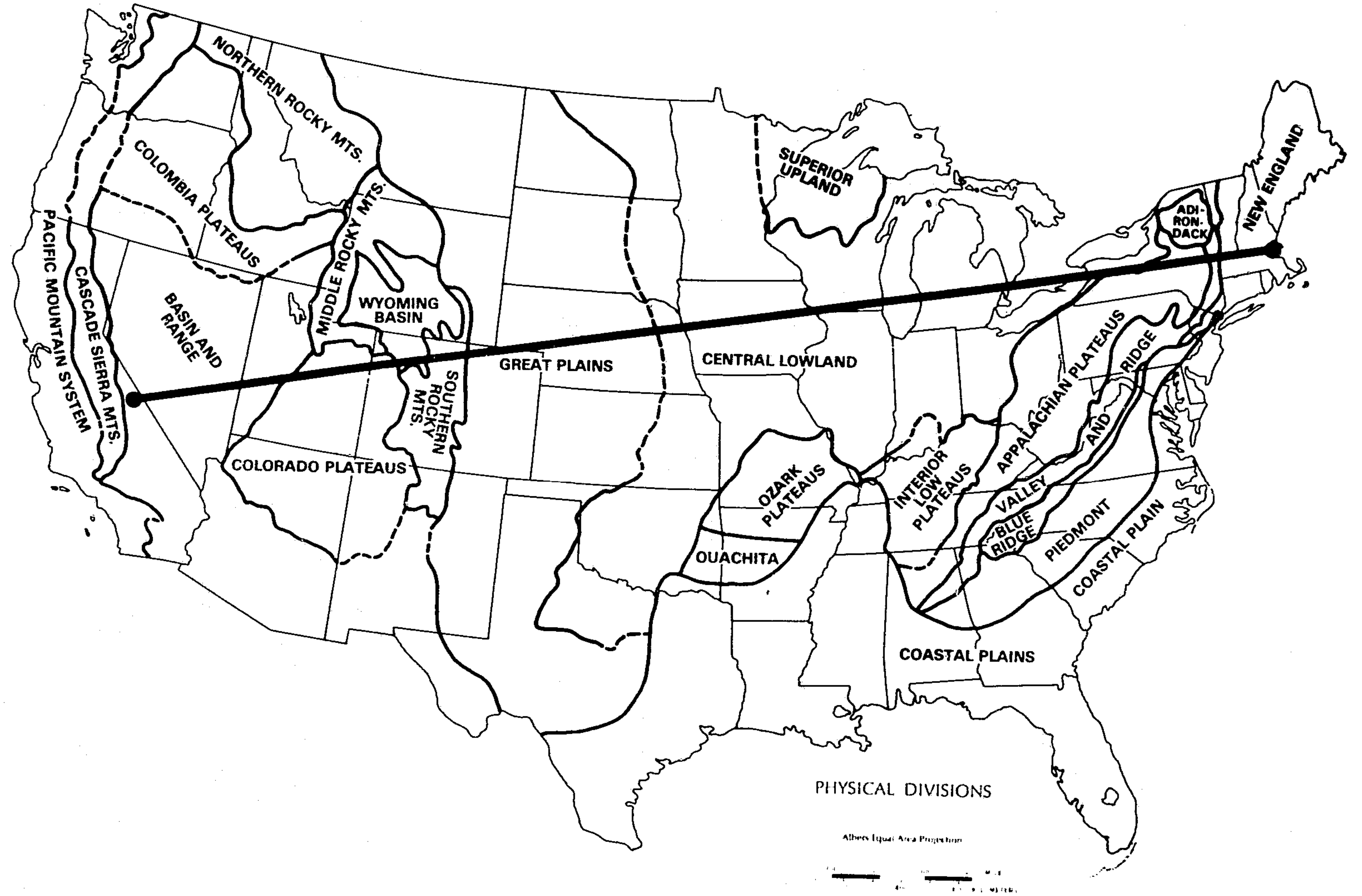

3-12
60

Figure 3-2. VLBI Experiments Between Owens Valley and Haystack

PLATE BOUNDARY DEFORMATION IN CALIFORNIA

OBJECTIVE AND BACKGROUND

NASA's geodynamic programs at Goddard and Jet Propulsion Laboratory (JPL) have now conducted geodynamic measurements at a few California sites over a sufficient time period to provide significant data related to crustal motion within the "slushy" border between the North American and Pacific Plates. Of particular interest is comparing these results with similar results obtained by conventional land-based surveys.

RECENT ACCOMPLISHMENTS

We have found that the relative motion between the North American and Pacific Plates, based on sea-floor magnetic striping patterns, is about 6 cm/year averaged over the last 3 to 4 million years. Results of ground line resurveying across this plate boundary by the National Geodetic Survey (NGS) in the Salton Sea area suggests a present day motion of 8 to 10 cm/year. Local ground surveys directly across the San Andreas fault show it has a maximum motion of 3.5 cm/year.

The SAFE program has measured a baseline shortening between Otay Mountain (San Diego) and Quincy (Northern California) of about 9 cm/year. This baseline crosses most of the major northwest trending California coastal faults and the baseline measurements are in general agreement with the Salton Sea measurements. The baseline measurements suggest that if 10 cm/year is the total interplate motion, then this motion is all being taken up along the coastal fault system, with a third along the San Andreas and the rest along parallel faults.

Results from the JPL ARIES program suggest an east-west extension between Goldstone and Pasadena of 5 cm/year, corresponding to a motion along the coastal fault system in this area of 5.6 cm/year. Because this baseline begins to the east of some of the major northwest trending coastal faults, this measurement may reflect only a portion of the total motion across the system. Conversely, it may indicate that some of the interplate motion is not being absorbed into the coastal fault system, but into the basin and range province to the east of California.

The results of these experiments suggest that:

- Relative motion today between the North American and Pacific Plates is about double the 3 million year average of 6 cm/year.

- Three cm of this motion is taken up by the San Andreas fault, and the rest is either absorbed by other California coastal faults parallel to the San Andreas or into the Basin and Range Province.

FUTURE EMPHASIS

Continued work on the plate boundary deformation problem in California is planned using all available pertinent data.

REFERENCES AND PUBLICATIONS

Allenby, R.J., "SAFE and ARIES Results Related to California Geodynamics," in progress

INTERCOMPARISON OF TRACKING SYSTEMS FOR PRECISE GEODETIC MEASUREMENTS

OBJECTIVES

The principal objective in this investigation is to perform a series of experiments designed to evaluate various systems' capabilities in making measurements of geophysical significance. Three such systems currently in operation are Satellite Laser ranging (SLR), DOP (Satellite Doppler), and the VLBI system. These systems are able to make valuable scientific contributions through precise measurements of length used in the determination of items such as crustal motion, Earth rotation, and polar motion. The first experiment performed was to compare the distance measurements between systems collocated at several locations in the United States.

BACKGROUND

The scientific community has long realized that precise measurements between points located great distances apart on the surface of the Earth could yield useful information on the physical processes occurring in the Earth's interior and observed on the Earth's surface. Direct measurement of tectonic plate motions could possibly explain Earth rotation, polar motion, and earthquake locations and frequencies.

Until the last decade the only practical method of obtaining these measurements was by traditional ground survey, which was limited by accuracy and frequency. During the 1970's, several new techniques emerged which promised to give intersite distances within centimeters on a routine basis. The systems which could supply this information include:

- SLR
- DOP
- VLBI
- Lunar Laser Ranging (LURE)

Since NASA has funded the development of several of these systems and has need of the data provided by them in order to carry out its mission, the question arises as to how good they are in performing their common objectives, and if in fact all these different types of systems are necessary. In an effort to evaluate the accuracy of the systems, it has been decided that a series of intercomparison experiments will be performed using SLR, DOP, and VLBI.

During the period January to March 1978 each of the above systems was operated from Owens Valley, CA, Goldstone, CA, and Haystack Observatory, MA. In addition, SLR was located at Greenbelt, MD during the experiment, and DOP was located at Greenbelt at a later time period. The purpose of this experiment was to compare the distance between each site as obtained by each type of system. Two teams (GSFC and JPL) independently used different data and techniques to reduce the VLBI data at Haystack and Owens Valley.

RECENT ACCOMPLISHMENTS

From this first experiment a comparison of the same distance measured by each system can be made. The SLR data collection and analysis was performed entirely by GSFC and the results were as follows:

- Satellite Tracked: Lageos.
- Tracking Dates: March 18, 1978 - March 31, 1978.
- Tracking Sites: Haystack, MA; Goldstone, CA; Owens Valley, CA; Greenbelt, MD.
- Number of Data Points: 16,000.
- Solutions Contained: New speed of light (299792.458 km/sec) New GM (398600.5 km)

The results for the chord difference obtained (meters) are given in table 3-1. The differences between the laser distance and distances obtained by other systems (centimeters) are given in table 3-2.

In general, SLR agrees well with VLBI, the largest difference being 27 cm between the Owens Valley-Goldstone (shortest) baseline.

This 27 cm may be due in part to the fact that the Owens Valley laser was somewhat erratic during the course of the experiment, measuring rms ranges of ±40 cm rather than the normal ±10 cm. SLR did not compare as well with DOP, the largest difference of 94 cm between the Greenbelt-Goldstone baseline. This may be due to the fact that the Doppler data at Greenbelt was not obtained during the same time period as the other Doppler data was taken.

Techniques in reduction of data have apparently caused the 5-cm difference in the Haystack-Owens Valley distance as determined by the two VLBI teams.

SIGNIFICANCE

This was the first direct comparison of the ability of precise measuring systems to determine intersite distances. As a consequence of this experiment, the VLBI teams from GSFC and JPL have agreed on data reduction techniques still to be implemented which will bring their results into better agreement. It has also been noted that SLR indicated station heights approximately 5 m higher than DOP heights. This apparent shift of the center of mass of one of the coordinate systems along the Z-axis will be investigated.

FUTURE EMPHASIS

These results are the first of a series of tracking system intercomparison experiments which are planned to be carried out under the direction of NASA Headquarters during the next few years.

Table 3-1. Baseline Chord Differences

Station From-To	Chord Differences (m)			
	Laser	Doppler	JPL/VLBI	GSFC/VLBI
Haystack-Owens Valley	3929896.72 ± 0.09	.69	.83	.78
Haystack-Goldstone	3899845.27 ± 0.07	4.68	.16	
Owens Valley-Goldstone	237190.94 ± 0.08	1.43	1.21	
Greenbelt-Haystack	602031.52 ± 0.05	2.36		
Greenbelt-Goldstone	3503665.33 ± 0.07	4.39		
Greenbelt-Owens Valley	3562310.78 ± 0.08	.50		

Table 3-2. Baseline System Differences

Station From-To	System Differences (cm)		
	Laser Minus Doppler	Laser Minus JPL/VLBI	Laser Minus GSFC/VLBI
Haystack-Owens Valley	3	-11	-6
Haystack-Goldstone	59	11	
Owens Valley-Goldstone	-49	-27	
Greenbelt-Haystack	-84		
Greenbelt-Goldstone	94		
Greenbelt-Owens Valley	28		

GSFC SITE STABILITY

OBJECTIVE

The objective of the GSFC site stability project is to monitor the site's geodetic stability.

BACKGROUND

The STALAS site near GSFC is the main reference station for the laser ranging programs. Accordingly, it is important to know the level of geodetic stability of STALAS. It is also important to detect any regional earthquakes which may influence measurements from STALAS.

RECENT ACCOMPLISHMENT

A field reconnaissance showed no convincing evidence of surface expressions of faulting and determined that the area is all tertiary and quaternary sediments of a poor grade of consolidation. A telemetered seismic station was established on the nearest bed rock exposure (Ellicott City, MD), and continues to monitor for possible local ground displacements.

FUTURE PLANS

A "hammer" refraction survey is planned for late spring to tie the STALAS site to the Maryland well log network. This will allow an accurate estimation of the elastic properties of the sediments at STALAS. A three day monitoring period will take place during the summer to measure the acoustic noise at the site. Two-Hz and 7-Hz sensors will be employed. This will allow a complete determination of the acoustic "transfer function" at STALAS. This effort is necessary since the STALAS pier does not go to bedrock. At the conclusion of the work, it will be possible to estimate the STALAS response to local seismic events seen on the Ellicott City system accurately.

GEODETIC STABILITY OF THE GREEN BANK, WEST VIRGINIA VLBI SITE

OBJECTIVE

A paper is being submitted to *Tectonophysics*, describing the results of a combined geological and geophysical study of the National Radio Astronomy Observatory at Green Bank. The study was undertaken in support of the VLBI program to assure the stability of the Green Bank site at the 2 to 5 cm level. It is essential to be sure that the sites on the east coast are really stable, locally, in order to use the precise continental-scale distance measurements from VLBI.

BACKGROUND

Because numerous lineaments, including the track of the so-called 38th parallel lineament, cross the region around Green Bank, a field survey was undertaken to measure any offset on the lineaments. Such offsets would indicate both the potential for movement and the magnitude over geologic time. Surprisingly, no offsets were found although the lineaments are clearly old, stratigraphically.

In addition to the field survey, a short-period high-gain seismometer has been in operation at NRAO for over two years. This system is intended to check for micro-earthquakes in the region around the observatory. Although no activity has been detected within 20 km of Green Bank, the previously known centers of activity near Elkins, W. VA and West-Central, VA, have been responsible for about 20 earthquakes with a maximum magnitude of 3 during the period of operation.

RECENT ACCOMPLISHMENTS

A major water impoundment project is being constructed by VEPCO about 35 km east of the observatory. Because of the possibility of impoundment-induced strain and loading-triggered microseismicity, monitoring at NRAO will be continued to assure that the current stability does not deteriorate as the resevoir is filled to capacity.

FUTURE EMPHASIS

Because one of the largest water impoundment projects east of the Mississippi is within 30 km of NRAO, seismic monitoring must continue for the assessment of impoundment-induced seismicity. A measurement of the acoustic noise spectrum in the vicinity of the 140-foot antenna is planned for late spring.

REFERENCES AND PUBLICATIONS

Webster, W.J., R.J. Allenby, P.D. Lowman, H.A. Tiedemann and L.K. Hutton, "Tectonic Motion Site Survey of the National Radio Astronomy Observatory, Green Bank, West Virginia," submitted to *Economic Geology*, published as NASA TM 79691, June 1979.

SPACEBORNE LASER RANGING SYSTEM

OBJECTIVES

In the spaceborne laser ranging system project, space methods will be used to detect and monitor very small crustal movements which are on the order of 0.3 to 0.5 cm/year in central California. A pulsed laser ranging system on a dedicated commandable spacecraft (free-flyer) can be used to provide continuous monitoring of crustal deformation in California as well as many other areas of the world and has the potential to provide an almost real-time system for detecting precursory ground motions before large earthquakes.

BACKGROUND

The concept of the spaceborne laser ranging system was developed as a technique for monitoring from space, frequently and over long time periods, the relative positions of a large number of geodetic reference points. The spaceborne laser ranging system consists of an orbiting spacecraft carrying a pulsed laser range measuring system which measures the range between the spacecraft and laser retroreflector arrays on the ground. By distributing these retroreflectors over regions of seismic activity and crustal deformations associated with tectonic plate boundary motion, earthquake zones, and ground motion due to fluid withdrawal, mountain building, or volcanic activity, this spaceborne technique conceptually would permit the monitoring of whole regions with a high density of points in a relatively short period of time, creating the impression of obtaining a geodetic "snapshot" of the area. Such measurement sets can be compared with other measurement sets obtained at appropriate intervals and the observed displacements used to develop regional maps of strain and strain-rate.

RECENT ACCOMPLISHMENTS

In order to assess the spaceborne laser ranging system's capabilities in the presence of known error sources, establish mission parameters, develop parameter estimation strategies and aid in system design specifications, it is standard procedure to perform computer simulations using covariance error analysis techniques. Many simulations have already been performed to study various aspects of the spaceborne laser system concept.

One such simulation was a survey of the State of California by the spaceborne laser ranging system. In the simulation, approximately 150 laser retroreflectors are distributed over California at a separation of about 50 km (see figure 3-3). We derived from the simulation estimates of the accuracy and precision with which the relative positions of the reflector arrays can be obtained. The error sources which were used to obtain these estimates of precision and accuracy are laser system noise and bias, perturbations of the spacecraft motion, and errors in the refraction calculations.

The orbit of the satellite is assumed to be circular at 1000-km altitude and 50-degree inclination to the equator. A medium inclination orbit was chosen because it provides ground tracks across California in almost orthogonal directions (southwest to northeast and northwest to southeast), and thus provides a strong geometric distribution of range measurements (see figure 3-4).

The simulation results in table 3-3 assume a six-day observation period with 50-percent cloud cover which effectively reduces the number of successfully observed tracks over the area from 18 to 9. The data on these tracks is simulated at a repetition rate of 10 pulses per second with a noise of $\pm$ 2 cm and a bias of .3 cm. The effect of the errors in the gravity field on the motion of the satellite were accounted for in this simulation by adopting the GEM 10 covariance model of the gravity field derived from satellite tracking and surface gravity data. The effects of solar radiation pressure and air drag on the satellite were assumed to be in error by a constant percentage in the estimation of their effects on the solution. The effect of atmospheric refraction was estimated through a two parameter (pressure and temperature) model. In this model, the temperature and pressure are assumed known at a limited number of locations in the region and are used to develop an atmospheric model of the whole region from which the temperature and pressure at each of the retroreflectors can be estimated. In table 3-3, both the accuracy and precision with which baselines between retroreflectors are obtainable is given over various distances and summarizes the error models and assumptions made in the simulation. The accuracy is the estimated total error in the baseline; the precision is the ability to repeat the measurement. The noise in the precision is approximately 1.44 times that of the accuracy while the systematic errors are generally smaller in the precision than the accuracy because of the correlations.

Table 3-3 shows that the error sources tend to increase as the baseline distance increases. The gravity model error dominates the accuracy while the solar radiation pressure and drag effects on the orbit are negligible in both accuracy and precision and over all distances. The noise level in precision is larger than that in the accuracy but the gravity contribution is significantly reduced in precision because the gravity error is largely systematic in nature, and is repeated from one simulation (or observation) to the next. The atmospheric refraction is larger in the precision than the accuracy, showing much of this error has the property of noise. The measurement bias contribution in precision also behaves much like noise since the bias on one track is independent of that from any other track.

SIGNIFICANCE

Based on this simulation study, it can be concluded that a survey of the complete state of California can be accomplished with a precision of ± 1 cm and an accuracy of ±5cm in about six days. By making allowance for an increase in our knowledge of the earth's gravity field over the next several years, we can safely establish as our objective an overall accuracy in the mid-1980's of ± 1 cm.

In the area of error due to atmospheric refraction, one possibility actively considered for error correction is use of a two-color laser system which operates in two colors separated enough in frequency that the total atmospheric refraction can be derived from the delay between the two pulses. This technique is still under development, but will become available within the next few years.

The spaceborne laser ranging system simulation demonstrates that the fundamental application of the system should be for the monitoring of crustal motions in seismic zones. This system has the capability of providing high accuracy geodetic measurements in a very short period of time, i.e., a "geodetic snapshot," and could have significant impact on our ability to study pre- and post-seismic motions.

FUTURE EMPHASIS

Future studies are to be expanded to determine the requirements for a global crustal monitoring system using a free-flyer. Such studies will include optimization of orbit altitude and inclination. Tracking, geometry, data precision, sampling rates, and data processing techniques will also be considered in arriving at a feasible mission for a free-flyer to monitor crustal movements on a global scale.

REFERENCES AND PUBLICATIONS

Vonbun, F.O., W.D. Kahn, P.O. Argentiero, D.W. Koch, "Spacebourne Earth Applications Ranging System (SPEAR)," *Journal of Spacecraft and Rockets, 14,* 8, 492-495, August 1977.

Kahn, W.D., and F.O. Vonbun, "Detectability of Land Subsidence from Space," International Association of Hydrological Sciences publication No. 121 and *Proceedings of the Anaheim Symposium,* 246-256, December 1976.

Gibbs, B.P. and E.M. Haley, "Error Analysis of Spacelab Geodynamics Laser Ranging System," Business and Technological Systems Report, BTS-TR-78-52, February 1976.

REFERENCES AND PUBLICATIONS (continued)

Mueller, I.I., B.H.W. Van Gelder, and M. Kumar, "Error Analysis for the Proposed Closed Grid Geodynamic Satellite Measurement System (GLOGEOS)," Report No. 230 of the Department of Geodetic Science, Ohio State University, September 1975.

Tapley, B., University of Texas, Austin, and D.E. Smith, NASA, workshop codirectors, "The Report from the Workshop on the Spaceborne Geodynamics Ranging System," Department of Aerospace Engineering, University of Texas, Austin, March 1979.

Smithsonian Astrophysical Observatory Staff, "Study of a Close Grid Geodynamic Measurement System," SAO Reports in *Geoastronomy*, No. 5, 1977.

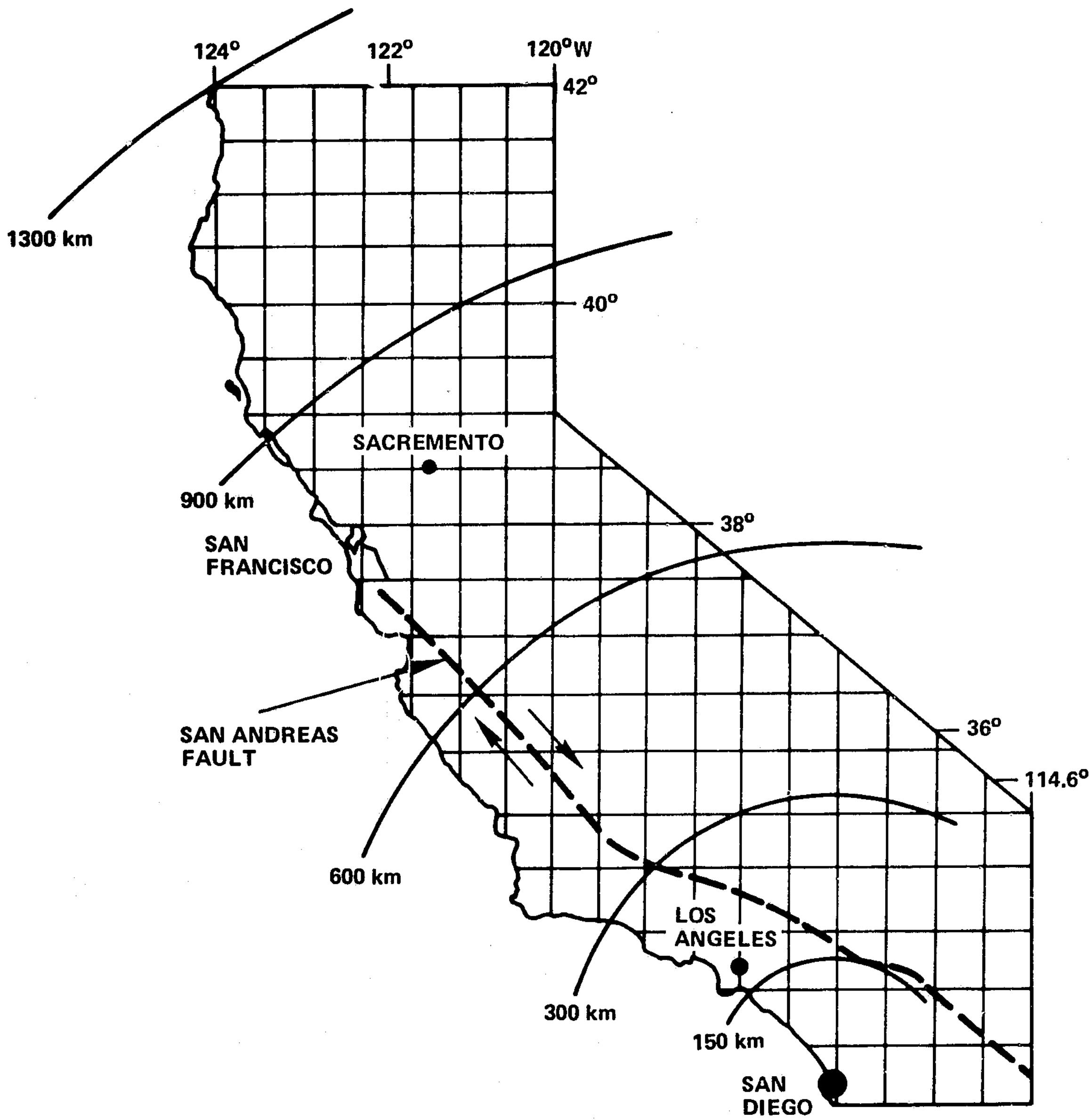

Figure 3-3. Distribution of Ground Targets for California Simulation (Spacing Approximately 50 Km)

Table 3-3. California Simulation: Baselines

	Accuracy							Precision						
Distance	Noise	Gravity	Atm. Refr	Meas Bias	Sol. Rad Press	Drag	RSS*	Noise	Gravity	Atm. Refr	Meas Bias	Sol.Rad Press	Drag	RSS
(km)	(cm)	(cm)	(cm)	(cm)	(cm)	(cm)	(cm)	(cm)	(cm)	(cm)	(cm)	(cm)	(cm)	(cm)
150	.18	.54	.10	.01	.00	.00	.58	.25	.10	.14	.01	.00	.00	.30
300	.20	1.06	.12	.01	.00	.00	1.09	.28	.19	.17	.02	.00	.00	.38
600	.24	1.65	.16	.02	.01	.00	1.68	.34	.24	.23	.04	.01	.00	.48
900	.27	2.21	.18	.03	.01	.00	2.23	.38	.33	.26	.05	.01	.00	.57
1300	.31	3.09	.25	.05	.02	.00	3.11	.44	.49	.35	.07	.03	.00	.75

*Root sum square.

Assumptions:

- Orbit

  Mean altitude: 1000 km
  Inclination: 50°

- Observation period: 6 days
- Cloud cover: 50%
- No. retroreflectors: 150 @ 50 km spacing
- Measurement noise: ± 2 cm single pulse, 10 pulses/sec
- Measurement bias: 0.3 cm
- Gravity uncertainty: GEM 10 covariances (ℓ, m=22)
- Atmospheric error model: 2 parameters

  Pressure noise: ± 1.0 mbar
  Pressure bias: 0.33 mbar
  Temp. noise ± 1.4 C

- Radiation pressure: 33% error
- Atmospheric drag: 22% error

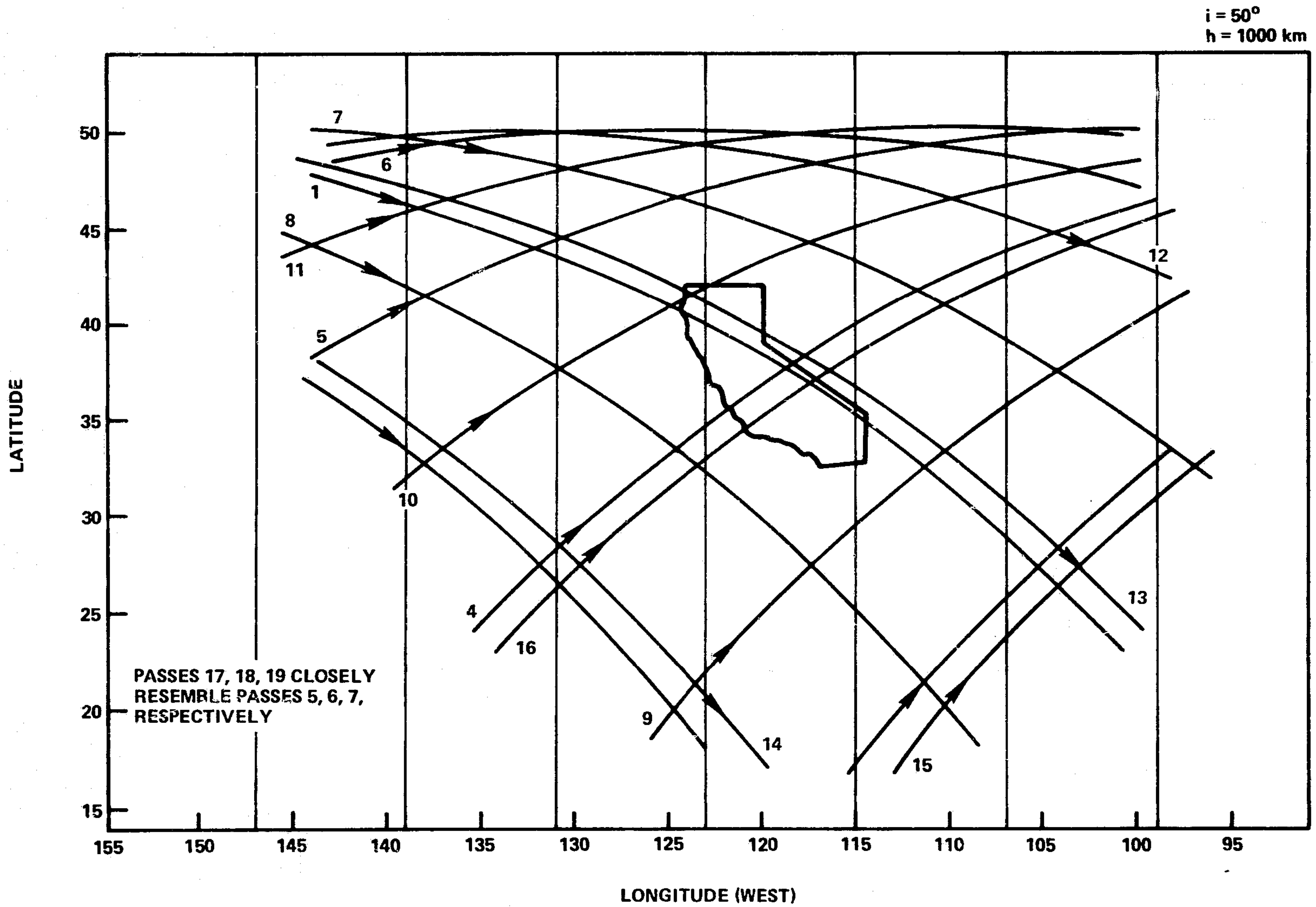

Figure 3-4. Data Collection Passes for the California Scenario

77

3-29

EARTHQUAKE MECHANISMS AND CRUSTAL DEFORMATION MODELING

OBJECTIVE

Research on earthquake mechanisms and crustal deformation modeling has as its central objective the elucidation of the physical processes associated with earthquakes, other fault motions, and regional deformations. During 1978, the research activities focused on three specific elements that relate to this objective: first was the study of the time-dependent deformations occurring coseismic to and following earthquakes; second was the simulation of earthquake dynamics; and third was the study of space techniques for measuring strain accumulation near active faults. Each of these topics is discussed separately in this section.

BACKGROUND OF COSEISMIC AND POSTSEISMIC SURFACE DEFORMATIONS

If the Earth were perfectly elastic then there would be no significant postseismic motions following an earthquake rupture. There is however considerable evidence from field studies, geodetic measurements, and laboratory rock mechanics experiments that there are anelastic forces within the Earth that may produce time dependent ground deformations. In order to model these forces and the attendant deformations, we have developed a model in which the Earth's lithosphere which extends from the surface to a depth of 50 to 125 km is represented by a standard viscoelastic solid. Such a substance response to an applied stress with an instantaneous elastic deformation. On a longer time scale of hours to months a transient viscoelastic response produces additional displacements. Below the lithosphere lies the asthenosphere. The asthenosphere also responds to a stress with an instantaneous elastic behavior; however, its viscoelastic flow continues as long as a stress exists. More to the point, the asthenosphere flows to relax an applied stress with a response time on the order of several years. The rheological model of the asthenosphere adopted in this work has these properties and is known as a Maxwell substance. Both this model and that of the lithosphere have been used extensively in the geophysical literature to explain rock mechanic, tectonic, and geological phenomena.

RECENT ACCOMPLISHMENTS IN COSEISMIC AND POSTSEISMIC SURFACE DEFORMATION MODELING

In the theoretical model an earthquake occurs at some depth in the lithospere and the fault along which the earthquake occurs is modeled as a dislocation in this layer. The displacements that occur at the time of the earthquake are a maximum at the fault and fall smoothly toward zero as the distance from the fault increases. The spatial scale for significant displacements increases with the depth of the earthquake source. For a lithospheric thickness of 100 km and a source depth of 25 km the coseismic displacement at 50 km from the fault is about 1/3 of that at the fault. At 150 km the displacement is reduced by an additional factor of two.

The postseismic displacements that occur in the model are due to viscoelastic flows. On the time scale of the lithospheric adjustment, the movements are in the opposite direction to those that occurred with the earthquake. While these displacements due to lithospheric viscoelasticity are less than the coseismic elastic displacements, they can be as much as several centimeters for major events. Such motions occurring in nature would significantly affect the interpretation of postseismic geodetic surveys.

On the time scale of the asthenospheric adjustment the ground motions are in the same direction as the coseismic displacements. The viscoelastic displacements can be a significant fraction of a meter and may be comparable to the elastic displacements at distances equal to a few times the lithospheric thickness from the fault.

SIGNIFICANCE OF COSEISMIC AND POSTSEISMIC SURFACE DEFORMATION MODELING

These results indicate that for all but very shallow earthquake significant time-dependent postseismic deformations can occur. Measurements of these deformations can be used in studies of Earth rheology and earthquake mechanisms.

FUTURE EMPHASIS IN COSEISMIC AND POSTSEISMIC SURFACE DEFORMATION MODELING

Several direct extensions of this work will be pursued in the next year. The surface strains and stresses associated with the postseismic ground motions will be calculated. The effects of variations in source depth, fault length, and material parameters will be studied. Alternative models of lithospheric and/or asthenospheric rheology will be formulated and their implications deduced.

REFERENCES AND PUBLICATIONS FOR COSEISMIC AND POSTSEISMIC SURFACE DEFORMATION MODELING

Cohen, S., "Postseismic Surface Deformations Due to Lithospheric and Asthenospheric Viscoelasticity," *Geophysical Research Letters, 6,* 129-131, 1979.

BACKGROUND SIMULATION OF EARTHQUAKE OCCURRENCE MODELING

Work on this topic has been divided into two subelements. A review of numerical and laboratory earthquake simulation studies has been prepared under an invitation from *Reviews of Geophysics and Space Physics*. This review focused on studying fault dynamics by representing earthquakes by blocks sliding under the influence of elastic springs. The role of viscoelasticity in producing transient and steady state creeps and in generating aftershocks was also considered.

Also completed in 1978 was research into the viscoelastic stiffness model of seismicity. This work, begun in 1977, offers a possible explanation for a number of dynamic features associated with faults. The model assumes that unstable sliding events occur along a fault whenever friction decreases with displacement less rapidly than the driving stress. The driving stress is assumed to be elastic on a short time scale or viscoelastic on a longer scale in accordance with the rheological model of the lithosphere discussed in connection with coseismic and postseismic surface deformation modeling.

RECENT ACCOMPLISHMENTS IN SIMULATION OF EARTHQUAKE OCCURRENCE MODELING

The review of sliding block models of earthquakes emphasezed the fact that such models are useful for representing large scale, general features of earthquakes. Thus they can be used to study correlations among seismic source parameters such as fault lenth and earthquake magnitude. They can also be features of rupture propagation and termination. They are less useful for studying effects of local geological conditions on earthquake properties and for studying the generation of high frequency seismic waves.

Calculations based on the viscoelastic stiffness theory of fault motion have revealed that viscoelastic forces and friction may play a significant role in producing postseismic creep and aftershocks. By contrast the interplay of elastic forces and friction can explain steady state creep, preseismic creep, main shocks, and creep episodes and slow earthquakes. The model also suggests that the observed occurrence of different magnitude shocks along a common fault can be explained by variations in the spatial scale of friction changes on the fault.

FUTURE EMPHASIS IN SIMULATION OF EARTHQUAKE OCCURRENCE MODELING

Since all currently planned work on this element is complete, there will be no major thrusts in this area in the immediate future.

REFERENCES AND PUBLICATIONS FOR SIMULATION OF EARTHQUAKE MODELING

Cohen, S., "The Viscoelastic Stiffness Model of Seismicity," *J. of Geophys. Res., 83,* 5425-5432, 1978.

Cohen, S., "Numerical and Laboratory Simulation of Fault Motion and Earthquake Occurrence," *Rev. Geophys. Space Phys., 17,* 61-72, 1979.

BACKGROUND OF SPACE SURVEYS OF CRUSTAL STRAINING

This study examined the precision with which crustal strain rates could be measured by space surveys. The study assumed that the survey sites are separated by 25 to 50 km and can be located relative to one another to a precision of one cm. The results can be scaled to other choices of site separations, and measured precision. The thrust of the study was to investigate how the selection of site geometry, number of sites, and resurvey period effect the precision in deducing strain rates.

RECENT ACCOMPLISHMENTS IN SPACE SURVEYS OF CRUSTAL STRAINING

The analysis indicates that measurement strain rate precisions of a few parts in 10^8 per year can be achieved within a few years with resurvey period of six months to a year. When compared to the expected strain rates along the San Andreas Fault of several parts in 10^7 per year, very favorable signal-to-noise ratios are found. A further order of magnitude improvement in the precision can be achieved by extending the survey over a decade or two.

SIGNIFICANCE OF SPACE SURVEYS OF CRUSTAL STRAINING

The implications of this analysis are that geophysically significant strain rates can be measured in a very timely manner using space techniques, that spatial variations in the straining on a scale of 50 km or longer can be determined, and that temporal variations on a scale of several years or longer can also be determined. Thus space surveys are potentially useful for studying strain variations along a fault, the relaxation of strain away from a plate boundary, and, possible, precursory and postseismic strain changes.

FUTURE EMPHASIS IN SPACE SURVEYS OF CRUSTAL STRAINING

Future thrusts will be directed toward analyzing data when it becomes available.

REFERENCES AND PUBLICATIONS FOR SPACE SURVEYS OF CRUSTAL STRAINING

Cohen, S., "Determining Crustal Strain Rates with a Spaceborne Geodynamic Ranging System," *Manuscripta Geodaetica, 4,* 245-260, 1979.

SEISMOGENIC MODELS FOR THE 1976 TANGSHAN EARTHQUAKE AND EARTHQUAKE PREDICTION IN THE PEKING REGION

OBJECTIVE

The goal of this project is to apply satellite gravity data to advance scientific understanding of intraplate earthquakes. This project extends and carries forward the existing computational programs in mantle convection patterns and subcrustal stress fields under Asia and focuses them on two specific objectives. These are, first, to propose a possible mechanism for the 1976 Tangshan earthquake and second, to predict major earthquakes in the Peking region.

BACKGROUND

Based on results from stress field analyses, geodetic measurements of crustal deformation, fault motion, and focal plane solutions, the Chinese geoscientists have concluded that under the influence of a principal compressive force, the strain energy was gradually accumulated within the interlocking portion of the rhombic Tangshan fault block and a large seismic focus was then developed. Unresolved is the question of where the principal compressive force originated. Most world seismicity has been related to rigid plate interaction, but the occurrence of the seismic zone in the Tangshan region, which is far from plate boundaries, cannot be attributed to that cause. It is, therefore, highly desirable to examine the applicability of the convection generated stress field as inferred from satellite gravity data for earthquake prediction and research in the Peking region.

RECENT ACCOMPLISHMENTS

Despite the success of earthquake prediction in China, the complete failure of the Chinese program to predict the 1976 Tangshan earthquake in which 655,000 people died indicates that the state of stress in the Peking region is still very poorly understood. Our research project examines the subcrustal stress field due to mantle convection flows under China as inferred from the satellite gravity data. This stress field enables us to determine the current stress regimes in the crust of the Peking region. Under the influence of this subcrustal stress field, the rectangular fault system in Peking region (figure 3-5) will cause stress concentration (figure 3-6). Conformal transformation and mapping of the convection generated stresses under North China have revealed stress concentration in the rhombic Tangshan fault block (figures 3-6 and 3-7). The magnitude and direction of the concentrated stress field in the Tangshan seismic district are in accord with the geodetic measurements of crustal deformation after the 1976 Tangshan earthquake. Therefore, it can be concluded that the mysterious principal compressional force which caused the 1976 Tangshan earthquake may be due to stress concentration resulting from mantle convection.

We have also modeled strain accumulation and stress release along the Taihangshan fault system in the Peking region. Since the correlations between the seismic data (figures 3-8 and 3-9) and the model results (figure 3-6) are consistent, the cyclic sequence permits us to predict major earthquakes in the Peking region as shown in figure 3-10. Figure 3-10 shows that a major earthquake m = 7.7 would occur in or before 1980 in the Peking-Tangshan area. The 1976 Tangshan earthquake M = 7.8 seems to verify this result. It is hoped that predictions as outlined in figure 10 will provide a basis for scientific and disaster planning and preparation in the Peking region.

Interiors

SIGNIFICANCE

Major programs aimed at earthquake prediction have been initiated in China. The routine announcements of reliable predictions have been successful for many small magnitude events. But particularly important and difficult to predict are large earthquakes. Since the duration of an anomaly is likely to be monotonically related to the magnitude of the subsequent earthquake, it is difficult to recognize the anomaly and to determine with any useful resolution the expected time for the earthquake. Therefore, the prediction of time, location, and magnitude of large earthquakes in the Peking region is especially noteworthy. While initial routine predictions will probably be made only for small events, we have demonstrated that the convection generated stress field inferred from satellite gravity data can make a major contribution in predicting large earthquakes in Peking region.

FUTURE EMPHASIS

The methods developed in this paper will be extended and applied to calculate stress concentration in the interiors and passive margins of tectonic plates. We plan to examine the applicability of the convection generated stresses as inferred from satellite gravity data for earthquake prediction and research in isolated zones of persistent and potentially hazardous seismicity.

REFERENCES AND PUBLICATIONS

Liu, H.S., "Convection Generated Stress Concentration and Seismogenic Models of the Tangshan Earthquake," *Physics of the Earth and Planetary Interiors, 19,* 307-318, 1979.

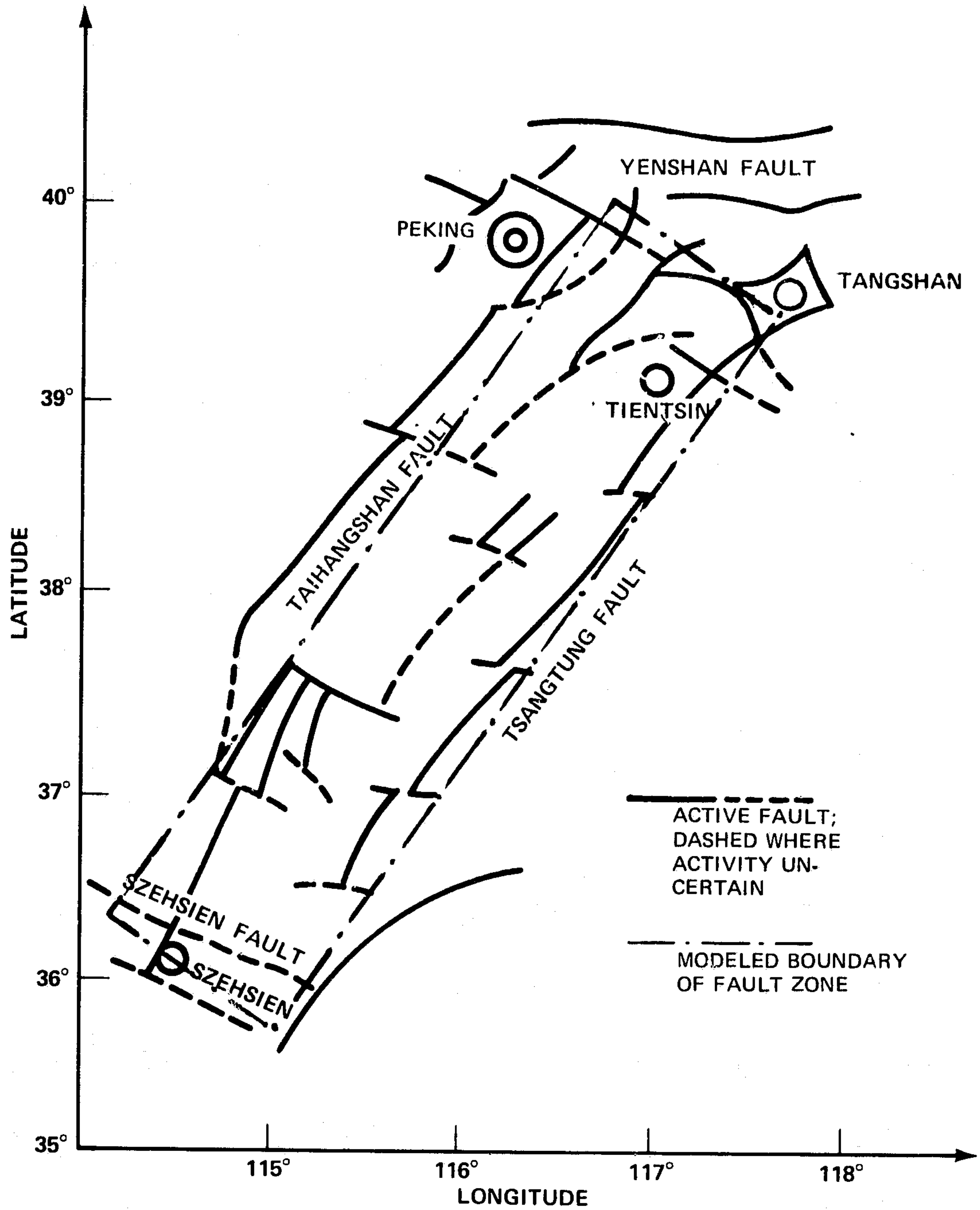

Figure 3-5. Fault System in the Peking-Tangshan Region

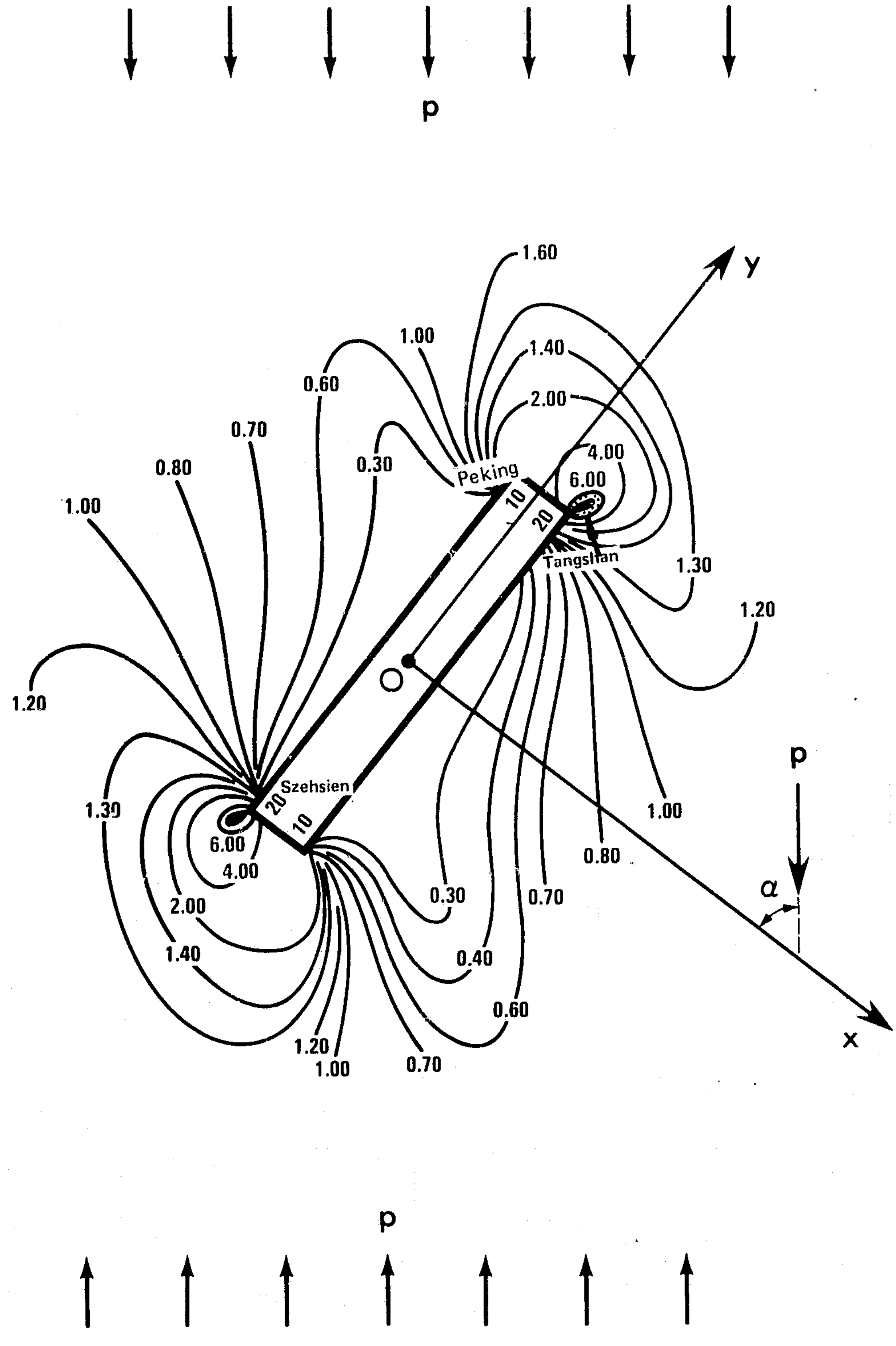

Figure 3-6. Stress Concentration in the Peking-Tangshan-Szehsien Region Caused by the Satellite Determined Tectonic Force P

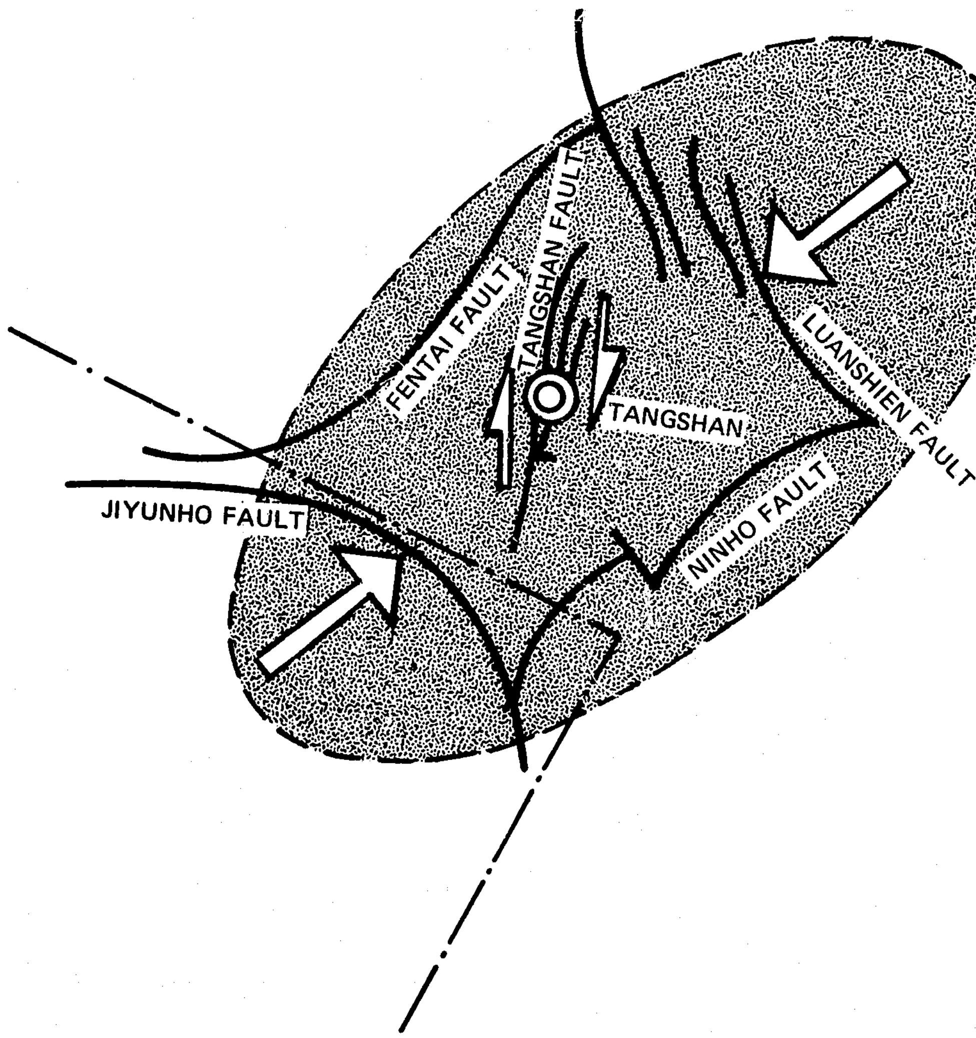

Figure 3-7. Seismogenic Model of the 1976 Tangshan Earthquake and the Satellite-Determined Stress Concentration

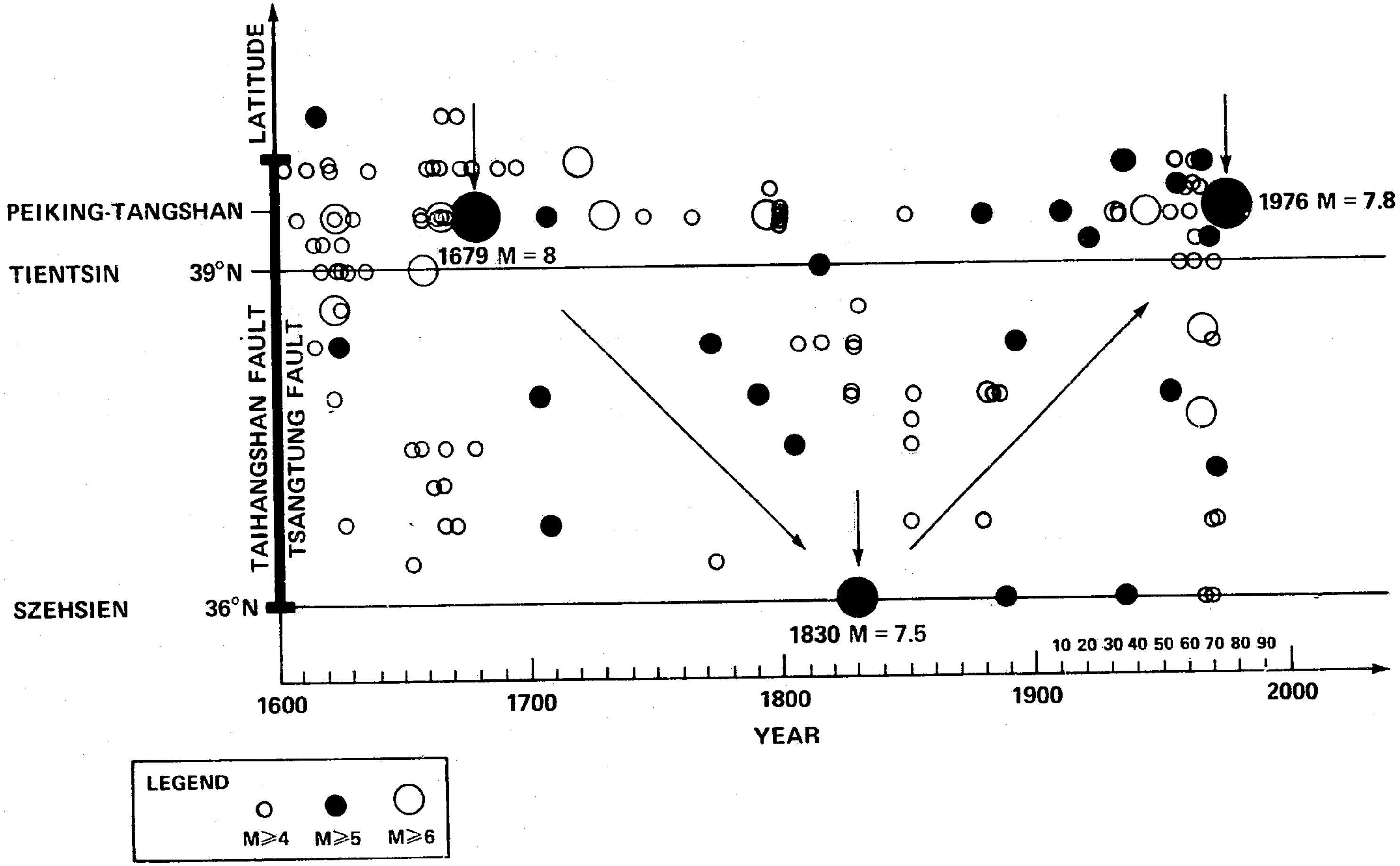

Figure 3-8. Magnitudes of Earthquakes in the Taihangshan-Tsangtung Fault System From 1600 to 1976

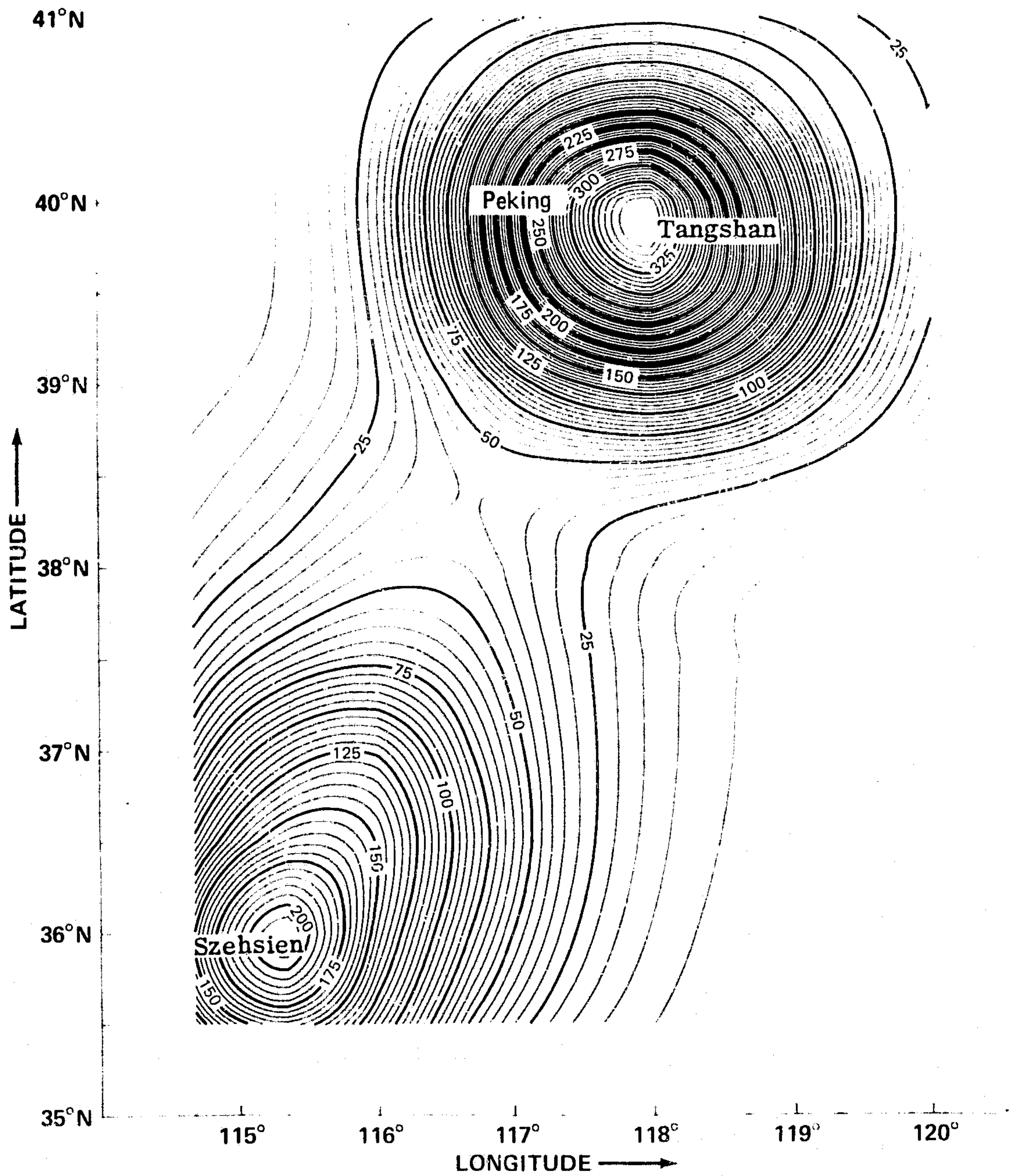

Figure 3-9. Strain Release Map of the Peking-Tangshan-Szehsien Region From 1830 to 1976

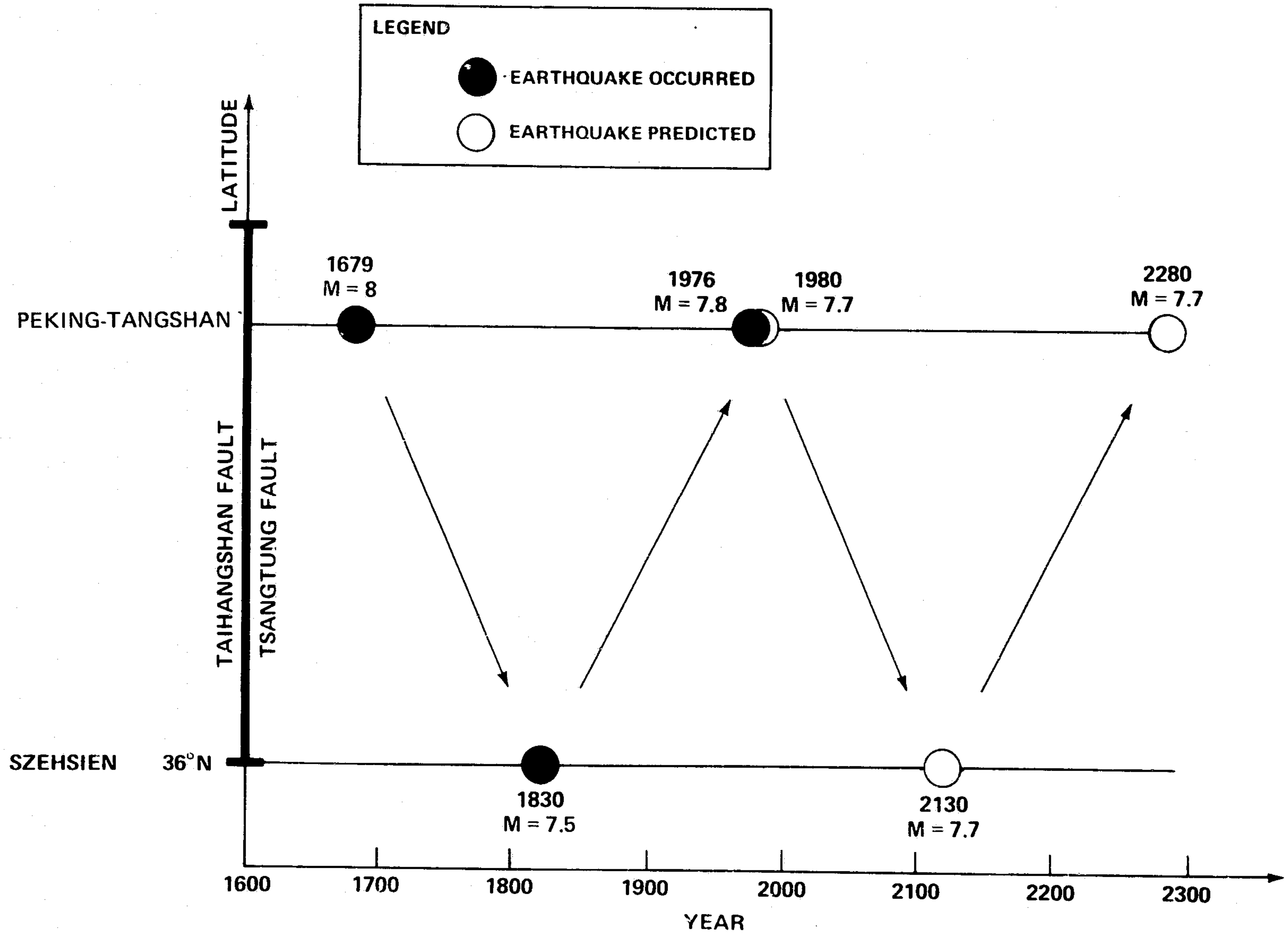

Figure 3-10. Historic and Predicted Major Earthquakes in the Peking Region

DEVELOPMENT OF A SEISMIC DATA COLLECTION PLATFORM

OBJECTIVE AND BACKGROUND

Geophysical data is now being collected all over the globe from a variety of remote and inhospitable locations. In order to develop any kind of a predictive system for natural crustal hazards, such as earthquakes or volcanic eruptions, near real-time collection of data is required. Off-the-shelf DCP's are now available for satellite relaying of low data rate information. A relatively inexpensive, field hardened system is not available that can relay the high data rate seismic information. In cooperation with GSFC Code 700, we have undertaken the development of a prototype seismic DCP.

RECENT ACCOMPLISHMENT

A DCP simulator has been constructed that utilizes an event detection algorithm developed by the USGS and compresses a short period seismic signal into a 100 bit per second GOES satellite channel. The simulator performs all the functions required of a field processor and includes additional features such as control from a printing terminal, variable buffer length, and variable microprocessor speed. An evaluation program to determine precise power budgets, optimum microprocessor speed, and buffer lengths is in progress.

FUTURE EMPHASIS

Completion of the evaluation program and preparation of a TM describing the system will mark the termination of this program.

REFERENCES AND PUBLICATIONS

Allenby, R.J., W.J. Webster, Jr., and J.E. Painter, "Satellite Relaying Geophysical Data," NASA/GSFC X-922-77-273, November 1977. A NASA Technical Memorandum describing the details of the design and performance is in progress. An abbreviated version will be submitted to *Geoscience Electronics*.

CHAPTER 4

GRAVITY FIELD MODELING

OVERVIEW

Gravity field model improvement is needed for geophysical studies of the Earth's interior and lithosphere in order to:

- Obtain more accurate orbits for analysis of satellite activity, polar motion and tidal parameters.
- Determine the baselines in crustal motion studies.
- Provide an improved ocean geoid for separating the dynamic and stationary sea surface topography for the identification and analysis of the broad features of ocean circulation.

This chapter describes the development of global gravity field models from satellite tracking data, surface gravity field data, and altimetry. Special investigations are also described, e.g., the use of satellite-to-satellite tracking for verification and increased resolution of the gravity field.

Contributors to this chapter include Michael Graber, Werner Kahn, Francis Lerch, James Marsh, Barbara Putney, David Rubincam, David Smith and C. A. Wagner.

GRAVITY MODEL DEVELOPMENT

OBJECTIVES

The primary objective of gravity model development research is a refined earth gravity field, which will provide a basis for further geophysical research. In particular, improved resolution of spatial variations of the field is needed for interpretation of density and stress irregularity. Moreover, a refined field for providing highly precise satellite orbits is required to investigate areas of geodynamics and ocean dynamics. Specifically, improved orbits will provide for more accurate baselines for the SAFE project and for better reduction in altimeter data for ocean dynamics.

BACKGROUND

NASA's geodynamics and ocean processes program requires knowledge of the global geoid to submeter levels of accuracy. Final realization of these goals over the Earth's oceans will rely on extensive analysis of GEOS 3 and Seasat altimetry in conjunction with improved understanding of basic oceanographic processes. At GSFC the emphasis has been on using as much of the precise satellite tracking and altimeter data as possible to develop improved comprehensive gravity models. More precise laser tracking has provided for improvement of the geopotential, better orbit determination, and in turn more effective use of GEOS 3 altimeter data.

RECENT ACCOMPLISHMENTS

Recent Goddard Earth Models (GEM's) have made extensive use of the data provided by the GEOS 3 mission to make major advancements in gravity modeling. Table 4-1 summarizes the evolution of these models.

GEM 9 is a gravity model based solely on optical, laser, and electronic observations taken on 30 satellites. GEM 10 is a combination solution containing a global set of 5^0 surface gravity anomalies (Rapp, 1977) along with the data in GEM 9.

The use of a modified least squares method (collocation) permitted GEM 9 to be a larger field than previous derived satellite models. GEM 9 having harmonics complete to 20 x 20 with selected higher-degree terms. The satellite data set has approximately 840,000 observations, of which 200,000 are laser ranges taken on 9 satellites equipped with retroreflectors. GEM 10 is complete to 22 x 22 with selected higher degree terms out to degree and order 30 amounting to a total of 592 coefficients. Comparisons with surface gravity and altimeter data indicate a substantial improvement in GEM 9 over previous satellite solutions.

GEOS 3 was the first unmanned geodetic satellite carrying a spaceborne altimeter. Two solutions, GEM 10A and 10B, have been made using this altimeter data. A significant improvement over GEM 9 and 10 has been obtained by combining the altimeter data into these models.

GEM 10A (Lerch et al., 1978) is a field which combines the GEM 10 satellite and surface data sets with 300 passes of GEOS 3 altimetry selected so that a $5^0 \times 5^0$ grid of coverage was obtained. GEM 10A is complete to 30 x 30 in harmonics. It made use of the collocation techniques applied in GEM 10 (at a lower strength) which was described by Lerch et al., (1977, section 3.2). GEM 10B Lerch et al., (1978) combined GEM 10 with over 700 passes of GEOS 3 altimetry producing a field complete to 36 x 36 in harmonics. Moreover, GEM 10B is a completely free adjustment without collocation. Using the harmonics of GEM 10B in Burn's formula (Heiskanen and Moritz, 1967, p. 85), a geoid has been computed (figure 4-1).

GEM 10C, a harmonic model complete to 180 x 180, has been produced as an extension of GEM 10B for terms beyond degree 36. It uses a global set of 1^0 means of altimeter sea surface heights and gravimetric geoid heights. Over 2300 passes of altimeter data have been used to produce a set of 26,800 $1^0 \times 1^0$ mean sea surface values which are shown contoured in figure 4-2. The gravimetric and altimetric information was combined to form a global set of 1^0 geoid heights for the computation of GEM 10C. In combining the data using a single value per 1^0 block, the altimeter information was given precedent over the surface data so that all altimeter derived mean sea surface heights were used. The directly measured part of these data sets are highly complementary with altimetric heights over most of the oceans and gravimetric anomalies over most land areas. In total, there were approximately 50,500 $1^0 \times 1^0$ equal angle blocks containing measured altimeter or surface gravity observations employed in the computation of GEM 10C.

Table 4-2 summarizes the estimated accuracy of recent GEM's. Advancement during 1978 towards the development of a more accurate and comprehensive gravity field has been substantial. GEM 10C provides for geoidal resolution which is an order of magnitude greater than GEM 9 with almost twice the overall accuracy of earlier fields.

FUTURE EMPHASIS

Future models, GEM 11 and 12, will use more precise satellite date from Lageos, BE-C, GEOS 3/ATS(SST), and Seasat. GEM 11 will provide for: (a) Better accuracy in the broad wavelength features of the geoid down to a few centimeters, (b) improved orbits for the reduction of Seasat and GEOS 3 altimeter data for ocean dynamics, and (c) improved BE 3 orbits for analysis of baselines in the SAFE project. New combination solutions GEM 12 (12A and 12B) will be derived by employing an improved set of surface gravity data and altimeter data. These latter solutions will provide for improved resolution in the geoid down to 100 km and analysis of sea surface topography for broad features of general ocean circulation.

REFERENCES AND PUBLICATIONS

Heiskanen, W. and H. Moritz, *Physical Geodesy*, W. H. Freeman and Company, San Francisco, 1967.

Lerch, F.J., C.A. Wagner, S.M. Klosko, R.P. Belott, R.E. Laubscher, and W.A. Taylor, "Gravity Model Improvement Using GEOS-C Altimetry (GEM 10A and 10B)," the *E⊕S Trans. AGU, 59*, 260 (abstract), 1978.

Lerch, F.J., R.P. Belott, S.M. Klosko, and E.M. Litkowski, "Laser Reference Orbits and Altimeter Validation for GEOS-3," supplement of paper presented at the Marine Geodesy Symposium, University of Miami, RSMAS, Virginia Keys, Miami, Florida, September, 1978.

Lerch, F.J., S.M. Klosko, R.E. Laubscher, and C.A. Wagner, "Gravity Model Improvement Using Altimeter Data of GEOS-3 (GEM 10A)," paper presented at the GEOS-3 Project Symposium, New Orleans, November, 1977.

Lerch, F.J., S.M. Klosko, R.E. Laubscher, and C.A. Wagner, "Gravity Model Improvement Using GEOS-3 (GEM 9 and 10)," *Journal of Geophysical Research, 84*, 3897-3916, 1979.

Rapp, R., "Potential Coefficient Determinations from 5° Terrestrial Gravity Data," *OSU*, No. 251, January, 1977.

Table 4-1. Goddard Earth Models

GEM	Harmonics	Data
GEM #9	20 x 20	Satellite Tracking
GEM #10	22 x 22	Satellite Tracking + Surface Gravity (1)
GEM #10A	30 x 30	Satellite Tracking + Surface Gravity (1) + Altimetry (1)
GEM #10B	36 x 36	Satellite Tracking + Surface Gravity (1) + Altimetry (2)
GEM #10C	180 x 180	Satellite Tracking + Surface Gravity (2) + Altimetry (3)

NOTE

Data:

1. Satellite Tracking: 30 Satellites Including GEOS 3.
2. Surface Gravimetry (1): 1654 5° (Equal Area) Mean Gravity Anomalies (Rapp 1977).
3. Surface Gravimetry (2): 38400 1° x 1° Mean Gravity Anomalies.
4. GEOS 3 Altimetry (1): 300 Passes Globally Distributed with 5° Spacing.
   Altimetry (2): 700 Passes Globally Distributed with 2° Spacing.
   Altimetry (3): 28000 1° x 1° Block Means Using 2300 Passes.

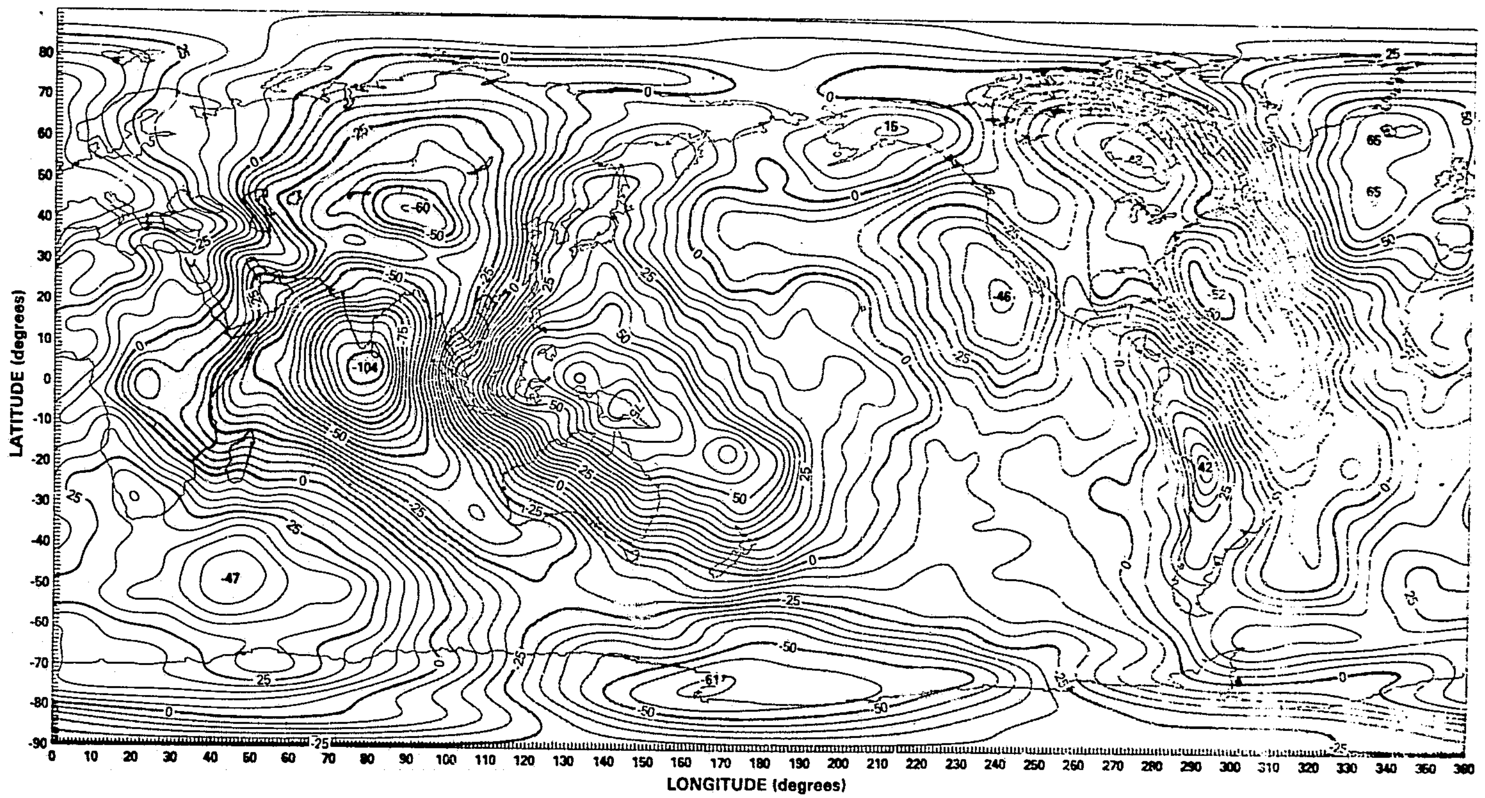

<u>NOTE</u>

Height in meters above the mean ellipsoid, f=1/298.257.

Figure 4-1. Geoid Surface Computed from the GEM 10B Model

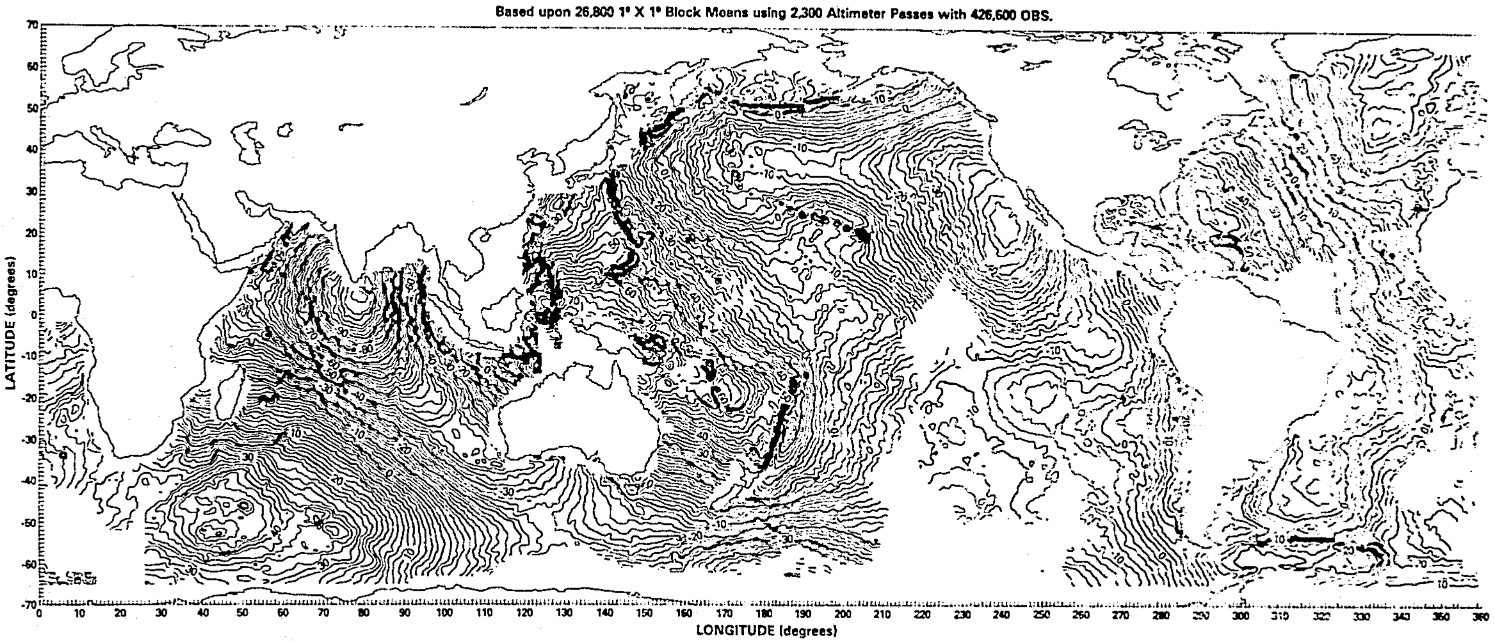

ORIGINAL PAGE IS
OF POOR QUALITY

Figure 4-2. Mean Sea Surface from GEOS 3 Altimetry

Table 4-2. Accuracy of Recent GEM's

Model	Complete Harmonic	Geoidal Resolution	Est. Comm. Error (m)	Est. Trun. Error (m)	Total Geoid Error	Approx. No. of Coef.
GEM 9(1977)	20	1000 Km	1.6	2.1	2.7	549
GEM 10(1977)	22	900 Km	1.4	1.9	2.5	592
GEM 10A(1978)	30	650 Km	1.4	1.6	2.4	958
GEM 10B(1978)	36	550 Km	1.3	1.3	2.2	1366
GEM 10C(1978)	180	100 Km	1.5	0.5	1.6	32758

DETERMINATION OF THE GEOCENTRIC GRAVITATIONAL CONSTANT

OBJECTIVE

The objective is to improve the accuracy of the geocentric gravitational constant (GM). It is a fundamental geodetic parameter, and a new value will provide a refinement in the Earth's reference ellipsoid for gravity anomalies and geoid undulations. Specifically, an accuracy is needed to provide an absolute scale of the geoid to within 10 cm for analysis of ocean circulation from spacecraft altimetry. Moreover, a precise scale is needed for satellite orbits for accurate utilization of spacecraft altimetry (±10 cm) and for absolute determination of baselines for plate motion studies where mixed observing systems may be used.

BACKGROUND

Most reductions of data from lunar and interplanetary probes have included re-estimation of the gravitational constant times the mass of the Earth, GM (Earth plus atmosphere). These missions include the Ranger, Surveyor, Lunar Orbiter, Pioneer, Mariner, and Viking series of flights, as well as a number of Russian interplanetary probes. The results of these GM estimations have been summarized by Esposito and Ng, 1976. The GM obtained from the best available interplanetary investigations has been adopted by the XVI General Assembly of the IUGG/IAG (Moritz, 1975). This value, based upon the IAG adopted value of the speed of light (c=299792.458 km/sec) is 398600.5 km^3/sec^2.

Laser ranging to the retroreflectors left on the moon during the Apollo Missions has been carried out at the McDonald Observatory in Texas since 1969. Williams (1974) has reported a value of GM obtained from these observations, which is in good general agreement with the interplanetary estimates. This value of GM and its uncertainty that he reported is 398600.48 $\pm$ .1 km^3/sec^2 for c equalling 299792.458 km/sec. King, et al. (1976) combined lunar laser and Alsep VLBI observations to obtain a value of GM of 398600.51 $\pm$ .03 for the IAG value of c.

In the present work (Lerch, et al., 1978), near-Earth laser ranging is used for a new determination of GM. It provides the most accurate estimate and, except for lunar laser ranging, it considerably reduces the uncertainty in GM.

RECENT ACCOMPLISHMENTS

Laser range observations taken on near-Earth satellites Lageos (a = 1.92 e.r.), Starlette (a = 1.15 e.r.), BE-C (a = 1.18 e.r.) and GEOS 3 (a = 1.13 e.r.), have been combined to determine an improved value of the geocentric gravitational constant (GM). The value of GM is 398600.61 km^3/sec^2, based upon a speed of light, c, of 299792.5 km/sec. Using the IAG adopted value of c equalling

299792.458 km/sec scales GM to 398600.44 km^3/sec^2. The uncertainty in this value is assessed to be ± .02 km^3/sec^2.

The GM 'ermination reported (Lerch, et al., 1978) was performed in the c lopment of the recent GEM 9 and 10 models (Lerch, et al, 1977). r the first time in the GEM series, these gravity models includ d an adjustment of GM.

Table 4-3 presents combined as well as individual solutions of GM using observations taken on four satellites. In all cases, the laser ranges were reduced in arcs of 5 days length. The value of c used was 299792.5 km/sec. Relativistic effects were modeled for light/time correction (Moyer, 1971) and reduced GM by .024 km^3/sec^2.

The individual satellite estimates of GM varied by less than .05 km^3/sec^2 from the combined result. Due to the high altitude of Lageos, its data dominated the combination solution as it has an order of magnitude greater capability than the other satellite data to separate GM from the orbital semimajor axis and station coordinate adjustments. Also, it is the only satellite that provides consistent subset solutions.

Table 4-4 intercompares the near-Earth laser determination of GM with other recent experimental results. The results obtained from our analysis (GM = 398600.44 ± .02 km^3/sec^2) generally confirms the latest results obtained from radiometric data taken when numerous interplanetary missions departed Earth and those obtained from lunar laser ranging. Moreover, the uncertainty assessed for GM determined from the near-Earth laser observations reduces the known uncertainty of GM (figure 4-1). These results are important for satellite missions requiring submeter radial orbital accuracies.

SIGNIFICANCE

It can be seen from table 4-4 that considerable improvement is made in GM, either in the uncertainty estimate or the actual value. Except for lunar laser ranging, at least a factor of 5 improvement is achieved. From the relationship

$$3 \frac{\Delta a}{a} = \frac{\Delta GM}{GM}$$

where a is the semimajor axis of the satellite, the new uncertainty estimate of GM (± .02 km^3/sec^2) reduces the radial scale error on geodetic satellites of approximately 1000-km altitude to about 10 cm. Baselines scale similarly as with the semimajor axis, hence baselines which are separated by 100 km should be accurate to about 2 cm as far as absolute scale is concerned.

FUTURE EMPHASIS

Because of the significance of GM as indicated above, it is desirable to see if GM can be reproduced from additional sets of data. Because of the capability of estimating GM from Lageos, Dr. David Smith, as project scientist for Lageos, has continued with this work. Six months of data have been employed in the work for Lageos, and presently, some preliminary values are being analyzed from 20 months worth of Lageos data. Subset solutions on a monthly basis show a steady decline in the estimated GM to about 20 lower than the above value. Hence, because of the importance of GM for scale, such as with baselines and a 10-cm absolute scale for the geoid, this work needs to be pursued.

REFERENCES AND PUBLICATIONS

Esposito, P.B. and S.K. Wong, "Geocentric Gravitational Constant Determined from Mariner 9 Radio Tracking Data," presented at the International Symposium on Earth Gravity Models and Related Problems, St. Louis, Mo., August 1972.

Esposito, P.B. and A.T.Y Ng, "Geocentric Gravitational Constant Determined from Spacecraft Radiometric Data," *Physics of the Earth and Planetary Interiors, 12,* 283-289, 1976.

King, R.W., C.C. Counseman, and I.I. Shapiro, "Lunar Dynamics and Selenodesy: Results from Analysis of BLBI and Laser Data," *Journal of Geophysical Research, 81,* 6251-6256, 1976.

Lerch, F.J., S.M. Klosko, R.E. Laubscher, and C.A. Wagner, "Gravity Model Improvement Using GEOS-3 (GEM 9 & 10)," NASA/GSFC X-921-77-246, September 1977.

Lerch, F.J., S.M. Klosko, R.E. Laubscher, D.E. Smith, P. Kolenkiewicz, B.H. Putney, J.G. Marsh, and J.E. Brownd, "Determination of the Gravitational Constant from Laser Ranging on Near-Earth Satellites," *Geophysical Research Letters, 5,* 12, 1031-1034, December 1978.

Martin, C.F., S.M. Klosko, and J.W. Regan, "Determination of the Masses of the Earth, Moon and Sun and The Size of the Earth from Mariner 9 Range and Doppler Observations," NASA/GSFC X-922-75-134, June 1975.

Martin, C.F., and I.H. Oh, "Utilization of Satellite-to-Satellite Tracking Data for Determination of The Geocentric Gravitational Constant, *J. Geophys. Res., 84,* B8, 3944-3950, July 1979.

Moritz, H., "Report of the Special Study Group No. 5.39 of IAG: Fundamental Geodetic Constants," presented at the Sixteenth General Assembly of IUGG/IAGG, Grenoble, France, August 1975.

REFERENCES AND PUBLICATIONS (continued)

Mozer, T.D., "Mathematical Formulation of the Double-Precision Orbit Determination Program (DPODP)," NASA/JPL TR32-1527, p. 17, May 15, 1971.

Williams, J.G., "Lunar Laser Ranging," presented at the 1974 Fall Annual Meeting of the American Geophysical Union, San Francisco, California, December 1974.

Table 4-3. Estimation of the Geocentric Gravitational Constant, GM, from Individual Satellite Laser Observations

Satellite Name	Semi-major Axis (Earth Radii)	Eccen-tricity	Inclina-tion (Deg.)	No. of 5D Arcs	No. of orbits	Recovered GM (km^3/sec^2)
Lageos	1.92	.004	109.83	32	88,800	398600.60
Starlette	1.15	.020	49.80	20	23,000	398600.61
BE-C	1.18	.026	41.19	20	18,500	398600.65
GEOS 3	1.13	.001	114.98	37	90,900	398600.60
Combined Results:				109	221,200	398600.61 $\pm$ .02

<u>Note</u>

Speed of light, c = 299792.5 km/sec

Table 4-4. Comparison of Recent Determinations of the Geocentric Gravitational Constant, GM

Investigators	Value of GM* (Km^3/Sec^2)	Type of Investigation
(A) Esposito and Wong, 1972	398600.63 $\pm$ .4	Interplanetary - Mariner 9
(B) Williams, 1974	.48 $\pm$ .1	Lunar Laser Ranging
(C) Martin et al., 1975	.66 $\pm$ .06	Interplanetary - Mariner 9
(D) Esposito and Ng, 1976	.55 $\pm$ .2	Interplanetary - Mariner 9
	.45 $\pm$ .2	Interplanetary - Mariner 10
(E) King et al., 1976	.51 $\pm$ .03	Lunar Laser Ranging and ALSEP VLBI
(F) Esposito, 1978	.40 $\pm$ .2	Interplanetary - Viking 1
	.60 $\pm$ .2	Interplanetary - Viking 2
(G) Martin and Oh, 1978	.35 $\pm$ .15	Near-Earth - Satellite-to-satellite Tracking on ATS 6/GEOS 3
(H) This paper	.44 $\pm$ .02	Near-Earth Laser Ranging on Four Satellites

*Assuming c = 299792.458 km/sec.

ANALYSIS OF THE GRAVITATIONAL SPECTRUM

OBJECTIVES

Objectives of the analysis of the gravitational spectrum research are:

- Calculation of the geoid spectrum to high degree from altimetry and gravimetry.
- Estimate of the strength of the crust from comparison of the topographic and geoid spectrum.
- Development of a method for predicting gravitational spectra directly from circular arcs of diverse data.
- Development of a method for predicting gravitational spectra directly from range-rate tracking of eccentric planetary orbiters.

BACKGROUND

Previous work, principally by Allan (1972) and Lambeck (1976) has established the usefulness of the gravitational spectrum in determining the depth of the sources (density contrasts) for the field. In addition, comparison of *regional* spectra of gravity with topography has generated new data on the strength of the crust (e.g., Dorman and Lewis, 1970; Banks, Parker and Huestis, 1977). In 1978, efficient methods were developed to get the gravitational spectra directly from spacecraft tracking as well as surface data. In addition, an overall comparison was made (no correlation) between the *global* spectra of gravity and topography, to establish one parameter of crustal strength related to the concept of regional isostatic compensation.

RECENT ACCOMPLISHMENTS AND SIGNIFICANCE

Smooth Spectrum of the Gravity Field

The smoothed spectrum of the gravity field to about degree 400 (50-km half wavelength) was derived from 81 long arcs of GEOS 3 and Skylab altimetry and 180 meridional arcs of 1 x 1 gravimetry. As part of this study, the spectrum of open ocean sea surface departure topography (above the geoid) was also evaluated below 1000 km half wavelength using tide functions, oceanographic charts, and differences of overlapping GEOS 3 altimetry. The results were that over most of the ocean, most of the time, the total sea surface spectrum is dominated by the geoid to 50 km half wavelength. The derived geoid spectrum itself (figure 4-3) is remarkably the same from either altimetry or gravimetry.

It is noted that the spectrum is significantly less powerful than Kaula's Rule up to about degree 50 and significantly more powerful above degree 100 to at least degree 400. Even if the gravitational field is known perfectly to a resolution of 100 km (1° x 1°), smaller scale geoidal undulations of about 50 cm are shown by these measurements.

Detailed Spectrum of the Free Air Gravity Field

The detailed spectrum of the free air gravity field to degree 36 (GEM 10B) and the smoothed spectrum from degree 36 to degree 180 was compared to a field derived for the crust only (to degree 180) for a range of strengths and depths of compensation (figure 4-3). The gravitational field for the crust was found from harmonic analysis of global 1° x 1° topography from Lee and Kaula, the Scripps Institution and U.S. Navy Bathymetric Soundings. The spectrum for an uncompensated (rigid) crust is obviously too powerful to explain the true field at long wavelengths though at short wavelengths the crust appears to be nearly unyielding. At the other extreme, the spectrum of a completely weak crust (for blocks greater than 110 x 110 km) can nearly match the measured field at intermediate wavelengths (20 n 40) for a constant depth of compensation of 30 km.

The weakness of the field spectrum of the fully compensated crust at lone wavelengths is attributed to significant density contrasts in the mantle. Its weakness at short wavelengths can be largely made up by giving strength to the crust over distances greater than 110 km. This strength can be interpreted most simply as resulting in a smoother compensating layer at depth than the 1° topography at the surface (regional compensation). The most reasonable combination of depth of compensation (average crust thickness) and extent of smoothing of the crust's bottom topography was found to be 25 and 220 km, respectively.

Gravitional Spectra Derived from Circular Orbit Satellite Tracking Data

The work on inverting altimetry and gravimetry (one dimensional) spectra to obtain (two dimensional) gravitational spectra has been generalized to include circular orbit satellite tracking data (range-rate). Harmonic analysis of three, 40-minute arcs of ATS-6 to Apollo/Soyuz four-way range-rates shows excellent agreement with the spectrum predicted from the Earth's gravitational field. Simulations show the method is capable of deriving accurate smoothed gravitational spectrum to high degree from just a few well-distributed arcs of such data. The arcs do not have to be global. But even with global arcs of data (e.g., gravity anomalies) much more and well-distributed data is required to derive accurate individual degree variances, than the smoothed spectrum. Nevertheless, as figure 4-3 shows, important geophysical information on the state of the crust and interior can be inferred by comparison of the easily derived smoothed spectra of gravity and topography.

Gravitational Spectrum Derived from Eccentric Orbit Satellite Tracking Data

The gravitational spectrum has been derived from range-rate tracking data on spacecraft in eccentric orbits. Here the distortion of the orbit causes significant power from low-degree harmonics to radiate into high-frequency range-rate fluctuations. In fact, the entire spectrum of fluctuations is influenced by every gravity harmonic, while for the circular orbit case, gravity disturbances radiate power only to the same or lower frequencies. The result (for the eccentric orbit) is a flatter and smoother spectrum which has significant variation with the observer's view of the orbit plane. The case of the highly eccentric Pioneer Venus orbiter has been worked out in detail for arbitrary start and stop positions with respect to periapsis, and arbitrary viewing angles. Significant gravitational signal should be observable in orbiter tracking from gravitational terms as high as 50 degree. However, because of high sensitivity to the data at periapsis, more passes need to be averaged to obtain a reliable gravitational spectrum than in the circular orbit case.

FUTURE EMPHASIS

In 1979 we will be working to derive global estimates of crustal strength from the *correlation* of gravity and topographic spectra. In addition, we will be trying to derive the density sources of a detailed global harmonic field from satellite tracking, altimetry, and gravimetry.

REFERENCES AND PUBLICATIONS

Allan, R.R., "Depth of Sources of Gravity Anomalies," *Nature Physical Science, 236,* 22-23, March 1972.

Banks, R.J., R.L. Parker, and S.P. Huestis, "Isostatic Compensation on a Continental Scale, Local Versus Regional Mechanisms," *Geophys. J.R. Astr. Soc., 51,* 431-452, 1977.

Dorman, L.M., and B.T.R. Lewis, "Experimental Isostasy, Theory of the Determination of the Earth's Isostatic Response to a Concentrated Load," *J. Geophys. Res., 75,* 3357-3365, 1970.

Lambeck, K., "Lateral Density Anomalies in the Upper Mantle," *J. Geophys. Res., 81,* 6333-6340, 1976.

Lerch, F.J., C.A. Wagner, S.M. Klosko, R.P. Belott, and G.T. Germana, "Goddard Earth Model Development for Oceanographic Applications," paper presented at the Marine Geodesy Symposium, Miami, Florida, October 1978, and accepted for publication in *Marine Geodesy,* 1979.

REFERENCES AND PUBLICATIONS (continued)

Wagner, C.A., "The Geoid Spectrum from Altimetry," NASA TM 79583, July 1978.

Wagner, C.A., and O.L. Colombo, "Gravitational Spectra from Direct Measurements," NASA TM 79603, August 1978.

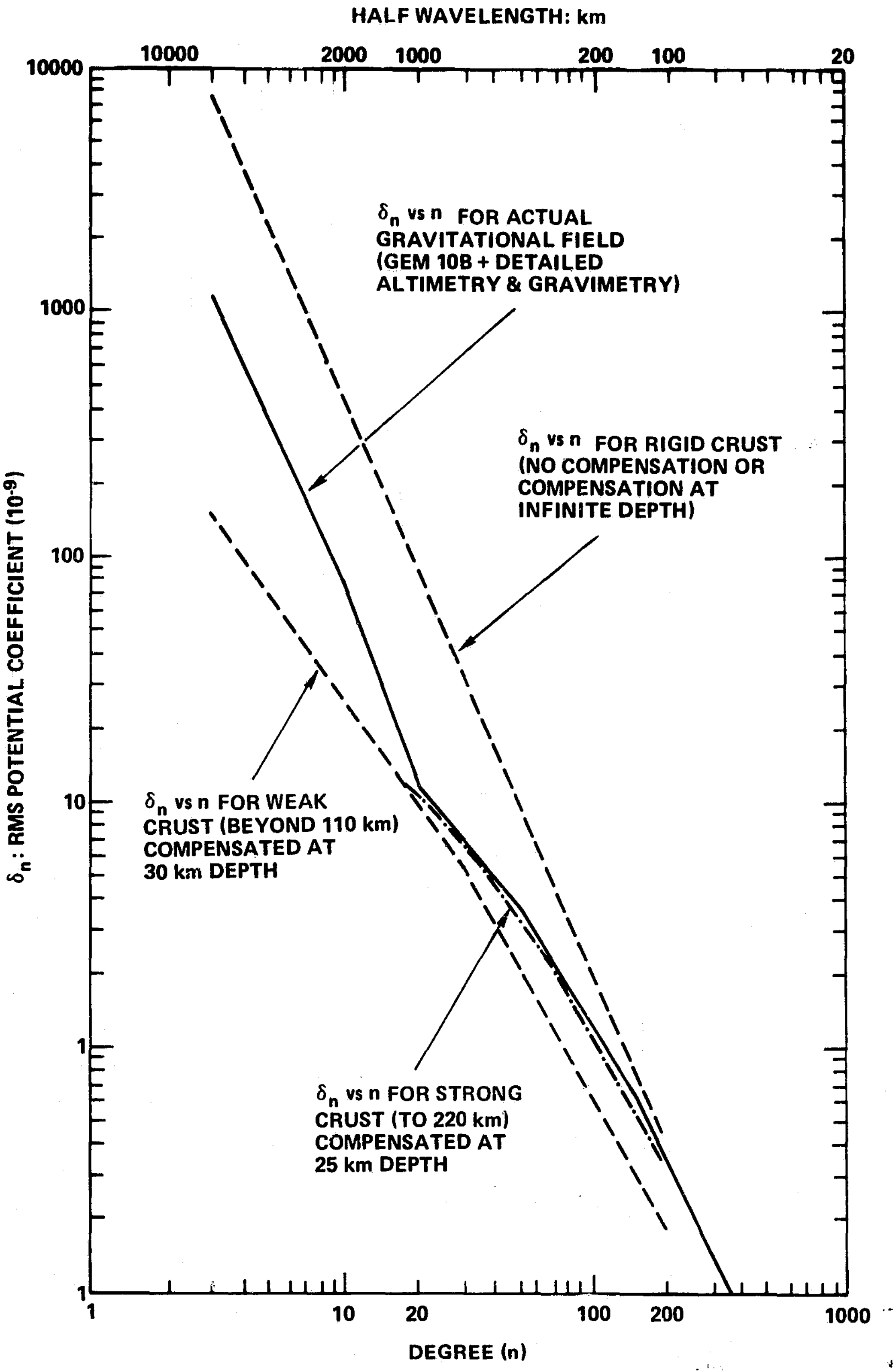

Figure 4-3. Geopotential Spectra from Measurements and Crustal Topography

GRAVITY ANOMALIES DETERMINED FROM TRACKING THE APOLLO DURING THE APOLLO-SOYUZ MISSION

OBJECTIVES

The objectives of a geodynamics experiment performed during the Apollo-Soyuz Mission in July 1975 were: (a) To demonstrate detectability of short wavelength (i.e., 300 km and larger) features of the Earth's gravity field; (b) to evaluate the high-low Satellite-to-Satellite (SST) tracking technique for geodynamic applications; and (c) to test the recoverability of short wavelength features of the Earth's gravity field.

BACKGROUND

Interest in the knowledge of more detailed structure of the Earth's gravity field has considerably increased during the past decade. Major factors fostering this interest were the tectonic plate hypothesis and the study of large ocean currents and ocean topography in general. The gravity anomalies with horizontal resolution within the range of 200 to 1000 km are of principal interest. Conventional analysis of satellite tracking data (e.g., angles, range, and range-rate) results in an earth gravity field model with a resolution of about 2000 km.

An experimental technique which can resolve gravity anomaly blocks of 2° x 2° and larger in areal extent is the "high-low" SST technique. This technique was tested during the joint US-USSR Apollo-Soyuz Mission flown in July 1975. High-frequency range-rate changes were observed between the "high" Applications Technology Satellite 6 (ATS 6) in a geosynchronous orbit and the "low" flying Apollo spacecraft in a near-circular near-earth orbit.

RECENT ACCOMPLISHMENTS

A total of 348 5° x 5° free-air gravity anomalies have been recovered using data from 30 processed Apollo revolutions from a total set of 108 revolutions in the region bounded by the Apollo orbit (52° N to 52° S) and the area covered by the ATS 6 satellite (64° W to 116° E) (see figures 4-4 and 4-5).

The rms error was found to be about 7 mgals. A comparison with anomalies independently determined from GEOS 3 altimeter data analysis, the Goddard Earth Model 10B (GEM-10B) and available surface gravity data was found to be in agreement with the 7 mgals quoted (refer to table 4-5).

SIGNIFICANCE

It can be concluded that the high-low SST system as tested during the Apollo-Soyuz mission demonstrated that system's capability to detect and recover mean free-air gravity anomalies. Furthermore, the SST system's potential as a sensor for mapping the global gravity field fine structure is also shown.

FUTURE EMPHASIS

The remaining Apollo data arcs not yet processed will be corrected for ionospheric refraction and a new solution for $5° \times 5°$ gravity anomalies will be made. The complete data set from Apollo will also be added into GEM models.

REFERENCES AND PUBLICATIONS

Vonbun, F.O., W.D. Kahn, W.T. Wells, T.D. Conrad, "Gravity Anomalies Determined from Tracking the Appollo-Soyuz," NASA TM 78031, December 1977.

Vonbun, F.O., W.D., Kahn, W.T. Wells, T.D. Conrad, "Geodynamics Experiment MA-128," Apollo-Soyuz Test Project Summary Science Report, I, NASA SP-412,177-191, 1977.

Vonbun, F.O., W.D. Kahn, J.W. Bryan, P.E. Schmid, W.T. Wells, T.D. Conrad,"Geodynamics Experiment MA-128," Apollo-Soyuz Test Project Preliminary Science Report, NASA TM X-58173, 12-1 to 12-16, February 1976.

Vonbun, F.O., W.D. Kahn, J.W. Bryan, P.E. Schmid, W.T. Wells, T.D. Conrad, "Gravity Anomaly Detection-Apollo/Soyuz," NASA/GSFC X-920-75-308, December 1975.

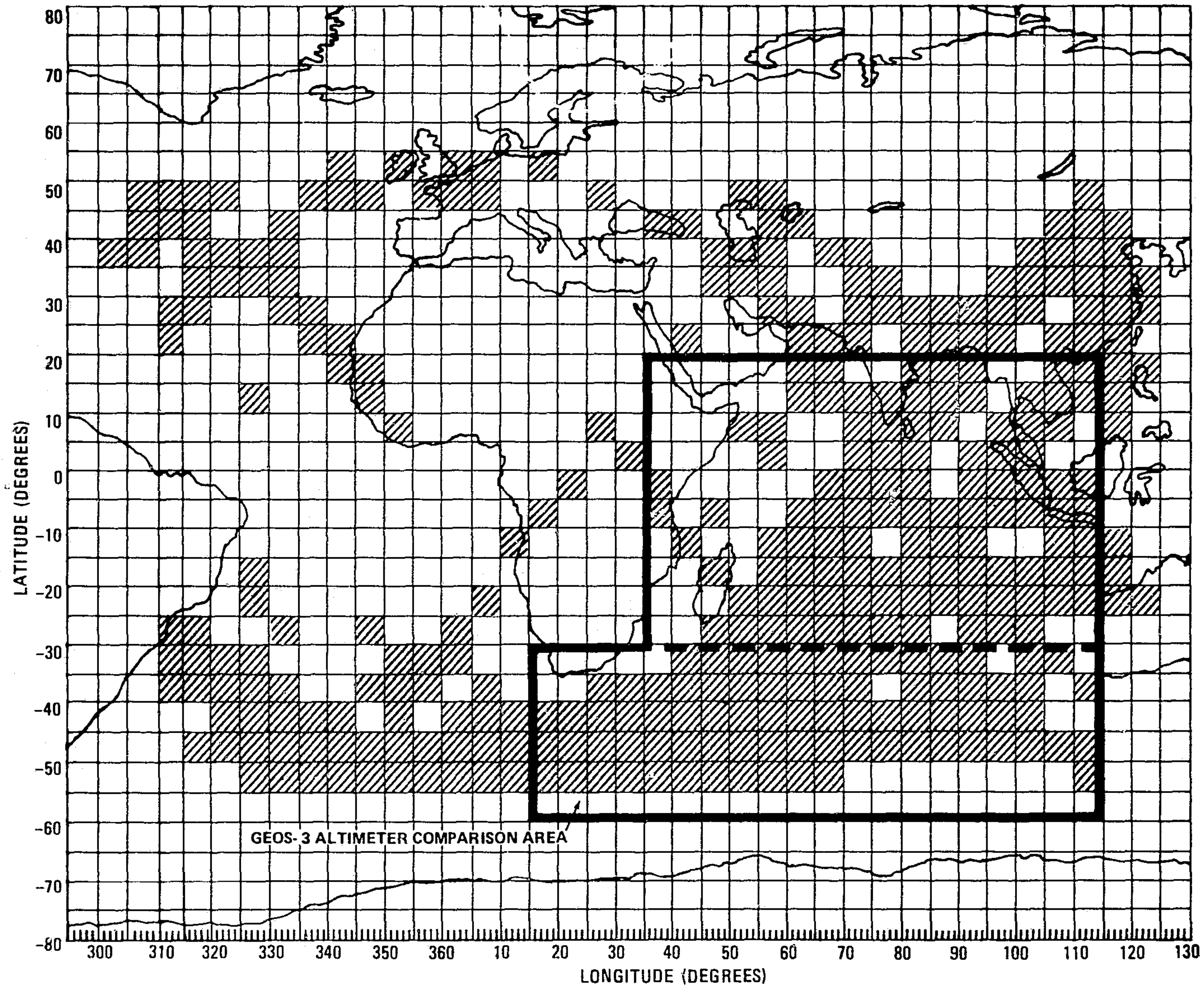

Figure 4-4. Free-air Gravity Anomalies

4-21

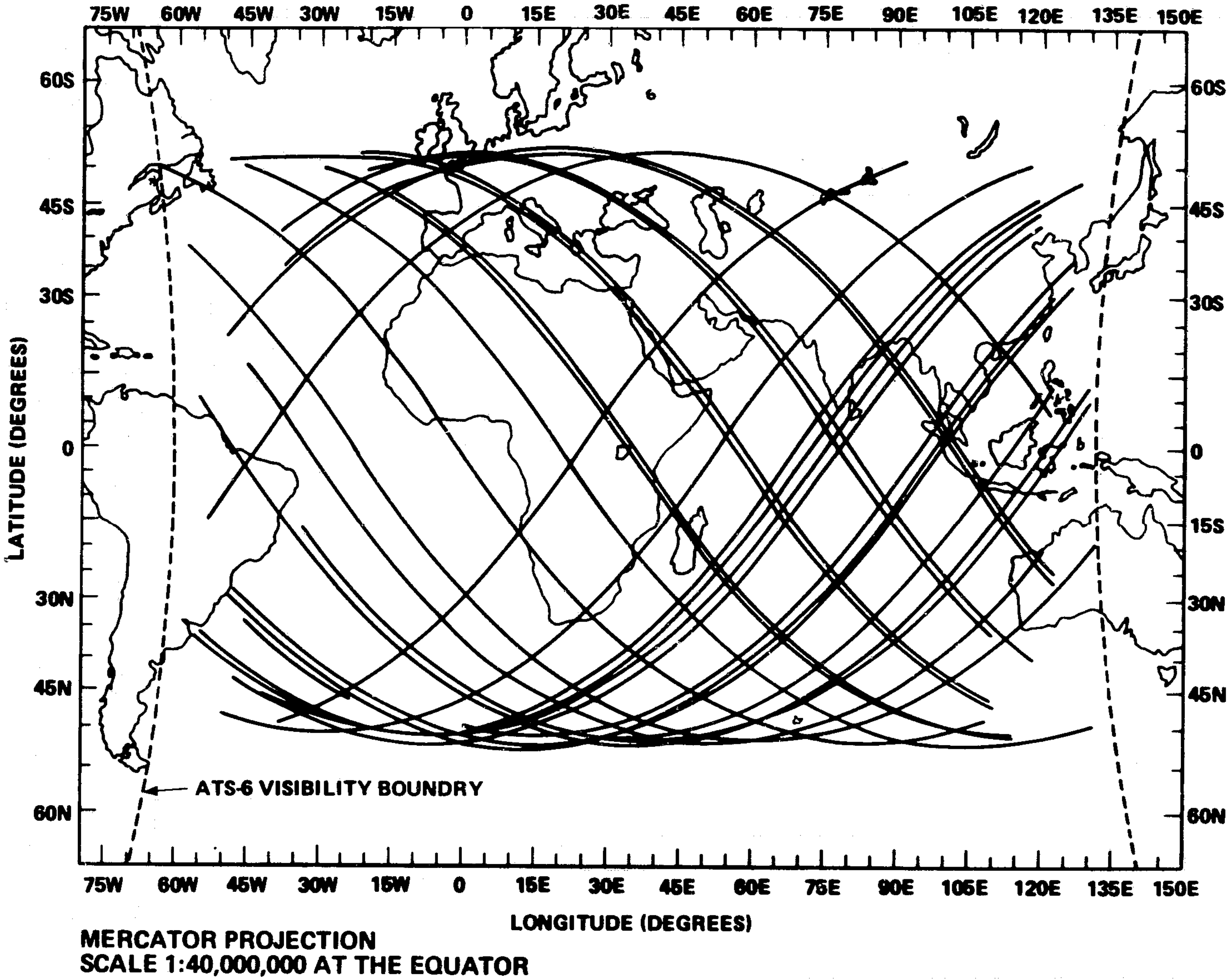

Figure 4-5. Apollo-Soyuz Ground Tracks

4-22
113

Table 4-5

Statistics of Comparisons for $5^\circ \times 5^\circ$ Mean Free-air Anomalies Recovered from Apollo

Description of Comparison	Total Number of Anomalies	Rms Difference (mgal)	Number of Anomalies Less Than 15 mgals*	Rms Difference (mgal)
Apollo/GEM 10B	348	10	313	7
Apollo/Surface Anomalies	348	15	261	8
Apollo/GEOS 3	73	7	69	6

*Error analyses have shown that with a system precision of ± 0.05 cm/sec or better a $5^\circ \times 5^\circ$, mean free-air gravity anomaly should be recoverable with an RMS uncertainty of 5 mgals (3σ = 15 mgals). Anomaly differences greater than 15 mgals should be viewed with caution.

UNEXPLAINED LAGEOS PERTURBATION

OBJECTIVE

The objective of the unexplained Lageos perturbation project is to explain and model a perturbation on Lageos.

BACKGROUND

The Lageos satellite has one unexplained orbital perturbation. This report describes the attempts made to explain it, so that it can be understood and adequately modeled in Lageos analyses. The perturbation is causing the semimajor axis to shrink at the rate of approximately 1 cm/week.

RECENT RESULTS AND SIGNIFICANCE

The effects of general relativity were investigated first as the possible cause of the perturbation. However, relativity predicts periodic changes in the semimajor axis with a period of one year. Data collected over a period of a year and half shows the semimajor axis is decreasing steadily; hence, relativity is not the cause. The relativity work is described more fully elsewhere.

Bruce Douglas (private communication) has suggested the perturbation might be due to a satellite resonance with a spherical harmonic term in the potential with degree $\ell = 52$ and order $m = 51$ and a period of about 400 days. But computations with Lageos data show the resonance to be poor, and rough calculations using Lagrange's planetary equations show the amplitude to be inadequate by orders of magnitude.

An attempt was made to account for the perturbation through the interaction of the satellite and the Earth's magnetic field. In particular, the field might despin Lageos and transfer its rotational angular momentum to the orbital distance, in analogy with tidal friction. However, a simple conservation-of-angular momentum argument shows that the total effect of stopping the rotation is 0.004 cm, which is not even adequate to explain a week of data.

The Poynting-Robertson effect was tried. This is a special relativity effect. The satellite absorbs sunlight and earthlight and is assumed to reradiate it isotropically in its own frame of reference. An observer on the Earth sees the reradiated light as blue-shifted in the direction of motion and red-shifted in the opposite direction. Since the photons jumping off the satellite in the front are more energetic than those in the rear, the satellite feels a force acting in a direction opposite to the motion. In other words, Poynting-Robertson acts as a drag. The force was put in a form suitable for the Gaussian form of Lagrange's planetary equations. The secular effect on the satellites semimajor axis was obtained by integrating over the true anomaly. The result was that the earthlight decreases the semimajor axis by 1 cm every 18 years, and sunlight by 1 cm every 428 days. This is too small to explain the perturbation acting on Lageos.

John A. O'Keefe (private communication) suggested the Yarkovsky effect. As the satellite rotates in the sunlight, the afternoon side of Lageos becomes the warmest part of it, much as afternoon is the warmest time of day here on Earth. So the most energetic photons jump off the satellite on the afternoon side, giving the satellite a sideways kick. The kick may act as a drag or impulse, depending on the orientation of the spin axis with respect to the sun. Calculations by Milt Schach and David Rubincam give an acceleration of about 10^{-7} cm S^{-2} due to the Yarkovsky effect for a reasonable temperature distribution. Putting this in a Gaussian form of Lagrange's equations gives a secular change of 0.01 cm/week, which is 2 orders of magnitude too small to explain the perturbation. However, the Earth's shadow has not been taken into account. Planetary perturbations (J. Kovalevsky, private communication) especially from Jupiter, have also been ruled out.

Atmospheric drag may be causing the perturbation. Densities for hydrogen and helium were computed for Lageos' altitude. (Other constituents of the atmosphere are too heavy to get up so high). This was done by taking the densities for hydrogen and helium at the critical level (400 km) from L.G. Jacchia (1977) and extrapolating them to the Lageos altitude (6000 km) using the equations of J.W. Chamberlin (1963). Hydrogen falls short by at least a factor of 10 to explain the observed decrease in semimajor axis. Helium at an exospheric temperature of 2000 k, however, gives precisely the right order of magnitude.

In summary, the following effects have been ruled out: General relativity; orbital resonance, magnetic field; Poynting-Robertson effect; and planetary perturbations. Possible causes are atmospheric drag, and the Yarkovsky effect.

FUTURE EMPHASIS

The Earth's shadow in the Yarkovsky effect will be taken into account in an analytical calculation, and the whole effect will be modeled in a computer calculation. Also, an attempt to correlate variations in the perturbation with solar activity will be made in order to test the atmospheric drag hypothesis.

REFERENCES AND PUBLICATIONS

Chamberlin, J.W., "Planetary Coronae and Atmospheric Evaporation," *Planetary and Space Science, 11,* pp. 901-960, August 1963.

Jacchia, L.G., "Thermospheric Temperature, Density, and Composition: New Models," SAO Special Report 375, March 1977.

GEODYN PROGRAM SYSTEM DEVELOPMENT

OBJECTIVES

The purpose of the Geodyn orbit determination and parameter estimation program is to recover geodetic and geophysical parameters from satellite data in a state-of-the-art manner.

BACKGROUND

In 1971 the Noname and Geostar programs were combined to form the Geodyn program. The philosophy of the development has been to mold the program very carefully to maintain computer efficiency and good program structure, appropriate orbit and Earth modeling, precise satellite measurement modeling, efficient numerical procedures and careful benchmarking. This care has paid off in the production of several GEM's, precise station locations, improved tidal, GM and polar motion values, consistent baseline determinations. Careful usage and modeling using laser, altimeter, and other satellite data from the GEOS satellites, BE 3, Starlett, Lageos, and currently the Seasat satellite as well as many others has allowed these accomplishments.

RECENT ACCOMPLISHMENTS AND SIGNIFICANCE

The Geodyn orbit determination and parameter estimation program has continued to evolve to meet new requirements in the areas of modeling, data handling and machine efficiency. Two major versions of the program were released during this year GDYN 7803 and GDYN 7808.

In support of Seasat several program modificatins were made and are still under development. In tuning up our models, the nutation and UT1 timing system computations were improved. The Hendershott ocean tidal model was corrected. A new satellite ephemeris file called the Seasat RV tape was created. Under current development is a variable area and reflectivity satellite model for the atmospheric drag and solar radiation computations, three dimensional accelerations for solar radiation, variable rotation rate of atmosphere and time dependent drag coefficient for atmospheric drag. A separate software package using the Bent model for the ionosphere was created to compute the ionsopheric correction to apply range, average range rate and altimeter observations. The processing of altimeter data was modified to allow Geodyn to substitute computed geoid heights, ocean tidal values, latitude and longitudes of the observations, and sea surface heights.

In support of Lageos, the relativity algorithms were studied and modified to be more correct, a network timing bias was created, and the procedure for polar motion was simplified.

Values of solar and magnetic flux and tables of universal and atomic time have been updated. Program documentation has been modified in a effort to reflect the current status of the software. Subroutines were modified to be more efficient and the overlay structure was updated.

In the software development, we have tried to be responsive to the current needs. Geodyn is a very complex program, consequently, all modifications are difficult. As we handle so many observation data types and complex earth models any modification in one area causes problems to the other areas. At times, the modifications seem to come slowly and when manpower and money are lowered, progress is even more difficult. Despite these problems, the program has performed adequately.

FUTURE EMPHASIS

In the near future the program will be upgraded to support Seasat in an optimal way. In particular, the variable area and reflectivity models, three dimensional acceleration time dependent drag coefficient, will be completed for better determination of the atmospheric drag and solar radiation perturbations on the satellite. In general, there will be a continued search for improved earth and orbit modeling such as an albedo model. As new satellite observation data types appear that are useful in this work, they will be added to the program. In addition, there will be a continued search for techniques and numerical procedures that will cut down on computer time and core size without sacrificing the required precision.

A background task is continuing to convert Geodyn to the CDC Star computer. With the predicted changeover of computer systems it is important to find a new machine to continue this work.

PRECISION ORBIT DETERMINATION SOFTWARE VALIDATION EXPERIMENT

OBJECTIVES

The objective of this effort is to intercompare orbit computation software and to identify the differences using simulated as well as real observational data.

BACKGROUND

Precision orbit determination is extremely important to projects such as Seasat which have stringent orbit accuracy requirements in order to meet the mission objectives. For example, the precision of both the altimeter data and the laser observations from Seasat is better than 10 cm. In order to be able to reliably investigate dynamic oceanographic phenomena i.e., topography effects such as cyclonic eddies, Western boundary currents, and equatorial and circumpolar currents at the sub-10 cm level, the radial component of the orbit must be known to this level also.

Orbit computation errors can be attributed to several sources. The most significant of these are due to: Inaccuracies in the models used; errors in the tracking data used, and errors associated with the numerical algorithms used in the orbit determination process. The latter errors are the result of runcation errors, roundoff errors, model approximations and machine or human blunders.

Detailed analyses of model accuracies, e.g., gravity model errors, have been carried out by a number of investigators and reasonable estimates have been established for most of the models. Comprehensive error budgets have also been established for the tracking systems. For example, in the case of the laser systems, rigorous verification and validation tests are continually performed to ensure that the data is of high quality. Many tests have been applied to the numerical algorithms used for orbit determination, separately and as a whole unit. However, until recently, detailed comparisons had not been carried out among the leading orbit computation programs in the world to ascertain the level of numerical consistency. As part of the Seasat altimeter/orbit determination team activities, a set of experiments were defined to identify the differences in orbit computation software used by the various groups.

RECENT ACCOMPLISHMENTS

Four groups with independently developed orbit determination software packages are involved in this experiment. They are: The Geodyn Program, developed by the Geodynamics Branch at GSFC; the Utopia Program developed by the Department of Aerospace Engineering at the University of Texas; the Celest Program developed by the Naval Surface Weapons Laboratory; and the program developed by the Groupe de Recherches de Geodesie Spatiale of the Centre National d'Etudes Spatiales in Toulouse, France. The programs are completely independent and in many instances use different techniques and procedures. Furthermore they are operating on different computers with different word lengths and so forth. Geodyn is run on the IBM 360/95, whereas the Utopia program is run on a CDC machine.

The experiment consisted of generating simulated data with various gravitational and nongravitational models. The simulated data consisted of laser ranges generated for the GEOS 3 orbit covering the time period of September 8 to 15, 1975. The perfect simulated data were generated at GSFC using the Geodyn program and they have been made available to the other organizations for their analysis. The final portion of the analyses consisted of the generation of an ephemeris based on the simulated data which can be compared with the original Geodyn ephemeris which was used to generate the simulated data. Differences between the Geodyn ephemeris and the other orbits, as well as the measurement residuals, have been used to identify problems in the programs.

The results of the experiment to date have been very encouraging. No major blunders have been discovered in the programs. Some differences and shortcomings have been revealed, however. For example, the linear interpolation of the nutation rotation matrix over a one-day interval in Geodyn was found to produce 10 cm orbit differences. Differences larger than 10 cm were noted when the solar radiation pressure perturbation was activated in Geodyn and Utopia. This is believed to be due to some limitations in the Utopia program.

In summary, our results to date indicate that the current level of consistency among the Geodyn, Utopia, and Celest programs is about 1 cm radially and well under 10 cm crosstrack and alongtrack. All options and combinations of force models have not yet been exercised in this experiment and this task is currently in progress.

An additional experiment has been undertaken using real laser observations on the Starlette satellite. An orbital arc of data seven days in length has been selected for this test. The current level of orbital agreement is 6 cm radially and 20 to 30 cm crosstrack and alongtrack. Further tests are in progress with this set of real data.

SIGNIFICANCE

With the sub-10 cm precision available from observational systems such as Dopplers, lasers and altimeters, and the many applications in many diverse areas such as studies of ocean dynamic processes, estimation of plate motion, variation in the Earth's rotation and the position of the pole, orbital accuracy requirements are reaching an unprecedented level. Although, during the development of the programs numerous checks on internal consistency were carried out, this experiment represents the first time that such comprehensive software comparisons have been made.

The current results indicate that radial orbit uncertainties due to software errors with real data on a relatively stable orbit such as Starlette are on the order of 5 cm.

FUTURE EMPHASIS

Future work will be concerned with an expansion of this experiment to include more details of the force models, particularly drag and solar radiation press and with the resolution of some of the existing differences. Further work will also be conducted with additional real observational data on other satellites such as Seasat and Lageos in addition to Starlette.

A GRAVITY FIELD SATELLITE

OBJECTIVES

The purpose of the gravity field satellite mission is to study the structure of the lithosphere, the physical properties of the mantle, and the velocity distribution of the ocean.

BACKGROUND

The possibility of flying a dedicated gravity field satellite mission, resulting in a worldwide set of gravity anomalies, promises to provide important data bases in the areas of solid Earth geophysics and oceanography. In solid Earth research, the study of the mechanical properties of the lithosphere, resource distribution, and total Earth density models each have important positions in GSFC's overall Earth physics research program toward a global geophysical model. The gravity anomalies give information about the bending of the lithosphere under the weight of mountain ranges. Models based on anomalous mass distributions under different geological regions can be tested by looking at the gravity anomaly structure. In the area of resource identification, calculations have been made at GSFC relating the gravity field to subcrustal stress fields and in turn demonstrating a correlation between tension stress and resource deposits. Information theory models have been formulated which convert the gravity field into a "most likely" interior density distribution.

In oceanography, the gravity field geoid can combine with altimetry to provide more accurate ocean circulation models. The geoid is by definition the surface of the ocean when it is at rest. The altimeter measures the surface of the actual dynamic ocean. The difference between these two surfaces can be used to infer the underlying velocities of ocean circulation. These circulation models are an integral part of the GSFC programs in climate and weather forecasting. Ocean circulation provides the primary mode of heat transport from the equatorial region to the high latitudes.

The data set to which Gravsat would contribute is currently composed of gravity anomalies acquired through land and ocean surface surveys. On 1° x 1° blocks, these vary in accuracy from 10 to 90 mgals, with the more accurate being on the land areas. A new data set is currently being made available based on the recent GEOS 3 altimetry. These measurements can be converted to gravity anomalies over the ocean areas. Papers being published in the next month claim that these GEOS 3 gravity anomalies are good to the 7 mgal level. This accuracy level has been demonstrated by comparison with highly accurate ship measurements which can be made on the 4-5 mgal level. GEOS 3 promises to map much of the ocean area from 65°S to 65°N latitude with ± 7 mgal, 1° x 1° gravity anomalies. The major mission areas are the land masses of South

America, Africa, and Asia (where the altimeter cannot measure the approximate geoid represented by the sea surface) and the polar areas (which are beyond the GEOS 3 orbital range).

RECENT ACCOMPLISHMENTS

During the current fiscal year, the main effort in the mission science area has been to define the goals in ocean sciences and Earth physics and to describe the programmatic inputs needed to achieve these goals. The two general goals which have been identified are improved weather forecasting capability and a global geophysical model. The inputs in the weather area include incident solar radiation, sea surface state, ocean circulation, etc. In the global geophysical model, one would consider tectonic processes, interior density models, polar motion, etc. Within these two program goals, Gravsat can provide improved data. We will study the error budgets in the various inputs and determine at what level the Gravsat analysis will have to proceed in order to contribute.

The National Academy of Sciences has held a workshop sponsored by NASA/GSFC to study the value and applicability of a dedicated gravity satellite. The report of this workshop provides a detailed analysis of the scientific data which would flow from a Gravsat Mission.

SIGNIFICANCE

The two support areas in this mission, namely, error analysis simulations and hardware design, require immediate study. There is at present a controversy in the error simulations as to whether the accuracy of the resulting gravity anomalies is primarily limited by the details of the numerical data reduction procedures or rather by the noise in the measurement hardware. If it is hardware limited, then we should put most of our effort into design feasibility studies. Auxiliary systems such as a Doppler transmitter (to allow tracking by the Tranet system) and a radar altimeter on the low orbiting satellites (to adjust intersecting orbits) might also make significant reductions in the Gravsat error budget.

FUTURE EMPHASIS

Studies will continue to establish the data requirements within the Gravsat scientific objectives and refine the mission specifications.

CHAPTER 5

GLOBAL EARTH DYNAMICS AND STRUCTURE

OVERVIEW

The goal of the Global Earth dynamics and structure program is to use space-derived and other related data to understand the global dynamics and structure of the Earth.

Data from the Earth's gravity field is derived from analysis of pertubations in satellite orbits and provides information on: The Earth's internal density distribution, mantle convection, elastic properties, and rotation; and the behavior of ocean tides and tidal friction in the Earth-Moon system.

Contributors to this chapter include Michael Graber, Hahn-Schou Liu, James Marsh, David Rubincam, Braulio Sanchez, and David Smith.

INFORMATION THEORY DENSITY DISTRIBUTION

OBJECTIVES

The objective of this project is to make a rational inference as to what the density distribution of the Earth is and investigate its geophysical significance, particularly with regard to convection in the mantle.

BACKGROUND

This is the problem: We do not have enough information about the Earth to say what the density distribution $\rho(r)$ actually is. For instance, if we know only the mass M_E and moment of inertia C_E of the Earth and assume the density distribution to be spherically symmetric, then we do not have enough information to determine $\rho(r)$. There are an infinite number of density distributions which satisfy the constraints of mass and moment of inertia. We cannot invert the data; we must infer a density distribution on the basis of incomplete data. We must find a rational method to pick out the "most likely" density distribution.

It is of extreme interest that the information theory approach of the physicist Jaynes (1975) gives us such a method. Jaynes' approach is to assign each possible answer to a problem (in this case, density distribution) a probability that it is the correct answer. The probabilities are then assigned magnitudes by maximizing Shannon's information measure

$$MI(P_1, P_2, \ldots P_N) = -K \sum_{i=1}^{N} P_i \ln P_i$$

subject to the known constraints (in this case, mass M_E moment of inertia C_E). The rationale for maximizing MI is that it is the measure of missing information, i.e., the amount of information needed to single out the correct answer. If MI is not maximized subject to the known constraints, then we are assuming information we do not have.

Since MI is analogous to the entropy function in statistical mechanics, this method is often called Maximum Entropy Method (MEM), but would be more appropriately named Information Theory Inference (ITI).

RECENT ACCOMPLISHMENTS

The problem of the spherical symmetric density distribution with constraints M_E and C_E was solved in the following way. The earth was divided into infinitesimal cubes of equal volume. Indistinguishable particles of identical mass were distributed among the cubes. The density at any point was then the number of particles in the cube in question times the mass of the particles, divided by the volume of the cube. Each possible distribution of particles amongst the cubes was given a probability P_i and MI was maximized subject to constraints $\Sigma P_i M_i = \overline{M}_E$ and $\Sigma P_i C_i = \overline{C}_E$, where M_i and C_i are the mass and moment of inertia, respectively of the ith model and $\overline{M}_E$ and $\overline{C}_E$ are experimentally measured values for mass and moment of inertia.

The problem was then shown to be completely analogous to the grand canonical ensemble in statistical mechanics, where particles are distributed among energy levels. The canonical ensemble methods were then used to obtain the average number of particles in each cube. The resulting average density distribution is a half-Gaussian:

$$\overline{\rho}(r) = 12.30e^{-1.46r^2/a_E^2} \text{ gm/cm}^3$$

and is shown in figure 5-1, along with K. E. Bullen's optimum distribution, based on all known (mostly seismic) information. The agreement is remarkably good, considering the information theory density distribution uses only two pieces of information: Mass and moment of inertia. This work described above was published in Rubincam (1978).

Subsequent work focussed on the lateral variations in the density distribution. The problem here was to find the most likely three-dimensional density distribution $\overline{\rho}(\vec{r})$ using the spherical harmonic coefficients $\overline{C}_{lm}$ and $\overline{S}_{lm}$ of the geopotential as constraints. The coefficients are almost the only source of information on lateral density variation. Only recently has seismic data given some crude information on this. The emphasis in this work is to relate the density variations to possible convection in the mantle.

The problem in lateral variation was solved using the statistical mechanical techniques described above, plus these important assumptions: The density distribution can be written as a sum of spherical harmonics of the form

$$\rho(\vec{r}) = \rho(r,\phi,\lambda) = \sum_{\ell=o}^{\infty} \sum_{m=o}^{\ell} \sum_{i=1}^{2} \overline{\rho}_{\ell mi}(r)\, \overline{Y}_{\ell mi}(\phi,\lambda)$$

and the lateral variations are taken to be small perturbations on top of the well-known spherically symmetric density distribution. In Dziewonski, et al., (1975), a parametrized model was taken to be in the gross radial distribution.

The resulting information theory coefficients in the above equation have the form $\rho_{\ell mi} \sim r^\ell$ where ℓ is the degree of the harmonic.

A computer program was written to compute and plot relative density variations in the mantle for shells of various radii and slices through the center of the Earth along various great circles (see figure 5-2). The results show that the total relative density variations are about 0.002 g/cm^3 in the mantle after subtracting off a model for 30 km of compensated crust, and about 0.02 g/cm^3 for the same thickness of uncompensated crust. The hydrostatic bulge is subtracted out in all cases, using a model of W. M. Kaula's (1967). The maps show diminishing variations towards the center of the Earth. Most of the variation is concentrated in the top of the mantle. A sample plot is shown in figure 5-3. The density increases from -3 to +3 units. The interval between units is 0.0001 g/cm^3. The great circle intersects the equator at 59° longitude and is inclined 33° to the equator.

SIGNIFICANCE

The information theory technique is definitely shown to be a practical as well as theoretical tool for understanding the Earth's structure. It also indicates that the density variations are very deep, and not confined to the crust and top of the mantle.

FUTURE EMPHASIS

Taking shells and slices here and there did not appear to give good indication of the three-dimensional structure of the variations, and work towards the end of the year concentrated on taking many slices through the Earth along fixed latitudes. This work, as well as interpretation of the variations, is now in progress. The method will also be extended to include estimates of the elastic parameters so that seismic data can be used in determining the Earth's structure.

REFERENCES AND PUBLICATIONS

Dziewonski, A.M., A.L. Hales, and E.R. Lapwood, "Parliamentary Simple Earth Models Consistent With Geophysical Data," *Phys. Earth Plan. Int.*, *10*, 12-48, 1975.

Jaynes, E.T., "Information Theory and Statistical Mechanics," *Phys. Rev.*, *106*, 620-630, and *108*, 171-190, 1957.

Kaula, W.M. "Geophysical Implications of Satellite Determinations of the Earth's Gravitational Field," *Space Sci. Rev.*, *7*, 769-794, 1967.

Rubincam, D.P., "Information Theory and the Earth's Density Distribution," NASA TM 78088, 1978, revised edition. NASA TM 80586; also submitted to *Geophysical Journal*, 1979.

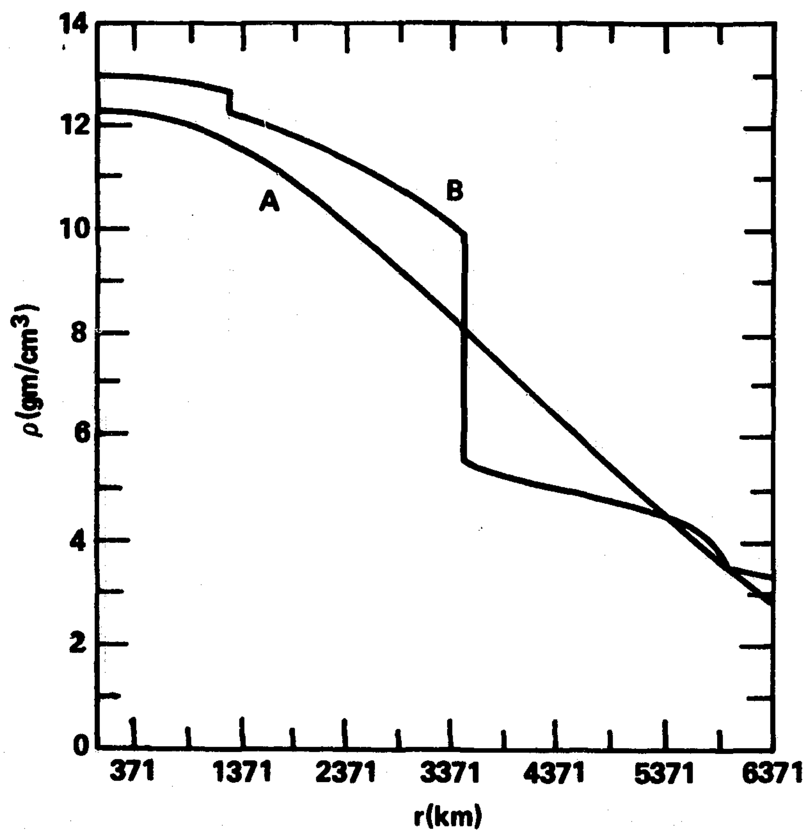

Figure 5-1. The Information Theory Density Distribution Using Maxwell-Boltzmann Statistics (Curve A) and the Optimum Density Distribution of Bullen, 1975 (Curve B) Shown as a Function of Radial Distance r

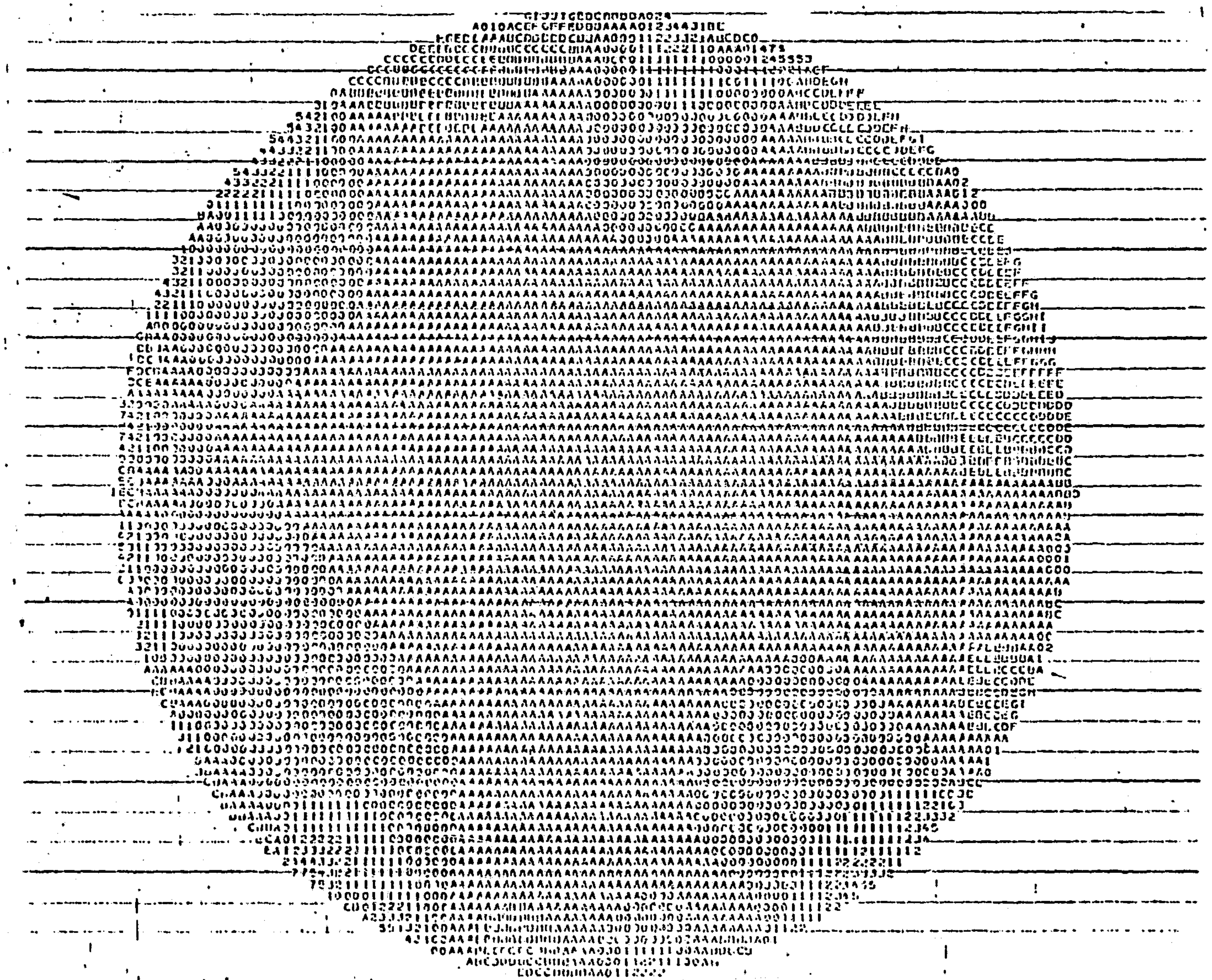

Figure 5-2. Computer Printout Used to Plot Earth's Density Distribution

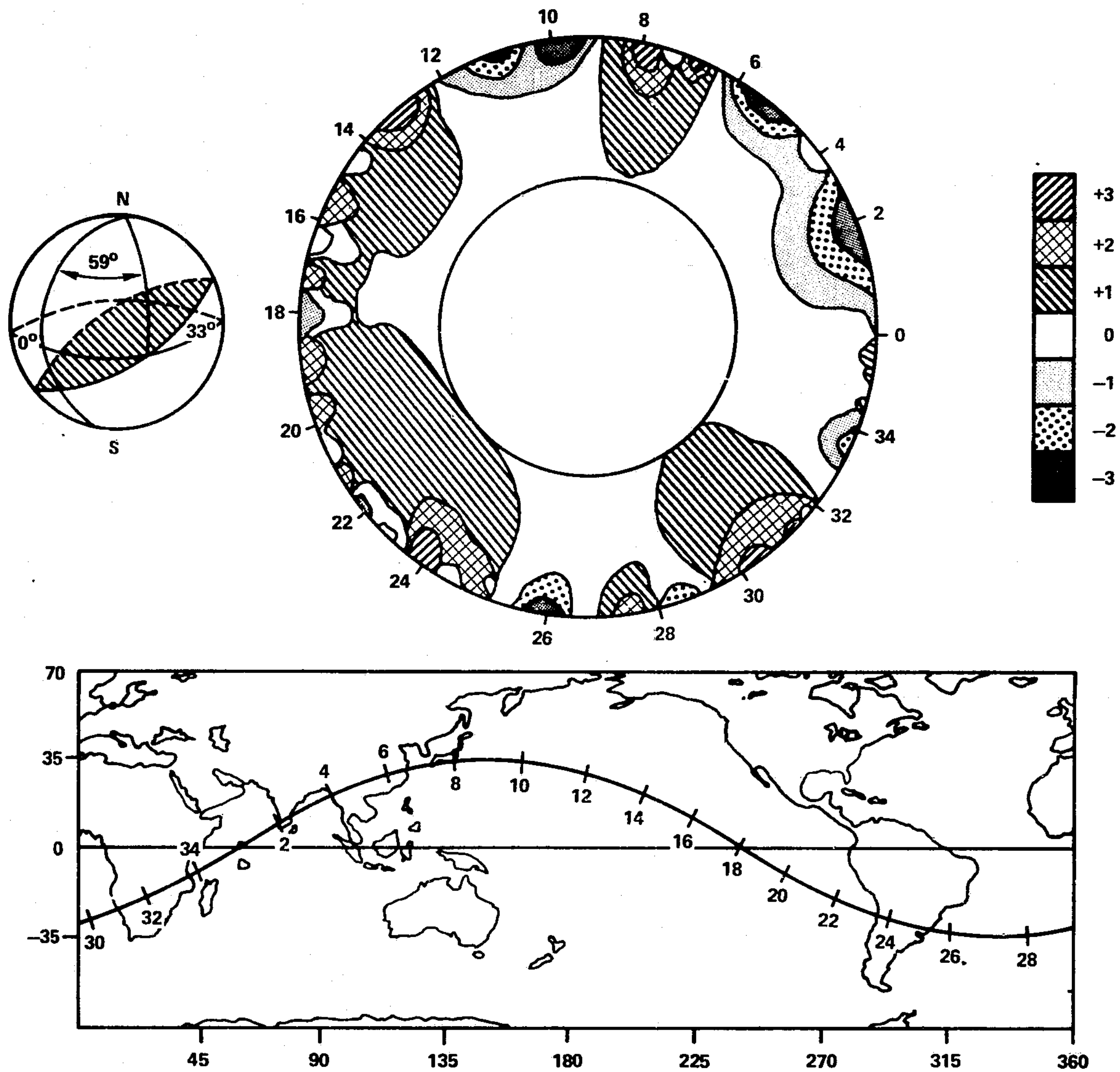

~~5-7~~ 131

Figure 5-3. Sample Plots Showing the Earth's Density Distribution

MANTLE CONVECTION AND SUBCRUSTAL STRESS

OBJECTIVES

Research in the theory of mantle convection is currently confronted with a variety of geodynamic problems of practical interest. Studies on tectonic forces as inferred from satellite gravity data have revealed a convection generated stress system which seems to provide a unifying mechanism for uplift, depression, rifting, seismicity, volcanicity, magmatism, magnetism and ore deposition in Africa. In order to extend the investigation of the applicability of the convection generated stresses for crustal deformation, this work proposes to calculate mantle convection patterns and subcrustal stress fields under Asia and Australia from satellite and surface gravity data.

BACKGROUND

The main problem of mantle convection currents is to determine their patterns from geodynamics data rather than on theoretical or speculative grounds. The departure of the Earth's gravity field from the hydrostatic model must be explained because of the importance of solid-state creep in the mantle in terms of the density differences driving the convection currents. It is therefore possible that most progress will be made in this important subject by searching for the geodynamics data of non-elastic behavior of the Earth from satellite observations of the geopotential and the geoid. For the development of a mechanism unifying geodynamic phenomena, the laminar viscous flow model of the Earth's mantle can be applied to the new satellite-derived geopotential fields for calculations of a stress system in the lower crust. The development of tectonic, seismic, and metallogenic features should be explainable in terms of this single stress system.

RECENT ACCOMPLISHMENTS

Mantle Convection Pattern and Subcrustal Stress Field Under Australia

Gravity data of the Earth have been applied to calculate the subcrustal stress field under Australia caused by mantle convection. According to the stress patterns, all interior regions in the Australian continent appear to be in a state of compression. The directions of these compressional stresses are about east-west and their magnitudes are in the order of 10^8 dyn cm^{-2}. It is found that the upwelling mantle convection flows under Australia diverge to the eastern region under the eastern highland belt and the regions under the uplifted western shield (see figure 5-4). The Australian basin systems seem to be related to the downwelling mantle convection flows (see figure 5-5).

The tensional stress fields, caused by the upwelling mantle convection flows, are shown to be regions of structural kinship characterized by major concentration of mineral and metal deposits in Australia (see figure 5-6). The relationship between current tension and ore deposits may be one involving uplift of the crust and thus explosure of the Precambrian basement rocks with fluid inclusions of ore deposits. The uplift of the eastern highland and western shield in Australia since the Pliocene time shows there exists a possible correlation between the upward movement of the fluid inclusions of ore deposits and the upwelling mantle convection flows under these regions.

The steps from gravity field, to mantle convection flows, to extentional tectonics, to mineral deposits are a long series of geology. It is difficult to make a good case for the jump from the first to the last. The essential question is one of geological time scale. In this paper, comparison of the mantle convection pattern and the Tertiary to Recent tectonic and igneous activities in Australia has been made to provide answers for the seemingly puzzling question.

The concept of ultimate mantle control, via zones of tensional weakness of the crust, on the distribution of mineral deposits is not new. Economic geologists have provided useful reviews of mineral exploration and genesis of ore deposits in the literature. Striking evidence of such megastructural controls on the distribution of certain economic minerals is emerging. A broader knowledge of tensional fractures of world importance, of their habits, their patterns and their mathematics, could have a profound bearing on an exploration policy. It is hoped that this contribution will not only enhance the economic geologist's ideas, but also present some useful guidelines for future mineral exploration in the continent. A full description of this work has been scheduled for publication in *Modern Geology* (Liu 1979).

Mantle Convection Pattern and Subcrustal Stress Field Under Asia

Gravitational models derived from satellite tracking and surface gravity have been used to derive the forces in the mantle of the earth under Asia. Based on studies of tectonic forces from these models, a subcrustal stress field under Asia has been obtained. The stresses are due to mantle convection.

According to the stress patterns, the east and west China crustal blocks and five seismic zones are identified. The tensional stresses exerted by the upwelling mantle convection flows under the crust of Tibet seem to be related to the Tibetan uplift. The compressional orogenic region from the southern tip of Lake Baikal, through Tien Shan, Hindu Kush and the Himalayas to northern Burma appears to be connected with the downwelling mantle convection flows. These tensional and compressional subcrustal stresses caused by mantle convection are shown in figure 5-7.

It has been found that the directions of the subcrustal stresses under China are disposed perpendicularly to the major fault systems and seismic belts (see figure 5-8). The results of stress calculations show that the crust of North China should be in compression and that stresses within it should be sufficient to form the Shansi Graben and Linfen Basin systems and fracture the lithosphere. This gives a possible explanation of why strong earthquakes occurred in North China which is an isolated narrow region of highest seismicity far from plate boundaries. The tensional stress fields, caused by the upwelling mantle convection flows, are found to be regions of structural kinship characterized by major concentrations of mineral and metal deposits in China (see figure 5-9). A description of this work has been published by Liu (1978).

SIGNIFICANCE

The subcrustal stress fields under Australia and Asia caused by convection flows in the upper mantle have been established to the twenty-fifth degree harmonics of the geopotential. The stress fields thus derived are consistent with the tectonic, metallogenic, and seismologic features in these continents. The results have provided a basis for seismogenic modeling of intraplate earthquakes and delineating target areas for ore prospecting.

FUTURE EMPHASIS

This work will be developed and applies to establish mantle convection patterns and subcrustal stress fields under North and South America.

REFERENCES AND PUBLICATIONS

Liu, H.S., "Convection Pattern and Stress System Under the African Plate," *Physics of the Earth and Planetary Interiors, 15, 60-68,* 1977.

Liu, H.S., "Mantle Convection Pattern and Subcrustal Stress Field Under Asia," *Physics of the Earth and Planetary Interiors, 16,* 247-256, 1978.

Liu, H.S., "Mantle Convection and Subcrustal Stresses Under Australia," *Modern Geology,* in press, 1979.

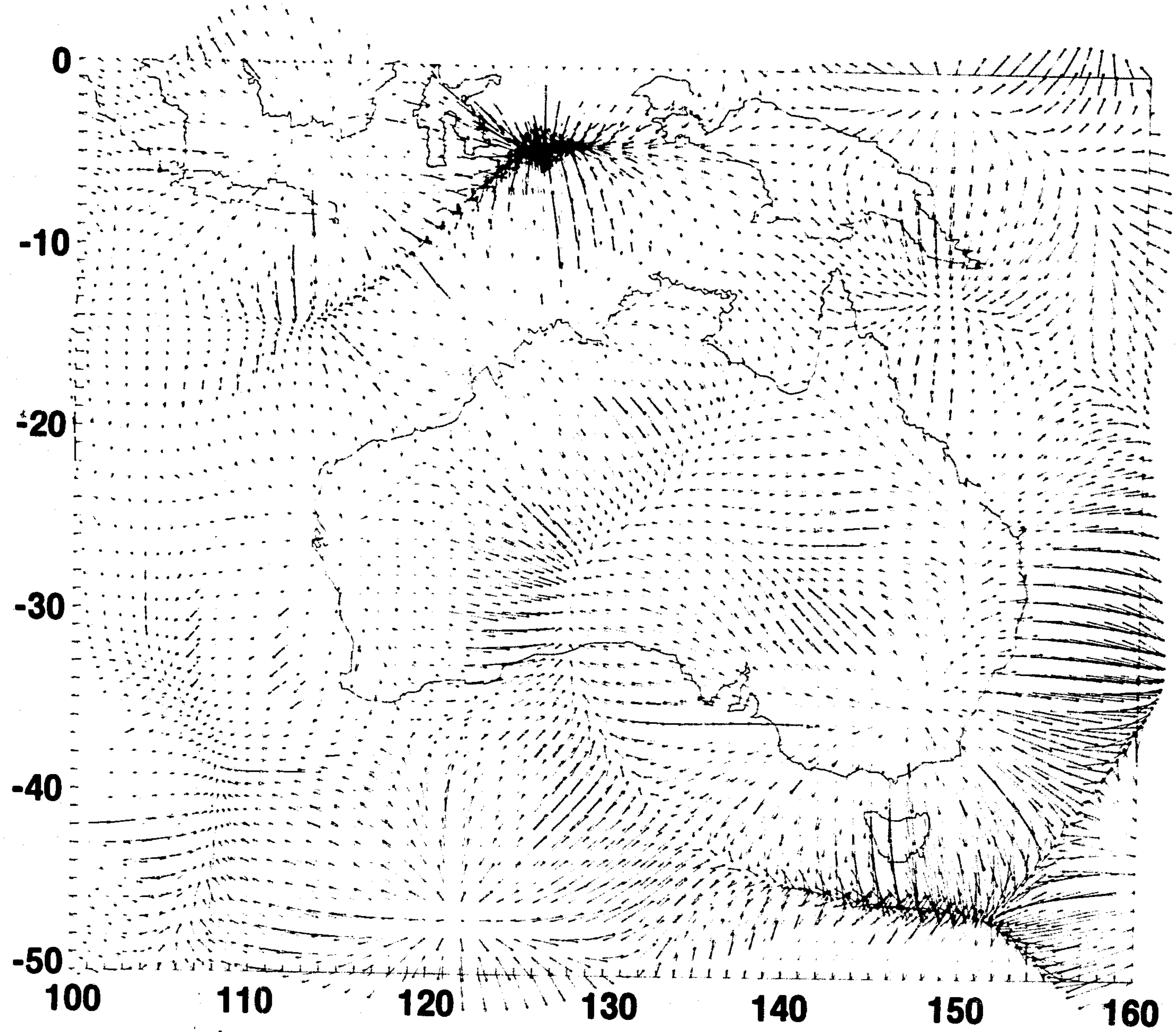

Figure 5-4. Subcrustal Stresses Exerted by Mantle Convection Under Australia

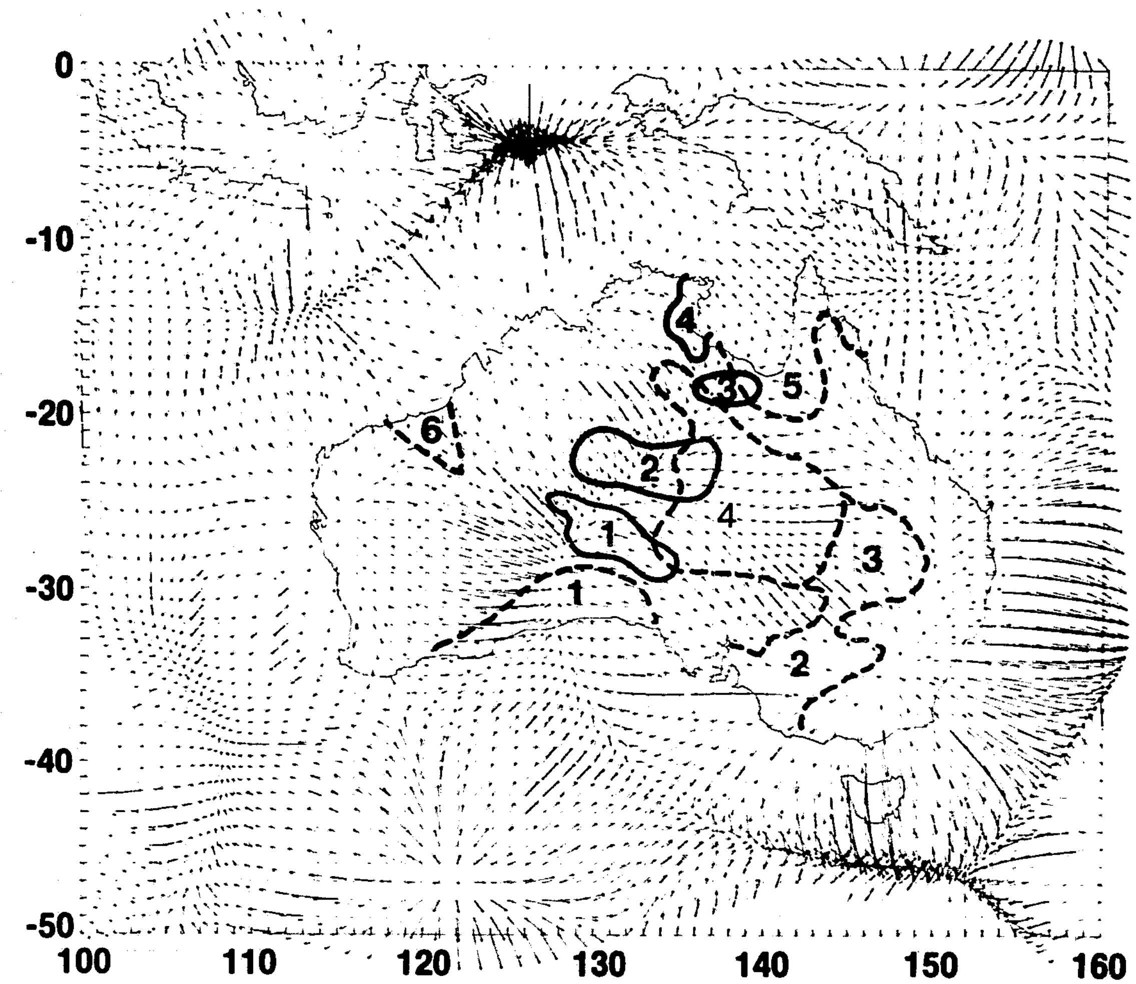

THE PRECAMBRIAN TO SILURIAN SYSTEM:
1. OFFICER BASIN
2. AMADEUS—NGALIA—GEORGINA BASIN
3. SOUTH NICHOLSON BASIN
4. ARAFURA—McARTHUR BASIN

THE TERTIARY TO QUATERNARY SYSTEM:
1. EUCLA BASIN
2. MURRAY BASIN, ST. VINCENT BASIN
3. DARLING—WARREGO BASIN
4. LAKE EYRE BASIN
5. CARPENTARIA BASIN
6. OAKOVER BASIN

Figure 5-5. Mantle Convection Pattern Under Australia and the Australian Basin Systems

ORIGINAL PAGE IS OF POOR QUALITY

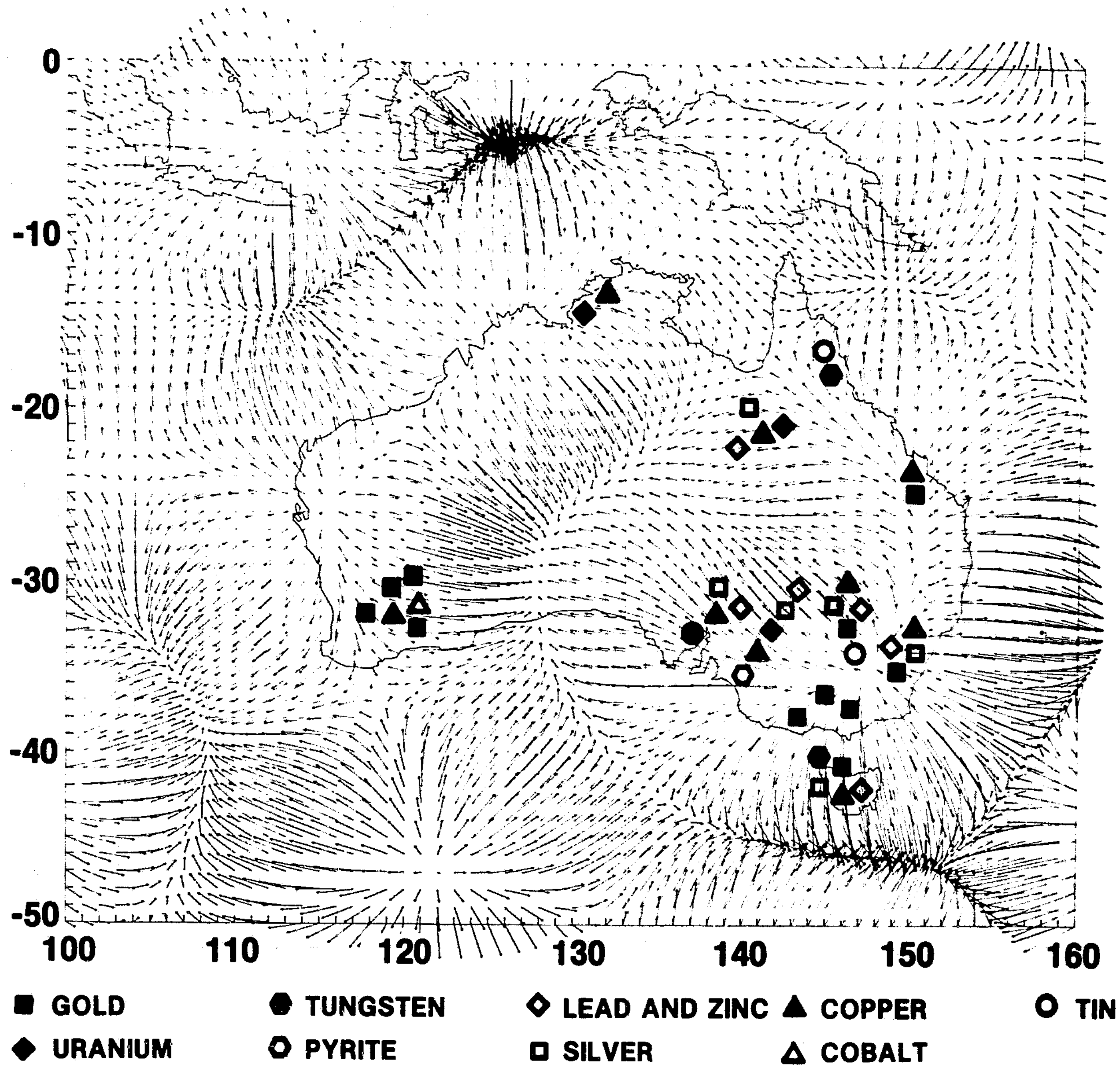

Figure 5-6. The Distribution of the Principal Mineral and Metal Deposits in Relation to the Tensional Subcrustal Stress Systems in Australia

5-13
137

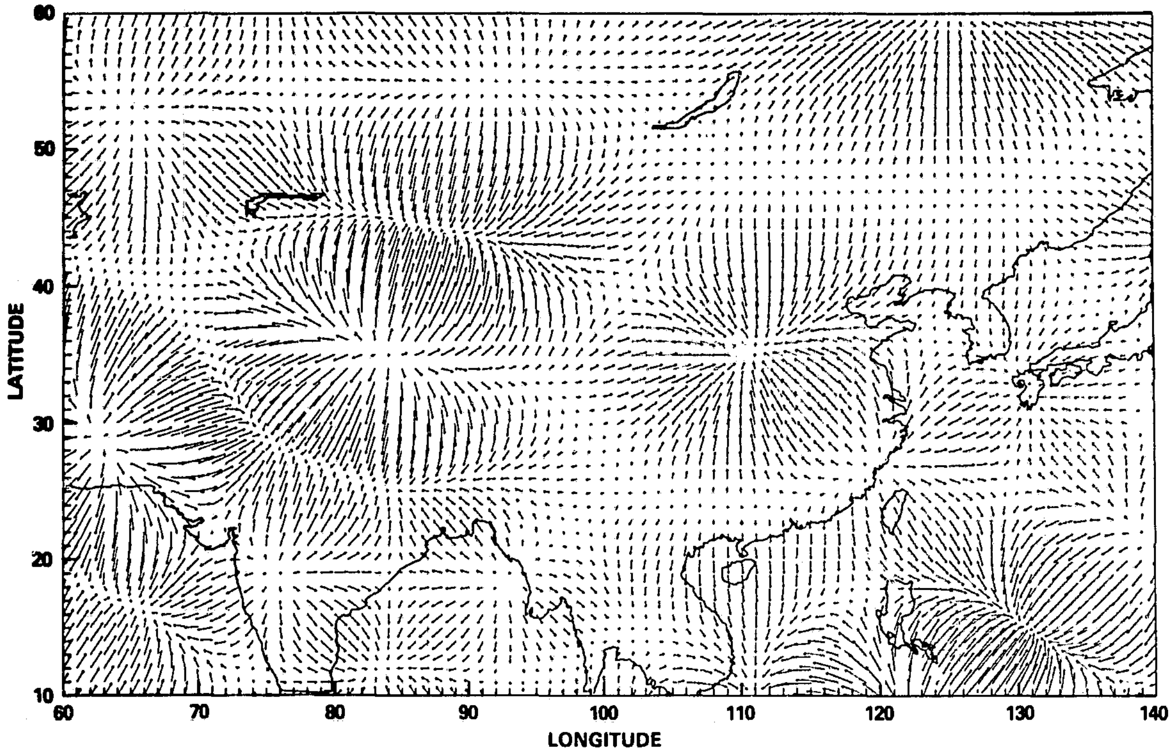

Figure 5-7. Subcrustal Stresses Exerted by Mantle Convection Under Asia

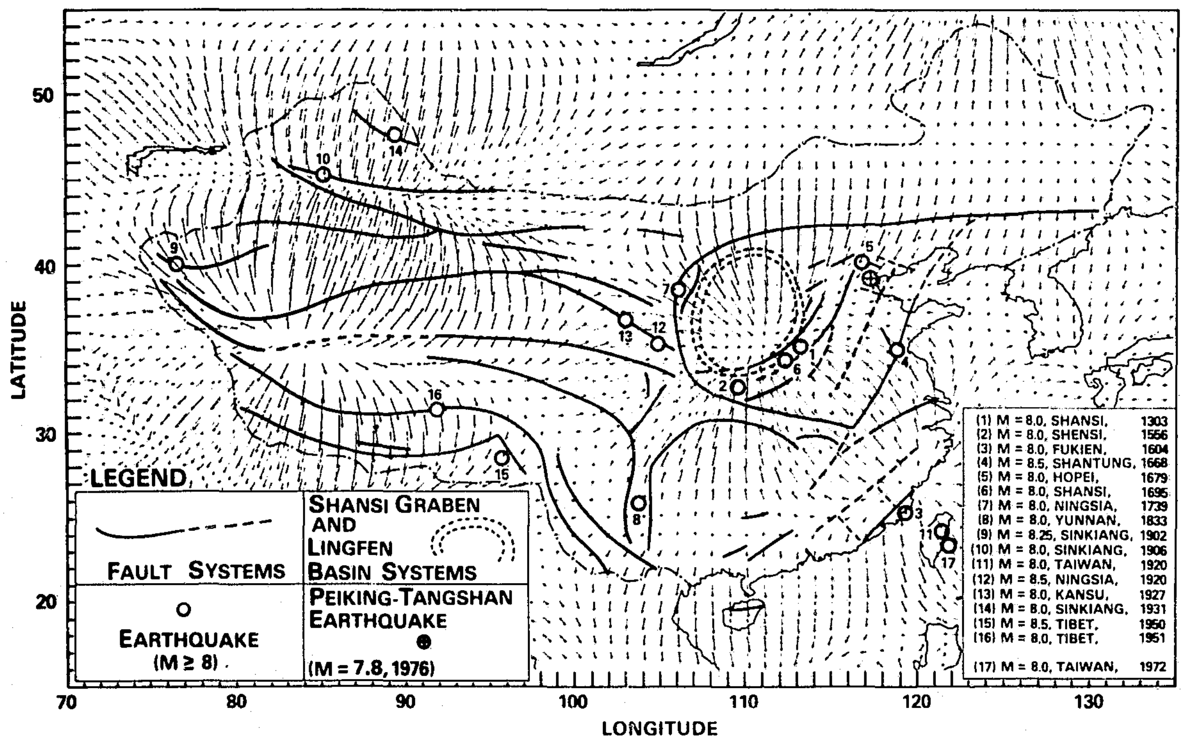

Figure 5-8. Subcrustal Stress Pattern and Seismological Features in China

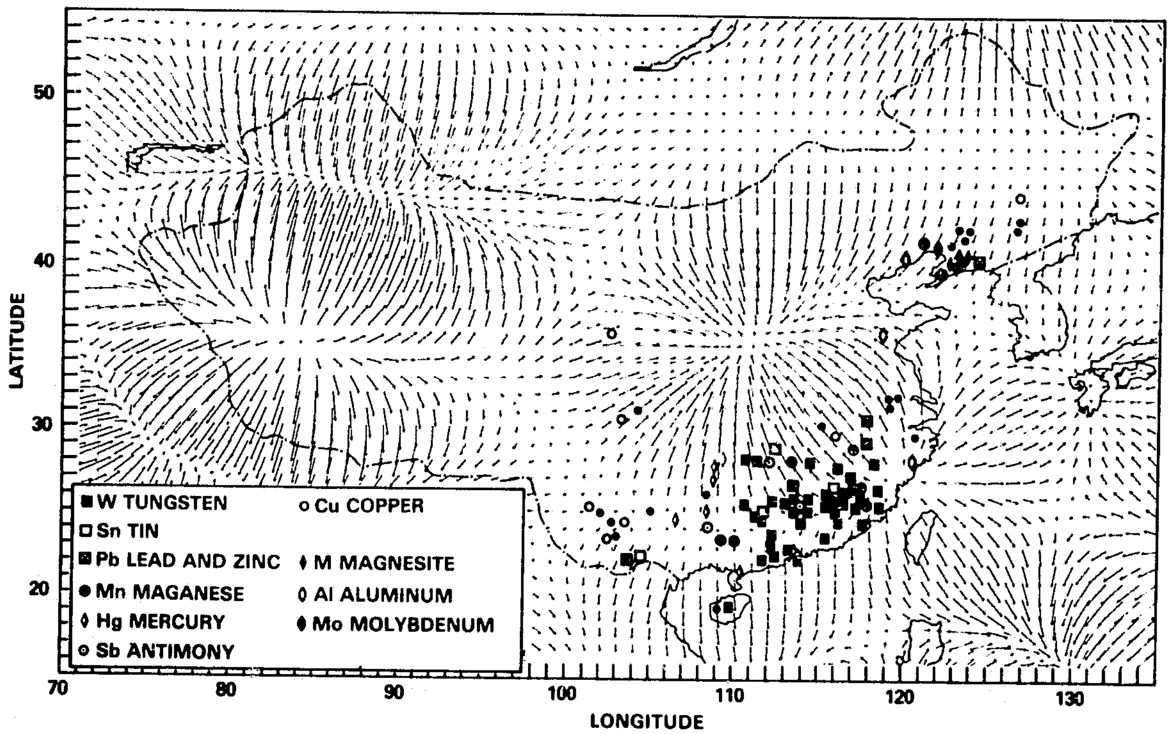

Figure 5-9. The Distribution of Mineral and Metal Deposits in Relation to the Tensional Subcrustal Stress System in China

GRAVITY ANOMALIES IN THE PACIFIC DERIVED FROM SATELLITE-TO-SATELLITE DOPPLER TRACKING DATA AND IMPLICATIONS FOR MANTLE CONVECTION

OBJECTIVE

The objective of this work has been to study the gravity undulations in the vicinity of the East Pacific Rise through the analysis of GEOS 3/ATS 6 SST Doppler tracking data.

BACKGROUND

Density variations within the earth give rise to convection and also produce gravity anomalies. The connection between gravity anomalies and thermal convection in the earth was clearly shown in a theoretical study by Pekeris (1935). Later, in drawing attention to the theorem by Von Zeipel which gives the conditions necessary for hydrostatic equilibrium within a rotating radioactive planet, Verhoogen (1949) used Pekeris's results and the Earth's gravitational field to estimate a convective velocity in the mantle of a few centimeters per year.

With the establishment of the kinematics of plate tectonics it has become increasingly clear that this model furnishes explanations for most of the magnetic, bathymetric, and heat flow anomalies observed in the ocean basins. It is now known that only second order variations in heat flow and bathymetry can be used to identify the style of convections within the mantle. However, theoretical and numerical studies (e.g., McKenzie, 1977) suggest a more direct, first order connection between thermal convection and gravity anomalies. In short, if the convection is strong enough to deflect the lithosphere, then an upwelling current will cause a positive gravity anomaly; the hot upwelling material alone, were it not able to deflect the surface upward, would of course cause a negative gravity anomaly. Current theories of mantle convection (Elsasser, et al., 1979), (Davies, 1977) propose that convection may be taking place at two levels in the Earth's mantle. Primary convection is believed to be taking place throughout the entire depth of the mantle. This whole mantle convection results in the formation of cells which have surface dimensions comparable to the sizes of the plates. Clear evidence of this phenomenon is presented in gravity anomaly maps which correspond to the low degree and order (up to 12,12) coefficients in the GSFC GEM gravity models.

In the circum Pacific area where the cold dense material is downwelling along the Pacific Plate boundary, a clear pattern of positive gravity anomalies is observed. Elsasser, et al., (1979) have also proposed that near surface (700 km) instabilities in the mantle should produce convection rolls within the overall large scale convection pattern. The laboratory experiments of McKenzie and Weiss (1975) have shown that the convection rolls will be established more rapidly under fast moving plates than under slow moving ones. The tentative absolute plate velocities determined by Minster, et al. (1974) suggest that only the Pacific, Nazca, and Cocos plates have been moving fast enough and long enough to have established the pattern of longitudinal rolls beneath them. Thus our analyses of gravity data have been concerned primarily with the Pacific plate.

In a world-wide study, Marsh and Marsh (1976) used a gravitational field model complete to the thirtieth degree and order (PGS110, Lerch 1976) to look for short wavelength gravity anomalies which might indicate a pattern of convection as suggested by theoretical studies (Richter and Parsons, 1975). They removed a field model complete to the twelfth degree and order and the highest order harmonics, beyond n, m=23, and found that this field consists almost wholly of anomalies possessing a wavelength of about 2000 km. Where correlations were possible, they found a close correlation between bathymetry and gravity and a close correspondence to surface gravity maps, although this latter correlation is not surprising since the field model contained a great amount of this same surface data in addition to satellite data. A peculiar pattern of anomalies of alternating sign was also found spanning the Pacific basin, striking approximately northwest. Along the east Pacific rise a hint of a correspondence between gravity and bathymetry was also noted. Many of the anomalies within the Pacific are of small amplitude (~10 mgal) while the uncertainties are often as large as 8 mgal. Although the pattern of anomaly uncertainties does not resemble the anomaly pattern, the map must be viewed with caution. Marsh and Marsh were also concerned with the possibility of introducing purely numerical perturbations into the resulting map through the procedure of truncation of the spherical harmonic field model.

RECENT ACCOMPLISHMENTS

East Pacific Gravity Anomalies

The present study was undertaken to obtain accurate gravity anomalies in the region of the east Pacific rise that: would be independent of any particular gravitational field model, could be used to check the higher degree and order part of existing field models, would not use a huge collection of spherical harmonic coefficients, and would supply much needed gravity data in this region which could be analyzed for the detection of convection rolls. Since there is little hope of obtaining extensive sea surface gravity measurements in this area, the new method of SST was used.

SST Doppler tracking data is obtained by using a stationary, relative-to-Earth, satellite (ATS 6) maintaining an altitude of 40,000 km to track a lower satellite (GEOS 3) flying in a nearly circular orbit (840-km altitude). See figure 5-10 for an illustration of this configuration. Doppler tracking furnishes range rates as a function of time which, when corrected for long wavelength orbital perturbations, can be easily converted to line-of-sight (between ATS 6 and GEOS 3) accelerations or gravity anomalies. By reducing the orbits using a gravitational field model complete to only the twelfth degree and order, gravity anomalies with wavelengths smaller than about 3,300 km could be revealed. The profiles of anomalies can then be used to construct a gravity map.

A total of 28 passes of satellite-to-satellite tracking data have been analyzed. The consistency of the data has been measured by comparison of signatures of passes having a similar ground track but separated by several weeks in time. These comparisons revealed a high level of repeatability. An example of such consistency is shown in figure 5-11 which presents results which agree quite well for revolutions 254 and 453 which are coincident. A test of the accuracy of the residuals is possible from passes which traverse the U.S. where the PGS-110 field and surface gravity data closely agree. Three such passes of SST residuals over the U.S. show excellent agreement with the residuals predicted by the PGS-110 model, thus confirming that the observed residuals can be attributed to high-degree perturbations in the gravitational field of the Earth.

Error analyses indicate that if orbital arc lengths of one revolution or less are used, the effects of high-order geopotential coefficients will indeed produce the dominant signature in the SST residuals.

At the outset of this investigation, orbit computations were performed for several revolutions using the PGS-110 coefficients through (4,4) in order to test the sensitivity of the data to the gravity field of the Earth. The residuals due to the unmodeled gravitational effects above (4,4) were quite large, amounting to about one cm/sec. Such residuals for revolution 240 are presented in figure 5-12. Theoretical residuals computed using the PGS-110 coefficients above (4,4) also shown in this figure, are in excellent agreement with these observed residuals. Since the main goal of this analysis was to study gravity anomalies defined by the higher degree and order terms, orbital solutions were subsequently computed using a (12,12) gravity model.

Figure 5-13 presents a contour map of the accelerations at the GEOS-3 altitude derived from the 28 passes of SST Doppler data. The uncertainty in the map is on the order of 5 mgals at the surface of the Earth.

A comparison of the SST derived gravity maps with corresponding maps computed using the PGS-110 gravity model, Rapp's model (1977) based solely upon surface gravity data and the GEM 10 model shows the maps to be essentially similar. The positives and negatives are generally in the same places. On closer inspection, however, the broad, undulating anomalies shown along track are more similar to the pattern of surface anomalies and the GEM 10 anomalies and less so to the somewhat shorter wavelength and more east-west striking PGS-110 anomalies. The amplitudes of the anomalies are generally about the same for all but the map of surface data, but recall that the 5° surface gravity anomalies estimated in this region were based upon sparse 1° data.

This analysis of satellite-to-satellite Doppler data for gravity anomaly perturbations in the Pacific has clearly indicated the presence of anomalies with wavelengths of about 2000 km. This direct observation has confirmed and provided additional detail for earlier gravity anomaly maps based upon sparse surface gravity data or conventional tracking data. The presence of such anomalies tends to imply that we may be observing upper mantle convection in this area. Additional analyses with the recently acquired satellite-to-satellite tracking data which covers the entire Pacific with a 1 to 2° resolution are expected to provide a clearer picture of the detailed gravity anomaly field in the Pacific Ocean area and thus provide an important basis for forming conclusions about convection in the mantle in this region. Further details on this work may be found in Marsh and Marsh, 1978 and Marsh, et al., 1977.

SIGNIFICANCE

The following important conclusions have been reached as a result of these analyses:

- The agreement is good between the SST-derived gravity anomalies and anomalies derived from conventional tracking techniques.
- Gravity anomaly signatures can be derived using simple computation techniques with SST data
- The SST data provide a very accurate test for existing gravity models.
- The data provide a means of accurately computing gravity data over land.

- The SST data provide a new data type for geophysical interpretations and the preliminary set of data available to date has indicated that gravity anomalies with wavelengths of about 2000 km exist in the Pacific which may be related to convection in the upper mantle in this area.

- It can provide an independent check on the altimeter-derived anomalies at intermediate wavelengths.

- The existing set of SST data provides a real data set for simulating the proposed gravity mapping satellite mission.

FUTURE EMPHASIS

After the previously discussed data were collected, the ground tracking stations were modified to record the Doppler data in a "nondestruct" mode. This modification increased the precision of the SST data from about 0.6 mm/s to less than 0.3 mm/s. With the new system, 5° gravity anomalies can probably be derived with an accuracy of about 1 mgal in the surface of the Earth. Over the past several months, we have collected a comprehensive grid of these data which provide about 1° to 2° coverage over the mid-Pacific Ocean area. These data are currently being analyzed and techniques are being developed so that they can be used to provide information on such problems as the mantle convection processes in the Pacific.

REFERENCES AND PUBLICATIONS

Elsasser, W.M., P. Olson, and B.D. Marsh, "The Depth of Mantle Convection," *J. of Geophysical Res., 84*, 147-155, 1979.

Davies, G.F., "Whole Mantle Convection and Plate Lectonics," *Geophys. J., 49*, 59-486, 1977.

Lerch, F.J., "The PGS-110 Gravity Model," private communication, 1976.

Marsh, B.D. and J.D. Marsh, "On Global Gravity Anomalies and Two-Scale Mantle Convection," *J. Geophys. Res., 81*, 5267-5280, 1976.

Marsh, B.D. and J.G., "Short Wavelength Gravity Anomalies in the Pacific," *J. Geophys. Res., 83*, 3555-3558, 1978.

REFERENCES AND PUBLICATIONS (continued)

Marsh, J.G., B.D. Marsh, T.D. Conrad, W.T. Wells, and R.G. Williamson, "Gravity Anomalies Near the East Pacific Rise with Wavelengths Shorter Than 3300 km Recovered from GEOS-3/ATS-6 Satellite-to-Satellite Doppler Tracking Data," NASA TM 79553, 1977.

McKenzie, D.P. and F. Richter, "Convection Currents in The Earth's Mantle," *Scientific American, 235*, 5, 72-89, 1977.

McKenzie, D.P. and N. Weiss, "Speculations on the Thermal and Tectonic History of the Earth," *Geophys. J. Roy. Astron, Soc., 42*, 131-174, 1975.

Minster, J.B., T.H. Jordan, P. Molnar, and E. Haines, "Numerical Modeling of Instantaneous Plate Tectonics," *Geophys. J. Roy. Astron. Soc., 36*, 541-576, 1974.

Pakeris, C.L., "Thermal Convection in the Interior of the Earth," *Monthly Notice of the Royal Astronomical Society, Geophysical Supplement, 3*, 8, 343-347, 1935.

Rapp, R.H., "Potential Coefficient Determinations from 5° Terrestrial Gravity Data," Dept of Geodetic Science, Ohio State University, Report No. 251, 1977.

Richter, F.M. and B. Parsons, "On the Interaction of Two Scales of Convection in the Mantle," *J. Geophys. Res., 80*, 2529-2541, 1975.

Verhoogen, J., "Von Zeipel's Theorem and Convection in the Earth," *Trans. Amer. Geophys. Union*, 32, 41-43, 1949.

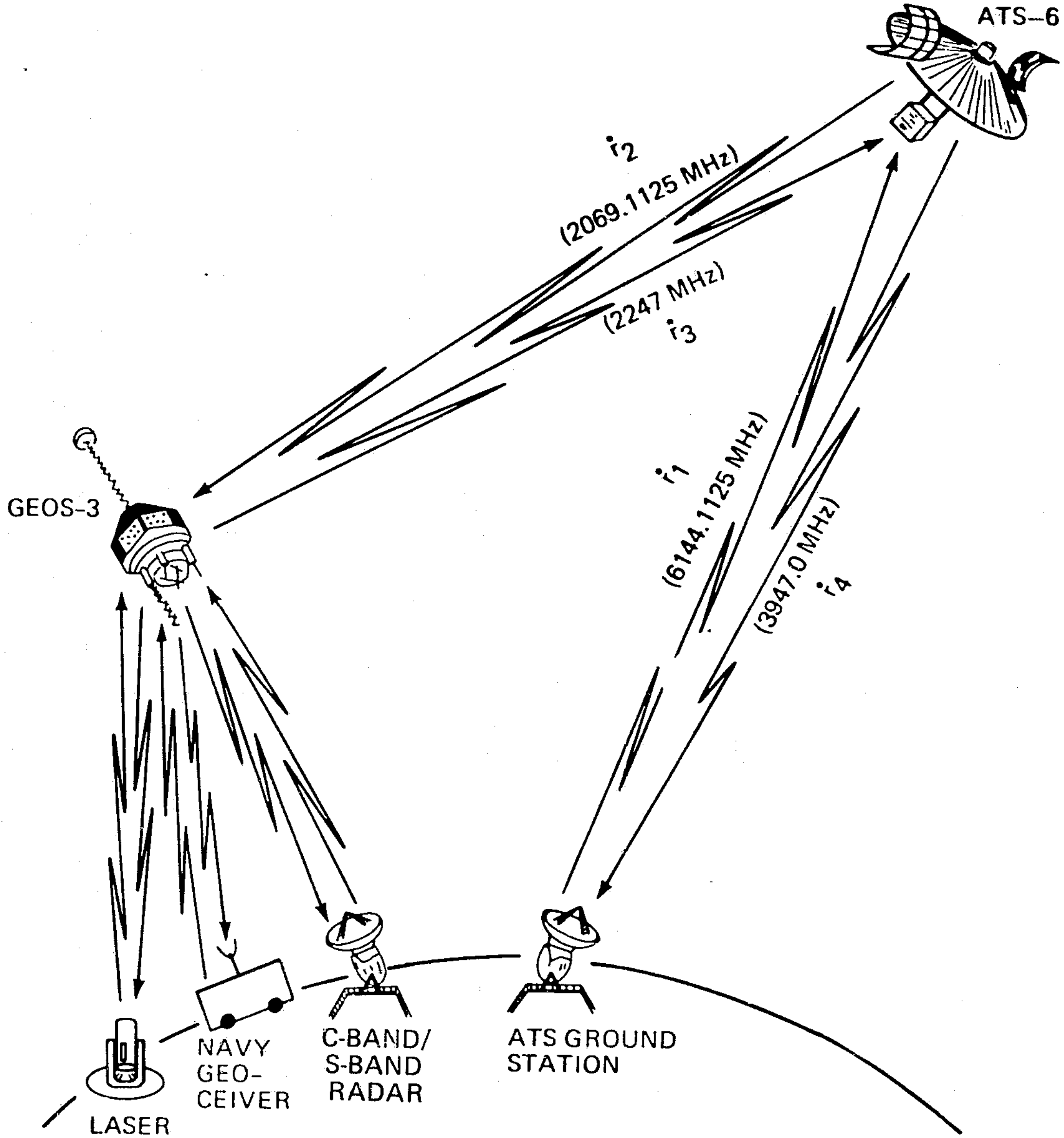

Figure 5-10. ATS 6/GEOS 3 SST Geometry

5-22

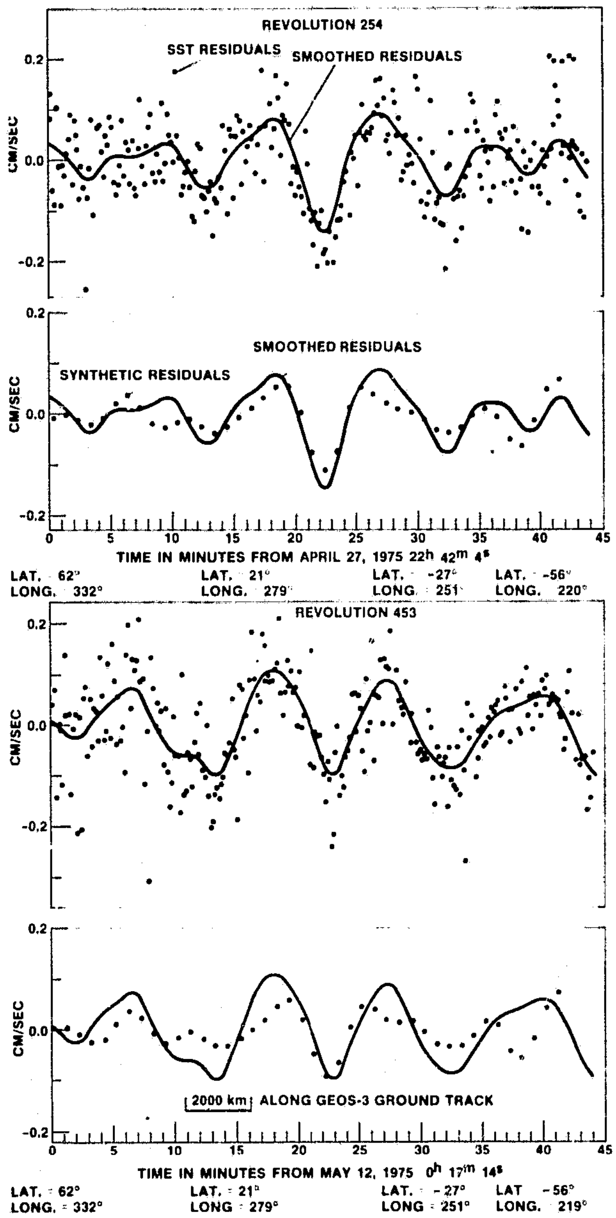

Figure 5-11. GEOS-3/ATS-6 SST/Range Rate Residuals Computed Using PGS-110 Gravity Model Coefficients to (12,12) Along Overlapping Ground Tracks

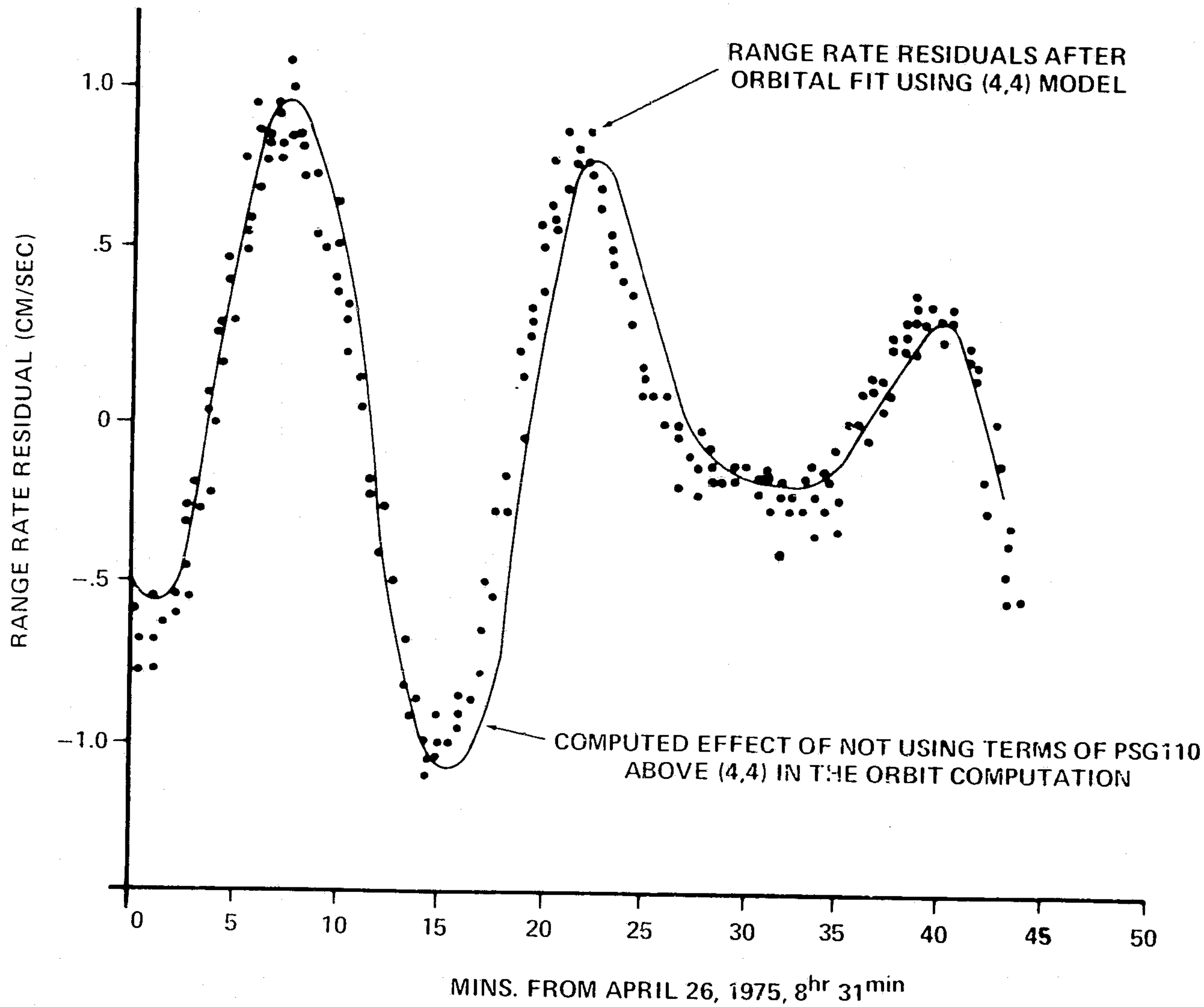

Figure 5-12. GEOS 3/ATS 6 SST Range Rate Residuals Computed Using PGS-110 Gravity Model Coefficients to Degree and Order (4,4)

5-24

148

ORIGINAL PAGE IS
OF POOR QUALITY

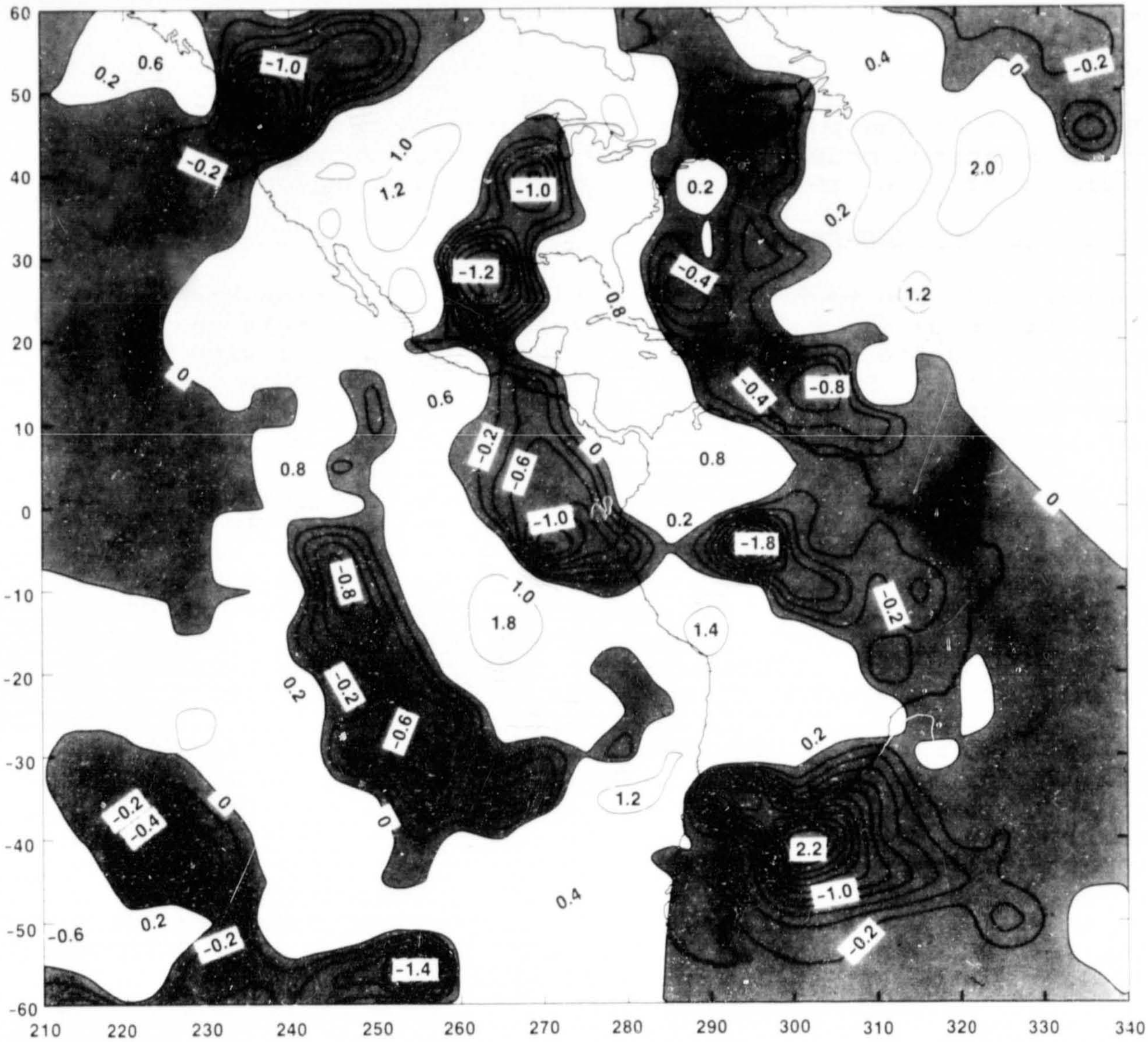

Figure 5-13. Contour Map Showing GEOS 3/ATS 6 Satellite-to-satellite Accelerations Relative to the PSG-110 (12,12) Gravity Model

POLAR MOTION RESEARCH

OBJECTIVES

The purpose of polar motion research is to study the motion of the rotation axis of the Earth in a coordiante system fixed within the Earth and to correlate this motion with other geophysical processes.

BACKGROUND

The motion of the pole was first measured 85 years ago. The introduction of modern high-speed computers has reopened the field, where the great masses of numbers made analysis difficult.

RECENT ACCOMPLISHMENTS

During 1978, two technical memoranda in polar motion research were completed and submitted to professional journals and are currently in the revision stage. These papers deal with the description of the statistical properties of the pole position time series as represented by the International Polar Motion Service measurements.

In the first paper, daily average latitudes were analyzed. As a result, significant differences in the annual wobble were noted for each observatory. Additional oscillations were noted for each observatory. Additional oscillations were noted at 304 days and 148 days. The residual spectrum was analyzed according to Schuster's test and it was concluded that there remained further time-dependent process in the data which would require a more accurate measurement technique for their solution.

In the second paper, the primary star pair observations (which produce the average latitudes) were analyzed. Using a least-squares approach, the high-frequency spectrum out to two cycles per day was analyzed. Unexpectedly large oscillations at one and two cycles per day were developed in the analysis. Because of the data acquisition technique used by the International Polar Motion Service, the peaks may be due to the mechanics of the instrument handling. As an independent check it is proposed to do a similar calculation using Lageos data.

SIGNIFICANCE

This area of research is important because the pole position time series is sensitive to the internal structural properties of the Earth. Differences in geophysical models show small differences in the polar motion. Determining the driving mechanism for the central 431-day process in the Earth's wobble will require detailed knowledge of the motion for its solution.

FUTURE EMPHASIS

The ability to model 50-day Lageos arcs to relatively small residuals opens up a new area of polar motion analysis at GSFC. Using standard Fourier analysis orders of magnitude, data over 50 days will provide a frequency resolution to the inverse of the data length, or 0.02 cycles per day. This provides sufficient discrimination to allow searching the high-frequency region for the presence of tidally-induced polar motion and to look for possible excitations near one or two cycles per day.

Since the Lageos data has typically only one satellite pass per day, the high-frequency cutoff would be at about one-half cycle per day. This cutoff can be extended by including passes from other satellites such as Starlette and BE 3. The data for each solution would be structured so that Lageos provides the long-term continuity (and thus high resolution) while the other satellite data provide the high-frequency sensitivity.

The typical manner for performing this type of analysis is to first solve for a series of pole positions and then to perform a Fourier analysis of this time series. However, with the satellite range data, the optimal method is to include the high-frequency component in the condition equation for the polar motion which is within the Geodyn computer program. This technique will solve for just two additional parameters, a phase and an amplitude. Preliminary tests indicate that a 30-day Lageos arc can fit the amplitude of a high-frequency sinusoid to 0".003.

The analyses represent a new region of polar motion time series analysis: the high frequencies above 0.25 cycles per day. It is expected that when they are completed, a new picture of the polar motion process will emerge.

REFERENCES AND PUBLICATIONS

M.S. Graber, "Analysis of Daily Latitude Variations," NASA TM 79585, 1978.

M.S. Graber, "Analysis of Star Pair Latitudes," NASA TM 79593, 1978.

POLAR MOTION FROM LAGEOS

OBJECTIVES

The objectives of our studies are to regularly determine the position of the pole from Lageos together with the appropriate statistics, and identify the major periods and significant features in the motion that could be ascribed to a geophysical origin.

BACKGROUND

The motion of the pole of rotation of the Earth is a sensitive measure of changes in the distribution of the Earth's mass. Earthquakes, atmospheric motions and the movements in the oceans are all sources of excitation of polar motion. Since the launch of Lageos in May 1976 and until the end of 1977, the position of the pole has been derived from laser tracking of the spacecraft. The tracking data were collected by systems of GSFC and the Smithsonian Astrophysical Observatory from sites in North and South America, and Australia, and the pole position has been determined every 5 days.

RECENT ACCOMPLISHMENTS

The method that was used to determine the pole was to initially form a series of contiguous precise orbital arcs of Lageos beginning at launch in May 1976 and continuing through December 1977, each about 30 days in length. During each orbital arc the station network was rotated every five days about the x and y polar axes to provide a new pole position. Further details of the method can be found in Smith, et al., (1978). Figure 5-14 shows the x and y coordinates of the pole determined from Lageos by this method. The constants used in the calculations were the GEM 10 gravity field out to degree and order 10 (Lerch, et al., 1977), the second degree Love number $k_2 = 0.29$, and station coordinates derived from the first eight months of the mission (Smith, et al., 1978). The major features of the polar motion are an annual period of 365 days and a Chandler period of about 430 days. Solving for an amplitude and a phase for each of these in the x-component we obtained the solid curve shown in figure 5-14. The residuals about the solid curve appear to be almost random and the curve seems to be a good approximation to the longterm polar motion in x. The standard deviation of a point about the solid line is about 0.025 arcseconds.

A similar fitting of the annual and Chandler motions to the y-component reveals a small 212-day period as well. Including this term as well, we obtain the solid line for y in figure 5-14. The standard deviation about the line is about 0.02 arcseconds.

The equations for the solid lines are:

$$x = 0.050534 - 0.0000491246\ t$$
$$-0.071442 \cos \omega_c + 0.059494 \sin \omega_c$$
$$-0.003751 \cos \omega_a - 0.186518 \sin \omega_a \text{ (arcseconds)}$$

$$y = 0.30374 - 0.0000864748\ t$$
$$+0.048845 \cos \omega_c + 0.171850 \sin \omega_c$$
$$-0.063426 \cos \omega_a - 0.025155 \sin \omega_a$$
$$-0.010541 \cos \omega_b + 0.017662 \sin \omega_b \text{ (arcseconds)}$$

Where $\omega_c = (\frac{2\pi}{430})t$, $\omega_a = (\frac{2\pi}{365})t$, $\omega_b = (\frac{2\pi}{212.2})t$ and t = day of year 1976.

The time dependent terms in x and y were obtained in order to absorb any effects due to periods long compared to the data span. No special interpretation can be given to the amplitudes of the annual and Chandler terms because of the shortness of the data span. Both appear to give amplitudes of about 0.2 arcseconds.

The center of curvature of the pole derived from the solid lines in figure 5-14 is shown in figure 5-15. Dramatic changes in the motion are shown to occur around certain dates (marked on the figure) but there appears to be no correlation with the occurrence of earthquakes. The largest earthquake that occurred during this period (May 1976 to December 1977 was near Indonesia, magnitude 7.9, on August 19, 1977, and is reported to have caused one of the largest free oscillations since the 1964 Alaska earthquake (A. Dahlen, 1978, private communication).

The excitation pole shown in Figure 5-15 is an extremely simplified version of the true motion because it is derived from approximation. The sudden changes in direction are probably not geophysically meaningful, particularly with respect to the data, but it is of interest to note that for over one year the motion of the excitation pole was located in a small region inside the general polar motion and in the general vicinity of the center. he data would seemingly suggest that for this period (September 1976 to September 1977) there were no major events that caused the excitation pole to move dramatically. Interestingly, this period includes the harsh northern winter of 1976/1977 which it has been speculated, might show in the polar motion due to the existence of large and long duration low-pressure regions. If however, one reads greater precision into the basic measurements, then this simple method of estimating the curvature is completely inadequate and it may be that a more careful derivation of the excitation pole might reveal further information.

SIGNIFICANCE

To date, this investigation has demonstrated that polar motion can be derived from laser tracking of Lageos by a few stations to an accuracy comparable to the classical astronomical method.

FUTURE EMPHASIS

It is evident that both a greater precision in the polar motion and a longer data span are necessary. The ultimate capability of this method is believed to be at least an order of magnitude better than is presently being achieved, and that the current major limitations are data quality and the locations of the tracking stations. Hopefully, improvements will be made in both these areas in the near future.

REFERENCES AND PUBLICATIONS

Lerch, F. J., S. M. Klosko, R. E. Laubscher, C. A. Wagner, "Determination of Polar Motion and Earth Rotation from Laser Tracking of Satellites," presented at the Eighty-second IAU Symposium, San Fernando, Spain, 1978. "Gravity Model Improvement Using GEOS-3 (GEM 9 & 10)," *J. Geophys. Res.*, *84*, 3897-3916, 1979.

Smith, D. E., R. Kolenkiewicz, P. J. Dunn, and M. Torrence, "Determination of Station Coordinates from Lageos," presented at the Second International Symposium on the Use of Artificial Satellites for Geodesy and Geodynamics, Lagonissi, Greece, 1978.

Smith, D. E., R. Kolenkiewicz, P. J. Dunn, and M. Torrence, "Determination of Polar Motion and Earth Rotation from Laser Tracking of Satellites," presented at The Eighty-second IAU Symposium, San Fernando, Spain, May 8-12, 1978.

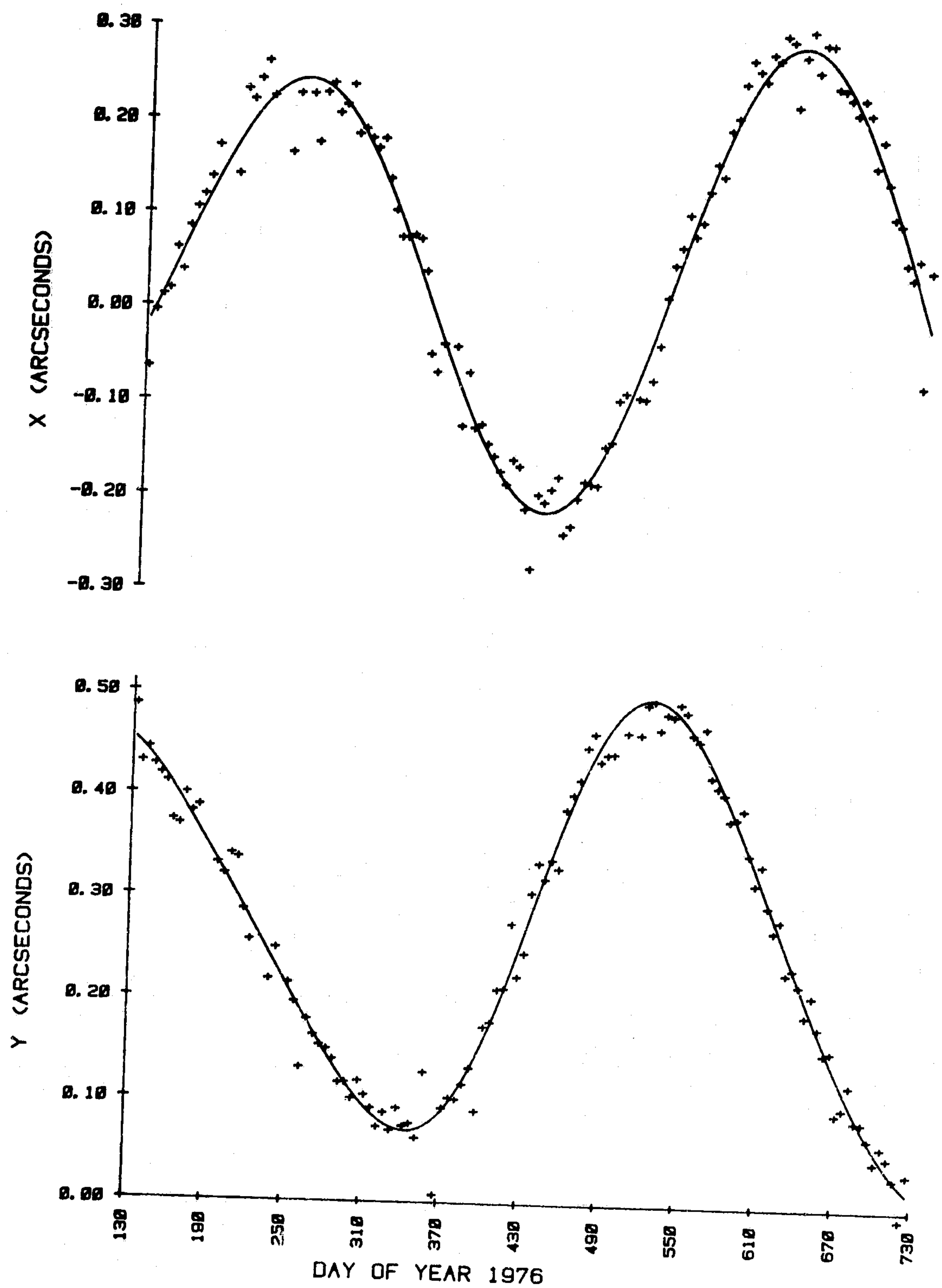

LAGEOS POLAR MOTION (JUNE 1976 - DECEMBER 1977)

Figure 5-14. Lageos Polar Motion (June 1976 to December 1977)

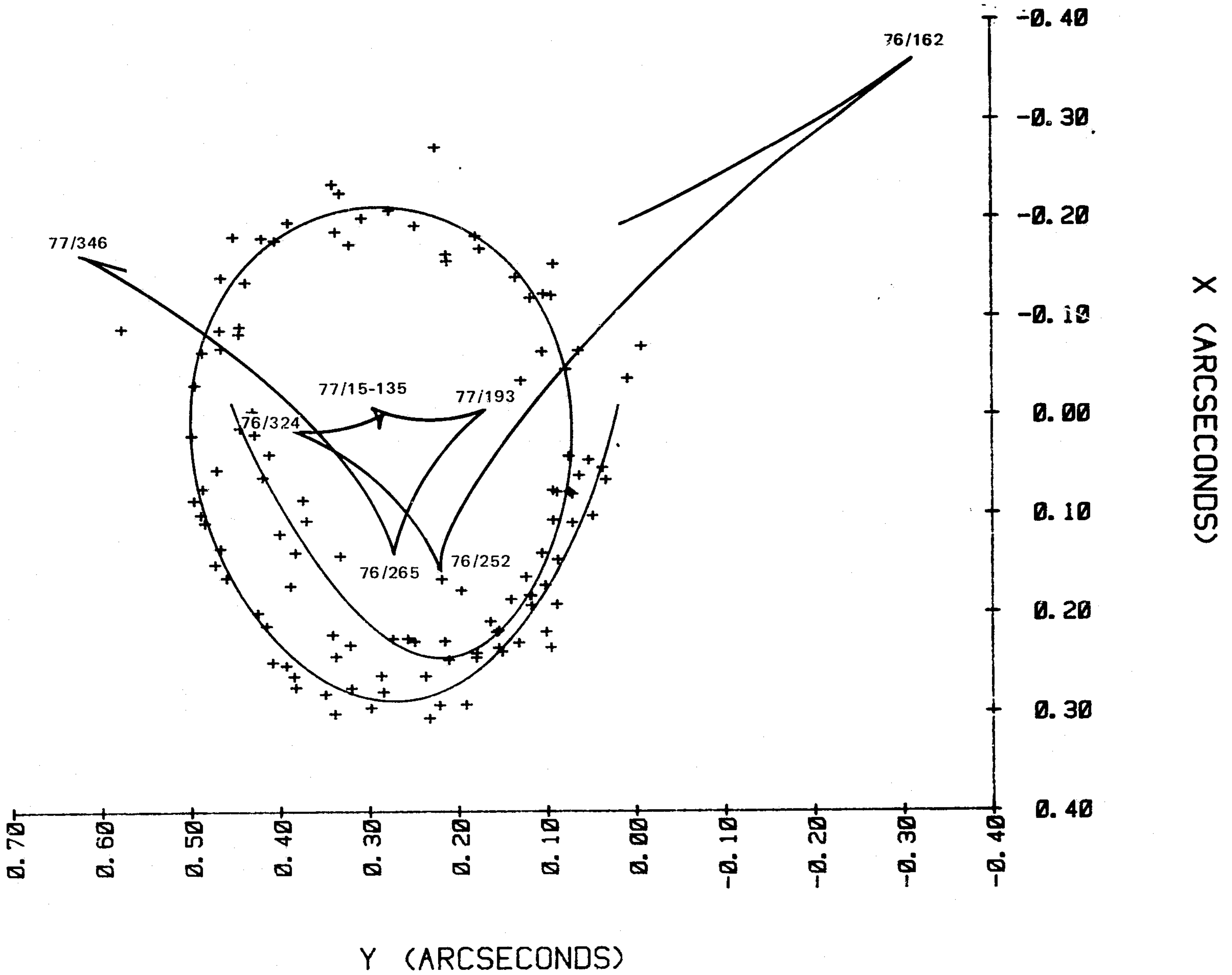

Figure 5-15. Polar Motion and Excitation Pole

5-32
156

OCEAN TIDAL EXCITATION OF POLAR MOTION

OBJECTIVE

The objective of this investigation is to ascertain the response of the rotational motion of the Earth to forcing functions produced by the water mass redistribution due to the ocean tides. In particular, it is desired to obtain the components of displacement of the rotation axis at the surface of the Earth. The investigation also addresses the larger question concerning the possibility of excitation of the Chandler wobble of the Earth.

BACKGROUND

One of the areas of interest in present day geophysics deals with the excitation of the polar motion of the Earth, that is, how do the different physical phenomena taking place inside and on the surface of the Earth affect the position of the rotation axis and the rate of rotation.

Among the many geophysical phenomena, one must consider the redistribution of the mass of the ocean produced by the gravitational tides due to the Sun and the Moon. Such a redistribution of mass yields changes in the inertia tensors of the Earth which themselves are the causes of changes in the position of the rotation axis and the rate of rotation. All the changes involved are functions of time with various periodicities.

RECENT ACCOMPLISHMENTS

In order to ascertain the ocean tidal effects the Liouville equations of motion for a nonrigid body have been simplified by neglecting higher order terms and an analytic solution has been found for the ω_x and ω_y components of angular velocity. Such a solution involves the magnitude of the changes in the products of inertia I_{xz} and I_{yz} due to the various ocean tidal components, as well as the frequencies of the tides and the natural frequency of rotation of the Chandler wobble.

The evaluation of the changes in I_{xz} and I_{yz} can be divided in two categories. Changes produced by ocean tides with periods of the order of a day and changes produced by long-period ocean tides, in particular the solar annual one. The method of evaluation depends on the category, and the effects produced by each are considerably different in order of magnitude.

The products of inertia due to the short-period ocean tides have been obtained by making use of spherical harmonic representations of the tide heights. These representations are fits to numerical solutions of the Laplace tidal equations and, as such, represent nonequilibrium solutions. In particular, the harmonic coefficients used were those provided by C. Goad (1978)* and the LTE solution used was provided on Estes (1977).

The long-period ocean tides were treated differently since no harmonic expansions were available. The equilibrium response of an ocean covering the entire surface of the Earth was formulated. The tidal height for the real Earth was then obtained by means of the ocean function which is equal to one over the oceans and zero over the continents. In particular the (8 x 8) ocean function harmonic expansion due to Munk and MacDonald was used. In order to solve for the products of inertia, it was then necessary to solve the integrals over the sphere of the product of three surface harmonics of arbitrary degree and order. Such a solution can be found in terms of the "3-j" symbols often found in quantum mechanics.

A summary of the results obtained for the products of inertia is given in table 5-1 where

$$I_{xz} = M_{xz} \cos (f_i t - \phi_{xzi})$$

$$I_{yz} = M_{yz} \cos (f_i t - \phi_{yzi})$$

and the subscript "i" refers to the particular tidal component. The magnitudes M_{xz}, M_{yz} are given in units of 10^{33} gm-cm^2. The corresponding results for ω_x and ω_y are given in table 5-2, where

$$\omega_x = W_x \cos (f_i t - \phi_{\omega xi})$$

$$\omega_y = W_y \cos (f_i t - \phi_{\omega yi})$$

The units for W_x and W_y are 10^{-16} radians per second. Table 5-3 gives the maximum displacements for the x and y components of position of the pole in cm units.

The results indicate that only the annual tidal component Sa yields a pole displacement of any significance. This is due to the proximity of its period (12 months) to the period of the Chandler wobble (about 14 months). The calculated tide heights for Sa are of the order of 0.88 millimeters.

SIGNIFICANCE

In general the results show the existence of a polar wobble as a response to each of the components of the ocean tides. The magnitude of the polar displacement depends on two factors: The amplitude of the tidal component, and its period (in relation to the Chandler period). The changes produced by the ocean tides in the products of inertia are periodic and regular; therefore, they cannot be the source of excitation of the Chandler wobble.

---

*Goad, C., NOAA, private communication, 1978.

FUTURE EMPHASIS

The investigation has considered only a few ocean tidal components. A natural and necessary extension will be to use Doodson's expansion of the luni-solar potential to obtain a more complete and systematic representation of the equilibrium (long-period) ocean tides and the resulting polar motion response.

Another possible line of development is to consider the changes in all the components of the inertia tensor (not just I_{xz} and I_{yz}) and to solve the fully nonlinear Liouville equations by means of numerical methods.

REFERENCES AND PUBLICATIONS

Estes, R., "A Computer Software System for the Generation of Global Ocean Tides Including Self-Gravitation and Crustal Loading Effects," NASA X-920-77-82, 1977.

Table 5-1. Products of Inertia Due to Short-period Ocean Tides, f_1-1

Tide	Period (f_1^{-1})	M_{xy}	ϕ_{xy}	M_{yz}	ϕ_{yz}
S_2	12 hr	2.61	-153.5°	1.58	-100.1°
M_2	12.42 hr	6.30	-146.8°	4.46	-114.7°
N_2	12.66 hr	1.16	-144.7°	0.81	- 13.5°
K_1	23.93 hr	9.27	109.6°	22.3	47.1°
O_1	25.82 hr	12.8	83.1°	12.6	49.6°
Sa	1 year	26.9	0°	13.2	0°

Table 5-2. Products of Inertia Due to Short-period Ocean Tides, Wx and Wy

Tide	W_x	$\phi_{\omega x}$	W_y	$\phi_{\omega y}$
S_2	2.97	-161.8°	2.49	- 83.6°
M_2	7.06	-161.4°	6.16	- 90.7°
N_2	1.37	-133.9°	1.22	- 31.0°
K_1	13.3	- 25.9°	13.4	63.9°
O_1	11.3	18.2°	11.3	116.0°
Sa	26436	149.2°	29758	-111.9°

Table 5-3. Products of Inertia Due to Short-period Ocean Tides, x and y

Tide	x	y
S_2	0.0026	0.0021
M_2	0.0061	0.0053
N_2	0.0012	0.0010
K_1	0.011	0.011
O_1	0.0099	0.0099
Sa	23.16	26.07

WHOLE-EARTH TIDAL NUMBERS

OBJECTIVE

The objectives of studying whole-Earth tidal numbers are to estimate the amplitudes and phases of the major gravitational tides produced by the combined effects of the solid-Earth, oceans, and atmosphere; and derive the present day acceleration of the Moon about the Earth.

BACKGROUND

The orbit of the GEOS 3 spacecraft has been analyzed to provide estimates of the amplitude and phase of the gravity tide at seven tidal frequencies: P_1, K_1, S_2, K_2, M_2, O_1, and N_2. The amplitudes of these tides suggest lower values for the diurnal tides compared to the semidiurnal tides indicating a larger ocean tide effect on the diurnal rather than the semidiurnal tides. In addition, the K_1 tide may be showing evidence of the predicted effect of resonance in the core. From the M_2 tidal numbers the acceleration of the moon in its orbit about the earth has been derived and the result of -32 ± 6 arcseconds centuries $^{-2}$ is in general agreement with other recent values.

RECENT ACCOMPLISHMENTS

During a 10-month period beginning shortly after launch in 1975, the orbit of the GEOS 3 satellite was regularly determined from laser tracking data acquired at the Greenbelt, Bermuda, and Grand Turk tracking sites. Each orbit was 24 hours in length, and a spectral analysis of the orbital inclination was obtained from the data. The basic perturbation of the orbital inclination is a large, long-period oscillation (S_2) modulated by a series of shorter-period tides that together cause a total displacement of the satellite of about 10^{-3} degrees in inclination. For the first approximation, the tidal perturbation can be represented by a Love number, k_2, of 0.265 with zero-degree phase (ε_2) for all frequencies. A comparison of the observed perturbation with the first approximation provides residuals that are almost random. Thus the method of obtaining the spectral amplitudes and phases was to remove from the orbital inclination the basic $k_2 = 0.265$, $\varepsilon_2 = 0$ effect for all frequencies, perform a spectral analysis on the residuals, and subsequently add back in the basic tidal perturbation. Figure 5-16 shows the power spectrum of the residuals in the GEOS 3 inclination after the major tidal effect has been removed. Many of the residual tidal terms are evident in this figure.

Turning the spectral amplitudes and phases in figure 5-16 and the basic tidal perturbation into effective Love numbers (whole-earth parameters), we obtain the values shown in table 5-4.

Table 5-4
Whole Earth Tidal Parameters

Tide	Love Numbers, k_2	ϵ_2 (degs)
P_1	0.263 ± 0.005	-2.2 ± 0.8
K_1	0.230 ± 0.004	+3.8 ± 1.0
S_2	0.281 ± 0.004	-0.9 ± 0.4
K_2	0.300 ± 0.015	0 ± 1.5
M_2	0.278 ± 0.006	+3.7 ± 0.6
O_1	0.231 ± 0.037	+13.0 ± 10.0
N_2	0.356 ± 0.050	0 ± 4.0

The conclusion that can be drawn from the values given in table 5-4 is that the three diurnal tides, P_1, K_1, and O_1 are much smaller than the semidiurnal tides. The primary reason that any of the k_2 values differs significantly from 0.30 derived from seismicity is that the ocean tides affect the motion of the satellite as well as the solid-Earth tides. Consequently, a first interpretation of the variation in k_2 can be to ascribe it to the different effects of the oceans at different frequencies and to conclude that this effect is greatest for the diurnal tides.

The second conclusion that can be drawn from the variation in values given table 5-4 is that our knowledge of the solid-Earth suggests only a very small phase lag in the tides is acceptable (~ 0.1 degrees). Consequently, the phases observed with GEOS 3 are also probably caused by the oceans. However, a negative phase lag, as we appear to have for P_1 and S_2, means that instead of tidal energy being dissipated in the Earth, the tides are being excited by the Earth. On face value this appears impossible but it is interesting to note that both P_1 and S_2 are solar induced tides and that in addition to solid-Earth and ocean-tides there are tides in the atmosphere, predominantly caused by solar heating that might be affecting our solution.

In addition, the effect of core resonance is predicted to cause a singularity in the value of the Love number, k_2, at a frequency of one cycle per day. This effect on the K_1 tide is believed to depress the Love number to about 0.26 so that some of the observed difference may be attributable to this resonance. However, without an accurate model of the K_1 ocean tide, it is impossible to isolate the solid-Earth contribution from that of the ocean. This explanation for K_1 cannot be used for P_1 or O_1 which, although nearly diurnal, are too far from the resonance frequency to be affected.

Finally, the values of M_2, N_2 and O_1 can be used to estimate the tidal acceleration of the Moon. The tidal bulge raised on the Earth by the Moon exerts a torque on the Moon proportional to its amplitude and the sine of the phase lag. The torque accelerates the Moon in its orbit thereby increasing the Earth-Moon distance in order to conserve angular momentum. After applying a small correction to M_2 arising from a fourth degree term in the ocean tides, which does not affect the lunar acceleration, we obtain for the lunar acceleration ($\dot{n}$) where

$$\dot{n} = -31.8 \pm 6 \text{ arcseconds centuries}^{-2}$$

which corresponds to an increase in the Earth-Moon distance of

$$4.7 \pm 0.9 \text{ cm/year}$$

Recent evaluations of $\dot{n}$ have ranged from -23.8 arcseconds centuries^{-2} (Williams, et al., 1978) to about -38 arcseconds centuries^{-2} (Oesterwinter and Cohen, 1972). Finally, the value of Q that we obtain for the oceans from the phase of the M_2 tide is 8±1 which suggests that if the moon were suddenly "switched off," the ocean tides on the Earth would effectively cease within a day or two.

SIGNIFICANCE

This analysis of the perturbation of the GEOS 3 satellite has provided estimates of the Whole-Earth Love numbers and phases at several of the major tidal frequencies. These parameters show a decrease in the tidal amplitude around one cycle/day that may be evidence of the existence of the diurnal resonance in the core that has been predicted theoretically (Molodenskii, 1961). To date, this resonance has not yet been positively identified in either tidal analyses or polar motion where the effect of the resonance is also expected to be evident. Observation of this resonance would confirm the existence of a liquid outer core that is observed seismically and a determination of the resonant frequency would provide a measure of the shape of the core-mantle boundary.

FUTURE EMPHASIS

Further work will be directed toward improving the estimate of lunar acceleration and to obtaining estimates on a regular basis for identification of possible changes in the dissipation of tidal energy and longterm variations in the Earth's rotation rate.

REFERENCES AND PUBLICATIONS

Molodenskii, M. S., "The Theory of Nutatious and Diurnal Earth Tides," *Obs. Roy. Belg. Comm.*, 188, and *S. Geoph. 58*, 25-26, 1961.

Oesterwinter, C., and C. J. Cohen, "New Orbital Elements for Moon and Planets," *Celestial Mechanics*, *5*, 317-395, 1972.

Williams, J. G., W. S. Sinclair, and C. F. Yoder, "Tidal Acceleration of the Moon," *Geophys. Res. Letters*, *5*, 943-946, 1978.

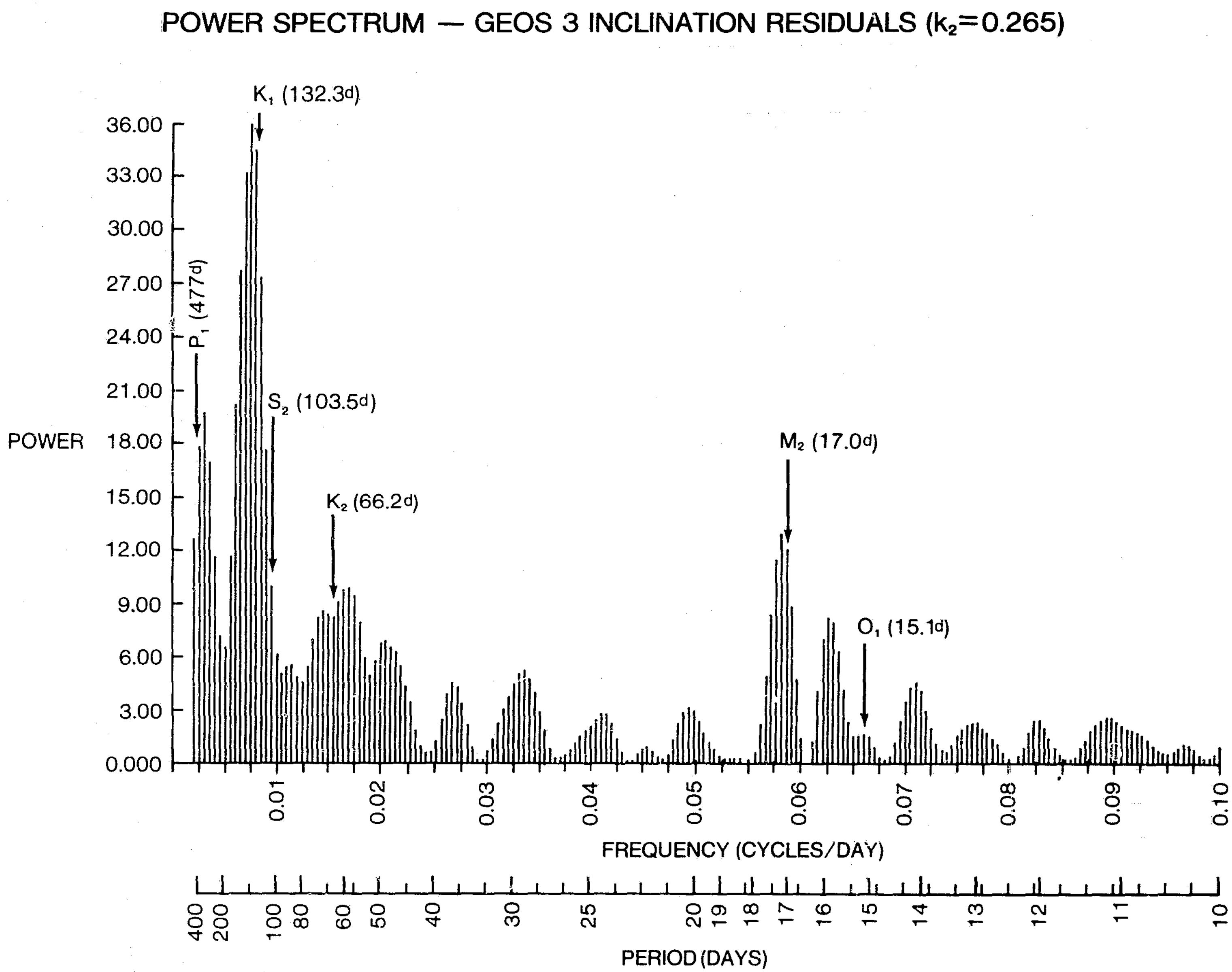

Figure 5-16. Power Spectrum of Residuals in GEOS 3 Inclination After Removal of Major Tidal Effect

CHAPTER 6

SEA SURFACE TOPOGRAPHY AND OCEAN DYNAMICS

OVERVIEW

The overall goal of this program is to apply remote sensing data to studies of dynamic ocean and Earth processes. The primary data types are satellite altimetry data, orbit perturbation data and gravity data. These data are analyzed in conjunction with surface observations, for example, ocean temperature and density measurements.

Global sets of satellite altimeter data have been collected during two satellite missions: The GEOS 3 mission (1975 to 1978) and the Seasat mission (1978).

Research programs are underway in the following areas to analyze and interpret the altimeter data:

- The development and implementation of techniques for the calibration and performance evaluation of the altimeter system.

- The computation of detailed gravimetric geoids which can be used as a basic reference surface for analyzing dynamic ocean topography associated with ocean circulation.

- The computation of regional as well as global mean sea surfaces for the analysis of temporal variations.

- Detailed analyses of the Gulf Stream and the associated eddy systems to improve our understanding of near surface as well as abyssal circulation.

- The analyses of orbit evolution data for the computation of ocean tidal parameters which are important for studies of dynamic ocean circulation modeling and for precision orbit determination.

A description of these programs is presented in the following sections.

Contributors to this chapter include Robert Cheney, Theodore Felsentreger, Werner Kahn, Ronald Kolenkiewicz, and James Marsh.

CALIBRATION RESULTS FOR THE GEOS 3 ALTIMETER

OBJECTIVE

The GEOS 3 satellite contained a radar altimeter capable of measuring heights with an accuracy of better than one meter. For some applications of the large quantity of altimeter data taken by the GEOS 3 intensive mode altimeter, an absolute calibration of the altitude data is needed. Such applications would include, for example, determination of the semimajor axis of the ellipsoid best approximating the geoid. To this end, the height bias of the altimeter has been determined.

BACKGROUND

The GEOS 3 spacecraft, launched on April 9, 1975, began operational activities on April 21, 1975. Since that time, the GEOS 3 altimeter has taken data on several thousand passes. On most of these, the altimeter was operating in the more precise short pulse, or intensive mode. In order to obtain full usage of these data a calibration (or height bias determination) of the altimeter is necessary.

The validation of the altimeter measurement from the spacecraft to the mean sea surface requires situations in which this distance can be accurately inferred, independent of the altimeter data itself. This can be done effectively using satellite passes which are nearly overhead at island laser tracking sites. This technique has the advantage that an accurate *a priori* knowledge of geoid heights is not required.

This was a particular problem with satellites such as GEOS 3, which incorporated no capability for orbit adjustments after orbital insertion. Calibration opportunities were thus dependent upon the groundtrack pattern of the orbit into which the spacecraft happened to be inserted. There were two island lasers in the GEOS 3 tracking schedule located at Bermuda and Grand Turk but near overhead passes were achieved only at Bermuda. Numerous groundtracks of the GEOS 3 satellite pass were in the vicinity of Bermuda. The Bermuda laser tracked on only two of these passes, but the two tracked were the two closest to being direct overhead passes (see figure 6-1).

One of the two overhead Bermuda passes (rev 4553) has been previously utilized for altimeter calibration (Martin and Butler, 1977), although without accounting for sea state effects on the altitude measurements and measured tide data on sea surface height. This pass did, however, have tracking by three lasers in the calibration area and should thus have a well-determined orbit. The other pass, rev 5471, had tracking by only two calibration area lasers, but the potential still exists for obtaining an accurate height of the spacecraft at the time of Bermuda overflight through the use of S-band tracking data taken from NASA STDN stations on earlier and later passes.

The aim is to obtain a best estimate of the GEOS 3 altimeter calibration bias, using the two available passes and reconciling differences between them.

The overhead calibration technique depends crucially upon obtaining the altimeter measurement which would be made directly over the tracking station, as if the altimeter were tracking to the normal ocean surface. The procedure for doing this is to smooth the data taken totally over water, and extrapolate to the point over the tracking station. To facilitate the smoothing operation, only measurement residuals are smoothed, with orbit, tropospheric propagation, a nominal tide from a tide model, and the best available gravimetric geoid all being removed.

To deduce the altimeter bias from residuals, we must consider the algorithm actually used for residual computation and what corrections or additions should be made to it. From the overhead calibration geometry shown in figure 4-2, the residual at the overhead point is the difference between the satellite distance to the ellipsoid based on the altimeter data plus appropriate tide and geoid models, and the satellite distance to the ellipsoid based on the tracking data and the station height above the ellipsoid. Neglecting the bias, the residual is expressed from figure 4-2 as

$$\text{Residual} = h_{alt} + \delta h + h_{tide} + h_{geoid} \quad \text{(Alt)}$$

$$- R - h_{MSL} - h_{geoid} \quad \text{(Sta)}$$

where

h_{alt} is the smoothed (and extrapolated) altimeter measurement corrected for tropospheric propagation effects.

δh is the nontidal deviation of the sea surface height from mean sea level. In the actual residual computation, this term is neglected.

h_{tide} is the tide height based on the Mofjeld tide model (2).

h_{geoid} (Alt) is the height of the geoid above the ellipsoid based on the Marsh-Chang 5' x 5' geoid model (3).

R is the satellite height above the tracking station, as deduced from the tracking data.

h_{MSL} is the tracking station height above mean sea level as determined by local survey.

h_{geoid} (Sta) is the geoid height used for the tracking station (=station height above ellipsoid - height above mean seal level).

It will be noted that the two geoid heights in the equation should exactly cancel at the point directly overhead the tracking station, assuming that the data reduction has used a station height consistent with the geoid model. In practice, we have chosen the station height on the basis of the station's estimated center-of-mass position, so a residual correction is necessary to account for the discrepancy. Other corrections which should be applied are:

- Correct h_{alt} for ionospheric propagation
- Correct h_{alt} for sea state effects
- Substitute the measured tide gauge height for the tide model value (automatically including δh).

RECENT ACCOMPLISHMENTS

Two GEOS 3 altimeter passes across Bermuda with tracking support by the Bermuda laser have been analyzed to estimate the bias in the altimeter measurements. The biases estimated were:

- Rev 4553: -5.75 ± .30m
- Rev 5471: -5.94 ± .21m
- Rev 4553 + Rev 5471: -5.88 ± .17m

Details of these calculations are shown in table 6-1.

Rev 4553 was supported by tracking by three lasers (Bermuda, Grand Turk, and Stalas), while rev 5471 had laser tracking only by Bermuda and the Patrick Air Force Base laser (not used). For supporting data on rev 5471, STDN range-rate data in a 3 revolution period around the pass of interest was used, and the orbit height over Bermuda was considered to be of comparable accuracy to that on rev 4553.

Sea surface height corrections are made for both passes based on measured tide gauge data. For rev 5471, tied gauge data appeared normal, but on rev 4553 it gave evidence of having been clogged although such was not indicated on the tide gauge records. However, rev 4553 did occur during a period of relatively high seas ($H_{1/3} \simeq 4$ m) and a sea state bias correction of 25 cm was applied. Because of the high seas and the uncertainty over the tide gauge data, rev 4553 was downweighted before combining with rev 5471 to obtain a best bias estimate of $-5.88 \pm .17$m. The individual bias estimates, however, are totally consistent to within the above listed uncertainties and are also consistent with the estimates made by the altimeter builders (4) on the basis of calculated spacecraft delays within the altimeter hardware and in data transfer. The G.E. estimate bias estimate was $-6.08 \pm .5$m.

The estimated altimeter bias has been obtained for low sea state conditions, or using corrections to "low sea state." Most GEOS 3 data has apparently been taken under such conditions and the above bias estimate can be applied to such data without a sea state correction. However, for sea states higher than 2 to 3 m a bias correction should be made if the data is to be used in geoidal analysis. Some further refinements in the technique used for making this correction appear necessary, particularly for unusually high sea states.

SIGNIFICANCE

The absolute bias calibration for the GEOS 3 intensive mode altimeter has been measured. This correction can be applied to this data to enable investigators to determine important geophysical parameters.

FUTURE EMPHASIS

The Seasat 1 spacecraft was launched on June 26, 1978. The satellite has an altimeter capable of measuring heights of less than 10 cm. This altimeter will be calibrated in the same manner used for calibration of GEOS 3. Results should be better since Seasat can be maneuvered to pass over the Bermuda laser.

REFERENCES AND PUBLICATIONS

Hofmeister, E.L., B.N. Keeney, T.W. Godbey, and R.J. Berg, "Data User's Handbook and Design Error Analysis — GEOS 3 Radar Altimeter," General Electric Company Report, *1* , prepared for NASA/Wallops Flight Center and the Johns Hopkins University/Applied Physics Laboratory, May 1976.

Marsh, J.G., and E.S. Chang, "5' Detailed Gravimetric Geoid in the Northwestern Atlantic Ocean," *Marine Geodesy, 1,* 3, 253-261, 1978.

Martin, C.F., and M.L. Butler, "Calibration Results for the GEOS 3 Altimeter," NASA CR-14143, September 1977.

Mofjeld, H.O., "Empirical Model for Tides in the Western North Atlantic Ocean," NOAA Technical Report ERL 340-AOML-15, October 1975.

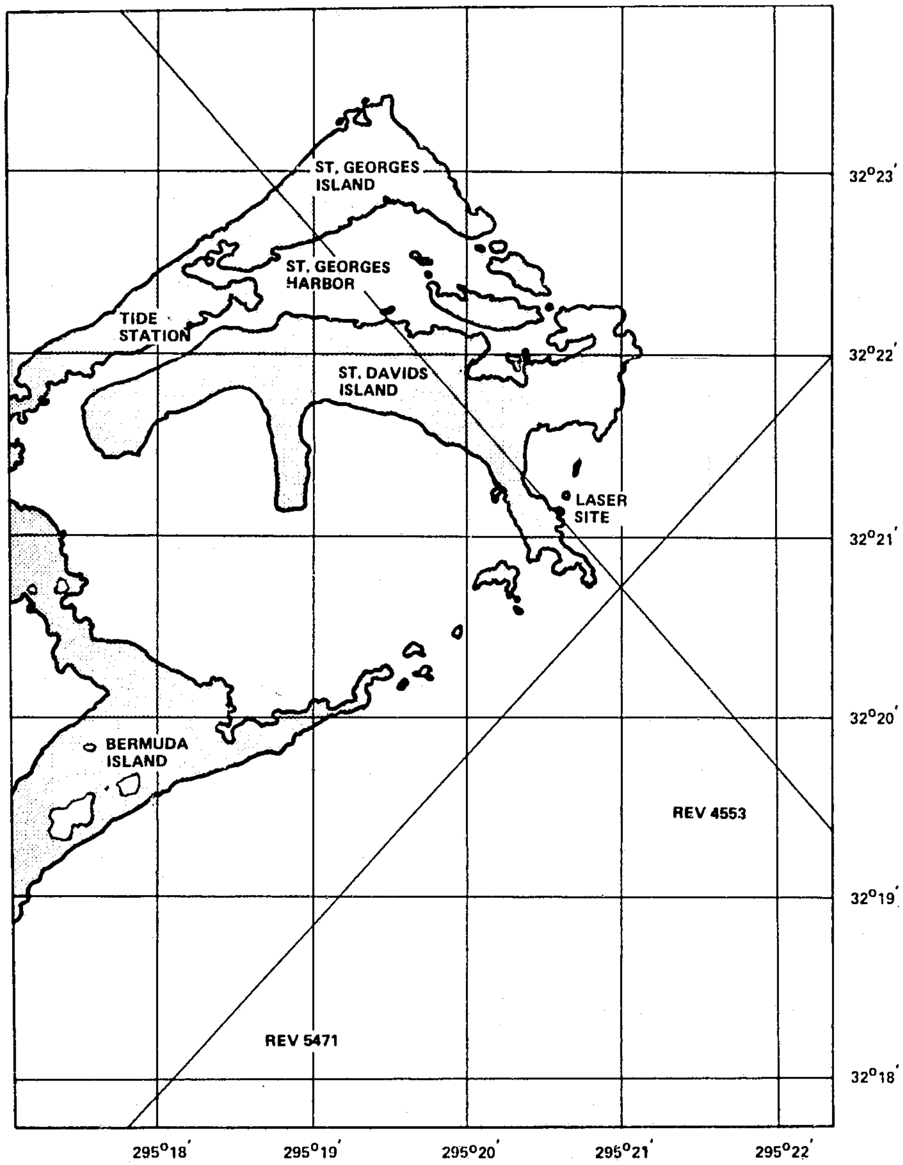

Figure 6-1. Ground Tracks of GEOS 3 Altimeter Calibration Passes

Table 6-1
Computation of GEOS 3 Altimeter Bias
Estimates Using Two Bermuda Overflights

Measurement Residual	Rev 4553	Rev 5471
+ Geoid Height used for Bermuda laser	1.45 ± .20 m*	0.79 ± .20 m*
- Geoid height at Bermuda laser from geoid model	-6.63 ± 0.0 m	-6.63 ± 0.0 m
+ Tropospheric propagation correction	0 ± .03 m	0 ± .03 m
+ Ionospheric propagation correction	-.05 ± .02 m	-.05 ± .02 m
+ Tide correction (Tide gauge—model)	-.27 ± .20 m	0 ± .03 m
+ Sea state bias correction	-.25 ± 0.10 m	0 ± .04 m
+ Orbit height correction	0 ± .03 m	0 ± .03 m
+ Correction for geoid model error	0 ± 0.0 m	-.05 ± .02 m
Estimated Pass Bias	-5.75 ± .30 m	-5.94 ± .21 m
Combined Bias	-5.88 ± .17 m	

*Uncertainty due to measurement noise.

DETAILED GRAVIMETRIC GEOID COMPUTATIONS

OBJECTIVES

The objective of this work is to compute a global detailed geoid by combining satellite-derived and surface-observed gravity data.

BACKGROUND

The earth gravity model development effort has provided the most accurate global representations available for features with wavelengths of about 500 km or longer. In order to supplement the highly accurate long wavelength data, techniques have been developed for computing geoids by combining this data with the precision short wavelength data provided by surface gravity data where it is available.

RECENT ACCOMPLISHMENTS

Detailed gravimetric geoids have been computed using a combination of GSFC potential field models and mean free-air surface gravity data. These computations have been carried out on a global scale (Marsh and Chang, 1978) by combining a set of $1^\circ \times 1^\circ$ mean surface anomalies with the GEM 8 model (Wagner, et al., 1977). More detailed computations have been made in the northwest Atlantic off the east coast of the U.S. by combining a set of 5' surface gravity data with the GEM 8 model (Marsh and Chang, 1978). Comparisons have been made between these detailed gravimetric geoids and satellite-derived tracking station coodinates and GEOS 3 altimeter data.

One-degree Global Gravimetric Geoid

The GSFC GEM 10 gravity field model was used to provide information on geoid undulations with wavelengths greater than 1500 km. This model was derived from a combination of satellite tracking data and surface gravity data. The satellite data set has approximately 840,000 observations, of which 200,000 are laser ranges taken on nine satellites. A set of 1654 equal area 5° mean gravity anomalies (Rapp, 1977) have been used along with these satellite data.

The set of 38,406 1° mean free-air anomalies used to describe the shorter wavelength geoid undulations were provided by Rapp (1978). These data primarily consisted of a set of observations obtained from the Defense Mapping Agency/Aerospace Center with additional data in Canada collected by the Canadian Department of Energy and Mines and data in the northwest Pacific Ocean collected by the Lamont Doherty Geological Observatory.

The following computational approach has been adopted (Rapp, 1967) for example:

$$N(\phi,\lambda) = N_1 + N_2 \tag{2}$$

where

$$N_1 = R \sum_{n=2}^{n_{max}} \sum_{m=0}^{n} \bar{P}_{nm} (\sin \phi) \, [\bar{C}^*_{nm} \cos m\lambda + \bar{S}_{nm} \sin m\lambda]$$

$$N_2 = \frac{R}{4 \pi \bar{\gamma}} \iint_{A_1} \Delta g_2 \, (\phi',\lambda') \, S \, (\psi) \, \cos\phi' \, d\phi' \, d\lambda'$$

ϕ, λ = geocentric latitude and longitude of the computation point

R = mean radius of the earth (6371 km)

$\bar{\gamma}$ = mean value of gravity (980 gals)

Δg_2 = residual free-air gravity anomaly = $\Delta g_T - \Delta g_S - \Delta g_A$

Δg_T = mean observed surface free-air gravity anomaly

Δg_S = satellite-derived free-air gravity anomaly

$$= \bar{\gamma} \sum_{n=2}^{n_{max}} \sum_{m=0}^{n} (n-1) \, \bar{P}_{nm} (\sin\phi) [\bar{C}^*_{nm} \cos m\lambda + \bar{S}_{nm} \sin m\lambda]$$

Δg_A = atmospheric correction to the gravity data (-0.853 mgal)

$\bar{P}_{nm}(\sin\phi)$ = normalized associated Legendre polynomial of degree n and order m

$\bar{C}^{*}_{nm}$ = $\bar{C}_{nm} - \bar{C}^{ref}_{nm}$

$\bar{C}_{nm}, \bar{S}_{nm}$ = normalized spherical harmonic coefficients of the potential field model

$\bar{C}^{ref}_{nm}$ = normalized spherical harmonic coefficients for the reference equipotential ellipsoid of degree n and order m. Only values for $\bar{C}^{ref}_{20}$ and $\bar{C}^{ref}_{40}$ were used.

$S(\psi)$ = Stokes' function

ψ = angular distance

In the computation of N_2, the residual surface gravity anomalies were integrated to 10° from the computation point. Since the Stokes' function $S(\psi)$ varies rapidly in the vicinity of the computation point, in order to obtain a more accurate value of $S(\psi)$ for the 1° x 1° blocks nearest the computation point, each block was divided into four equal blocks and values of $S(\Psi)$ were calculated at the centers of the sub-blocks and then averaged.

The parameters used were those recommended by the Special Study Group 5.39 of the International Association of Geodesy (Moritz, 1975):

a_e = 6378.140 km

$1/f$ = 298.257

GM = 398600.5 km^3/s^2

ω = 7.292115×10^{-5} rad/s

Figure 6-2 presents a contour map of the 1° global detailed geoid (Marsh, 1979). With the current set of 1° mean surface gravity data, numerous short wavelength features in the geoid are now visible. Most notable are the steep gradients associated with the major oceanic trenches in the Pacific, for example, the Mariana-Bonin-Japan-Kuril trenches, the Philippine Trench, the Java Trench, the Aleutian Trench, and the Peru-Chile Trench. In the Atlantic, the Puerto Rico Trench is also visible. In the vicinity of Hawaii the height of the geoid increases by about 16 m over a distance of 2°. Longer wavelength geoidal lows are observed in the Indian Ocean south of India (N = -102 m), the Hudson Bay (N = -49 m), and the Pacific Ocean off Baja, California (N = -46 m). Significant geoid highs are observed over the Andes (N = 57 m), south of Iceland (N = 70 m), and over New Guinea (N = 87 m).

This map contains numerous short wavelength features, which cannot be detected by the GEM 10 field model. Differences on the order of 10 to 15 m are associated with most trenches, except over the Tonga-Kermadec Trench, where a difference of -28 m occurs. A difference of +18 m occurs in the southern portion of India; however, the differences over the geoidal low in the Indian Ocean are only a few meters, indicating that this feature is primarily accounted for by the GEM 10 model. Over the Andes, a difference of 18 m is shown. In Central Africa, there is a broad feature, approximately 20° in extent and with a total amplitude of 26 m. The cause of this large deviation is not presently understood.

As a means of testing the precision of the detailed geoid, comparisons have been made with geoceiver and astrogeodetic-derived geoid heights at 98 well-distributed locations over the United States. The accuracy of these geoid heights is on the order of 1 to 2 m (Strange, 1976, private communication; Carroll and Wessells, 1975). The rms differences between the geoceiver/astrogeodetic geoid heights and the 1° detailed geoid were 1.7 m. A similar comparison with the geoid derived solely from the GEM 10 model resulted in an rms difference of about 2 m for the geoceivers and the astrogeodetic stations. The rms differences of about 2 m indicate that the GEM 10 model provides a good description of the geopotential over the United States.

This detailed gravimetric geoid has also been compared with the geoid of Europe computed by Levallois and Monget (1975). This latter solution was based upon a combination of astrogeodetic and gravimetric data. After making the necessary datum transformations, the rms difference was about 3 m.

Five-Minute Detailed Gravimetric Geoid

A high resolution gravimetric geoid has been computed for the northwest Atlantic Ocean off the east coast of the U.S. The computation technique employed was similar to that employed for the 1° geoid discussed earlier. The long wavelength undulations were computed using the GEM 8 potential field model consisting of a set of spherical harmonic coefficients complete to degree and order 25 with higher order resonant coefficients. The surface gravity data were in the form of 5' x 5', 15' x 15', and 1° x 1° mean free air anomalies provided by the Defense Mapping Agency/Aerospace Center (Seppelin, 1975, private communication). In the application of Stokes' formula, the 5' mean residual anomalies were integrated from 0° to 2° around the computation point, the 15' mean residual anomalies were integrated from 2° x 3° and the 1° mean residual anomalies were intergrated from 3° to 20°.

Figure 6-3 presents a contour map of the 5' x 5' detailed gravimetric geoid for the area extending from 16° to 39°N latitude and from 278° to 300°E longitude. Several features are apparent in this map. Near the center of the map there is a relatively flat area covering about 4° in longitude and 12° in latitude, which corresponds to the Hatteras Abyssal Plain. In the vicinity of Bermuda, there is a feature with a height of approximately 5 m covering an area of about 1° x 1°. This is attributed to the steep rise of the island of Bermuda from the ocean floor. Traces of the New England Seamont Chain are also observable in the northeast corner of the geoid map. Over the Puerto Rico Trench, there is a geoid trough with a depth of 22 m relative to the northern coast of Puerto Rico. This depression in the geoid is in good agreement with the gravimetric results obtained by Von Arx (1966). Also shown in the map is a steep gradient which corresponds to the Blake Escarpment, where the depth of the ocean floor changes by about 3,600 m over half a degree in longitude. North of the Blake Escarpment a geoidal feature corresponding to the Blake Bahama Outer Ridge is observed.

A contour map of the differences between the 5' detailed gravimetric geoid and the geoid derived from the GEM 8 potential field model was computed. This map represents the short wavelength information provided by the detailed surface gravity data. A difference of -16 m occurs over the Puerto Rico Trench. Differences in the range of ±8 m are frequently observed in the Caribbean area. In the northeast portion of the calibration area, a large positive feature with a maximum value of 14 m is noted as occurring in the vicinity of Bermuda.

As a check on the precision of the 5' detailed gravimetric geoid, comparisons have been made with geoid heights computed for ten geoceiver stations distributed along the east coast of the United States (Strange, 1976, private communication). These stations are being used in the new adjustment of the North American Datum (Bossler, 1976). The accuracy of the center of mass coordinates derived for these stations has been assessed to be 1 to 2 m (Strange, et al., 1975). Geoid undulations at these geoceiver stations have been computed by differencing the satellite-derived station heights above the reference ellipsoid and the heights above mean sea level. Precise astrogeodetic measurements have also been made at locations occupied by the geoceiver stations. Geoid heights derived from the astrogeodetic data are accurate to approximately 2 m (Carroll and Wessels, 1975). The rms difference between the gravimetric geoid heights and those calculated from the geoceiver heights was 1.2 m. Similar results were obtained for the astrogeodetic data. The equatorial radius implied by this set of geoceiver stations is 6,378,135 ±2 m.

This high resolution geoid has been primarily computed to provide ground truth for the GEOS 3 and Seasat altimeter experiments and to provide a basis for the detection of departures of the sea surface from the equipotential surface due to dynamic ocean phenomena. Figure 4-6 presents a comparison between the 5' geoid and the sea surface height above the reference ellipsoid as measured by GEOS 3 along a profile extending from south of the Puerto Rican Trench to the Chesapeake Bay. The general agreement is on the order of a meter or so, with both data types clearly depicting features such as the Puerto Rican Trench, the Hatteras Abyssal Plain, and the Continental Slope.

Comparisons of GEOS 3 altimeter data and the 5' x 5' geoid in the vicinity of the Gulf Stream by Leitao, et al. (1978) have indicated the presence of expected geostrophic height differences across the Gulf Stream. Recent comparisons with Seasat altimeter data in the Northwestern Atlantic Ocean by Cheney and Marsh (1979) have clearly indicated the location and magnitude of dynamic topography over the Gulf Stream as well as shorter wavelength warm and cold water eddies.

SIGNIFICANCE

A global geoid with an accuracy of about two meters in most areas has been computed on a 1° grid. In the northwest Atlantic a geoid has been computed on a 5' grid. These geoids are being used for geophysical analyses such as mantle convection studies and also for oceanographic applications such as the detection of the sea surface from the equipotential surface due to dynamic ocean phenomena.

FUTURE EMPHASIS

Future work will be concerned with further interpretation and analysis of the geoids for geophysical and oceanographic applications. More detailed computations will be conducted using recently acquired data sets which will enhance the precision and resolution of the geoids.

REFERENCES AND PUBLICATIONS

Bossler, J.D., "The New Adjustment of the North American Horizontal Datum," *EØS Trans. AGU, 57,* 557-562, 1976.

Carroll, D.G., and Wessells, C.W., "A 1975 Astrogeodetic Geoid for the United States," presented to the Sixteenth General Assembly of the International Union of Geodesy and Geophysics, Grenoble, France, 1975.

Cheney, R., and J.G. Marsh, "A Preliminary Look at Seasat Altimetry in Gulf Stream Region," *Gulf Stream,* Department of Com-Commerce/NOAA publication, *5*, 2, 3-7, April 1979.

REFERENCES AND PUBLICATIONS (continued)

Leitao, C.D., N.E. Huang, and C.G. Parra, "Remote Sensing of Gulf Stream Using GEOS-3 Radar Altimeter," NASA Technical Paper 1209, April 1978.

Lerch, F.J., S.M. Klosko, R.D. Laubscher, and C.A. Wagner, Gravity Model Improvement Using GEOS-3 (GEM 9 and 10)," NASA/GSFC X-921-77-246, 1977, and *Geophys. Res. 84,* B8, 3897-3920, 1979.

Marsh, J.G. and E.S. Chang, "Global Detailed Gravimetric Geoid," accepted for publication by *Marine Geodesy,* and published in *Journal of Marine Geodesy, 2,* 2, 145-159, 1979.

Marsh, J.G. and E.S. Chang, "5' Detailed Gravimetric Geoid in the Northwestern Atlantic Ocean," *Journal of Marine Geodesy, 1,* 3, 253-261 June 1978.

Marsh, J.G. "GEM-10 Detailed Gravimetric Geoid," in progress.

Moritz, H., "Report of Special Study Group No. 5.39 of IAG: Fundamental Geodetic Constants," *Bull. Geod.*, 118, 398-408, 1975.

Rapp, R.H., "Combination of Satellite and Terrestrial Data for a Detailed Geoid," *Trans. AGU, 48,* 1967.

Rapp, R.H., private communication, 1976.

Rapp, R.H., "Potential Coefficient Determinations from 5° Terrestrial Gravity Data," Ohio State University Report No. 251, January 1977.

Von Arx, W.S., "Level Surface Profiles Across the Puerto Rico Trench," *Science, 154,* 1651-1653, 1966.

Wagner, C.A., F.J. Lerch, J.E. Brownd, and J.A. Richardson, "Improvement in the Geopotential Derived from Satellite and Surface Data (GEM-7 and GEM-8)," *J. Geophys. Res., 82,* 5, 901-914, February 1977.

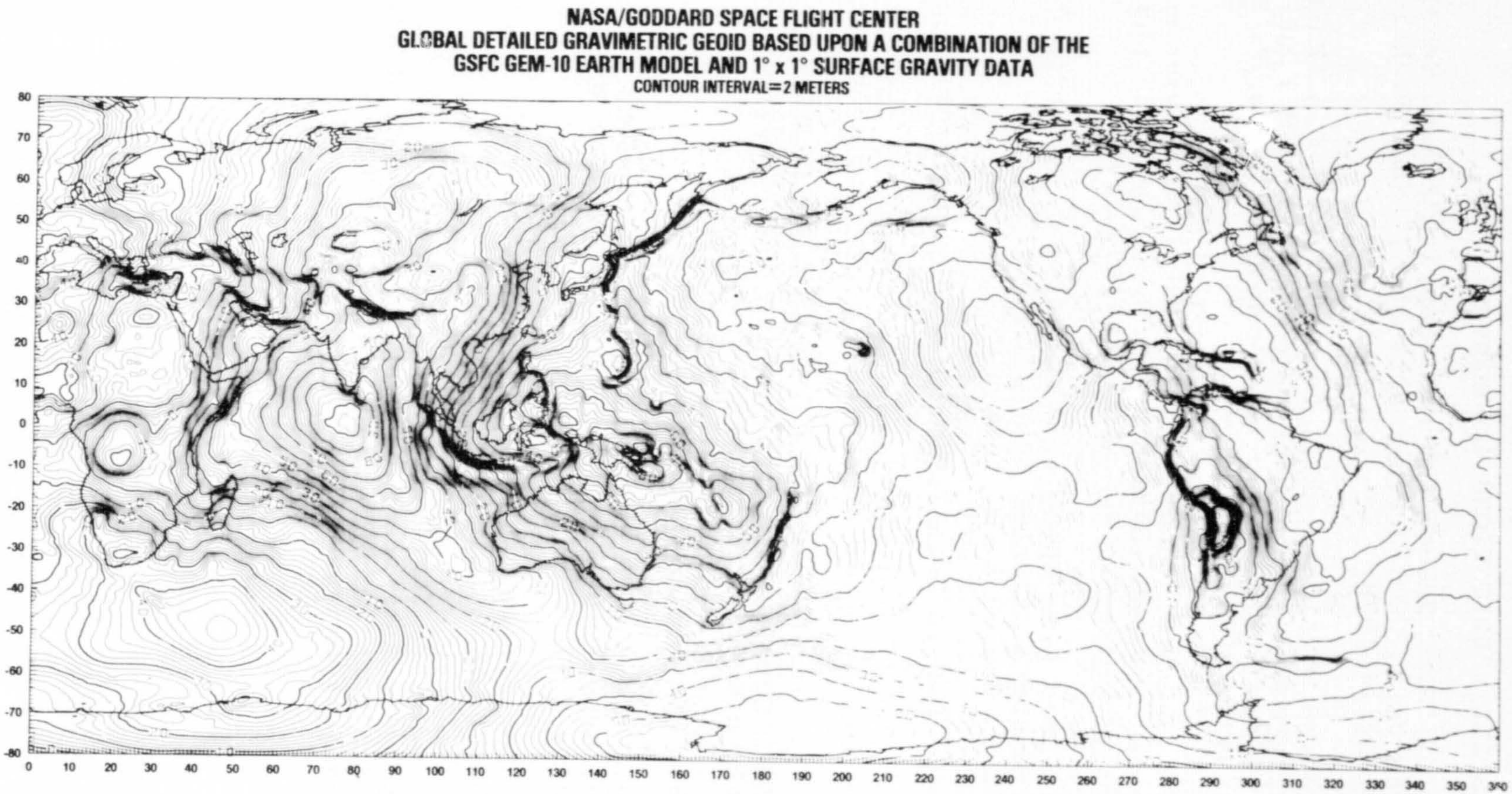

Figure 6-2. Contour Map of Global Detailed Gravimetric Geoid

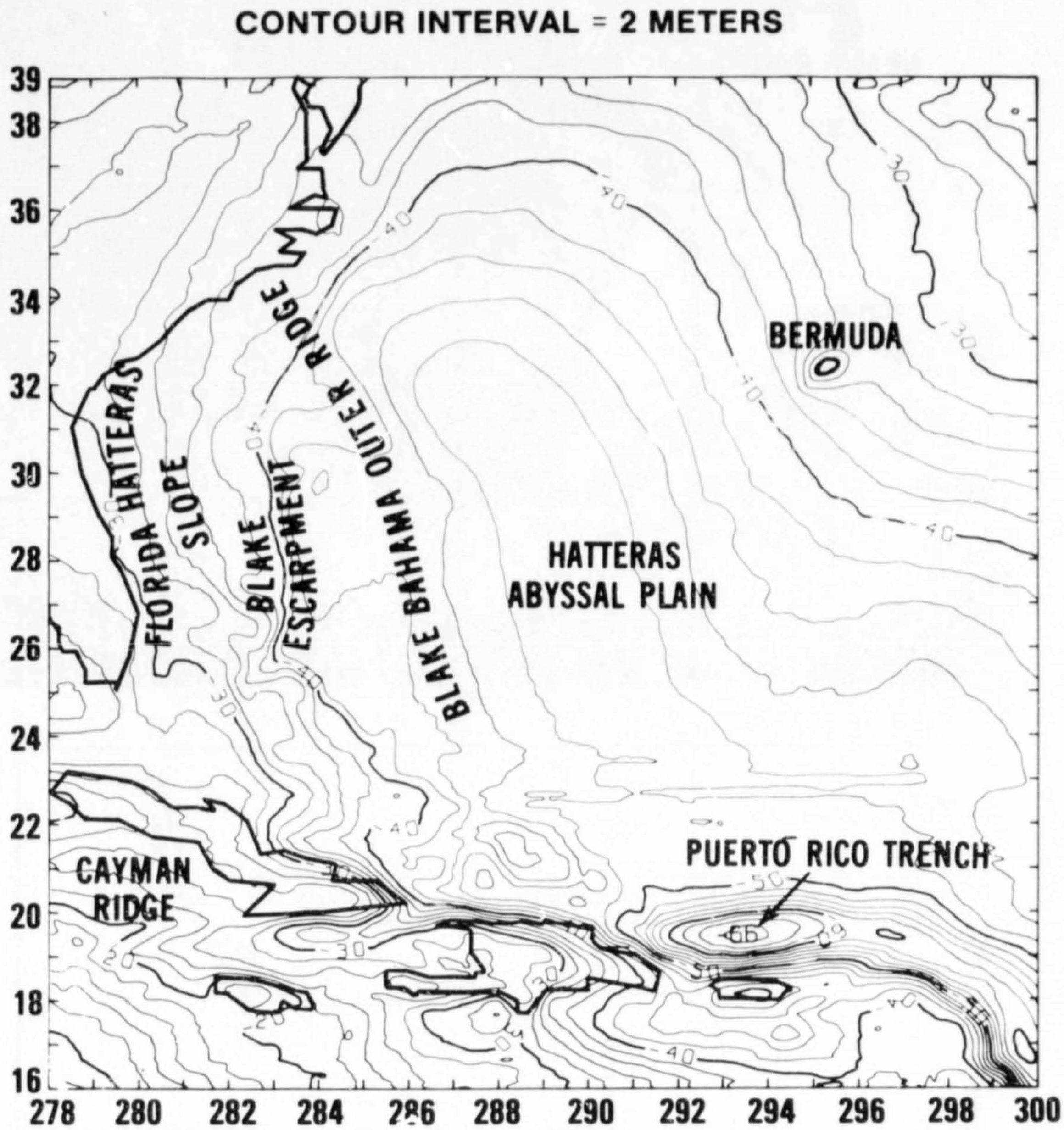

Figure 6-3. Contour Map of Detailed Geometric Geoid for U.S./Bermuda/Caribbean Area. Based on Combination of 5' 5', 15' 15', and 1° x 1°GEM 8 Earth Model

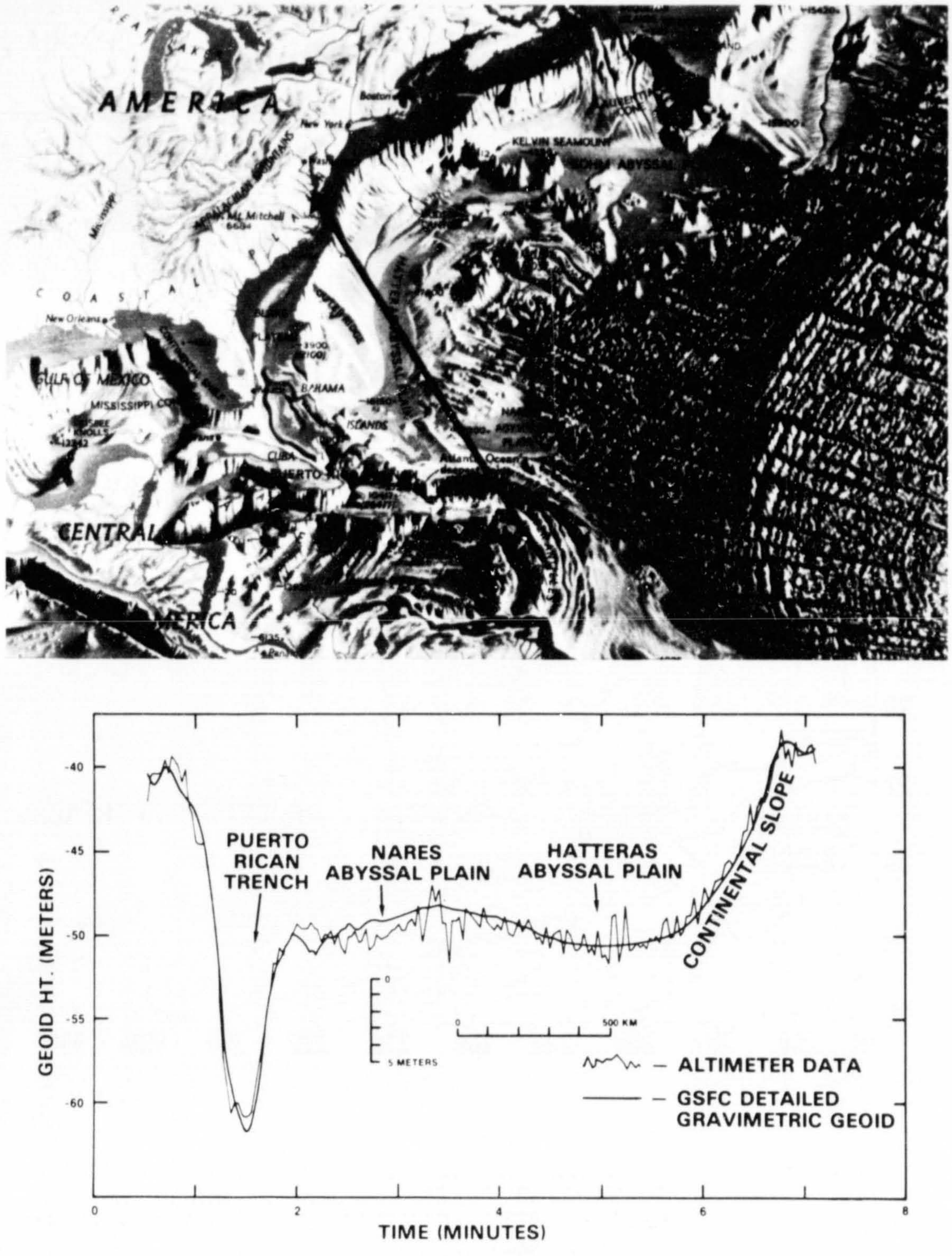

Figure 6-4. Comparison of GEOS 3 Altimeter Pass 260 and GSFC Detailed Gravimetric Geoid in the Northwest Atlantic

ORIGINAL PAGE IS
OF POOR QUALITY

MEAN SEA SURFACE COMPUTATION USING GEOS 3 ALTIMETER DATA

OBJECTIVES

The objective of this work is to compute a global mean sea surface ($\sim$ the geoid) using precision reduced GEOS 3 altimeter data and to interpret the surface for geophysical implications such as mantle convection or plate tectonics and to use the surface as a basis for the study of dynamic ocean processes.

BACKGROUND

The GEOS 3 radar altimeter experiment conducted during the period of 1975 to 1978 has provided a major revolution in the computation of the geoid in ocean areas. This experiment has provided a homogeneous grid of altimeter data over the oceans with a resolution in most areas of a fraction of a degree. The precision of these data is on the order of 30 to 50 cm.

Techniques have been developed for combining these data with precision orbital data based upon laser tracking data and the individual profiles have been combined to calculate a uniform mean surface for the ocean areas.

RECENT ACCOMPLISHMENTS

The mean surfaces of several regions of the world's oceans have been estimated using GEOS 3 altimeter data. Included in these computations are: The northwest Atlantic, the northeast Pacific off the coast of California, the Indian Ocean, the southwest Pacific, and the Phillipine Sea.

The technique of crossover adjustment was used to eliminate orbital errors and other time-varying error sources (e.g., changes in the sea surface height due to tides, storms, etc.) from the determination of the mean sea surface. The technique initially involved finding the locations of the intersection points of the ascending and descending passes of GEOS 3. The data files were then scanned to find the approximate time and location of each crossover. A quadratic interpolation using data extending to 0.2° on either side of the crossover was used to obtain the precise time, latitude and longitude of the crossover. The values of the sea surface height measurements for both the ascending and descending passes were similarly interpolated in time and were separately evaluated at the calculated crossover time. This procedure yielded a data set consisting of the time, latitude, and longitude of the crossover point and the altimeter-derived sea surface height measurements at that point obtained on the ascending and descending passes.

The sea surface height crossover differences (ascending pass height-descending pass height) were then used in a least squares adjustment process to compute a bias and a tilt for each pass, which were used to correct the sea surface measurements. Since orbital errors are primarily long wavelength in nature, the biases and tilts in the relatively short passes absorbed a significant portion of the orbit error.

The adjustments which minimize the sum of the squares of the crossover differences will eliminate the relative errors in the sea surface heights, and will define the shape of the sea height surface. However, the adjustment does not provide any information on the orientation of the surface with respect to the center of mass of the earth. In order to fix the surface in space relative to the center of mass of the Earth, six 5-day arcs of globally distributed laser data were held fixed in the solution.

These reference orbits were selected to maximize the global distribution of laser data and to obtain altimeter data from as many of the chosen ocean regions as possible in each arc. These orbits were computed using the laser station coordinates derived by Marsh, Williamson, and Martin (1977), where the value of GM = 398600.64 km^3/s^2, the value of the speed of light = 2.997925×10^8 m/s. The GEM 10 (Lerch et al., 1977) and GEM 10B (Lerch, et al., 1978) Earth gravity models are used. After comparisons were made between the GEM 10 and GEM 10B orbits, GEM 10B was chosen for the control orbits since the radial orbit accuracy obtained with this model was about a meter, whereas the GEM 10 orbital accuracy was about 1.5 meters.

Biases and tilts were computed for the remaining altimeter passes in a least squares adjustment process. These biases and tilts were then applied to the data and new crossover differences were computed. This correction procedure was repeated for several iterations. After each iteration, the rms crossover difference was computed. On the next iteration, any crossover difference whose magnitude was greater than four times the rms difference was flagged and was not used in computing the subsequent corrections. This editing procedure removed only a small number of points which had extremely large crossover differences. After the final iteration, the tilt and bias corrections were applied to the data of each pass, and the corrected sea surface height values were saved.

In contouring the sea surface heights, the grid points were spaced at 0.25° in the northwest Atlantic and 2° in the other regions, which corresponds closely to the spacing of the crossover data. The surfaces are referenced to an ellipsoid of a_e = 6378140 m and a flattening of 1/298.255.

Figure 6-5 shows the sea surface contour map of the northwest Atlantic derived from the GEOS 3 altimeter data with the orientation provided by the precise laser orbits. Several features of the ocean floor topography are clearly reflected in the sea surface topography. Bermuda is clearly visible, and the relatively flat area in the center corresponds to the Hatteras abyssal plain. To the west, the Blake Bahama outer ridge and the Blake escarpment are visible. Line indicating the 200 m, 2000 m, and 4000 m bathymetry contours have been added. Notice how the sea surface contours follow the 2000-m line along the entire North American coastline. In the region of the Blake Bahama Outer Ridge, the 4000-m line extends out into the Atlantic, and this feature is clearly shown in the contour lines of the sea surface.

The 5' x 5' GEM 8 detailed gravimetric geoid (Marsh and Chang, 1978) covers a portion of the same area as the sea height surface presented here, and thus may be used for comparison with this surface. The Marsh-Chang geoid is a detailed gravimetric geoid presented on a 5' x 5' grid which incorporates both a satellite-determined geoid (GEM 8) and surface gravity anomaly data.

The differences between the 5' gravimetric geoid and the mean sea surfaces were calculated after removal of an overall Δx, Δy, Δz, tilt and the rms difference was 1.1 meters. In the central portion of the region the differences are generally less than 50 cm. The areas of great differences occur either at the edges of the region where it is expected that the mean sea surface may be less accurately determined due to the sparsity of data, or in the southernmost portion of the surface, where the surface is very convoluted due to the presence of many islands and other bathymetric features.

To check the consistency of the calculated sea surface in the northwest Atlantic with the orbital and altimeter data which were used in the sea surface computation, we have compared the sea surface heights from our calculated sea surface with the sea surface heights obtained directly from the altimeter measurements of several passes. The difference in the two sea surface heights should indicate both the short wavelength time-dependent errors due to eddies, storms, etc., and long wavelength orbital errors which should appear as biases and tilts in the height differences.

Figure 6-6 presents plots of altimeter residuals for four passes through the northwest Atlantic during a five-day orbit. These residuals indicate orbit errors which are generally less than 50 cm. Some of the systematic trends noted in the residuals, e.g., at 23^m and 24^m on the 13^h pass, may be due to an oceanographic phenomenon in this pass which is not contained in the mean sea surface.

Figure 6-7 presents a contour map of the mean sea surface computed for the area between Japan and Australia. The tectonically complex structure in the vicinity of the Mariana, Bonin, and Japan Trenches is reflected in the ocean surface. Comparisons of individual GEOS 3 and Seasat altimeter tracks with this mean surface are expected to reveal eddies, rings, and meanders of the Japan current in this region.

Similar contour maps of the other ocean areas are contained in a more complete report by Marsh, et al., 1978.

SIGNIFICANCE

Using radar altimetry and precise laser ranging data, techniques have been developed for the computation of mean sea surfaces on a global scale. Using these techniques, mean sea surfaces have been computed for six areas of the Earth's oceans. The spatial resolution achieved varies from 0.25° in the northwest Atlantic to 2° in some ocean areas. The surfaces are referenced to the center of mass of the Earth with an accuracy of one meter and have relative accuracies ranging from 30 to 70 cm. These mean sea surfaces will form an important basis for future investigations of dynamic ocean processes as well as geodynamical analyses in ocean areas.

FUTURE EMPHASIS

Future work in this area will be concerned with the interpretation of this newly developed data type for geodynamic investigations such as mantle convection and the development of techniques for the detection and monitoring of dynamic ocean processes.

REFERENCES AND PUBLICATIONS

Lerch, F.J., C.A. Wagner, S.M. Klosko, R.P. Belott, R.E. Laubscher, and W.A. Taylor, "Gravity Model Improvement Using GEOS 3 Altimetry (GEM 10A and 10B)," presented at Spring Annual Meeting of the American Geophysical Union, Miami Beach, Florida, April 1978.

March, J.G., R.D. Williamson, and T.V. Martin, "Tracking Station Coordinate Investigation," Final Report of GEOS 3 Investigation presented at New Orleans, Louisiana, November 1977.

REFERENCES AND PUBLICATIONS (continued)

Marsh, J.G., T.V. Martin, J.J. McCarthy, and P.S. Chovitz, "Estimation of Mean Sea Surfaces in the North Atlantic, the Pacific and the Indian Ocean Using GEOS 3 Altimeter Data," presented at the Second International Symposium on the Uses of Artificial Satellites for Geodesy and Geodynamic, Lagonissi, Greece and published in the proceedings, May 1978; also published as NASA TM 79704, February 1979.

Marsh, J.G. and Chang, E.S., "5' Detailed Gravimetric Geoid in the Northwest Atlantic Ocean," *Marine Geodesy, 1*, 3, June 1978.

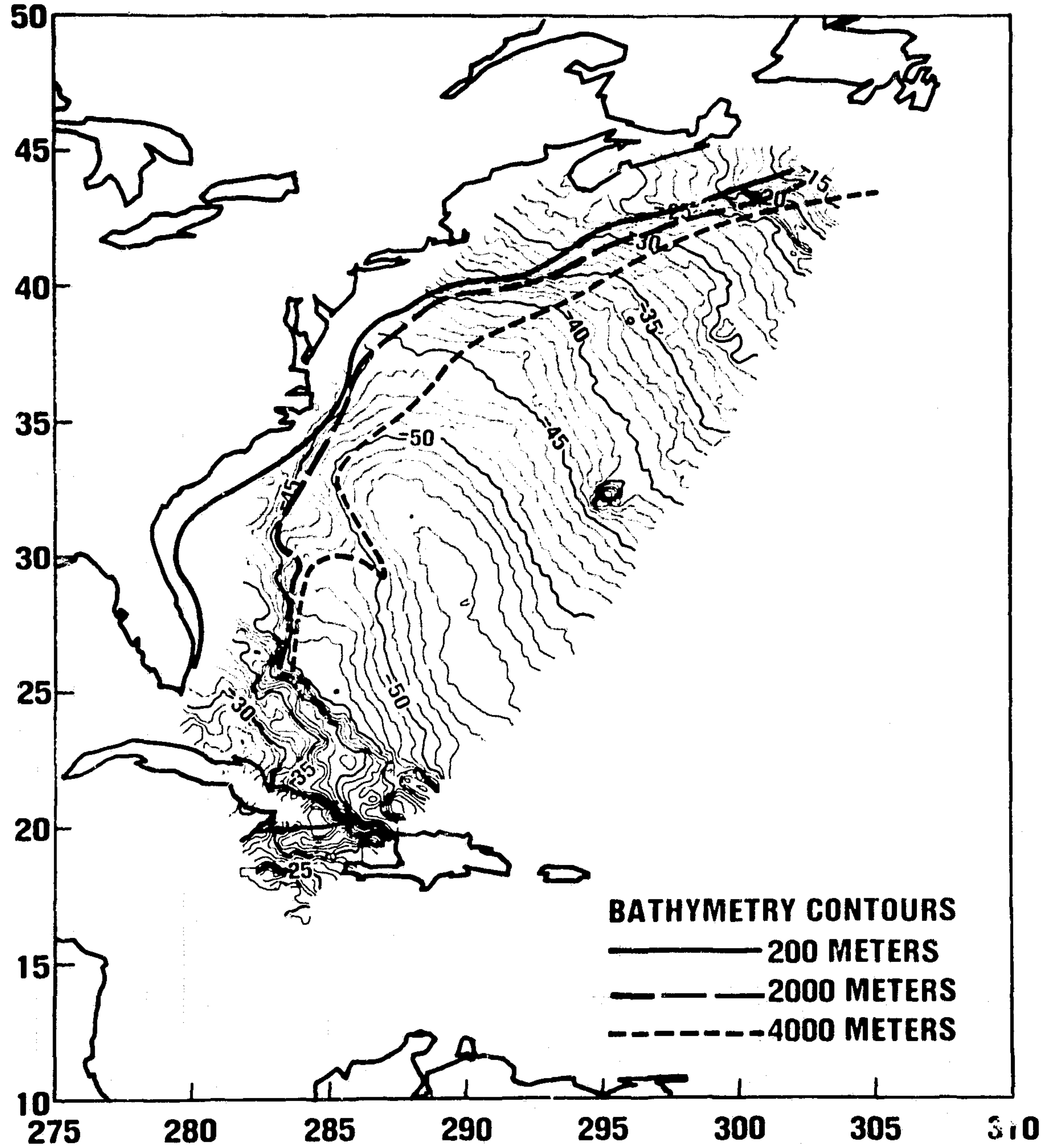

Figure 6-5. Contour Map of the Ocean Surface Derived from GEOS 3 Altimeter Crossover Data, Contour Interval 1 Meter. The Earth semimajor axis equals 6378140 meters.

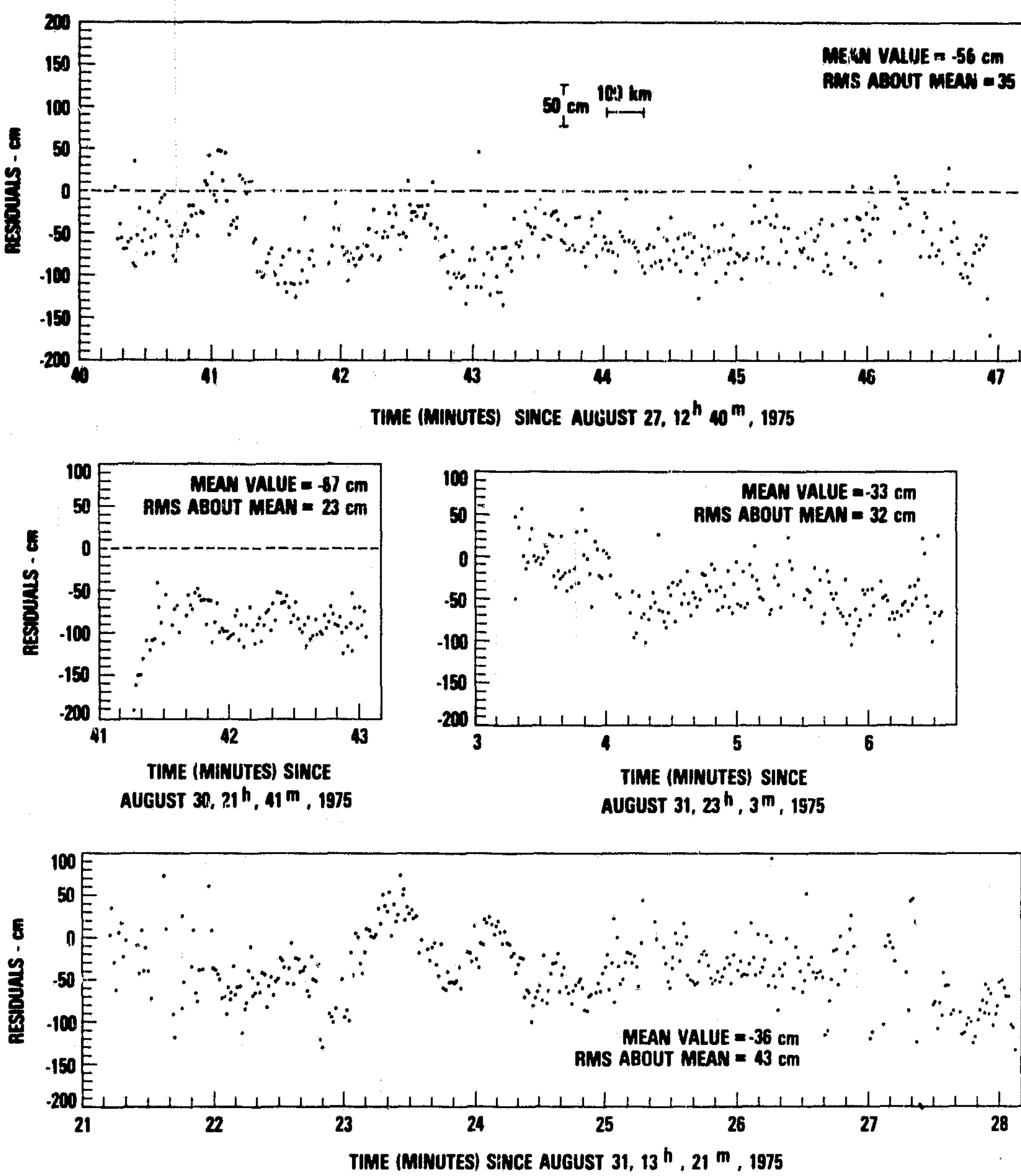

Figure 6-6. GEOS 3 Altimeter Residuals Based on a 5-day laser Orbit and the Altimeter-derived Mean Sea Surface

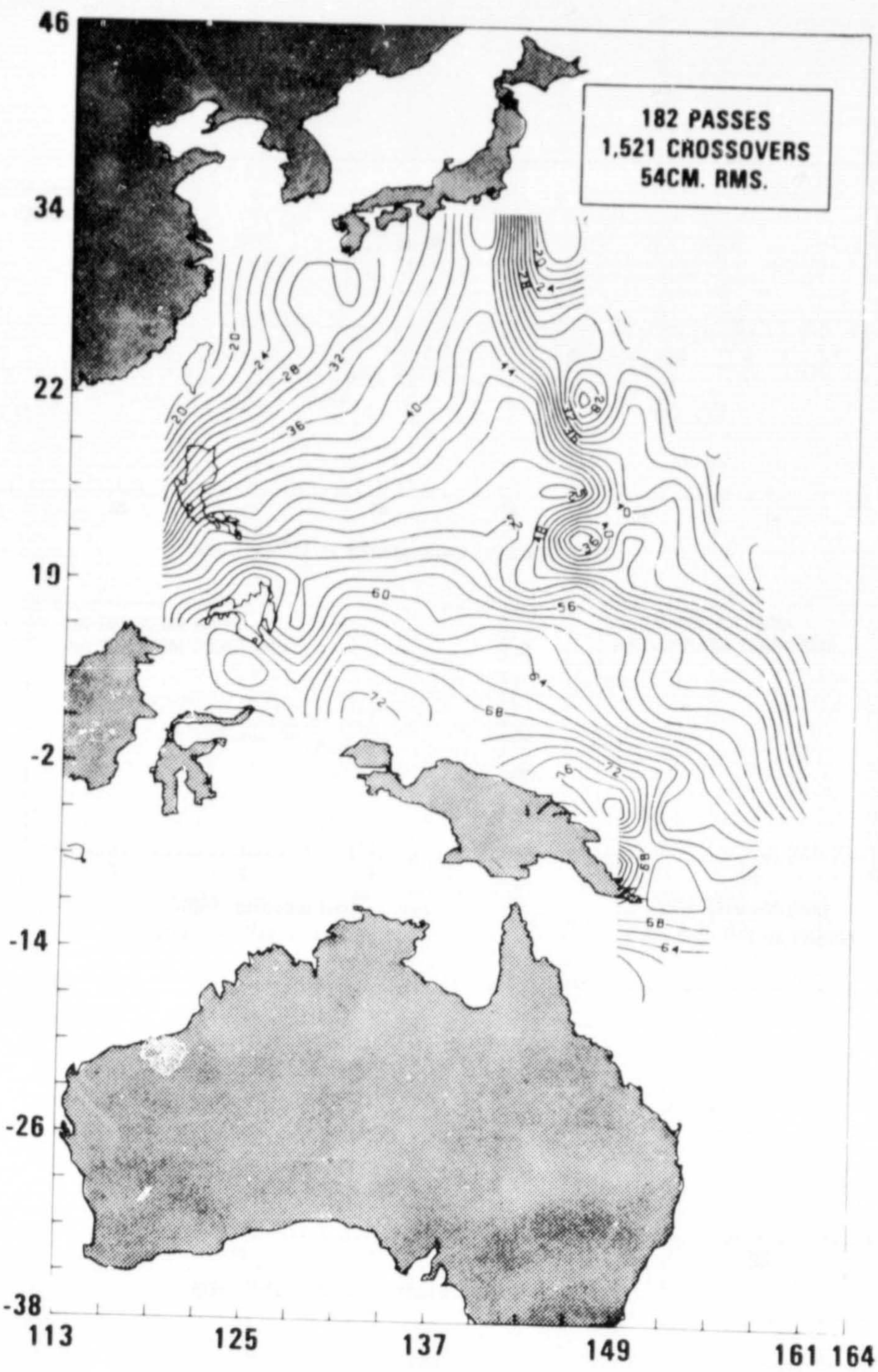

Figure 6-7. Contour Map of the Ocean Surface Derived From GEOS 3 Altimeter Crossover Data

MEAN SEA SURFACE FOR THE GULF OF ALASKA

OBJECTIVES

The primary experiment on the GEOS 3 satellite was the radar altimeter. This experiment's major objective is to demonstrate the utility of measuring the geometry of the ocean surface, i.e., the geoid with absolute height resolution of ± 5 meters and a relative height precision of ± 1 to ± 2 meters.

BACKGROUND

Satellite tracking contributions to the determination of the current ocean geoid have a spatial resolution corresponding to a half wavelength of approximately 11° to 15° (1250 to 1650 km). Although the addition of surface gravity permits local representations with finer resolution, in the 1° to 5° (110 to 550 km) range, these data are available over only about 50 percent of the ocean surface.

The GEOS 3 altimeter has demonstrated the capability to determine the fine structure of the mean sea surface. When this instrument is operating in the short-pulse mode, a measurement is produced every 4 km along the satellite subtrack. With this resolution capability, it will be possible to describe sea surface topography to a detail of less than 1°, depending on the degree of data smoothing used and the spacing between subtracks.

RECENT ACCOMPLISHMENTS

GEOS 3 altimeter data from 100 altimeter passes were used to construct a mean sea surface for the Gulf of Alaska region, bounded by Longitudes 200° E to 240° E and Latitudes 20° N to 55° N. The resultant sea surface correlated very well sea bottom topography (see figure 6-8).

For the computation of the mean sea surface, the GEM 7 gravity field model was used as the reference field. This gravity field model is complete through order and degree 16. GEM 7 does not properly model intermediate and short wavelength features ranging from 2000 km and below, hence the rms deviation from GEM 7 was 4.5 m. This large rms deviation from the GEM 7 reference gravity field model indicated the presence of information in the intermediate and short wavelength portion of the spectra. Further analyses of the sea surface heights was thus performed by estimating both 5° x 5° and 2° x 2° mean free-air gravity anomalies.

Estimates of 35 $5^\circ \times 5^\circ$ mean free-air gravity anomalies were obtained from 98 passes of altimeter data. The values are given in figure 6-9 and the comparison of the estimated values with terrestrial anomalies published by Professor R. Rapp, of Ohio State University and those published by Talwani and Cochran (1977 are given in Figure 6-10. The comparison with Rapp over all anomaly blocks estimated gave an rms difference of 7.6 mgals. The comparison with Cochran and Talwani which was made over a smaller number of anomaly blocks gave a rms difference of 3.6 mgals. Clearly, the comparison with Rapp is more extensive and meaningful. It is felt that the recovered $5^\circ \times 5^\circ$ mean anomalies have an average uncertainty of $\pm$ 5 mgals since for some areas the terrestrial anomalies used for the comparison themselves have large uncertainties associated with them.

The estimation for 192 $2^\circ \times 2^\circ$ mean free gravity anomalies for the same area utilizing the same altimetry data used for the $5^\circ \times 5^\circ$ estimation solution is shown in figure 6-11 By comparing the estimated anomalies with terrestrial gravity anomalies, the comparisons as seen in figure 6-12 show slightly smaller rms differences with Professor Rapp's terrestrial anomalies than those of Cochran and Talwani.

It seems that the average uncertainty of the recovered $2^\circ \times 2^\circ$ gravity anomalies is $\pm$ 12 mgals. As stated before, the uncertainties for some of the terrestrial anomalies is too high, implying that those anomalies themselves are not well determined.

SIGNIFICANCE

The feasibility of gravity anomaly recovery using altimetry data is proven. A new sea surface augmented by the estimated $2^\circ \times 2^\circ$ gravity anomalies will provide a better model of the mean sea surface than that shown in figure 6-8. Furthermore, additional reduction of the rms error in the mean sea surface for the Gulf of Alaska region is anticipated by using additional altimeter data now available for the region. Only 40 percent of the total data available are used.

FUTURE EMPHASIS

A marine geoid for the Gulf of Alaska region will be computed by using all available GEOS 3 and Seasat 1 altimetry data available for that region.

REFERENCES AND PUBLICATIONS

Kahn, W.D., B.B. Agrawal, R.D. Brown, "Mean Sea Level Determination from Satellite Altimetry," NASA/GSFC C-921-77-41, March 1977.

Kahn, W.D., J.W. Siry, R.D. Brown, W.T. Wells, "Ocean Gravity and Geoid Determination," NASA/GSFC X-921-77-259, October 1977.

Talwani, M. and R.J. Cochran, "Free-Air Gravity Anomalies in the World's Oceans and Their Relationship to Residual Elevation," *Geophys. J.R. Astr. Soc., 50*, 495-552, 1977.

Watts, A.B. and A.R. Leeds, "Gravimetric Geoid in the Northwest Pacific Ocean," *Geophys. J.R. Astro. Soc., 50*, 249-278, 1977.

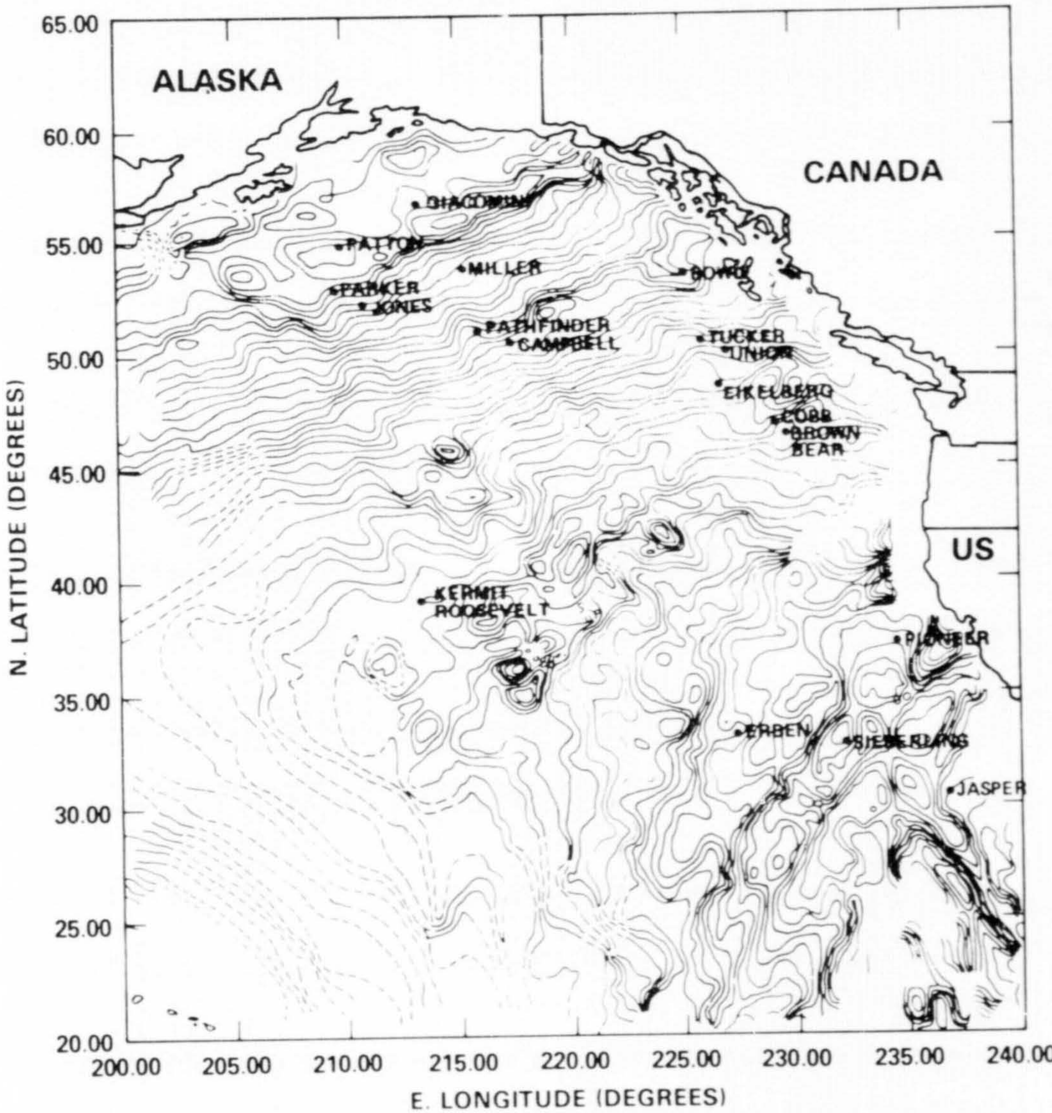

- DATA SPAN: 4/75 TO 6/76
- NUMBER OF ALTIMETER PASSES USED: 100
- NUMBER OF ALTIMETER MEASUREMENTS USED: 96,053
- REFERENCE GRAVITY FIELD USED: GEM-7 (l, m = 16)

DEVIATION FROM GEM-7

BIAS: −0.8 METERS

NOISE: ± 4.5 METERS

CONTOURS: 1 METER INTERVALS

Figure 6-8. GEOS 3 Altimeter Geoid for Gulf of Alaska Area

6-30
195

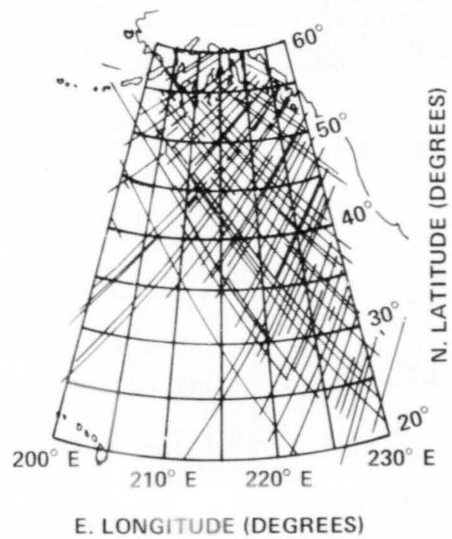

DATA DISTRIBUTION OF GULF
OF ALASKA SOLUTION AREA

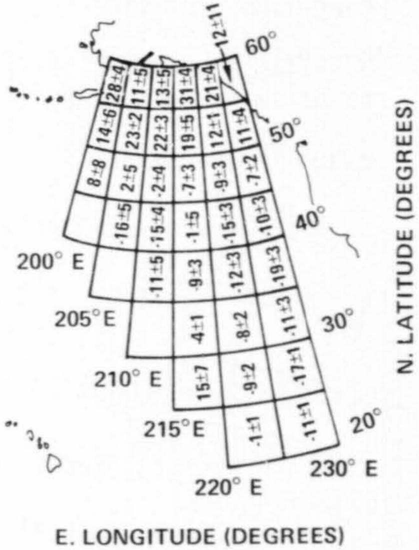

$5^0 \times 5^0$ GRAVITY ANOMALIES
(mgal)

- NUMBER OF PASSES USED: 98
- NUMBER OF OBSERVATIONS USED: 95,791
- REFERENCE GRAVITY FIELD USED: GEM-7 (COMPLETE THROUGH ORDER AND DEGREE 16)
- R_e: 6378145 METERS
- f^{-1}: 298.25
- GM: 3.986008×10^5 km^3/sec^2
- STANDARD DEVIATION OF FIT: ± 2.6 m

Figure 6-9. 5° x 5° Gravity Anomaly Recovery Solution for the Gulf of Alaska Area

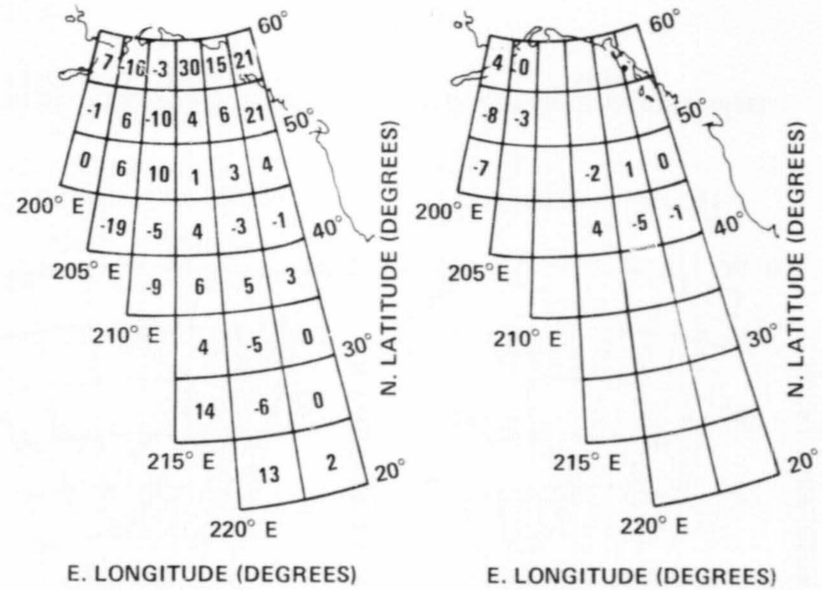

*(a) ANOMALY DIFFERENCES RESULTING FROM COMPARISON WITH $1^{0} \times 1^{0}$ MEAN FREE AIR GRAVITY ANOMALIES (R. RAPP 1976) (RMS DIFFERENCE: 7.6 mgals)

*(b) ANOMALY DIFFERENCES RESULTING FROM COMPARISON WITH MEAN FREE AIR GRAVITY ANOMALIES (COCHRAN & TALWANI 1977) (RMS DIFFERENCE: 3.6 mgals)

- REFERENCE GRAVITY FIELD USED: GEM-7 (COMPLETE THROUGH ORDER AND DEGREE 16)
- R_e: 6378145 METERS
- f^{-1}: 298.25
- GM: 3.986008×10^{5} km^{3}/sec^{2}
- STANDARD DEVIATION OF FIT: $\pm$ 2.6 m

Figure 6-10. Differences Between Estimated 5 × 5 Gravity Anomalies and Ground Truth

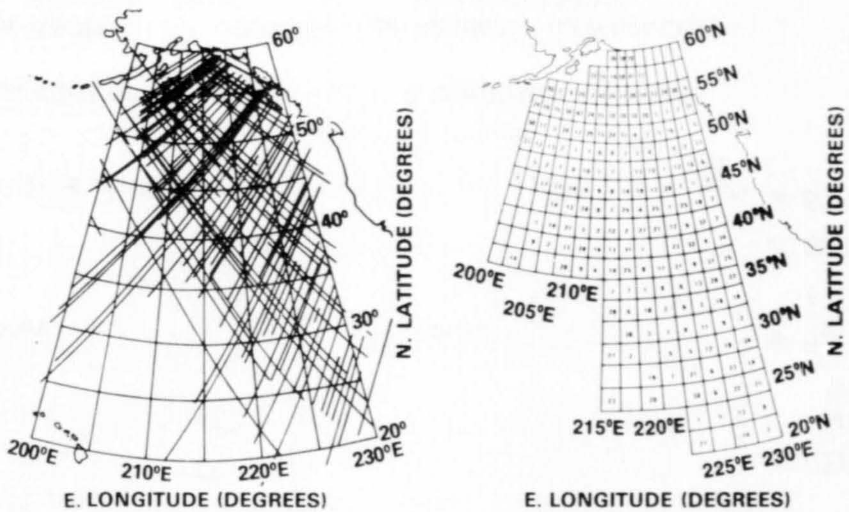

DATA DISTRIBUTION OF GULF OF ALASKA SOLUTION AREA

$2^\circ \times 2^\circ$ GRAVITY ANOMALIES (MGAL)

- **NUMBER OF PASSES USED: 98**
- **NUMBER OF OBSERVATIONS USED: 95,791**
- **REFERENCE GRAVITY FIELD USED: GEM-7 (COMPLETE THROUGH ORDER AND DEGREE 16)**
- **R_e: 6378145 METERS**
- **f^{-1}: 298.25**
- **GM: 3.986008×10^5 km^3/sec^2**
- **STANDARD DEVIATION OF FIT: ± 2.1 MET**

Figure 6-11. $2^\circ \times 2^\circ$ Gravity Anomaly Recovery Solution for Gulf of Alaska

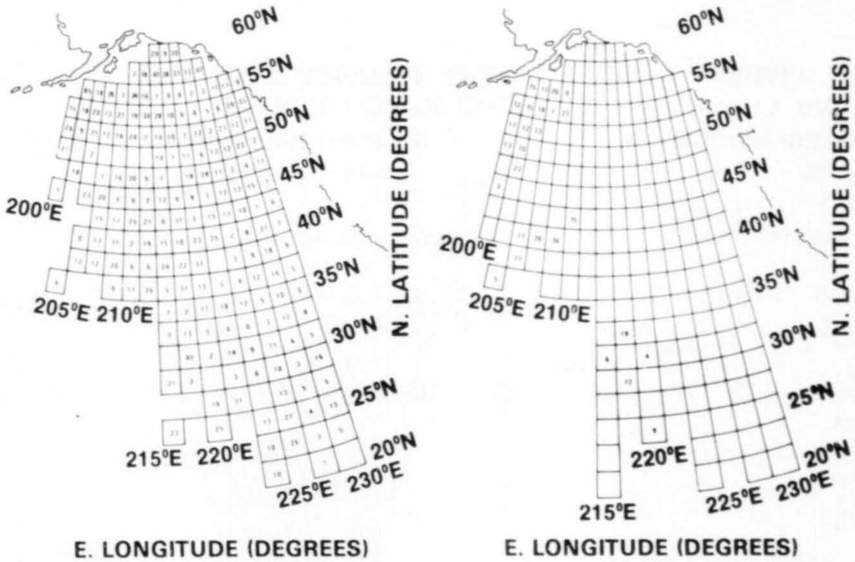

- REFERENCE GRAVITY FIELD USED: GEM-7 (COMPLETE TO ORDER AND DEGREE 16)
- R_e: 6378145 METERS
  f^{-1}: 298.25
- GM: 3.986008×10^5 km^3/sec^2
- STANDARD DEVIATION OF FIT: ± 2.1 METERS

(a) ANOMALY DIFFERENCES RESULTING FROM COMPARISON WITH 1° x 1° MEAN FREE AIR GRAVITY ANOMALIES (R. RAPP 1976) (RMS DIFFERENCE: 13.1 MGAL)

(b) ANOMALY DIFFERENCES RESULTING FROM COMPARISON WITH MEAN FREE AIR GRAVITY ANOMALIES (COCHRANE & TALWANI 1977) (RMS DIFFERENCE: 15.4 MGAL)

Figure 6-12. Differences Between Estimated 2° x 2° Gravity Anomalies and Ground Truth

GULF STREAM STUDIES

OBJECTIVE

The use of satellite altimetry in the study of ocean circulation is a newly emerging technique which carries great promise. Dynamic sea surface slopes from which current velocity can be inferred can be computed by standard oceanographic methods only with a knowledge of the ocean's density structure, and even then assumptions must be made regarding the "level of no motion." Direct, satellite-based measurements of sea height, together with an accurate gravity model, could vastly improve our understanding of near-surface as well as abyssal circulation.

BACKGROUND

The Gulf Stream system is being used as a testing ground for assessing the altimeter's ability to correctly identify ocean features. Studies presently underway include the tracking of Gulf Stream rings (eddies) with free-drifting buoys, construction of sea height maps from subsurface thermal data, and comparison of Seasat altimetry with surface truth observations.

ACCOMPLISHMENTS

Tracking Cyclonic Rings with Satellite-tracked Drifters

In an effort to provide surface truth information for use with Seasat altimetry, three cyclonic rings were "tagged" with free-drifting buoys parachuted into their centers from a Coast Guard aircraft (see figure 6-13). The drop was made from an altitude of 150 m. Once in the water, explosive cutters, sea-soluble tablets, and corrodible magnesium links cut the parachute away, deployed the drogue, and freed the buoy from its wooden pallet and drogue housing. Positions of the buoys during their 6-months duration are computed daily by Nimbus 6. This was only the second time that such an operation had been attempted, but the deployments were highly successful. The trajectory of one of the drifters shown in figure 6-14 demonstrates how one ring (called ring No. 4) migrated 350 km westward between September 1978 and January 1979. The ring initially moved westward at 8.7 cm/sec before coming to an abrupt halt at 72.5° W, where it remained for two months. Tracking of this same ring by conventional oceanographic methods extends back to July 13, 1978. Figure 6-15 shows examples of this ring's signature in two Seasat altimetry passes in July and August. The 60- to 65-cm sea surface depression characteristic of the cyclonic ring is clearly apparent near 33° N.

A Simple Method of Estimating Sea Surface Slopes

Biweekly maps of sea surface topography are being constructed from subsurface oceanographic observations available during the period of Seasat's operation (July to October 1978). The result will be oceanic "weather maps," charting regions of high and low sea height which should appear in the Seasat altimetry records. The data base consists primarily of bathythermographs, or vertical profiles of temperature. In order to simplify the construction of topographic maps, empirical relationships between thermal parameters and dynamic heights are being derived. The example shown in figure 6-16 demonstrates that given the temperature at 350 m (the depth limit of bathythermographs routinely dropped by Navy aircraft), dynamic height of the sea surface relative to a deep pressure surface is known to within an accuracy of 10 cm, or about the same accuracy as the Seasat altimeter. Data was obtained from 133 stations in the western North Atlantic. Standard deviation of the points about the second degree fit is 10.4 cm. Such relationships permit the calculation of sea surface slopes from thermal data alone.

Comparison of Seasat Altimetry With Surface Truth

Sea surface topography maps constructed thus far have been compared with the few available Seasat passes. Results for some of the tracks are impressive. Two of the best examples were shown in Figure 6-15, in which altimeter sea heights were differenced with the Marsh 5' geoid (1978). The Gulf Stream Stands out clearly and the North Wall position corresponds well with that observed in satellite infrared imagery. Regions in which subsurface temperature measurements indicate no major anomalies appear flat, as they should. Known ring positions correspond with unmistakable sea surface depressions. The profiles further serve to illustrate the extremely low noise level of the altimeter measurements. These high-quality data should produce accurate, altimetry-derived topographic maps of the sea surface for July and August 1978.

SIGNIFICANCE

Full utilization of the air-deployed drifter technique to obtain surface truth for altimetry will have to await a replacement for Seasat. Success of the buoy experiments conducted thus far indicates that surface drifters can be used to track rings for several months. We anticipate a large scale ring tracking program as part of the next satellite altimetry effort, and the airborne buoy capability provides the first reasonable method for attempting this.

With the present Seasat data we hope to show that ocean features such as currents and rings can be accurately detected with a satellite-borne altimeter. If this concept can be verified, it will provide a unique tool for attacking a variety of ocean circulation problems: Current meandering, the level of no motion, seasonal variability of currents, distribution and movement of both mid-ocean eddies and the more intense current rings, tidal analysis, and relationships between atmospheric and oceanic circulations.

FUTURE EMPHAISIS

We have looked at only a few Seasat altimetry passes through the Gulf Stream region; much work remains to be done. Individual passes will be examined for meso scale ocean features with particular emphasis on the western North Atlantic, the western North Pacific, and the southern ocean surrounding Antarctica. Maps of sea surface topography will be generated from all existing Seasat data in an attempt to describe the ocean eddy population and the distributions of potential and kinetic energy. Drifting buoy experiments will be continued in cooperation with the Naval Oceanographic Office and the Coast Guard. More work may also be done with the GEOS 3 altimetry data base.

REFERENCES AND PUBLICATIONS

Cheney, R.E. and B.P. Blumenthal, "Tracking Gull Stream Rings With Air-Deployable Surface Drifters," *Gulfstream, 6,* 10 NOAA National Weather Surface publication, 1978.

Cheney, R.E. and B.P. Blumenthal, "Air-Deployable Ocean Drifters," *Polymode News,* 57, 1978.

Cheney, R.E., P.L. Richardson, and K. Nagasaka, "Tracking a Kuroshio Cold Ring With a Free-drifting Surface Buoy," *Deep-Sea Research* in press, 1979.

Cheney, R.E. and J.G. March, "Comparison of Seasat Altimetry with Thermally Derived Sea Heights in the Western North Atlantic," *E@S Trans. AGU, 60,* 232 (abstract), 1979.

Marsh, J.G. and E.S. Chang, "5' Detailed Gravimetric Geoid in the Northwestern Atlantic Ocean," *Journal of Marine Geodesy, Atlantic 1,* 3, 253-261, June 1978.

Richardson, P.L., R.E. Cheney, and L.A. Martini, "Tracking of a Gulf Stream Ring With a Free Drifting Surface Buoy," *Journal of Physical Oceanography, 7,* 4, 580-590, 1977.

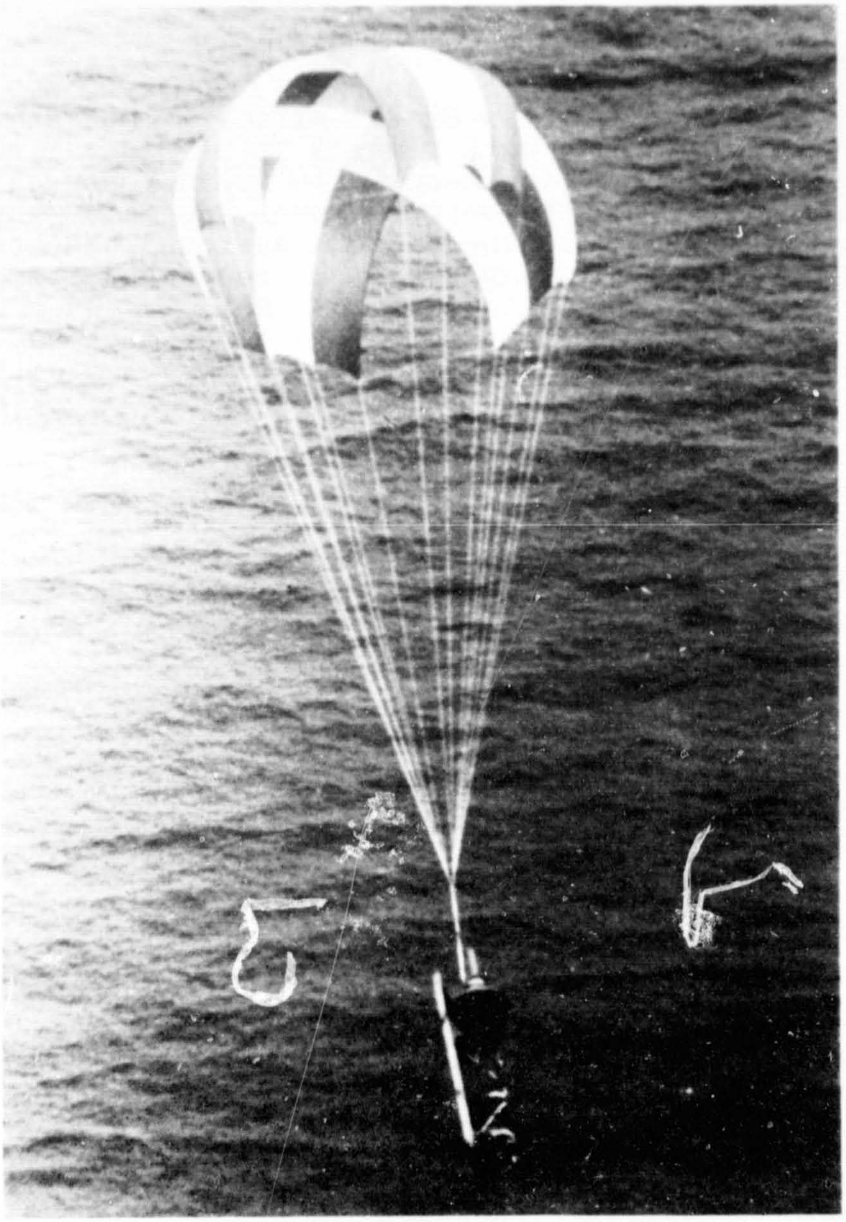

ORIGINAL PAGE IS
OF POOR QUALITY

Figure 6-13. Ocean Drifter Being Parachuted
Into a Gull Ring, September, 22, 1978

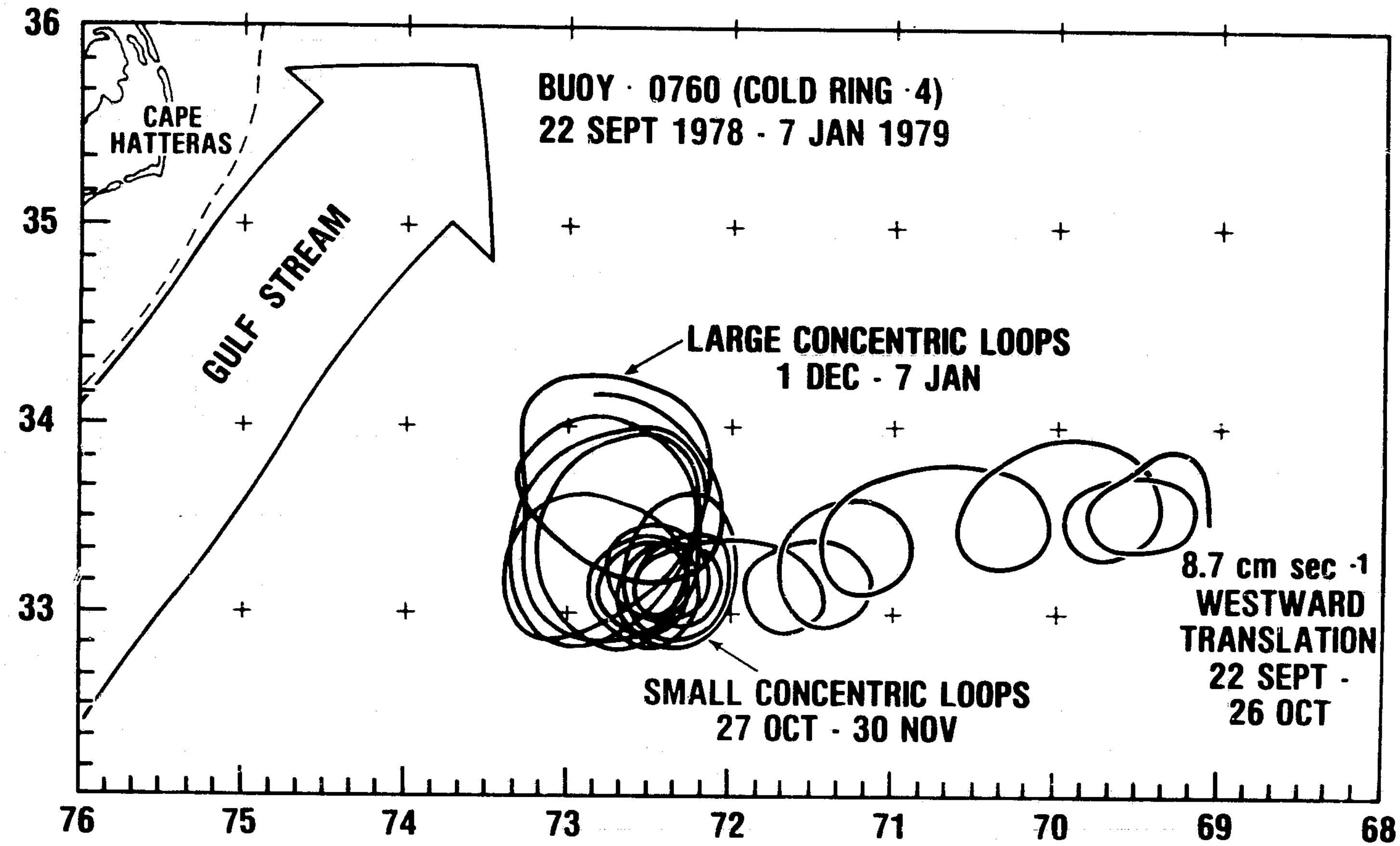

Figure 6-14. 107-day Trajectory of Buoy No.0760 Trapped in a Cyclonic Gulf Stream Ring West of Bermuda

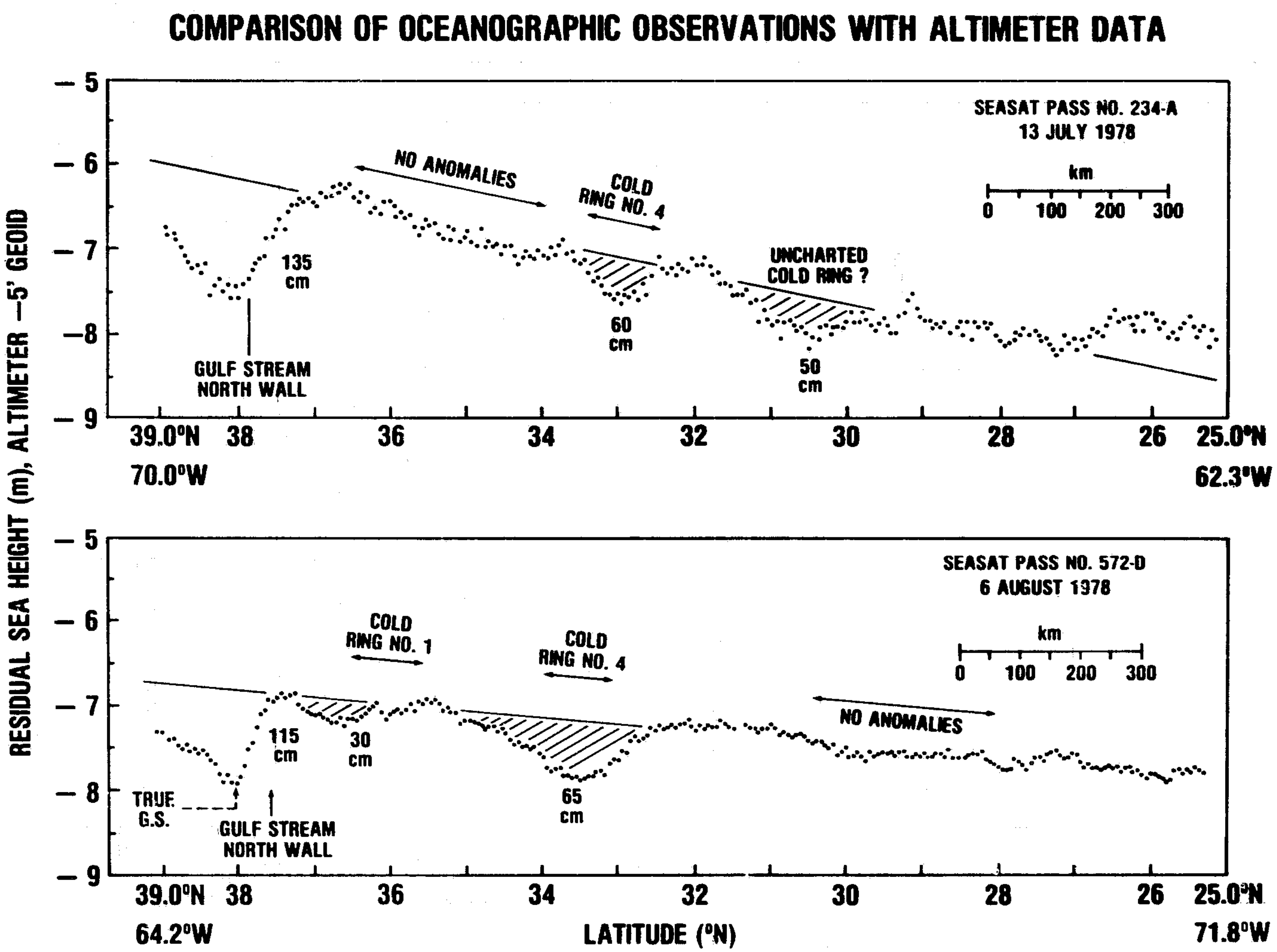

Figure 6-15. Comparison of July and August 1978 Oceanographic Observations with Seasat Altimeter Data

6-40
205

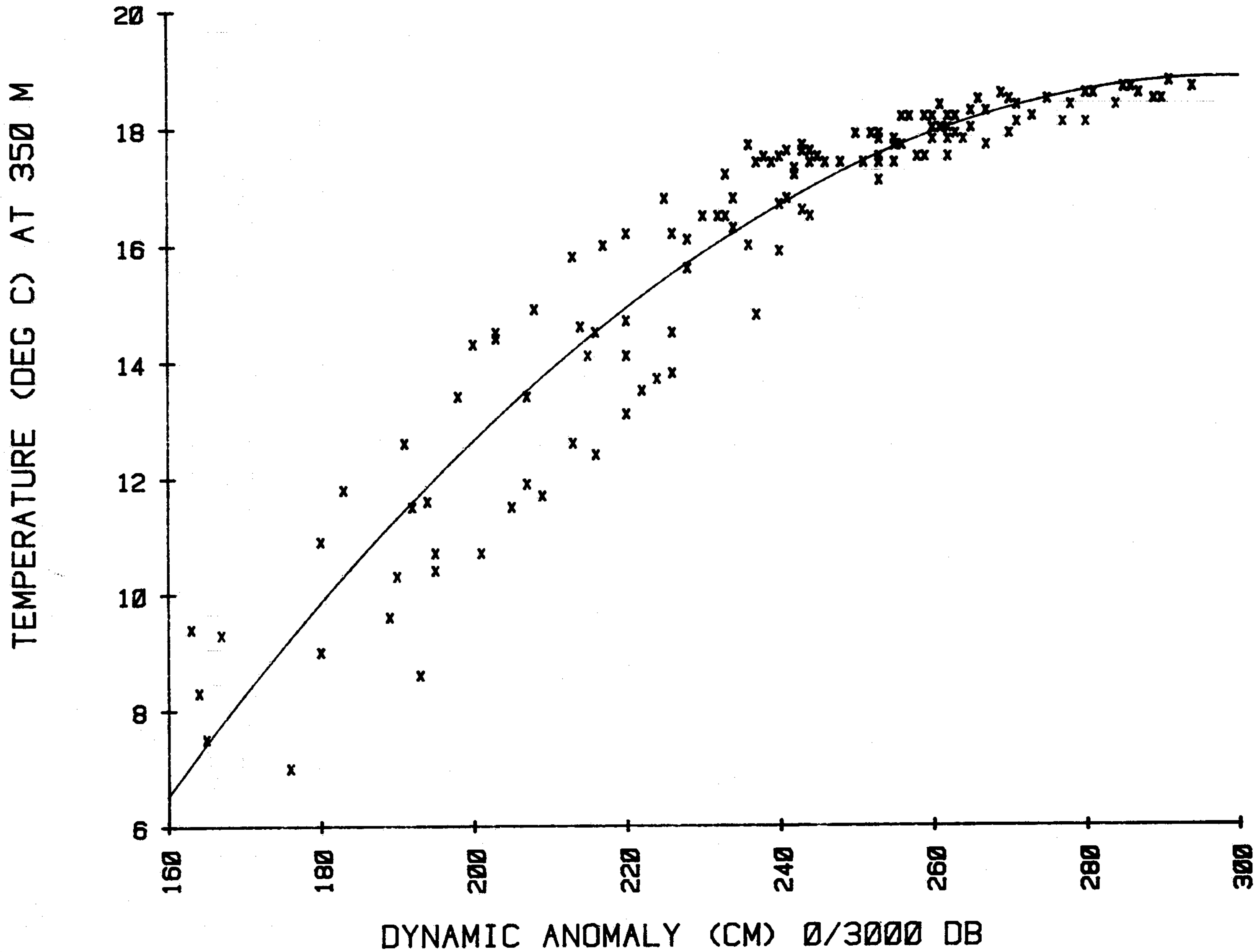

Figure 6-16. 350-m Temperature Plotted Against Dynamic Height of the Ocean Surface Relative to 3000 dB (Approximately 2958 m)

OCEAN TIDAL STUDIES FROM SATELLITE ORBIT DATA

OBJECTIVES

The objective of this work was to obtain information about the M_2 (the principal lunar semidiurnal) ocean tide from the observed effect of this tide on the orbits of artifical Earth satellites. Accurate modeling of the ocean tides provides a fundamental data type for increasing our knowledge of the dynamics of the Earth and this knowledge is also necessary for improved satellite orbit determination.

BACKGROUND

Ocean tidal effects are most easily observed in the inclination histories of the satellites, it being the best behaved of the orbital elements for tidal studies. In some instances, the perturbations can be seen satisfactorily in the longitude of the ascending node. Tidal constituents such as S_2, K_1, K_2, and P_1 typically cause variations in these orbital elements up to several tenths of an arc second in amplitude, with periods of tens or hundreds of days.

The most intriguing ocean tide to study is the M_2 because it has the greatest effect on the Earth's oceans. However, its influence on satellite orbital elements is small, usually no more than a few hundredths of an arc second in amplitude with periods averaging about two weeks. As a consequence, very precise data must be derived in order to obtain a significant recovery of parameters for the M_2 ocean tide.

RECENT ACCOMPLISHMENTS

M_2 Ocean Tide Parameters

An estimation has been made of the principal long-period spherical harmonic parameters in the representation for the M_2 ocean tide from the orbital histories of three satellites: 1967-92A (transit), Starlette, and GEOS 3. The data used were primarily the evolution of the orbital inclinations of the satellites, with the addition of the longitude of the ascending node from GEOS 3.

Figures 6-17, 6-18, 6-19, and 6-20 display the data used in this study. These data consist of the "residuals" remaining in the orbital elements after all known perturbations, including solid-Earth tides, have been accounted for. The ocean tide effects are discernible in these residuals. Frequency analyses were performed on the residuals to ascertain the periodicities to be included in a series of least squares fits to the residuals. These least squares analyses produced amplitudes and phases for the observed harmonic variations in the residuals. Figures 6-17, 6-18, 6-19, and 6-20 also display the least squares fits, along with the observed amplitudes for the M_2 effects. The oscillations caused by the M_2 tide can be clearly seen in each instance. The rms of fits for the four figures are .036, .051, .030, and 0.34 arc seconds, respectively.

A subsequent least squares solution was then performed in order to recover the M_2 ocean tide parameters. In this solution, use was made of the amplitudes and phases for the M_2 tide obtained in the breakdown of the residuals. In addition, the following perturbation equations (derived from an expression for the ocean tide potential) were used:

1967-92A:

$$\Delta I = \frac{0.01003 \text{ arc sec}}{\text{cm}} C_{22}^{+} \sin (2\Omega - 2\lambda' + \varepsilon_{22}^{+})$$

$$+ \frac{0.009606 \text{ arc sec}}{\text{cm}} C_{42}^{+} \sin (2\Omega - 2\lambda' + \varepsilon_{42}^{+})$$

Starlette:

$$\Delta I = \frac{0.006268 \text{ arc sec}}{\text{cm}} C_{22}^{+} \sin (2\Omega - 2\lambda' + \varepsilon_{22}^{+})$$

$$- \frac{0.01190 \text{ arc sec}}{\text{cm}} C_{42}^{+} \sin (2\Omega - 2\lambda' + \varepsilon_{42}^{+})$$

GEOS 3:

$$\Delta I = \frac{0.01288 \text{ arc sec}}{\text{cm}} C_{22}^{+} \sin (2\Omega - 2\lambda' + \varepsilon_{22}^{+})$$

$$- \frac{0.003267 \text{ arc sec}}{\text{cm}} C_{42}^{+} \sin (2\Omega - 2\lambda' + \varepsilon_{42}^{+})$$

$$\Delta\Omega = \frac{-0.002394 \text{ arc sec}}{\text{cm}} C^+_{22} \cos\left(2\Omega - 2\lambda' + \varepsilon^+_{22}\right)$$

$$- \frac{0.03464 \text{ arc sec}}{\text{cm}} C^+_{42} \cos\left(2\Omega - 2\lambda' + \varepsilon^+_{42}\right)$$

where

I = inclination of satellite

Ω = longitude of ascending node of satellite

λ' = mean longitude of the Moon (referred to ecliptic)

C^+_{22}, C^+_{42} = long period spherical harmonic parameters, expressed in cm (recovered in the solution)

$\varepsilon^+_{22}, \varepsilon^+_{42}$ = phase angles (recovered in the solution)

The results are shown in table 6-2, along with several other recent determinations. The uncertainties are the formal standard deviations of the solution; the realistic errors are probably somewhat larger.

Deceleration of the Moon's Mean Longitude

Dissipational tidal friction in the oceans is known to provide the largest contribution to N, the observed deceleration in the lunar mean longitude. Further, only the second degree components of the ocean tide contribute significantly to this secular decay. The main ocean tide variations in N are provided by the second degree terms for the M_2, N_2, and 0_1 constituents. The contributions from these constituents (derived from the ocean tide potential) are presented in table 6-3. In order to compute a value for N from these expressions, we use our satellite-derived M_2 parameters presented in table 6-2 and the N_2 and 0_1 models of R. Estes of Business and Technological Systems, Inc., Seabrook, Maryland:

N_2		0_1	
C^+_{22}	$^+_{22}$	C^+_{21}	$^+_{21}$
.58 cm	358°	2.70 cm	159°

The result is a value for N of -25 ± 3 arc seconds/century^2. Table 6-4 presents a comparison of this estimate with several other recent determinations.

SIGNIFICANCE

The satellite-derived $(2,2)^+$ parameters for the M_2 ocean tide are in accord with the numerical models of Estes and Schwiderski and the satellite solution of Goad and Douglas (1978), if one assumes the realistic uncertainties to be at least 50 percent larger than the formal standard deviations. The $(4,2)^+$ values are in good agreement, with the noticeable exceptions of the C^+_{42} of Schwiderski and the ϵ^+_{42} of Estes. The data used by Goad and Douglas (1978) form a subset of the data used in the present investigation, so the consistency between the two models is not unexpected. However, the agreement with the numerical models is quite satisfying.

The credibility of our M_2 ocean tide solution is further enhanced by the close accord between our computed value for the deceleration of the lunar mean longitude and the other recently reported estimates. The major contribution to the N comes from the $(2,2,)^+$ parameters for the M_2 ocean tide.

It is evident from the results of this investigation that studies of close Earth satellite orbits are able to provide important information about the tidal forces acting on the Earth. A more detailed discussion of this work may be found in Felsentreger et al., 1979.

FUTURE EMPHASIS

Studies of the sort just described, while providing valuable information about the ocean tides, can furnish only the gross properties of ocean tidal models. Tidal variations on the order of centimeters must be modeled for oceanographic studies such as current or eddy tracking to be successful. Consequently, work has been planned to use satellite altimetry data to develop global ocean tide models accurate to this level.

REFERENCES AND PUBLICATIONS

Calame, O., and J.D. Mulholland, "Lunar Tidal Acceleration Determined From Laser Range Measures," *Science, 199,* 977-978, 1978.

Felsentreger, T.L., J.G. Marsh, and R.G. Williamson, "M_2 Ocean Tide Parameters and the Deceleration of the Moon's Mean Longitude From Satellite Orbit Data," *J. Geophys. Res.,* in press 1979.

Goad, C.C., and B.C. Douglas, "Lunar Tidal Acceleration Obtained from Laser Range Measures," *Science*, *199*, 977, 1978.

Goad, C.C. and B.C. Douglas, "Lunar Tidal Acceleration Obtained From Satellite-Derived Ocean Tide Parameters," *J. Geophys. Res.*, *83*, 2306-2310, 1978.

Morrison, L.V., and C.G. Ward, "An Analysis of The Transits of Mercury 1677-1973," *Mon. Not. Roy. Astron. Soc.*, *173*, 183-206, 1975.

Muller P.M. "Determination of the Cosmological Rate of Change of G and the Tidal Accelerations of Earth and Moon from Ancient and Modern Astronomical Data," JPL Special Publication 43-36, Jet Propulsion Laboratory, Pasadena, California, 1976.

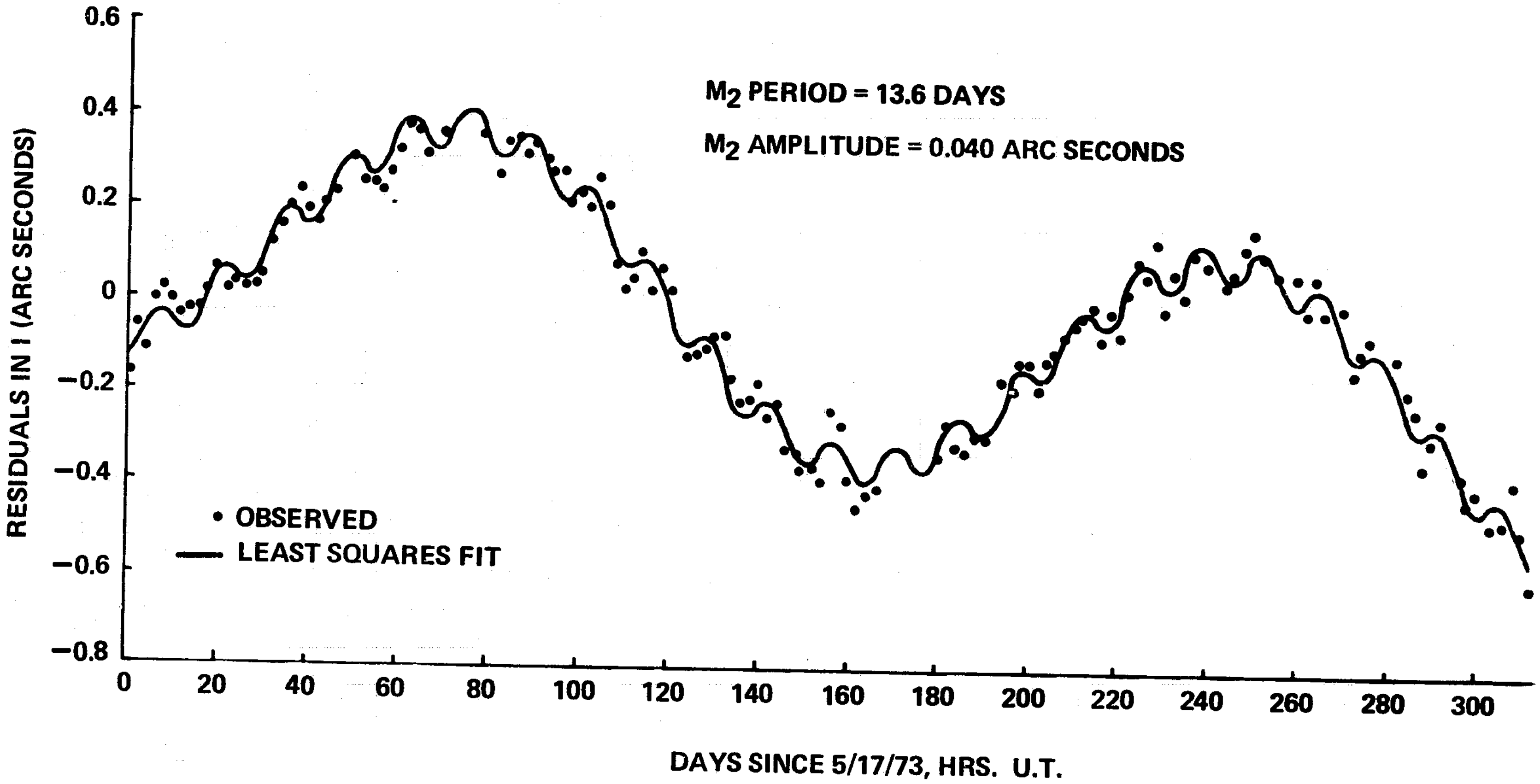

Figure 6-17. Inclination Residuals for 1967-92A (Transit)

6-47
2/2

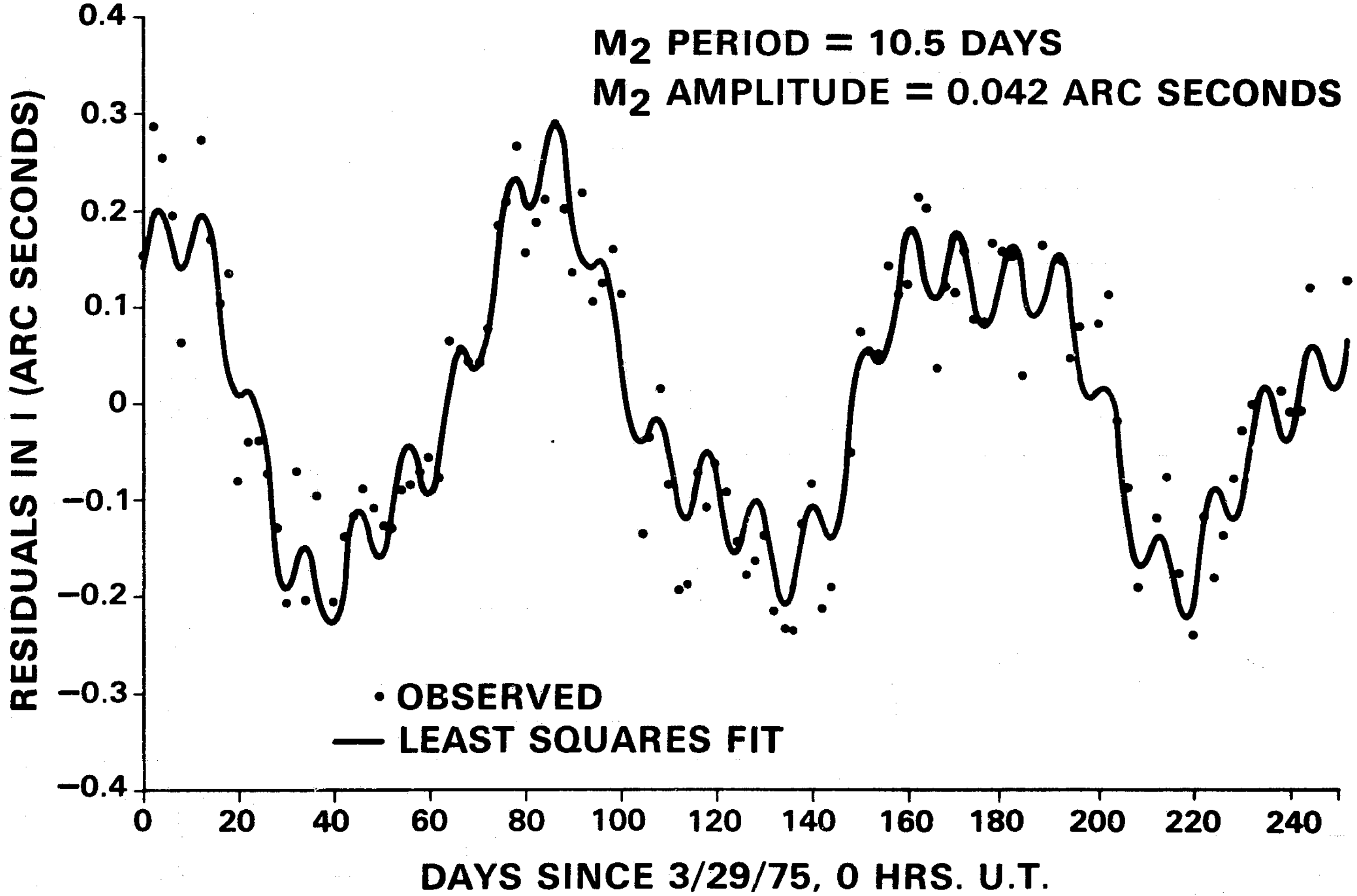

6-48
213

Figure 6-18. Residuals in Inclination for Starlette

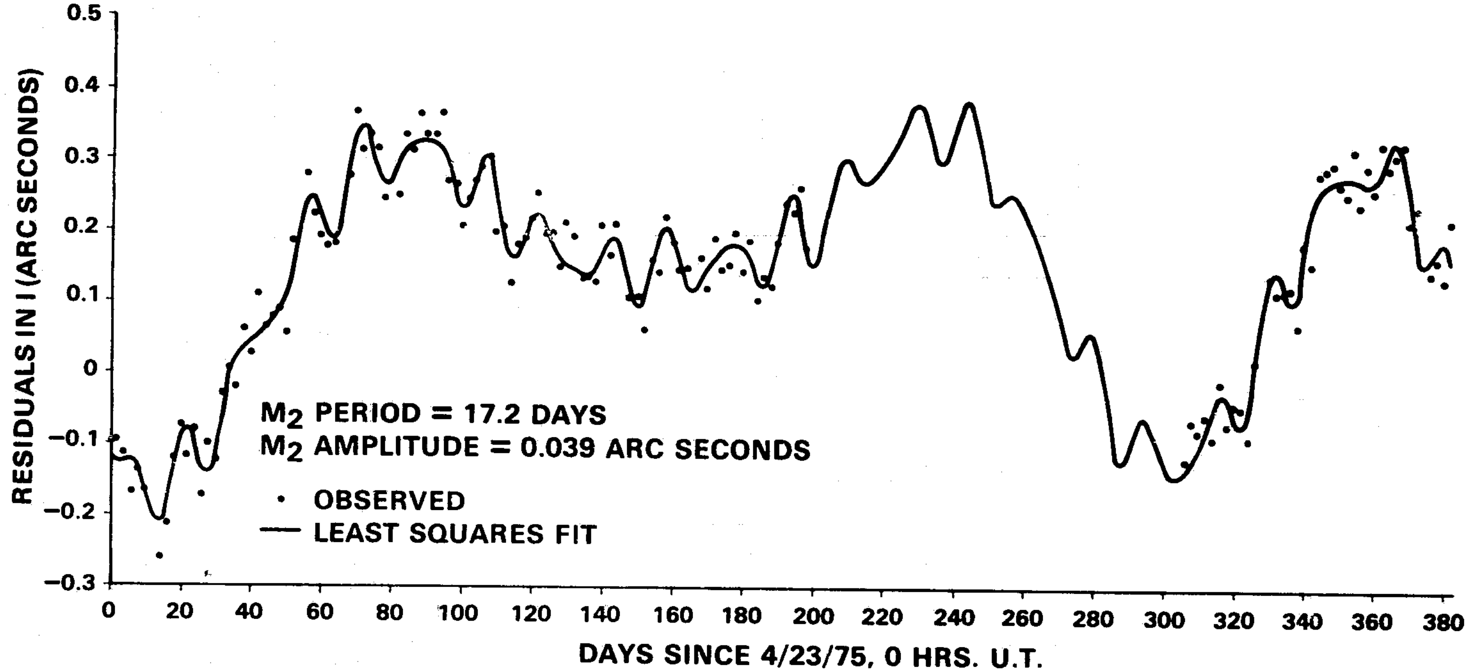

Figure 6-19. Inclination Residuals for GEOS 3

#118
6-49

6-50
215

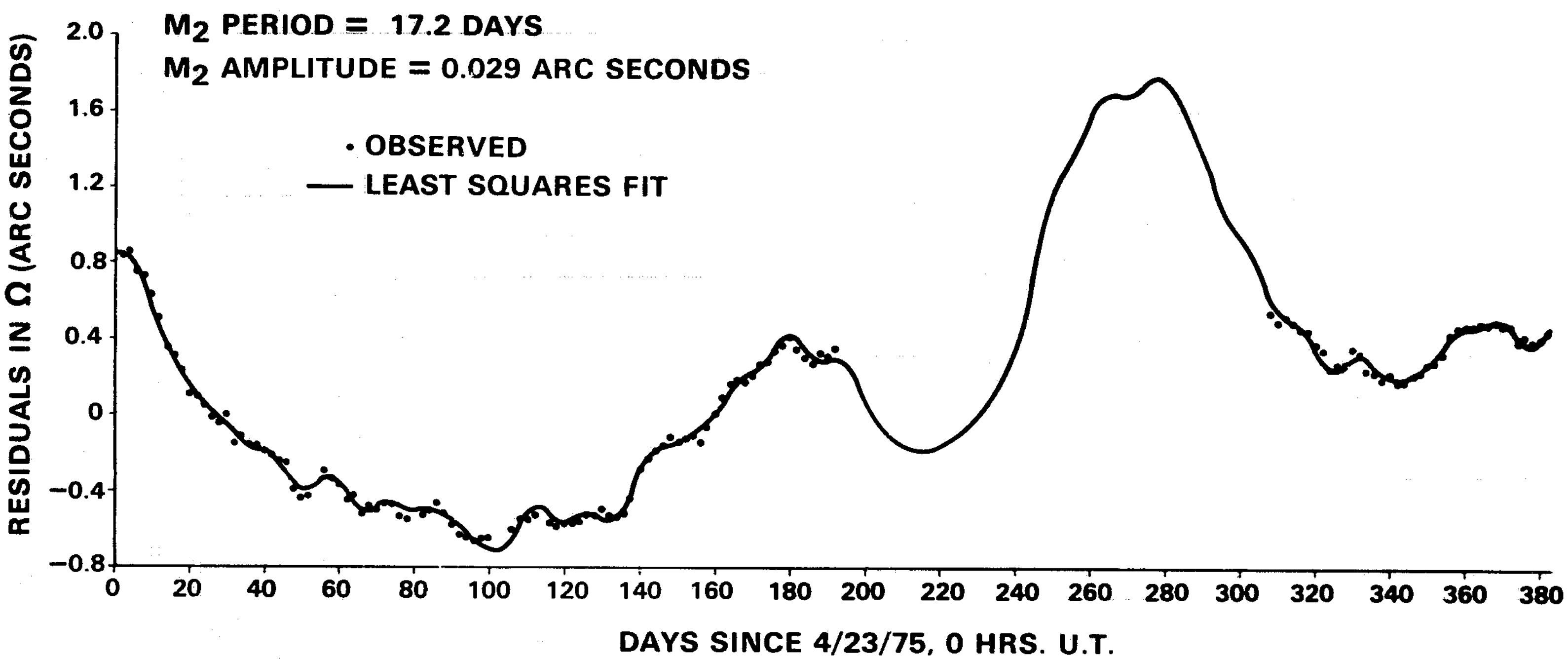

Figure 6-20. Residuals in Longitude of Ascending Node for GEOS 3

Table 6-2
M_2 Ocean Tide Parameters With Recent Solutions

Source	C^+_{22} (cm)	ε^+_{22} (deg)	C^+_{42} (cm)	ε^+_{42} (deg)
Felsentreger et al.[1]	3.42 ± 0.24	325.5 ± 3.9	.97 ± 0.12	124.0 ± 6.9
Goad and Douglas (1978)[1]	3.23 ± 0.25	331 ± 6.0	.87 ± 0.19	113 ± 6.0
Estes (BTS)[2]	3.31	333	.96	145
Schwiderski (NSWC)[3]	3.59	326	1.34	126

[1] Satellite Solutions.

[2] Business and Technological Systems, Inc., Seabrook, Md., numerical solution.

[3] Naval Surface Weapons Center, Dahlgren, Va., numerical solution.

Obtained from C. Goad, private communication.

Table 6-3
Summary of Principal Ocean Tidal Effects on the Deceleration of the Moon's Mean Longitude

Tidal Constituent	$\Delta\dot{N}$ (Arc Seconds/Century^2)
M_2	C^+_{22} $(-8.04 \cos \varepsilon^+_{22} + 0.22 \sin \varepsilon^+_{22})$
N_2*	C^+_{22} $(-2.32 \cos \varepsilon^+_{22} + 0.06 \sin \varepsilon^+_{22})$
O_1*	C^+_{21} $(-0.32 \cos \varepsilon^+_{21} - 1.41 \sin \varepsilon^+_{21})$

*Estes (BTS) numerical models (obtained from C. Goad, private communication).

Table 6-4
Recent Values for the Deceleration of the Moon's Mean Longitude

Source	$\dot{N}$ (Arc Seconds/Century^2)
Felsentreger et al.[1]	-25 ± 3
Goad and Douglas (1978)[2]	-26 ± 3
Morrison and Ward (1975)[3]	-26 ± 2
Muller (1976)[4]	-27.2 ± 1.7
Calame and Mulholland (1978)[5]	-24.6 ± 1.6

[1]Satellite solution.

[2]Satellite solution.

[3]From transits of Mercury.

[4]From ancient eclipses and transits of Mercury.

[5]From lunar laser ranging.

CHAPTER 7

LAND RESOURCES

OVERVIEW

The management of our resources, both natural and man-made, requires accurate and timely information. The Landsat satellites and other remote sensors afford a unique, synoptic view of our resources and can potentially yield accurate information in a more rapid and inexpensive manner than conventional data collection methods. The common goal of the land resource projects is to develop and evaluate the capability of remote sensing techniques and sensors to provide the information required for intelligent resource management decisions.

Six scientists are involved in land resource projects, and they are investigating remote sensing applications for a variety of resource managers. The forest insect investigation is demonstrating the usefulness of Landsat data for the planning of infestation suppression operations by responsible agencies. The surface mine project is developing remote sensing methods for the monitoring of mine reclamation by the Environmental Protection Agency. The census project is applying Landsat data to the acquisition of information required by the Bureau of the Census for the management of the urban environment.

Despite the diversity of resource applications under investigation, the projects share several research objectives. One such objective is the integration of Landsat data with other data sources, such as terrain data (i.e., elevation, slope, aspect), soils information, and census survey data. Other common goals are the detection of environmental changes and the development of methods to assess the accuracy of information derived from remotely sensed data. The pursuit of these objectives will be greatly facilitated by the implementation of an Automated Geographic Information System (AGIS). An additional common research interest addresses the removal of extrinsic effects on remotely sensed data due to variations in illumination, atmosphere, and topography. The topographic effect project is developing a method to eliminate data variations due to changes in slope angle and aspect.

These research projects are related to both present and future satellite systems. Landsat 1, 2, and 3 data are being used to develop new analytical techniques. The potential of Landsat D's Thematic Mapper is being evaluated, while the requirements for the next generation of Earth observation sensors is being pursued.

Contributors to this chapter include Arthur Anderson, Jerrold Christenson, Brent Holben, James Irons, Christopher Justice, Lee Miller, and David Toll.

FOREST INSECT AND DISEASE INVESTIGATION

OBJECTIVE

The objective of the investigation is to develop and evaluate remote sensing techniques and sensors to facilitate the use of present and future satellite systems to detect, monitor, and assess accurately the intensity and spatial distribution of major forest insect infestations in the northeastern U.S.

BACKGROUND

Historically, the magnitude of the annual losses incurred by our nation's 500-million acres of forest land due to forest insect infestations has been estimated to exceed 5-billion board feet: enough lumber to build at least 1-million houses. To initiate timber salvage and/or infestation suppression operations, the responsible agencies must have accurate, timely, standardized and efficient methods of detecting and mapping the insect damage. Present-day survey techniques consisting of ground inspection and low altitude aerial surveillance and photography are often found to be obsolete, prompting federal and state agencies to request help in the research and development of techniques to facilitate the use of satellite remotely sensed data for monitoring insect infestations.

Preliminary research conducted at GSFC has indicated that Landsat MSS data can be utilized to detect deciduous forest lands heavily defoliated by the gypsy moth caterpillar during their late June/ early July feeding cycle. However, these preliminary findings indicated that additional research and development is needed to devise techniques: (a) To eliminate errors of commission (i.e., misclassification) with non-forest areas when classifying defoliation, and (b) to delineate more consistently areas of light to moderate defoliation (i.e., those areas where insect populations are increasing).

RECENT ACCOMPLISHMENTS

Geometrically registered Landsat data sets depicting both nondefoliated (July 19, 1976) and defoilated (June 27, 1977) forest stand conditions have been created for two test sites in central Pennsylvania. Image differencing techniques have been investigated and applied to these data sets as a means of enhancing the visual delineation of areas of defoliation (i.e., change detection). To eliminate the potential of errors of commission with non-forest cover types during the digital classification of defoliation, a hierarchial classification procedure has been successfully developed for masking out (i.e., removing) all nonforest areas in the image data.

SIGNIFICANCE

The combined effect of these accomplishments is that gypsy moth defoliation can be detected and isolated with greater accuracy and efficiency, thus increasing the probability of future operational use of the satellite data for this application.

FUTURE EMPHASIS

Given Landsat MSS spatial, spectral, and radiometric resolution, and the rather subtle changes which must be detected to differentiate healthy forest from light defoliation, light from moderate, and moderate from heavy, it is important that peripheral effects on the imagery due to the atmosphere, illumination and topography be removed to provide standardized reflectance values of ground objects. The future emphasis of the research will be to investigate and develop techniques to delineate accurately and consistently the severity of defoliation during the June/July feeding cycle by accounting for as many of these peripheral effects as possible.

REFERENCES AND PUBLICATIONS

Williams, D.L., and M.L. Stauffer, "Monitoring Gypsy Moth Defoliation by Applying Change Detection Techniques to Landsat Imagery," *Proceedings of the Symposium on Remote Sensing for Vegetation Damage Assessment, American Society of Photogrammetry*, 221-229, Falls Church, Virginia 1978.

Williams, D.L., and L.D. Miller, "Monitoring Forest Canopy Alteration Around the World with Digital Analysis of Landsat Imagery," *Proceedings of the ISP/IUFRO International Symposium of Remote Sensing Observation and Inventory of Earth Resources and the Endangered Environment*, 1721-1762, Freiburg, West Germany, 1978.

SURFACE MINE MONITORING

OBJECTIVE

The purpose of the surface mine monitoring project is the evaluation of new remote-sensing techniques and sensor packages for the monitoring of surface mines in the eastern United States. The project addresses the impact of the increased spatial resolution and additional spectral bands provided by potential new sensors on monitoring capabilities. The evaluation will result in the designation of operational monitoring procedures by the EPA.

BACKGROUND

The EPA Office of Monitoring and Technical Support is conducting a comparative study of remote-sensing techniques for the monitoring of eastern, midwestern and western surface mines. The current project at GSFC was initiated by the EPA as a part of this overall study. The EPA hopes to develop rapid, cost-effective, remote-sensing techniques to meet the monitoring requirements set forth in the Federal Surface Mining Control and Reclamation Act of 1977 (Public Law 95-87).

Three test areas in central Pennsylvania have been selected for this project. The areas are located on the Appalachian Plateau and contain a variety of abandoned, reclaimed, and active mines. Remotely-sensed data collected over the areas during the fall of 1978 are being gathered. The General Electric Company has been contracted for data analysis and HRB Singer, Inc. is providing ground data.

The data from the fall included EPA-Daedalus 11-channel scanner data, Landsat MSS data, and Landsat-3 Return Beam Vidicon (RBV) data. Landsat MSS imagery and Computer Compatible Tape (CCT's) have been delivered, and RBV CCT's will be ordered as soon as the digital data become available. Daedalus scanner data is currently being reformatted by the EPA for analysis on GE's Image-100 processing system.

The ground data provided by HRB Singer, Inc. consists of 1:24,000 and 1:12,000 scale aerial photographs accompanied by acetate overlays. The overlays delineate land-use categories, slope classes, bare soil and spoil surface colors, water bodies, and vegetative categories within the test areas. Measurements of the acreage covered by surface mines in the areas will also be provided.

RECENT ACCOMPLISHMENTS

Analysis has begun on the Landsat MSS digital data. The analysis will result in thematic maps showing the extent of surface mine activity, rehabilitation, and revegetation in the test areas. The accuracy of the thematic maps will be determined by comparisons to ground data.

SIGNIFICANCE

The data analysis will permit a comparison of the various sensors. The improved RBV resolution will be compared to MSS data. The additional spectral bands of the Daedalus scanner will be analyzed to determine an optimal set of bands for mine monitoring.

FUTURE EMPHASIS

The data analysis will be repeated for data collected over the test areas during the Spring of 1979. HRB Singer, Inc. will again collect ground data. In addition to MSS, RBV, and Daedalus scanner data, Landsat-D TM simulator data may be acquired. Following data analysis, GSFC will recommend the optimal sensor packages and time of year for monitoring. Furthermore, GSFC will designate the required data processing techniques for the operational monitoring of eastern surface mines by the EPA.

NASA-CENSUS APPLICATIONS PILOT TEST URBAN AREA DELINEATION

OBJECTIVES

The overall program objective is to apply image analysis techniques to Landsat data for the delineation and periodic updating of urbanized areas in the United States and to transfer that technology. Specific objectives are to: (a) Assess the accuracy, timeliness, savings (time and money); cost effectiveness, and increased capability provided by Landsat data analysis; (b) Train Census Bureau personnel; and (c) Disseminate methods and techniques to other user groups.

BACKGROUND

This project is in support of a continued and expanding need of the Bureau of the Census for current and accurate information about the urban environment. The Bureau of the Census is required by law to delineate the urbanized area for each standard metropolitan statistical area in the United States at specific time intervals. Recent legislation and requirements of several federal and state funding programs have increased the need for more frequent updates of selected demographic variables.

RECENT ACCOMPLISHMENTS

Recent accomplishments of the program include:

- Landsat data analyses were completed for five geographically distinct urbanized areas. Seattle, Boston, Richmond, Austin, and Orlando were the test sites. Results of the analyses were provided to the Census Bureau for evaluation.

- Line printer thematic maps (1:24,000) were produced to match Census Bureau Metropolitan Map Series.

- A technique was developed so that Landsat land cover statistics can be listed by census tracts.

- Techniques to superimpose census tract boundaries on urban satellite data through two input modes, television scanner, and digitizer were developed.

- An Image Based Information System (IBIS) was tested on the Richmond, Virginia test area. The test was designed to show the integration of Landsat data with ancillary census data into a graphical display for use by the Census Bureau.

- An image differencing (pixel-by-pixel subtraction of data from two separate dates) change detection scheme was developed to monitor growth in the urban fringe zone in Austin, Texas. Of ten new residential areas constructed in the study area, eight were identified correctly.

- Theoretical aspects of classification accuracy evaluation were studied. Various approaches to accuracy evaluation were discussed, with identification for future developments.

- Preliminary output from a textural features program gives promise for future work. The texture features quantitatively describe the spatial distribution of spectral information across an image. The program should aid in detecting various land cover features in an urban area.

- Five image reformatting and enhancements were tested and evaluated for Landsat urban area images. A cubic-convolution resampling provided the best visual results. A high pass filter to enhance linear features requires further development.

- Monthly urban area cloud cover probabilities relative to Landsat imagery were obtained. The information will assist Census Bureau personnel in determining "windows" of available imagery.

SIGNIFICANCE

Current research efforts at GSFC indicate that the techniques being developed will be of considerable value for use in urban area analysis. The Landsat information extraction techniques will provide land cover data which can be compiled through a geographic reference grid that corresponds with the user's data base. The land cover data extracted from Landsat can then be an effective tool for monitoring the large number of urbanized areas in the U.S. (300 by 1980).

FUTURE EMPHASIS

<u>Urban Change Detection Technique Development</u>

One approach, "image differencing," is being used to subtract two anniversary Landsat scenes, one from the other. Significant changes in reflectance values are and will be identified and evaluated for their land cover change. Other change detection approaches will be investigated more thoroughly for two additional cities, Denver and Richmond.

Quantitative Accuracy Assessment

A computer spatial data plane representing a topographic map will be utilized as "ground truth" to test the Landsat thematic output map.

Evaluation Material to the Census Bureau

Output products in user compatible formats similar to those developed in the test phase baseline approach will be produced.

Technology Transfer

Successful techniques will be implemented by the Bureau for future census in: 1980 - base imagery (initial image data): 1983 - change detection for preparation of urbanized areas (if mid-decade census is required); 1987 - change detection for 1990 census.

Interface RBV and Thermal Data With MSS for Urban Areas

A systematic approach to derive land cover feature boundary information from the high resolution RBV data will be developed. The use of enhanced thermal data for urban feature discrimination will be evaluated.

Urban Surface Texture Information

Techniques to improve land cover classification among areas of similar spectral response by introducing textural information into the decision process will be evaluated.

Classification Improvement Using Digital Terrain Data

The terrain parameters most likely to improve MSS classification accuracies will be identified. The optimum scale and the most effective method of incorporating digital terrain data with Landsat data will be examined.

Future Sensor Definition

This task will utilize the results of a JPL sensor study task and will combine the findings with the results of a related literature search to initiate a proposal for future sensor systems optimized for urban land use monitoring.

REFERENCES AND PUBLICATIONS (continued)

Abdullah, A., and Harper, J., of Computer Sciences Corporation, Silver Spring, Maryland, "Technical Notes on the Classification Problems," NASA/GSFC TM 78/6000, April 1978.

Christenson, J.W., "Urbanized Area Analysis Using Landsat Data," presented at Harvard Computer Graphics Laboratory's International User's Conference on Computer Mapping, Cambridge, Mass., 1978.

Christenson, J.W., presented at the American Society of Photogrammetry, Annual Meeting, Washington, D.C., "Developing Techniques in Landsat Digital Data Processing for Landcover Mapping in the Urban Fringe Zone," 1978.

Dietrich, D.L., Lachowski, H.M., and Christenson, J.W., presented at the Twelfth International Symposium on Remote Sensing of Environment, Manila, Philippines, "Identification and Delineation of Urbanized Areas Using Landsat Data," 1978.

McKinney, R.L., of Computer Sciences Corporation, Silver Spring, Maryland, "Comparison of Large Scene Image Enhancement Capabilities at GSFC," NASA/GSFC TM 78/6089, March 1978.

Ramapriyan, H.K., Chang, S.H., and McKinney, R.L., of Computer Sciences Corporation, Silver Spring, Maryland, "Use of Textural Features in the Analysis of Landsat Images,: TM/78/6100, April 1978.

Tom, C., Miller, L.D., Christenson, J.W., "Spatial Land-Use Inventory, Modeling, and Projection/Denver Metropolitan Area, With Existing Maps, Airphotos, and Landsat Imagery," NASA/GSFC Technical Paper G-7816, STAR Category 43, p. 98, 1978.

LANDSAT AND ANCILLARY DATA INPUTS TO AUTOMATED GEOGRAPHIC INFORMATION SYSTEM

OBJECTIVES

The objective of this activity is to review the state-of-the-art of Automated Geographic Information System AGIS software, evaluate currently available systems, and recommended the implementation of an AGIS which will fulfill Census Bureau Applications Pilot Test (APT) requirements. Other objectives are to:

- Acquire the recommended AGIS and implement an IBM 360 and HP 3000.

- Perform a preliminary test and evaluation of the increased utility of Landsat by combining raw and classified data with ancillary data in the AGIS, and specifically address the procedures for improving Landsat cover classification (incorporating digital terrain data) and the procedures for modeling urban development suitability.

- Identify and analyze AGIS concepts including composite mapping, integrated terrain unit mapping, scale, and composite accuracies.

BACKGROUND

A current research effort initiated as part of the Census APT is concerned with the potential applications of combining Landsat data with ancillary data to improve the utility of Landsat for urbanized area delineation. Recent studies have shown that remotely sensed satellite data may be of greatest value when used as a spatial data source in combination with other spatial and nonspatial data. A project has been designed to demonstrate the utility of incorporating remotely sensed data with digital terrain data and existing environmental data sources for multispectral classification improvement and urban residential development suitability analysis.

RECENT ACCOMPLISHMENTS

During the past year, a review of AGIS software was performed and a recommendation to acquire ESRI AGIS software was made. An urban residential development suitability demonstration project was designed and a test site near Denver, Colorado, was selected. Topographic, thematic, remotely sensed, and digital data were acquired and, where necessary, digitized. Programs to read and analyze the digital terrain data were implemented on the Image 100 and ESL

IDIMS systems. Using the terrain data, measurements of surface morphology were calculated. Digital Landsat data were geometrically corrected and registered to a topographic map base.

SIGNIFICANCE

By combining Landsat ancillary data in an AGIS, it will be possible to develop improved classification techniques to utilize multilevel resource analysis procedures, and to assess the utility of Landsat data for urban and residential development suitability modeling. AGIS procedures will permit spatial statistical analysis of the automated integration of remotely sensed satellite data with environmental data obtained by conventional data collection methods.

FUTURE EMPHASIS

Remotely sensed satellite data processing algorithms which incorporate ancillary data will be developed. Land cover classification procedures will be optimized, using both Landsat and ancillary data. An assessment will be made of the optimum resolution of digital terrain data for surface cover mapping improvement in areas of different terrain. An examination will be made of the application of integrated terrain unit concepts (which overlay natural factors, e.g., landforms, soils, geology, hydrology, etc.) to AGIS methodologies. Landsat data inputs into urban residential suitability models will be evaluated, and the requirements for integrating change detection and AGIS techniques will be analyzed.

EXAMINATION AND MODELING OF THE TOPOGRAPHIC EFFECT ON THE RADIOMETRIC RESPONSE OF NADIR LOOKING VISIBLE AND NEAR IR SENSORS

OBJECTIVES

The objectives are: (a) To design and test an incident solar radiation model to simulate the topographic effect on sensor response, and (b) to establish a method of eliminating the topographic effect on multispectral satellite data by incorporating digital terrain data with the incident solar radiation model.

BACKGROUND

Recent studies have shown that spectral response variations due to topography pose difficulties to multispectral cover classification and the use of multitemporal data, and that the topographic effect varies with the date of imaging. It has been shown that the topographic effect is caused by differential solar irradiance which is a function of solar elevation, solar azimuth, slope angle and slope aspect. There is now a need to quantify and define clearly the topographic effect and establish a method of eliminating the topographic component of the satellite data prior to multispectral classification.

RECENT ACCOMPLISHMENTS

A theoretical incident solar radiation model was established and tested for eight solar elevations using field data consisting of measurements taken with a handheld radiometer of a uniform sand surface. Multiple correlation analysis also was undertaken on the theoretical and field data sets. High correlation coefficients of greater than .95 were computed for the majority of cases and the limitations of the theoretical model were defined. Eighty percent of the first objective has now been achieved. Digital terrain data have been acquired (from the USGS) at horizontal intervals of 200 feet and 50 feet. Programs have been written and implemented to input these data on the Image 100 and ESL IDIMS interactive systems. Registration of the digital terrain data and the Landsat data and the computation of the morphometric terrain parameters, such as slope and aspect, are now being undertaken on the IDIMS system.

SIGNIFICANCE

The solar radiation model simulates the variations in spectral response due to slope angle and aspect. By applying the incident solar radiation model to multispectral satellite data, it should be possible to improve surface cover classification in areas of variable terrain. It will also be possible to extract coarse slope angle and aspect data from remotely sensed data for areas where existing morphometric data are available.

FUTURE EMPHASIS

The following will be undertaken: Examination of the diffuse radiation component and incorporation within the model, examination of variations in the slope angle and aspect spectral response model for different cover types, examination of the optimum resolution of digital terrain data for multispectral cover classification improvement in different terrain types, examination of the sensitivity of the Landsat sensors to variations in slope angle and aspect and development of a topographic effect correction technique as applied to Landsat multispectral data.

REFERENCES AND PUBLICATIONS

Holben, B.N., and C.O. Justice, "Quantification and Modeling of the Topographic Effect on the Radiometric Response of Nadir Looking Visible and Photographic Infrared Sensors, in preparation, to be submitted to *Photogrammetric Engineering and Remote Sensing*, 1979.

Justice, C.O., "An Examination of the Relationships Between Selected Ground Properties and Landsat MSS Data in an Area of Complex Terrain in Southern Italy," *Proceedings of The American Society of Photogrammetry, Fall Technical Meeting*, Albuquerque, New Mexico, 303-328, October 1978.

Justice, C.O., and B.N. Holben, "Evaluation and Modeling of the Topographic Effect on the Spectral Response from Nadir Pointing Sensors," NASA TM 80305, June 1979.

Justice, C.O. and B.N. Holben, "Examination of Lambertian and Non-Lambertian Models for Simulating The Topographic Effect on Remotely Sensed Data," NASA TM 80557, September 1979.

CHAPTER 8

AGRICULTURAL REMOTE SENSING

OVERVIEW

The agricultural remote sensing program endeavors to determine those agronomic variables which can be measured by remote spectral sensors and to define the spectral, spatial, temporal, and radiometric resolutions best suited to such measurement.

Although a wide variety of vegetation environments exists over the Earth's surface, there is great scientific value in studying narrowly defined geographical locations under controlled and well-monitored conditions. Particular photosynthetic organisms may have difficulty surviving and growing in certain environments, but each strain of vegetation (or phenotype) shares characteristics with other members of its species. Additionally, understanding the physiological differences imposed on an organism by its environment requires quantitative comparison with rigorously defined baseline information.

NASA obtains the necessary baseline information by remotely acquiring spectral data for vegetation during the period from emergence to harvest, and under conditions of controlled and/or known crop treatment and development. The range of spectra extends from the visible (400 nanometers) into the infrared (14,000 nanometers). Additional spectra in the C,L and S-bands of the microwave region are taken. The degree of correlation between spectral information and agronomic characteristics provides a basis for defining those characteristics which can be measured by remote sensors and also provides the rationale for the selection of the potential spectral bands. The studies are supported through these major elements: (1) Planting maintenance, and agronomic measurements of five crop species by the Agricultural Research Center, Beltsville, Maryland; (2) Visible/Infrared spectral measurements of crops by portable two- and three-band radiometers; (3) Visible/Infrared spectral measurements using a scanning teleradiometer; (4) passive microwave spectral measurements; and (5) measurement of polarized light components.

The agronomic and spectral quantitative data obtained provide the basis for correlations necessary to define the optimal spectral regions for measuring important agronomic parameters. The results will influence future spacecraft sensor design.

While an empirical approach is currently emphasized in the overall program objectives, use of remotely sensed information could be increased by an improved understanding of the biophysical phenomena which give rise to specific vegetational spectra, i.e., the interaction of electromagnetic radiation with the plants' chromogenic pigments.

The spectral manifestations of these interactions are influenced by the physical state of the photosensitive materials along with their cellular environment. While studying these interactions will present a formidable challenge because of the variables involved, it will allow exploitation of "fingerprint" parameters that could be used for crop discrimination and assessment of crop status and eventual yield.

Contributors to this chapter include John Barker, Emmett Chappelle, Donald Deering, Brent Holben, Daniel Kimes, John Schutt, and Compton Tucker.

SPECTRAL CROP DEVELOPMENT STAGES

OBJECTIVE AND BACKGROUND

The purpose of the project is the use of remotely sensed multispectral imagery to monitor the condition of agricultural crops and predict yields. Our expertise in this area has advanced rapidly. By necessity, much of this effort has been coupled with ground-based data on crop development and climatic conditions throughout the growing season. Several numerical schemes for recording stages of crop development were devised. However, one of the problems that arose in trying to monitor crop condition and predict yields was our inability to collect on-the-ground developmental data over the large area generally surveyed in remote sensing projects; i.e., it was not feasible to collect developmental data on crops to supplement satellite imagery for any large-scale agricultural monitoring project. In foreign locations, access was often impossible and in locations such as North America or Australia, labor costs were sometimes excessive. The solution for this problem was to generate a remotely sensed crop development value whose inputs would come entirely from remote sensing sources. This approach included collecting remotely sensed data by a two-channel hand-held radiometer recording red and photograpic infrared spectral radiances.

RECENT ACCOMPLISHMENTS

Five stages of Spectral Crop Development (SCD) were observed for corn and soybean (see figures 8-1 and 8-2):

- Stage 1: For both crops, the Vegetation Index (VI) for the bare soil before crop emergence and after emergence up to 20 to 30 percent cover was negative.

- Stage 2: The rapid increase in vegetative crop cover for both corn and soybeans prior to bloom was indicated by a rapid increase in VI.

- Stage 3: Once vegetative crop cover was complete, VI reached a plateau. SCD stage 3 continued during bloom and until chlorosis was detected.

- Stage 4: During the period of crop maturation and dry-down, VI declined gradually. Leaves became chlorotic and were often lost from the plants.

- Stage 5: The soybean lost all leaves and the corn lost all color, i.e., the crops were ripe and ready for harvest. The VI resembled that measured at crop emergence.

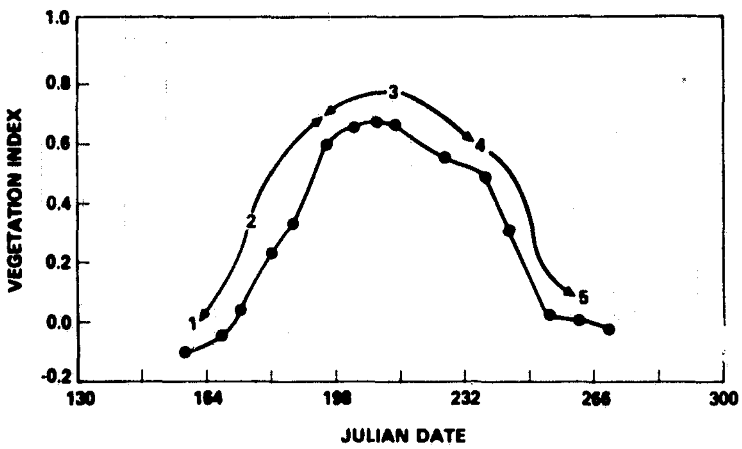

Figure 8-1. Spectral Crop Development Stages for Corn

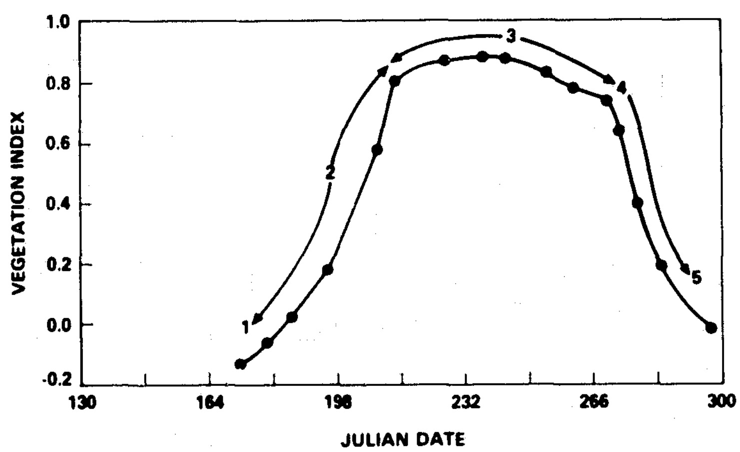

Figure 8-2. Spectral Crop Development Stages for Soybean

SIGNIFICANCE

The relationship between the VI and crop development that we observed indicated that crop condition could be assessed through spectral measurements. Attaining and sustaining full vegetative cover stage is an important factor in the final yield of any crop.

The spectral assessment of the stages of crop development could be important in the prediction of yield by remote sensing.

FUTURE EMPHASIS

Additional and more detailed studies are planned for the 1979 growing season using two- and three-band hand-held radiometers.

OPTIMAL BANDS FOR CANOPY COVER, CROP HEIGHT, AND CROP NODES

OBJECTIVES

Using a new radiometer constructed by Barnes Engineering Corporation according to GSFC specifications (0.4 to 2.5 μm) investigations have been conducted during the past year on corn, soybeans, and alfalfa to determine those bands critical for the best correlation with crop canopy, crop height, and crop nodes. The eventual goal is the utilization of certain bands for the prediction of crop yield.

BACKGROUND

For the past two years, NASA has been involved in a cooperative research program with the U.S. Department of Agriculture (USDA) Beltsville Agricultural Research Center (BARC). Their contribution has been the planting, management, and measurement of agronomic variables for three crops: corn, soybeans, and alfalfa. Since May 1978, the Barnes radiometer has been used to make weekly spectral measurements on corn, soybeans and alfalfa, from emergence to harvest. A uniqueness of the Barnes radiometer lies in its ability to measure electromagnetic radiation through two separate apertures: An object and a reference channel. These measurements are made alternately at 50 μ/sec intervals, which allows extremely accurate reflectance signals.

RECENT ACCOMPLISHMENTS

Only a preliminary analysis of the data has been completed at this time. We believe that with the large number of spectral bands at our disposal, a multivariate statistical approach will yield the most significant information. Working with a limited number of soybean and corn plots, it is indicated that the bands necessary for correlation with canopy cover, crop height and crop nodes include 1.22, 1.66, and 2.2. It must be stressed that these conclusions are still considered quite preliminary. It is possible that additional bands will be found that correlate with other agronomic parameters.

SIGNIFICANCE

The band correlation is best with those agronomic variables studied to date which fall in the boundaries of TM5 and TM6 of the Thematic Mapper.

FUTURE EMPHASIS

The analysis of the data collected during 1978 will be completed and the results will be submitted for publication. The emphasis of the spectral analysis for 1979 will be on crop yield prediction.

CROP BIOMASS AND YIELD

OBJECTIVE

The objective of the crop biomass and yield studies is to investigate and quantify the red and photographic infrared radiance relationship to total the above-ground dry biomass accumulation and grain yield of winter wheat using handheld radiometry.

BACKGROUND

Many investigators have shown a relationship between linear spectral transformations and biomass grain yield, but full potential has not been realized due to limits of data collection. Handheld radiometry has recently been shown to have great potential to exploit this spectral/biomass grain yield relationship. Twenty winter wheat plots at the USDA/BARC were spectrally monitored on 21 dates with a two-band radiometer. Grain yield at harvest, and total dry biomass accumulation data were also collected. A two-fold range of grain yield and total dry biomass accumulation resulted from normal, within-field variability.

RECENT ACCOMPLISHMENTS

This work demonstrated that spectral data explain approximately 80 percent of the biomass variation and approximately 65 percent of the grain yield variation in a field of winter wheat (see figure 8-3) for a plot of the coefficient of determination (r^2), versus Julian date, from 21 separate regressions of the VI regressed against the total above ground dry biomass harvested on June 23, 1978. Note the broad plateau region approximately from date 104 to 145 in which the r^2's vary between 0.7 and 0.8+. It is also possible to integrate the spectral transformations over accumulated heat units rather than time without degrading the biomass grain yield predictability (see figure 8-4) for a visual representation of an integration technique of the spectral curve for all plots. Integration areas under selected portions of the curves were regressed against the harvested grain yield. Coefficients of determination were identical or in some cases better than Julian date when substituted for growing degree days.

SIGNIFICANCE

Prediction of grain yield and vegetative biomass is possible. Good predictability of biomass accumulation suggests a potential approach to quantifying a major component of carbon cycling for seasonally dynamic ecosystems.

FUTURE EMPHASIS

An expansion of the 1978 experimental design is planned using three spectral bands (TM3, TM4, and TM5) and three different wheat fields. The ability of Thematic Mapper bands TM3, TM4, and TM5 to spectrally estimate grain yield and total dry biomass accumulation will be evaluated.

REFERENCES AND PUBLICATIONS

Holben B., and C.J. Tucker, "Evaluation of Irradiational Conditions as They Limit The Application of a Ground-Based Nondestructive Tropical Rain Forest Leaf Area Index Technique Using Spectral Measurements," *Photogrammetric Engineering and Remote Sensing*, in press, 1979.

Tucker, C.J., B. Holben, J.H. Elgin, Jr., and J.E. McMurtrey, III, 1979, "Remote Sensing of Winter Wheat Total Dry Matter Accumulation," to be submitted to *International Journal of Remote Sensing*, 1979.

Tucker, C.J., B. Holben, J.H. Elgin, Jr., and J.E. McMurtrey, III, "The Relationship of Red and Photographic Infrared Spectral Data to Grain Yield Variation Within a Winter Wheat Field," submitted to *Photogrammetric Engineering and Remote Sensing* and published as NASA TM 80318, July 1979.

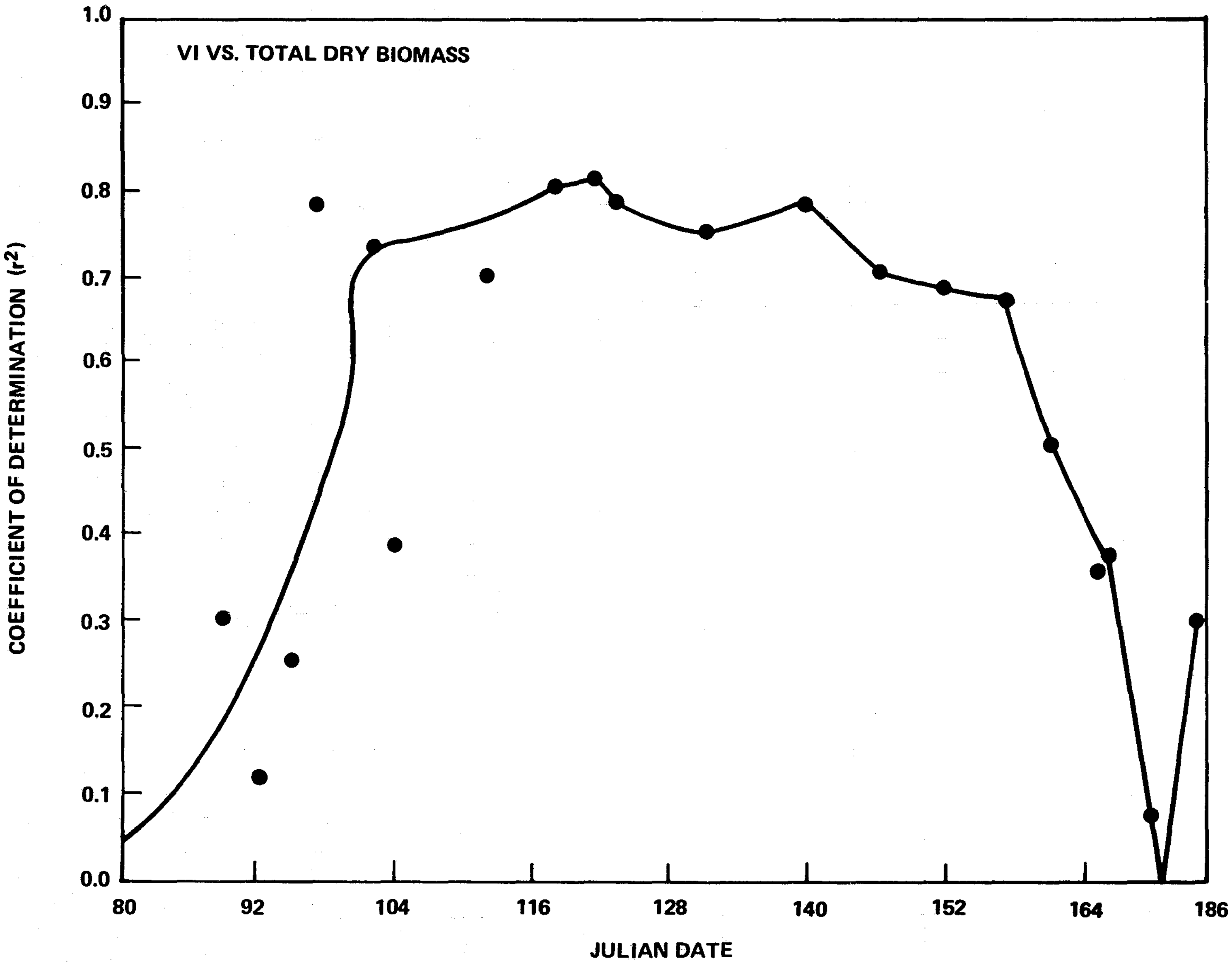

Figure 8-3. Plot from 21 Separate Regressions of the VI Regressed Against June 23, 1978 Above Ground Biomass

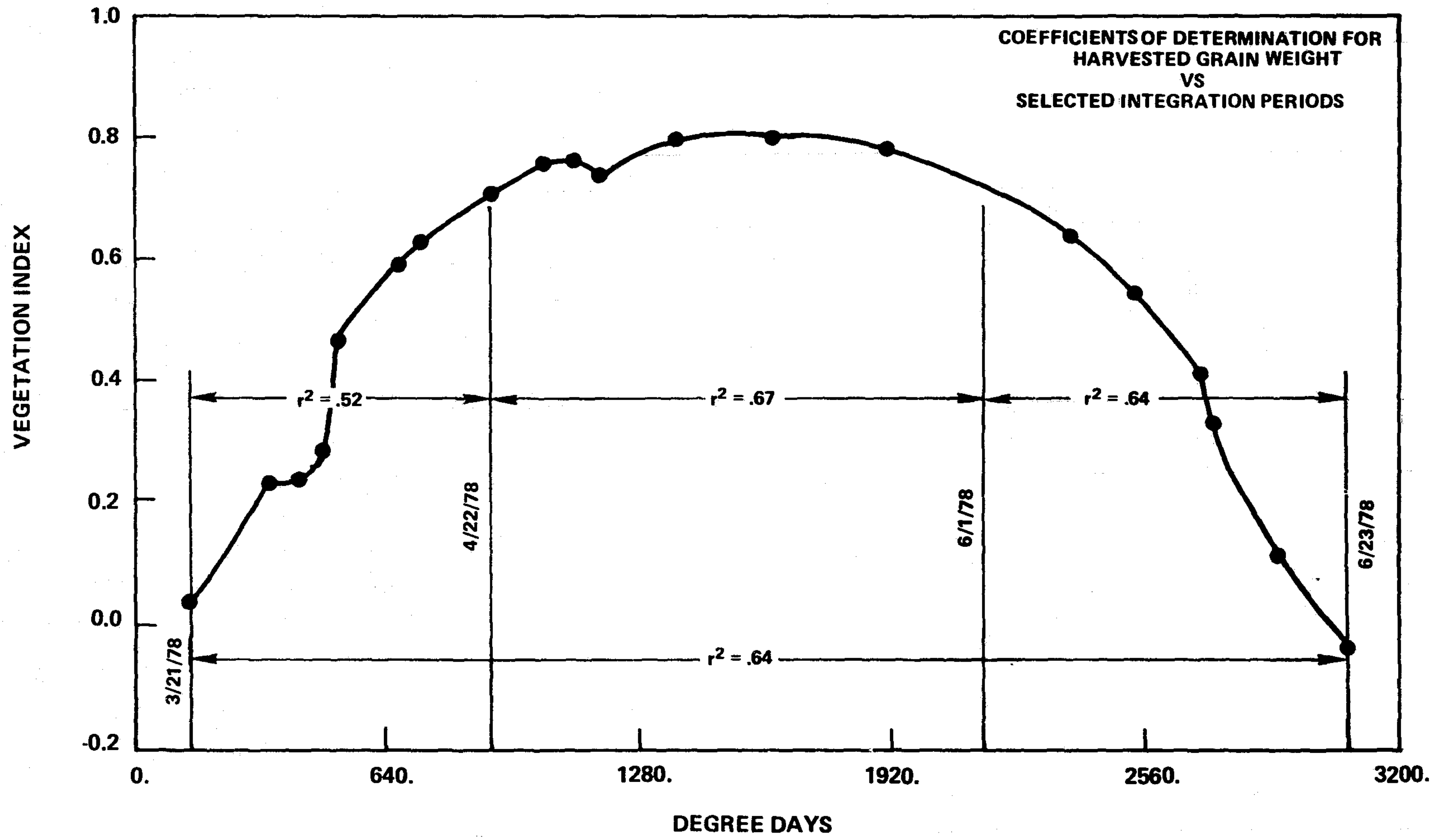

Figure 8-4. Visual Representation of Integration Technique of Spectral Data Curve for All Plots

PASSIVE MICROWAVE TECHNIQUES FOR REMOTELY ESTIMATING MOISTURE IN BARE AND VEGETATED SOILS

OBJECTIVE

The overall objective of the passive microwave research of the agricultural field program is to determine the optimum sensor parameters for spaceborne microwave radiometers for sensing soil moisture under various vegetation covers. The objective of the work in 1978 was to determine the relationships between brightness temperatures at 21.4 (L-band), 11.3 (S-band), and 6 cm (C-band), and soil moisture in bare and vegetated soils.

BACKGROUND

Past studies have demonstrated that the ability of brightness temperature to correlate with soil moisture is dependent on wavelength, polarization, surface roughness, viewing angle, and depth. For an ideally smooth surface the L-band radiance receives its maximum contribution from a depth of about 5 cm. In practice, however, the maximum correlation does not reach 5 cm because an ideally smooth transmitting surface with a uniformly dense subsoil seldom exists.

RECENT ACCOMPLISHMENTS

Observed brightness temperatures were found to correlate well ($r^2 > 0.9$) with gravimetric soil moisture data averaged over the top 2 cm for all bands, provided the soil densities were 1.25 gm/cc or greater. Values of the slopes of regression equations of microwave brightness temperature versus soil moisture decreased from C- to S- to L-band observations. While the sensitivity to soil moisture decreased in this band progression, the soil moisture range of linear correlation increased. Well-worked lower density soils of less than 1 gm/cc had higher brightness temperatures than soil with densities from 1.25 to 1.5 gm/cc and the same soil moisture content. Observations of vegetated soil showed brightness temperatures between the lower and higher density soils, for identical moisture levels. Correlation coefficients were found to drop by about 10 percent for the vegetated soils, indicating a lower sensitivity and accuracy for measuring soil moisture in all three bands.

SIGNIFICANCE

The usefulness of L-band for detecting soil moisture to at least a depth of 2 cm has again been demonstrated. S- and C-bands were shown to give correlations between brightness temperatures and soil moisture to a depth of 2 cm for a nominally rough soil surface. It was also shown that soil density does not interfere significantly with brightness temperature soil moisture relationships unless the soil density approaches 1.

FUTURE EMPHASIS

The results reported above were produced from the 1977 field season data. The 1978 primary field data were collected at the end of the growing season and involved measurement of bare ground under artificially controlled moisture conditions and measurement of a mature corn crop. These data will be analyzed during 1979. In addition to analyzing the 1978 data, the principal objective of the microwave study during the 1979 growing season will be to determine the magnitude of the plant canopy contribution to microwave emissions from vegetated soil areas (principally a corn crop) throughout the growing season. Also, extensive measurements will be made for understanding microwave emissions in C-L, L-, and P- (50-cm) bands under a wide range of soil moisture and roughness conditions.

COLORADO DROUGHT PROJECT

OBJECTIVE

The objectives of the Colorado drought project are to evaluate the monitoring of drought conditions in Colorado using Landsat data, and to study the ability of Landsat data for the monitoring of drought conditions over large semiarid regions.

BACKGROUND

The Earth Resources Department at Colorado State University is conducting this research for NASA/GSFC. The years of 1973 (a "wet" year), 1976 (a dry year), and 1977 (a very dry year) are being compared. Various green vegetation indices are being used to evaluate the effects of drought upon primary productivity in the rangeland, forest, and agricultural sectors of Colorado.

SIGNIFICANCE

The anticipated significance of the project is the development of digital or photographic assessment of drought conditions over large areas using Landsat imagery.

FUTURE EMPHASIS

The project will officially end in December of 1979. A final report will be published at that time.

REFERENCES AND PUBLICATIONS

Tucker, C.J. and F.M. Smith "A Survey of Nondestructive Biomass Estimation Techniques," *Journal of the British Grassland Society*, in press, 1979.

Tucker, C.J., "Post Senescent Grass Canopy Remote Sensing," *Remote Sensing of Environment, 7*, 3, 203-210, 1978.

Tucker, C.J., "A Spectral Method for Determining the Percent of Live Herbage Material in Clipped Samples," *Remote Sensing of Environment*, in press, 1980.

Holben, B., and C.J. Tucker, "Evaluation of Irradiational Conditions as They Limit The Application of a Ground-Based Nondestructive Tropical Rain Forest Leaf Area Index Technique Using Spectral Measurements," *Photogrammetric Engineering and Remote Sensing*, in press, 1979.

REFERENCES AND PUBLICATIONS (continued)

Tucker, C.J., J.H. Elgin, Jr., J.E. McMurtrey III, and C.J. Fan, "Monitoring Corn and Soybean Crop Development with Hand-held Radiometer Spectral Data," *Remote Sensing of The Environment, 8*, 3, 237-248, 1979.

Tucker, C.J., J.H. Elgin, Jr., and J.E. McMurtrey III, "Temporal Spectral Measurements of Corn and Soybean Crops," *Photogrammetry Engineering and Remote Sensing, 45*, 5, 643-653, 1979.

Tucker, C.J., J.H. Elgin, Jr., and J.E. McMurtrey III, "Relationship of Red and Photographic Infrared Spectral Radiances to Alfalfa Biomass, Forage Water Content, Percentage Cover, and Severity of Drought Stress," *International Journal of Remote Sensing*, in press, 1980.

Tucker, C.J., "Are Two Photographic Infrared Sensors Required?" *Photogrammetric Engineering and Remote Sensing, 44*, 3, 289-295, 1978.

Tucker, C.J., "A Comparison of Satellite Sensor Bands for Vegetation Monitoring," *Photogrammetric Engineering and Remote Sensing, 44*, 11, 1369-1380, 1978.

Tucker, C.J., B. Holben, J.H. Elgin, Jr., and J.E. McMurtrey, III, "The Relationship of Red and Photographic Infrared Spectral Data to Grain Yield Variation Within a Winter Wheat Field," submitted to *Photogrammetric Engineering and Remote Sensing*, 1979, and published as NASA TM 80318, 1979.

Tucker, C.J. B. Holben, J.H. Elgin, Jr., and J.E. McMurtrey, III, "Remote Sensing of Winter Wheat Total Dry Matter Accumulation," to be submitted to *International Journal of Remote Sensing*.

Tucker, C.J., and B. Holben, "Evaluation of Irradiational Conditions as They Limit the Application of a Ground-Based Nondestructive Tropical Rain Forest Leaf Area Index Technique Using Spectral Measurements," *Photogrammetric Engineering and Remote Sensing*, in press.

SUN ELEVATION AND SENSOR LOOK ANGLE EFFECTS ON REMOTE SENSING OF VEGETATION

OBJECTIVES

The overall study objective was to evaluate the effect of sun elevation and sensor-look angle on measuring important agronomic variables with remote sensing techniques. The first phase is to determine the magnitude of the diurnal sun elevation or attendant shadow influences on red (R) and near infrared (IR) radiances and the ability to discriminate different quantities of green biomass.

BACKGROUND

The agricultural field project is principally directed toward determining the agronomic variables which can be measured by remote spectral sensors and defining the spectral regions which can be utilized as satellite remote sensing surrogates for important agronomic variables. Due to time constraints and other physical limitations involved in crop measurement using the sophisticated broad spectral region, scanning reflectometer, most spectral measurements are made at or near local solar noon. In satellite applications of remote sensing techniques the effects of solar elevation differences resulting from different overpass times of the day, different latitudes, and different seasons of the year must be considered. In addition, with future satellites (e.g., the Multispectral Resource Sampler [MRS]) being designed to look off-nadir, the effects of sensor look angle must also be understood.

The interactions of red and near infrared radiation with green plant material have been studied for several years and are fairly well understood. Techniques have been developed to determine the amount of green plant material or green biomass on the ground with remote sensors that utilize both the red and infrared spectral regions. It is not known, however, how this determination is affected by changes is sun elevation or the increased amount of shadow within the plant canopy.

During the first phase of the study, different amounts of green biomass were created in small plots within a uniform and "all green" crop of alfalfa. Spectral measurements were taken on the plots in a sampling mode with a two-channel (0.66 and 0.80 μm) hand-held radiometer at selected time intervals throughout the day under clear sky conditions. In addition, the same plots were monitored under hazy and cloudy skies on different days.

RECENT ACCOMPLISHMENTS

Individual red and infrared radiances, the IR/R ration, and the Normalized Difference (ND) parameter (IR-R)/ (IR+R) were all found through linear regression analyses to be similarly (ignoring sign) highly correlated with the quantity of dry green biomass over the range of 0-4000 kg/ha and for all sun elevations evaluated (ranging from about 15° to 45°). However, the functional relationships between the four spectral parameters and green biomass are observed to be quite different (see figures 8-5 and 8-6). It is evident that conventionally applied linear regression analyses are inadequate to evaluate these data.

The preliminary analysis reveals that for sun elevations greater than approximately 40° (which occurred at the local solar noon +1.5 hours on October 11, 1978) red and infrared radiance differences were negligible. However, at the lower sun elevation not only were the radiances appreciably reduced, but the spectral sensitivities to green biomass differences were also reduced.

Both of the spectral band differencing techniques evaluated were found to eliminate most of the sun angle effects, particularly for sun elevations greater than 30°. Consequently, the sensitivities of IR/R and ND were essentially the same for sun elevations within the range of approximately 30° to 45°. The ND parameter appears to be highly sensitive to green biomass differences in the range of 0 to 2500 kg/ha, whereas IR/R is most sensitive to biomass differences at the higher levels of green biomass (1000 to 4000 kg/ha).

SIGNIFICANCE

These preliminary results indicate that green biomass estimates can be made with equal accuracy over the range of sun elevations from 30 to at least 45 by using red and infrared radiance measurements in certain spectral band differencing transformations (e.g., IR/R and ND). However, applications utilizing radiance values for these spectral bands individually may be seriously impacted by the sun angle effect.

FUTURE EMPHASIS

Research during the 1979 growing season will provide a more comprehensive evaluation of both sun elevation and look angle influences. A wide range of sun elevation (up to about 85°) and look angles (up to 50°) will be examined for greenhouse grown wheat plants and field grown crops. Green biomass and foliage projection cover (canopy cover) will be the key agronomic variables evaluated.

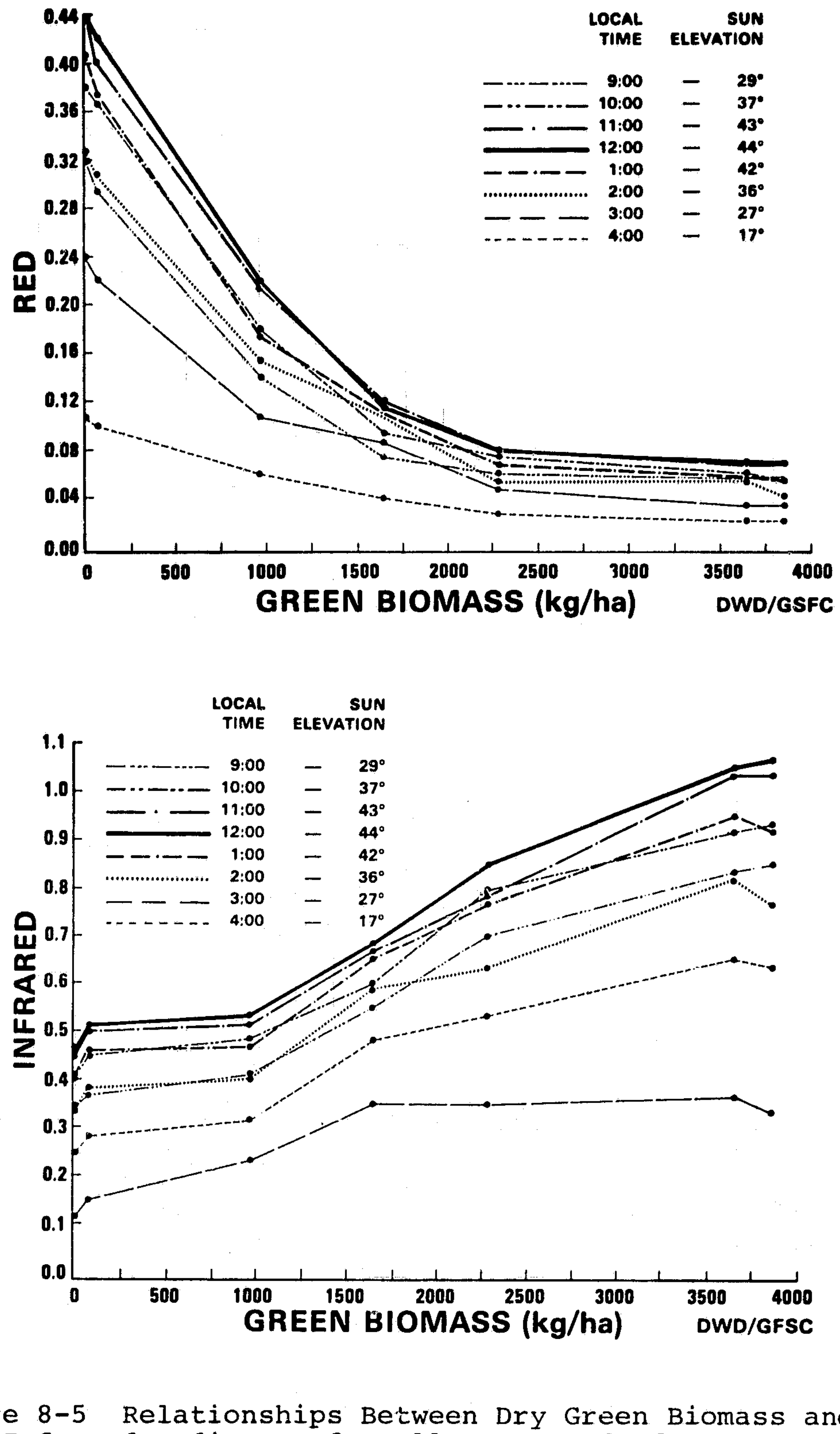

Figure 8-5 Relationships Between Dry Green Biomass and Red and Near Infrared Radiances for All Green Alfalfa, October 11, 1978

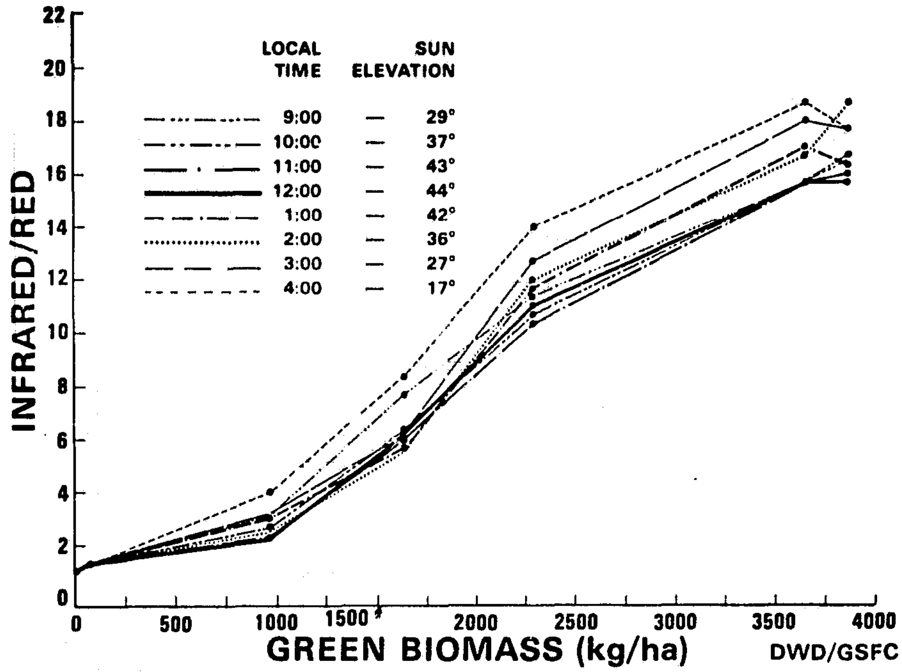

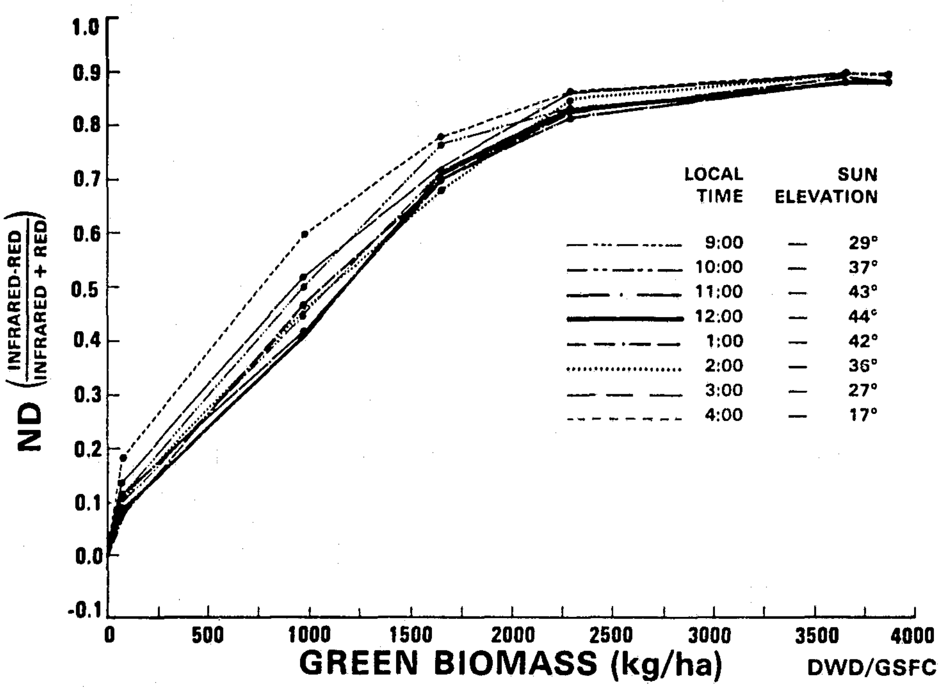

Figure 8-6. Relationships Between Dry Green Biomass and Infrared/Red Ratio and ND Parameter for All Green Alfalfa, October 11, 1978

SPECTRAL DISCRIMINATION OF WHEAT

OBJECTIVE

The primary objective of the research was to develop and exercise a quantitative relative evaluation of proposed Landsat D TM band options in eight spectral regions from 0.4 to 2.4 m for the discrimination of winter wheat from its confusers in Finney County, Kansas.

A secondary research objective was to analyze the inherent spectral discrimination of crops through the preparation of a temporal atlas of reflectance and divergence spectra in the Finney County, Kansas LACIE Intensive Test Site during the 1975/1976 winter wheat season.

BACKGROUND

This research task is part of a major research objective to examine the feasibility of incorporating remotely sensed data into growth, yield and production models for the purpose of observing, monitoring and forecasting the condition and amount of economically significant food, feed, and fiber crops. The limited agricultural objectives of this task are to use existing spectral and ancillary data to compare the relative performance of the Landsat MSS scanner to the proposed TM scanner for the discrimination of winter wheat from confusers in Kansas.

As a part of the LACIE field measurements program, more than 12,000 helicopter FSS/S191-H spectra over the Finney County site in 1975/1976 became available to researchers through the LARS facility at Purdue University. Supporting ground, aircraft and Landsat observations were also provided by LARS throughout the growing season. The spectral data available from LARS were and are the most geographically representative of significant wheat producing regions.

RECENT ACCOMPLISHMENTS

A figure-of merit was developed for comparing eight spectral regions. It contains factors for both the probability of correct classification of two classes and the probability of a specific spectral region independent from the other seven regions. Absolute values for the figures-of-merits were converted into rank order in table 8-1.

The results given in table 8-1 indicate that TM4 and TM6 will probably be the two most valuable bands for discriminating one crop from another crop.

An average figure-of-merit was also used to place the seven dates in an approximate rank order based on the ability to discriminate dry land winter wheat from irrigated winter wheat on that date. The order of dates from best to worst discriminability is October 21, March 18, May 6, June 12, November 11, April 18, and March 31, 1978.

An unexpected, and as yet unexamined, result was the observation of apparent fine structure within several of the eight spectral regions, i.e., the bands within these spectral regions were not equally effective in separating winter from its confuser crops. Initial indications are that the spectral regions given in table 8-2 may contain maxima in the discrimination function.

The two spectral regions not examined for optimum band center location were TM2 (.54-.62 m) and TM3 (.62-.68 μm).

Using the data compiled, a draft of a temporal crop atlas was produced, along with supporting ancillary data.

SIGNIFICANCE

The analysis of over 12,000 spectra is the most extensive study of spectral discriminability of wheat from confusers ever undertaken. The results were used as agricultural justification for the addition of TM6 on Landsat-D, with or without the mission of one of the original five reflective bands.

An improvement factor of more than three was estimated for the six reflective TM bands relative to the current MSS bands. This reduced margin of error promises to improve the performance of Landsat-D.

The temporal analysis suggests that it would be worthwhile to develop statistical weighting factors when combining imagery form more than one data. These factors could then be examined for possible programming of smart sensor systems to acquire data within specific time windows.

The indication of apparent fine structure within the individual spectral regions is strong justification for further analysis and collection of field spectra which might be used to identify more optimal bands for future missions.

FUTURE EMPHASIS

Several different objectives and additional data are being considered for future research involving analysis of both point spectra and spatial imagery collected as part of the LACIE field measurements program. Some possibilities include adding: Yield data, data from ARS research stations taken with EXOTECH spectraradiometer, intensive test sites, and data from more than one growing season.

REFERENCES AND PUBLICATIONS

Barker, J.H., F. Gordon, and A. deGasparis, "Selection of Spectral Bands for Winter Wheat," presented at the ASP meeting, Remote Sensing and Interpretation Division, in Washington, D.C., March 2, 1978.

Table 8-1. Rank Discrimination of Winter Wheat Versus All Confuser Crops for Eight Spectral Regions

Crops	Rank Discrimination for Spectral Regions (0.40 to 2.35 μm) with Thematic Map Designation*							
	0.40 to 0.52 (TM1)	0.54 to 0.62 (TM2)	0.62 to 0.68 (TM3)	0.70 to 0.95 (TM4)	0.95 to 1.15 (A)	1.15 to 1.40 (B)	1.55 to 1.75 (TM5)	2.15 to 2.35 (TM6)
Dry Winter Wheat vs. Confuser Crop	6	7	8	2	1	4	5	3
Irrigated Winter Wheat vs. Confuser Crop	7	8	6	1	2	3	4	5
Dry Winter Wheat vs. Irrigated Winter Wheat	5	7	8	2	4	3	6	1

*One (1) is the best discrimination.

Table 8-2. Parameters for Spectral Regions That May Contain Maxima in the Discrimination Function

Spectral Region	Band Center (μm)	Range (μm)	Band Width (μm)
1	0.420	0.404 - 0.436	0.032
2	0.500	0.484 - 0.536	0.052
3	0.825	0.750 - 0.900	0.150
4	1.075	1.025 - 1.125	0.100
5	1.225	1.253 - 1.298	0.045
6	1.375	1.351 - 1.399	0.048
7	1.575	1.557 - 1.593	0.036
8	1.699	1.663 - 1.737	0.074
9	2.525	2.185 - 2.321	0.136

LANDSAT SPECTRAL WHEAT CALENDAR

OBJECTIVE

The objectives of the Landsat spectral wheat calendar research task are: (1) To develop and evaluate nonlinear mathematical formulations for relating satellite observations of Landsat MSS bands to ground observations of Leaf Area Index (LAI) for winter wheat in Kansas, and (2) to develop a mathematical model for a "Landsat Spectral Wheat Calendar," a time plot of transformed combinations of MSS bands.

BACKGROUND

This task is part of a major research objective to examine the feasibility of incorporating remotely sensed data into growth and yield models for the purpose of observing, monitoring, and forecasting the areal extent and condition of economically significant food, feed, and fiber crops. The limited objectives of this task are for computational development and analysis of current Landsat 1, 2, and 3 imagery as applied to the extraction of information on the status of winter wheat in a few counties in Kansas; and secondly, for simulating future performance capabilities for the TM sensor on Landsat 4 and other possible sensor systems based on spectra of winter wheat taken in Kansas, North Dakota, and Maryland.

Various investigators have demonstrated the feasibility of using visible and IR spectra for measuring vegetation. Field measurements according to information available in the spectral region from 0.5 to 1.1 mm are: (1) An infrared reflectance band (0.75 to 0.80 mm) directly related to green biomass, and (2) a red reflectance band (0.63 to 0.69 mm) inversely related to the chlorophyll contents of plants. Deering and others have demonstrated the utility of the normalized difference of (MSS 6-MSS 5)/ MSS 6+MSS 5) for measuring biomass on rangeland. Kanemasu and others have shown linear relationships between combinations of MSS bands and LAI for wheat.

It would be useful to develop a set of self-consistent, nonlinear mathematical models for relating spectral crop calendars of transformed MSS values versus time. It would also be useful to develop growth curves of LAI versus time to a nonlinear LAI versus MSS model by eliminating time as a parameter. If analytical functions could be developed whose fitted coefficients in the time domain can be used to derive an MSS/LAI relationship, then there would be two significant benefits: (1) More data would be brought into self-consistency with fewer degrees of freedom, and (2) the potential for testing hypotheses on the agronomic significance of the various fitted parameters would be increased.

RECENT ACCOMPLISHMENTS

Spectral crop calendars for winter wheat in Kansas have been developed for several transformations of the four Landsat MSS bands based on the modeling of correlations between measured values of LAI, and Landsat imagery for the same fields taken throughout the growing season.

Both LAI and reduced Landsat values were originally collected as part of a growth model study in 1974, 1975 and 1976 by E.T. Kanemasu at the Kansas State University Evapotranspiration Lab for winter wheat in Riley, Ellsworth, and Finney Counties.

Fourteen subsets of this LAI/MSS data were used to evaluate numerous linear and nonlinear transformations for the two growing seasons. The r^2 values for linear correlations of LAI with transformed indices are as follows:

- For the untransformed bands, MSS 7 gave the highest values, ranging from 0.3 to 0.9 for individual subsets and 0.3 for the correlation of all data;

- Principal components indicated that the vegetative information is contained within the orthogonal components with the lowest absolute value of radiance variability. This indicates that the four MSS sensors on Landsat are more responsive to nonvegetative effects such as illumination level and atmospheric conditions than to the variations in the degree of vegetation;

- There was no significant correlation of this fourth principal component for the collection of all data or for the three individual county subsets, which, in combination with the correlation of fall and spring subsets, suggests that local variations in scene radiances from crops with identical LAI limit the predictive value of this transformation;

- MSS ratios of 6/5 and 7/5 were consistently higher than 6/4 and 7/4;

- Normalized differences such as (7-5)/(7+5) and (6-5)/(6+5) were higher than (7-4)/(7+4) and (6-4)/(6+4);

- Normalized differences of (7+6-5-4)/(7+6+5+4) and (7-5-4)/(7+5+4) gave the highest individual subset and collected values.

SIGNIFICANCE

Since harvested yield has a high correlation with both the maximum values of LAI and its duration, for small grains (such as wheat) coefficients from the LAI/MSS model provide a potential method of predicting yield from Landsat imagery.

FUTURE EMPHASIS

Analysis of the 1974-1975 and 1975-1976 data will be extended to include: (1) Nonlinear correlation models of LAI and MSS, and (2) Landsat spectral wheat calendars which incorporate these nonlinear transformations.

Ground data have been collected by Kanemasu for the 1977/1978 season. Landsat imagery will be supplied from Goddard. The analysis will be a collaborative effort. The possibility of making atmospheric corrections to the imagery will be examined.

Field spectra and helicopter spectra will be used to simulate Landsat D performance.

HAND-HELD RADIOMETER DEVELOPMENT

OBJECTIVE

To develop a hand-held radiometer suitable for field use which operates in the 0.40 2.50 μm region of the spectrum.

BACKGROUND

There currently is a need for rapid, convenient, and accurate *in situ* ground-based remote sensing data collection instruments for measuring vegetation. This data is needed principally to increase our understanding of the information available in the spectral reflectance-vegetation interaction. A greater understanding of this coupling between spectral reflectance and vegetation will lead to two objectives: (1) A greater understanding of satellite and aircraft remote sensing imagery of terrestrial vegetation; and (2) the use of these techniques for nondestructive ground-based studies of vegetation by itself. Regardless of the altitude of the sensors in question (2 m, 2000 m, or 700 km), the same information is potentially available.

Our understanding of vegetational remote sensing will be increased via controlled *in situ* experimentation. The easiest and most controlled way to do this is with a ground-based method. It has proven to be extremely difficult to accurately and precisely reconstruct the status of vegetation in Landsat pixels, for example. For these we not only must consider atmospheric effects, sun angle effects, etc., but we also must sample enough pixels on the ground to represent a valid and controlled sample (each pixel equals 0.45 ha).

Previous efforts to better understand the spectral reflectance of vegetation have used spectrometers in various field configurations. This has proven to only partially alleviate the dirth of controlled *in situ* data from vegetation, however.

Spectrometers are capable of providing detailed spectra from vegetated targets. They sacrifice mobility and hence wide area coverage in achieving the capability of detailed wavelength measurements.

RECENT MAJOR ACCOMPLISHMENTS

A prototype device with two silicon and one lead sulfide channel has been developed and currently is being tested (see figure 8-7).

SIGNIFICANCE

Additional and numerous ground-based remote sensing studies are needed immediately to expand our understanding of spectral reflectance from vegetation targets, but cannot proceed if only field spectrometers are used.

Discrete-band radiometers configured by custom-made interference filters have been proven to overcome the limitations of spectrometers. Spectrometers are needed, however, to define those wavelength regions to be used in the discrete band radiometers. A previous effort in this area has been reviewed and documented.

FUTURE EMPHASIS

A production run of 20 three-band devices will be undertaken as soon as preliminary testing is completed (April 1, 1979). These units will be used for a joint USDA-NASA testing and evaluation program during the 1980 and 1981 growing seasons. Instruments will be delivered to the USDA in late 1979.

REFERENCES AND PUBLICATIONS

Holben, B., and C.J. Tucker, "Evaluation of Irradiational Conditions as They Limit the Application of a Ground-Based Nondestructive Tropical Rain Forest Leaf Area Index Technique Using Spectral Measurements," *Photogrammetric Engineering and Remote Sensing*, in press.

Tucker, C.J. and F.M. Smith, "A Survey of Nondestructive Biomass Estimation Techniques," *Journal of the British Grassland Society*, in press.

Tucker, C.J., "Post Senescent Grass Canopy Remote Sensing," *Remote Sensing of Environment, 7*, 3, 203-210, 1978.

Tucker, C.J., "A Spectral Method for Determining The Percent of Live Herbage Material in Clipped Samples," *Remote Sensing of Environment*, in press, 1980.

Tucker, C.J., J.H. Elgin, J.E. McMurtrey, and C.J. Fan, "Monitoring Corn and Soybean Crop Development with Hand-held Radiometer Spectral Data," *Remote Sensing of Environment, 8*, 3, 237-248.

Tucker, C.J., J.H. Elgin, and J.E. McMurtrey, "Tropical Spectral Measurements of Corn and Soybean Crops," *Photogrammetry Engineering and Remote Sensing, 45*, 5, 643-653.

Tucker, C.J., J.H. Elgin, Jr., and J.E. McMurtrey, III, "Relationship of Red and Photographic Infrared Spectral Radiances to Alfalfa Biomass, Forage Water Content, Percentage Cover, and Severity of Drought Stress," *International Journal of Remote Sensing*, in press, 1980.

Tucker, C.J., B. Holben, J.H. Elgin, Jr., and J.E. McMurtrey, III, "The Relationship of Red and Photographic Infrared Spectral Data to Grain Yield Variation Within A Winter Wheat Field," submitted to Photogrammetric Engineering and Remote Sensing and published as NASA TM 80318, July 1979.

REFERENCES AND PUBLICATIONS (continued)

Tucker, C.J., J.H. Elgin, Jr., and J.E. McMurtrey, III, "Remote Sensing of Winter Total Dry Matter Accumulation," will be submitted to *International Journal of Remote Sensing*.

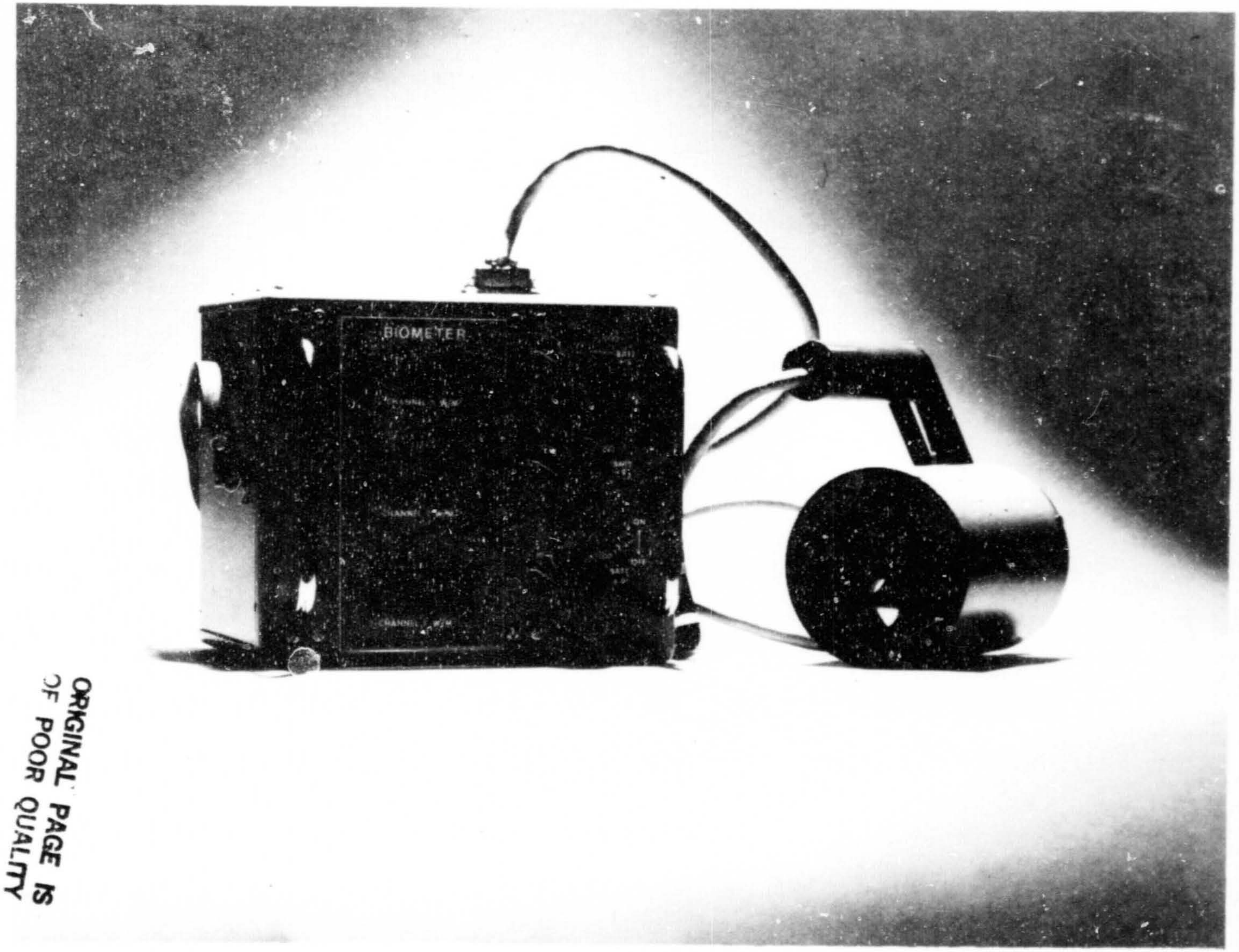

Figure 8-7. Prototype for Hand-held Radiometer

ORIGINAL PAGE IS
OF POOR QUALITY

PLANT/CROP STRESS MODELING

OBJECTIVE

The objectives of the plant/crop stress modeling project are to test the relationships established from laboratory data for their utility in estimating crop water status, and modify these relationships to optimize their utility.

BACKGROUND

During 1978 a cooperative effort was begun with the Plant Stress Laboratory of the U.S. Department of Agriculture, Beltsville, Maryland, to carry out reflectance measurements on cotton, soybeans and corn subjected to varying levels of water stress. Previous work by Thomas et al. at Texas A&M University (1971) correlated spectral reflectance with gravimetric water content of leaves by incorporating turgid and dry leaf reflectances as parameters into the functional form of the correlation. For field and remote applications, this approach is not feasible because turgid and dry leaf reflectance data are not obtainable except from laboratory experimentation. Approaches useful to field and remote sensing applications must rely upon self-referencing rather than referencing to separately derived data.

RECENT ACCOMPLISHMENTS

It has been found that leaf water content can be related to reflectance provided: (1) Knowledge of the rate of water loss from an excised leaf during the time of the optical measurement is known; (2) effect of water content upon leaf contour can be corrected for : and (3) leaf composition is established as a noninterferring factor. Leaf water contents were corrected to the average level present during the optical measurement by using previously established rate of evaporation curves. The roughness of leaves having less than 75 percent water is less than those with moisture contents greater than 80 percent. It has also been found that in some cases the effect of roughness can be minimized by computing the ratio of reflectance at the 1.42 and 1.92 water bands to the reflectance at 1 micron. Without recourse to analyzing leaves for their starch and protein contents, correlations between leaf water content and reflectance of cotton plants of the same age have given r^2 values from 0.75 to 0.86 for all wavelengths from 1 to 2.2 microns. Leaf water contents were in the range of from 60 to 75 percent.

SIGNIFICANCE

The adaptation of existing correlations between leaf water content and IR reflectances to canopies provides a basis for identifying water stress, and estimating water content from lift truck and satellite.

FUTURE EMPHASIS

Since the method of correlating water content with IR reflectance spectra for plants containing less than 75 percent water has been worked out, efforts will be brought to bear on finding correlations for water contents greater than 75 percent. At this time it appears as though such relationships will have to account for protein and carbohydrate levels, as well as that of water. Using a specially constructed reflectance/transmission cell built at USDA, spectra of solution suspensions of protein and carbohydrate in water will be obtained as a function of simulated leaf thickness and compared with leaf spectra. The leaf will then be analyzed as a check on the modeling procedure.

AGRICULTURAL MANAGEMENT INFORMATION

OBJECTIVE

The objective of the Agricultural Management Information (AMI) research effort is to develop and test methods for the incorporation of remotely sensed data into agricultural management decisions in increasing productivity and/or efficiency of domestic agriculture. This objective focuses on crop production (including rangeland and forest management).

BACKGROUND

Agriculture and related activities account for a significant portion of the nation's gross national product, and its well-being in terms of efficiency and productivity is important for the U. S. balance of payments (in terms of foreign trade). In assessing the potential use of remote sensing technology in agriculture, forestry, and range management the Space Applications Board of the National Academy of Sciences has pointed out the potential of developing this technology for agricultural information requirements. The Applications Survey Group for Agriculture (1976 under the auspices of JPL) proposed explicitly that satellite remote sensing be used to aid the producer in farm management.

RECENT ACCOMPLISHMENTS

With the aid of a non-GSFC external steering committee, GSFC, NASA, universities, other federal agencies and industrial personnel, a preliminary plan for research and development in the AMI project has been developed and a preliminary draft compiled. This document contains a discussion of the tasks undertaken in defining an effective AMI program. The plan contains the methodology which was used by the AMI project investigators and advisers in identifying in economic terms agricultural management information requirements (e.g., specified crops, area of country, farm management practices employed, and level of farm manager making the decisions) and the research and development necessary to fulfill them. Also discussed are the major sub-objectives decided upon and, for each of these the availability of the technology and models required. Five sub-objectives have been identified and a research and development plan has been developed for each. These sub-objectives were: Irrigation scheduling, range management, soil productivity, plant antagonist control, and weed control.

SIGNIFICANCE

The significance of the AMI plan lies in the construction of a set of objectives (sub-objectives) which will contribute to the information available to the agricultural producer. Each of these sub-objectives is based on an "application system" that is defined as a total chain of research and technology which leads from an information requirement to the utilization of that information through identification of "weak links in the chain" which require further research and development in remote sensing technology.

FUTURE EMPHASIS

Any additional work in this area awaits NASA Headquarters guidance and resources.

REFERENCES AND PUBLICATIONS

"Agricultural Management Information-AMI- Preliminary Plan for Research and Development: Summary of Program Planning Activities at GSFC 1978-1979," preliminary draft, 137 pp., 1978. Appendices B, C, D, E, F, and M entitled as follows:

"User Needs Survey of Agricultural Management Information," Appendix B, Volume I, prepared by Ecosystems International, Inc., Gambrills, Md., under NASA contract NAS5-25003, 114 pp., 1978.

"User Needs Survey of Agricultural Management Information," Appendix C, Volume II, prepared by Ecosystems International, Inc., Gambrills, Md., under NASA contract NAS5-25003, 101 pp., 1978.

"User Needs Survey of Agricultural Management Information," Appendix D, prepared by Ecosystems International, Inc., under NASA contract NAS5-25003, 162 pp., 1978.

"A Survey of Farm Management Decision Models," Appendix E, prepared by ECON, Inc., Princeton, N.J. under NASA contract NAS5-20940, 153 pp., November 1977.

"The Plan for The Economic Evaluation of Research for Improved Agricultural Management Decisions," Appendix F, prepared by ECON, Inc., Princeton, N.J., under NASA contract NAS5-20940. 47 pp., April 1978.

"Agricultural Management Decisions: A Preliminary Benefit Assessment," Appendix G, prepared by ECON, Inc., Princeton, N.J., under NASA contract NAS5-20940, 162 pp., May 1978.

"Research Feasibility: GE Report," Appendix M, prepared by General Electric, Inc., Valley Forge Space Center, Pennsylvania, 176 pp., February 1976.

WHEAT YIELD STUDY

OBJECTIVE

The objective of the wheat yield study is to develop and evaluate methods and techniques of using remotely sensed data for the determination of yield in grain crops, particularly wheat. The specific data orientation is the spectral bands representing those on the Landsat D TM. Implicit in the study is comparison of the utility of TM data to this end, as compared with yield results that can be obtained using the MSS data.

BACKGROUND

The ultimate goal of any agriculturally oriented remote sensing program is to determine expected productivity of the various crops of interest and to detect any factors that could affect that productivity. This implies an ability to identify the crops of interest, measure their acreage, and qualitatively and quantitatively evaluate their growth state and condition.

Any study of crop yield using remotely sensed data must concentrate on crop conditions at specific growth stages and how these may affect anticipated yields. The extent to which remotely sensed data can be compared to agronomic parameters, and thus be used to anticipate crop yield, depends on the magnitude of sensor response over spectral regions of sensor perceptivity.

Most studies to date have been based on the data available from the four bands from the Landsats 1, 2, and 3. The Goddard program in this area has been oriented toward data that will be available from the Landsat-D TM. Prior to launch of Landsat-D in September 1981, this must be simulated from whatever sources may be available and the constraints of these simulations taken into account in any results. To date this project has primarily used data residual at LARS/Purdue and available from two sensor systems: (1) The JSC FSS/S191-H spectroradiometer, and (2) the Exotech spectroradiometer. By using this radiometrically scanned data, backed up with the LACIE spacecraft collection of agronomic and mensuration "ground truth," an attempt has been made to associate TM-like spectral data with the two basic essentials of yield determination: Identification of crop and its agronomic state.

The prime data source for the first portion of this investigation (which was related to identity of crop) was the Fine Sun Sensor (FSS) data collected during the 1975/76 winter wheat growth year in Finney County, Kansas (LACIE ITS number 1988). The FSS radiometric scanner (which was helicopter mounted) collected the data in 63 individual wave bands, ranging from about 0.4 μm to 12.5 μm. This project decided only to use wave bands in the reflective region of this spectrum and chose the bands primarily from 0.4 μm to 2.35 μm.

Initially the FSS bands in this region were statistically grouped into 27 bands grouped in the several spectral regions of agronomic interest. Eventually these were subgrouped into those bands which represented the various reflective bands that were at that time considered for the TM. The subgroups are: TM1, 0.45-0.52; TM2, 0.52-0.60; TM3, 0.63-0.69; TM4, 0.76-0.90; TM5, 1.09; TM6, 1.55-1.75; TM7, 2.08-2.35.

Using Purdue/LARS EXOSYS and LARSYS systems statistical and separability routines, the interrelations among these bands relative to the crops identity were studied. Using a figure of merit designed to reflect the relationships of interest, it was determined that the addition of bands 6 and 7 did add to the discrimination ability of the remote sensor (compared with those that were only limited to the range that generally approximated those of the MSS) while addition of the 1.09 band did not improve the discriminability of this significantly.

RECENT ACCOMPLISHMENTS

Since the initial phase on TM band identity power, the emphasis has been on the use of TM data to determine agronomic yield. Much of this effort has been in the formative stages of determining what data to use and how and where best to use it.

Two radiometrically scanned data sources have been chosen for study and one spatially scanned source. The two radiometrically scanned data sources are the FSS data taken over Hand County, South Dakota in 1976/77 wheat season, and the Exotech data taken at the Williston AES during the spring of 1977. The spatially scanned data are those taken by the JSC TM simulator system in June of 1978 over Hand County, South Dakota.

To date the Hand County and Williston data have been used in the EXOSYS/LARSYS to make some preliminary statistical studies, which indicate some promise with regard to identity of growth stage, particularly using some band rationing of the TM bands. No definitive results are available yet.

The JSC TM simulator data have only recently come in-house and have been entered into the IDIMS system. Most of their analysis is planned for in conjunction with this system. These data are the only spatially-scanned TM simulation data that are available to date, to our knowledge.

SIGNIFICANCE

To date, the work with the simulated TM data has been one of the few research efforts that has attempted to quantify the merits of the additional and altered spectral bands of the TM (relative to MSS), using data that has a substantive amount of "ground truth" associated with it. The initial work has pointed out some of the limitations of this approach and also some of the additional needs and shortcomings of the "ground truth" information acquired, even in some of the most comprehensive programs, such as LACIE. These findings are being factored into the planning and strategies of the BARC program.

Work with the simulated TM data has also helped formulate some of the limitations associated with simulating spatially scanning remote sensing systems with radiometric scanning systems. Those problems associated with geometrics of spatial/spectral sensors can only be evaluated in a real sense with systems that work in that domain.

FUTURE EMPHASIS

The use of the TM simulator data (JSC aircraft) will be the base for the future comparison of yield results in this study. It will be necessary to supplement this study with radiometrically scanned data, because of present scarcity of the TM data at this time. The GSFC IDIMS system will be the primary analysis system for the evaluation of the use of TM bands to determine yield within two to three years. After that, it is expected that the Landsat-D Assessment System facilities and computers may offer opportunities to expand what is done on the IDIMS. The immediate objective is to try to evaluate and expand some of the identity and state work that has been and is being done with the radiometric data. This work is planned to tie in with the agricultural field project, Landsat spectral wheat project, and LAS project.

CHAPTER 9

ADVANCED STUDIES IN EARTH RESOURCES

OVERVIEW

The advanced studies program aids GSFC engineers and managers in the design of future satellite systems and sensors based on current remote sensing research and evaluates the utility of the data these systems produce. We have planned and evaluated the approved Landsat D system and the proposed Multispectral Resource Sampler (MRS) sensor. We have also investigated the potential benefit of Landsat D's TM sensor compared to existing or proposed sensors.

Contributors to this chapter include Charles Schnetzler, Compton Tucker, and Darrel Williams.

LANDSAT-D ASSESSMENT SYSTEM

OBJECTIVE

The objective of the Landsat-D Assessment System (LAS) is to provide a facility and capability to perform analyses that will quantify the engineering and technological advantages afforded by the Landsat-D system, and in particular, the TM.

BACKGROUND

The four major objectives of the Landsat-D project are: (a) To assess the capability of the TM to provide improved information for Earth resources management, (b) to provide a transition for both domestic and foreign users from MSS data to the higher resolution and data rate of the TM, (c) to provide system level feasibility demonstrations in concert with user agencies, and (d) to encourage continued foreign participation in the program. Within the total project framework is a ground segment component, referred to as the LAS, to ensure that these major objectives are achieved. LAS activities will be primarily devoted to assessing the ability of the TM but will include: (a) Data quality tests to define and validate output products relative to user applications, (b) TM versus MSS performance evaluation tests to quantify the advantages of the TM improved spatial, spectral, and radiometric resolution in comparison to the MSS, (c) data systems applications tests to demonstrate the ability of the Landsat-D system to provide useful results in a timely manner, and (d) operational sensors and data system studies to determine what might be the appropriate characteristics for an operational system.

RECENT ACCOMPLISHMENTS

A preliminary LAS implementation plan has been drafted which calls for the creation of five Discipline Experiment Teams (DET) to represent the major Earth resources disciplines of agriculture, forest and rangeland, water resources, geology, and land use. Each DET will plan and conduct those activities required to define and validate the TM and Landsat-D system data output as applicable to its respective discipline. An internal DET advisory group has been appointed to assist the project scientist in defining and/or reviewing the LAS facility layout, software requirements, data formats, optimum orbital altitudes, etc.

SIGNIFICANCE

Via this early planning, every effort is being made to ensure that the LAS organizational structure and computer facility will be operational by the time Landsat-D is launched in the third quarter of CY 1981.

FUTURE EMPHASIS

Future emphasis will include: (a) The continued evaluation and determination of system and software requirements, (b) formulation and release of an Announcement of Opportunity in order to determine actual DET membership, and (c) analysis of TM simulator aircraft data to become more familiar with TM bands and resolution.

MULTISPECTRAL LINEAR ARRAY SENSOR DEVELOPMENT

OBJECTIVE

The objective of the program is to design conceptually an experimental Multispectral Linear Array (MLA) sensor for spacecraft flight in the mid-1980's. This will aid in providing new and unique Earth survey research capabilities beyond those possible with current sensor systems, and will be an engineering test of the new MLA technology.

BACKGROUND

An electromechanical scanner, such as the MSS on Landsat 1, 2, and 3, and the TM, which will fly on Landsat-D, are representative of NASA's present remote sensing capabilities from space platforms. However, these types of sensors have reached a plateau of development where any additional improvement in performance will be extremely costly. The next generation of satellite sensors will probably use linear arrays, each composed of a large number of solid state detectors in the pushbroom mode, i.e., a mode where the forward motion of the satellite sweeps the array of detectors, which are oriented perpendicular to the ground track, across the scene. Advantages to such a mode include the elimination of complex mechanical scan mechanisms; increased geometric fidelity, both across track and between bands; and higher sensitivity, due to longer dwell time of each detector. A clear disadvantage is the need for calibration of a much larger number of detectors.

Early in the calendar year GSFC was asked by NASA Headquarters to begin work on a potential FY 1980 new start for an MLA sensor which would be ready for spaceflight by 1985.

ACCOMPLISHMENTS

Over the year, the emphasis has been on defining the required sensor parameters from the scientific researchers' point of view and from this, developing a phase A systems specifications and design. On the scientific side, a science advisory group, composed of remote sensing researchers in diverse fields, was formed and has held two meetings. Input from this group plus other scientists was used to define the optimum sensor parameters for multidisciplinary use. Compared to the TM, the sensor as presently designed will provide improved temporal, spectral and spatial resolution. Across track pointing of up to ±40° will provide 1 to 2 day frequency of observation. Along track pointing of ±55° will allow atmospheric measurements to be made so that corrections can be made to the scene radiometry. Additionally, along track pointing will enable the requisition of stereo images. Spatial resolutions of the MRS will be 15 meters with a swath width of 15 kms. Filter wheels over each of four arrays will allow an inflight choice of five spectral bands per array. It will be possible to select bands as narrow as 20 nm.

SIGNIFICANCE

The work to date on defining optimum sensor parameters will be the basis for our ongoing effort to get a future new start for an MLA sensor.

FUTURE EMPHASIS

The effort in CY 1979 will be to continue to refine the sensor parameters and to gather interest and support from the user (research) community. Several more meetings of the science advisory group will be held, and a workshop of 50 to 75 remote sensing researchers is planned for May. If funds are available, several lines of "proof-of-concept" research will be pursued, particularly on utility of bidirectional and polarization measurements, techniques for using the sensor for corrections of atmospheric scattering, and under sampling schemes. The MLA sensor concept will be reproposed to Headquarters in the fall for an FY 1981 new start.

REFERENCES AND PUBLICATIONS

"Multispectral Linear Array Advisory Group Meeting-Summary Report of June 1-2, 1978 Meeting," ORI Report dated June 1978.

"Multispectral Resource Sampler Advisory Group Meeting-Summary Report of Second Meeting, October 30, 1978," ORI Report dated December 1978.

Schnetzler, C.C. and L.L. Thompson, "Multispectral Resource Sampler: An Experimental Satellite Sensor for the Mid-1980's," (abstract) presented at ASP Meeting, March 1979.

LANDSAT-D PRELAUNCH ASSESSMENT OF SPECTRAL RESOLUTION AND SPECTRAL BANDS

OBJECTIVE

The objective of the research is to quantitatively assess the TM's spectral bands vis-a-vis other existing (RBV, MSS) or proposed (Colvocoresses operational Landsat and the French SPOT) satellite sensor systems for monitoring vegetation resources.

BACKGROUND

The first four Landsat-D TM sensor bands were evaluated and compared to: the RBV and MSS sensors from Landsats 1, 2, and 3; the Colvocoresses' proposed operational Landsat three-band system; and the French SPOT three-band system by using simulation/integration techniques and *in situ* collected spectral reflectance data. Sensors were evaluated with regard to their ability to measure vegetation biomass, chlorophyll concentration, and leaf water content.

SIGNIFICANCE

The significant results of the research are:

- Thematic Mapper sensors TM1, TM2, TM3, and TM4 were found to be very well situated spectrally for remote sensing of vegetated targets (refer to tables 9-1 and 9-2).
- Significant improvements can be expected from the TM over the MSS of Landsats 1, 2, and 3, resulting from optimal spectral resolution alone.
- Colvocoresses' proposed three-band system was found to have two poor bands for monitoring vegetation (see figures 9-1 and 9-2).
- The French satellite SPOT three-band system has three well placed bands for monitoring vegetation. The SPOT bands are very similar to TM bands TM2, TM3, and TM4, respectively.
- Sensor bandwidths must be restricted to regions of the spectrum where the same vegetation-spectral reflectance relationship predominates. Combining different vegetation-spectral reflectance relationships within the same sensor bandwidth seriously reduced the vegetational utility of the combined sensor, especially for more complex canopy situations.

- Complex canopy situations necessitate a more specific spectral subset of the less complex canopy situation spectral regions. As such, the more heterogeneous or complex conditions are of predominant value for selecting sensors of the greatest and most persistent vegetational utility.

FUTURE EMPHASIS

Future plans include use of hand-held radiometers for prelaunch *in situ* extensive tests to further expand the existing research areas.

REFERENCES AND PUBLICATIONS

Tucker, C.J., "Are Two Photographic Infrared Sensors Required?" *Photogrammetric Engineering and Remote Sensing, 44*, 3, 289-295, 1978.

Tucker, C.J., "A Comparison of Satellite Sensor Bands for Vegetation Monitoring," *Photogrammetric Engineering and Remote Sensing, 44*, 11, 1369-1380, 1978.

Table 9-1. Coefficient of Determination (r^2) Values Resulting from the Regressions Between Integrated Radiance and the Various Sampled Canopy Variables for the June Data

Sensor	Bandwidth (μm)	Total Wet Biomass	Total Dry Biomass	Leaf Water Content	Dry Green Biomass	Dry Brown Biomass	Total Chlorophyll Content
RBV 1	.475- .575	.73	.66	.76	.67	.24	.77
RBV 2	.580- .680	.88	.81	.91	.82	.32	.91
RBV 3	.690- .800	.65	.63	.65	.63	.51	.65
MSS 4	.500- .600	.78	.71	.81	.73	.27	.81
MSS 5	.600- .700	.88	.80	.91	.82	.32	.91
MSS 6	.700- .800	.63	.62	.63	.61	.54	.65
MSS 7*	.800-1.100	.72	.71	.73	.71	.61	.73
TM 1	.450- .520	.69	.61	.72	.63	.19	.74
TM 2	.520- .600	.70	.72	.82	.74	.28	.83
TM 3	.630- .690	.88	.80	.91	.82	.32	.91
TM 4	.760- .900	.78	.76	.78	.76	.63	.78
SPOT 1	0.50- 0.59	.76	.69	.79	.71	.26	.81
SPOT 2	0.61- 0.69	.88	.81	.91	.82	.32	.91
SPOT 3	0.79- 0.90	.77	.75	.77	.75	.63	.78
Colvo 1	.470- .570	.71	.65	.75	.66	.23	.76
Colvo 2	.570- .700	.88	.80	.91	.82	.32	.91
Colvo 3*	.760-1.050	.74	.73	.74	.72	.62	.75

*Data was incomplete for the 1.00-1.1 μm interval. The simulations for MSS7 and Colvo 3 used 1.00 μm as their upper wavelength limits.

Table 9-2. Coefficient of Determination (r^2) Values Resulting from the Regressions Between Integrated Radiance and the Various Sampled Canopy Variables for the September Data

Sensor	Bandwidth (μm)	Total Wet Biomass	Total Dry Biomass	Leaf Water Content	Dry Green Biomass	Dry Brown Biomass	Total Chlorophyll Content
RBV 1	.475- .575	.31	.28	.41	.21	.10	.25
RBV 2	.580- .680	.40	.38	.64	.24	.07	.33
RBV 3	.690- .800	.48	.51	.41	.43	.29	.39
MSS 4	.500- .600	.25	.22	.37	.16	.07	.20
MSS 5	.600- .700	.39	.38	.65	.23	.06	.33
MSS 6	.700- .800	.53	.55	.48	.47	.30	.44
MSS 7*	.800-1.100	--	--	--	--	--	--
TM 1	.450- .520	.56	.54	.69	.41	.19	.45
TM 2	.520- .600	.22	.20	.33	.14	.06	.18
TM 3	.630- .690	.43	.25	.70	.41	.07	.36
TM 4*	.760- .900	--	--	--	--	--	--
SPOT 1	0.50- 0.59	.25	.17	.35	.22	.08	.20
SPOT 2	0.61- 0.69	.42	.24	.68	.41	.07	.35
SPOT 3*	0.79- 0.90	--	--	--	--	--	--
Colvo 1	.470- .570	.33	.23	.43	.30	.11	.26
Colvo 2	.570- .700	.37	.22	.62	.35	.12	.32
Colvo 3*	.760-1.050	--	--	--	--	--	--

*The September data only covered the 0.350-0.800 μm region. Some sensors, therefore, could not be simulated.

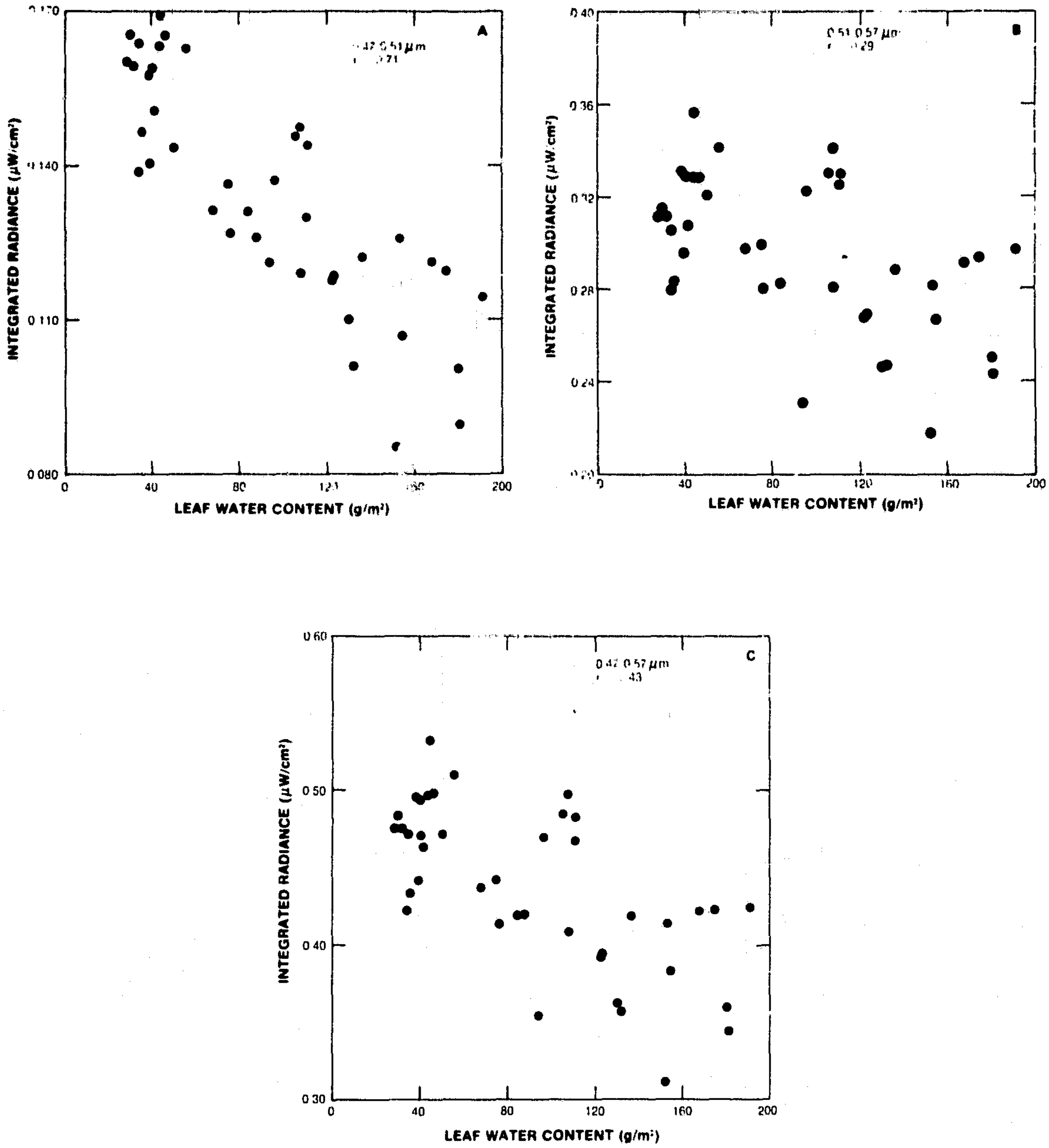

NOTE

Plot A is 0.47 to 0.51 μm, B is 0.51 to 0.57 μm, and C is 0.47 to 0.57 μm. Note how two different effects occur within Colvocoresses' proposed band 1. The combination of these two wavelength regions seriously reduces the vegetational utility of this proposed sensor.

Figure 9-2. Integrated Radiance for Three Wavelength Intervals Plotted Against the Leaf Water Content for the September Sampling Period Colvocorresses' Band 1

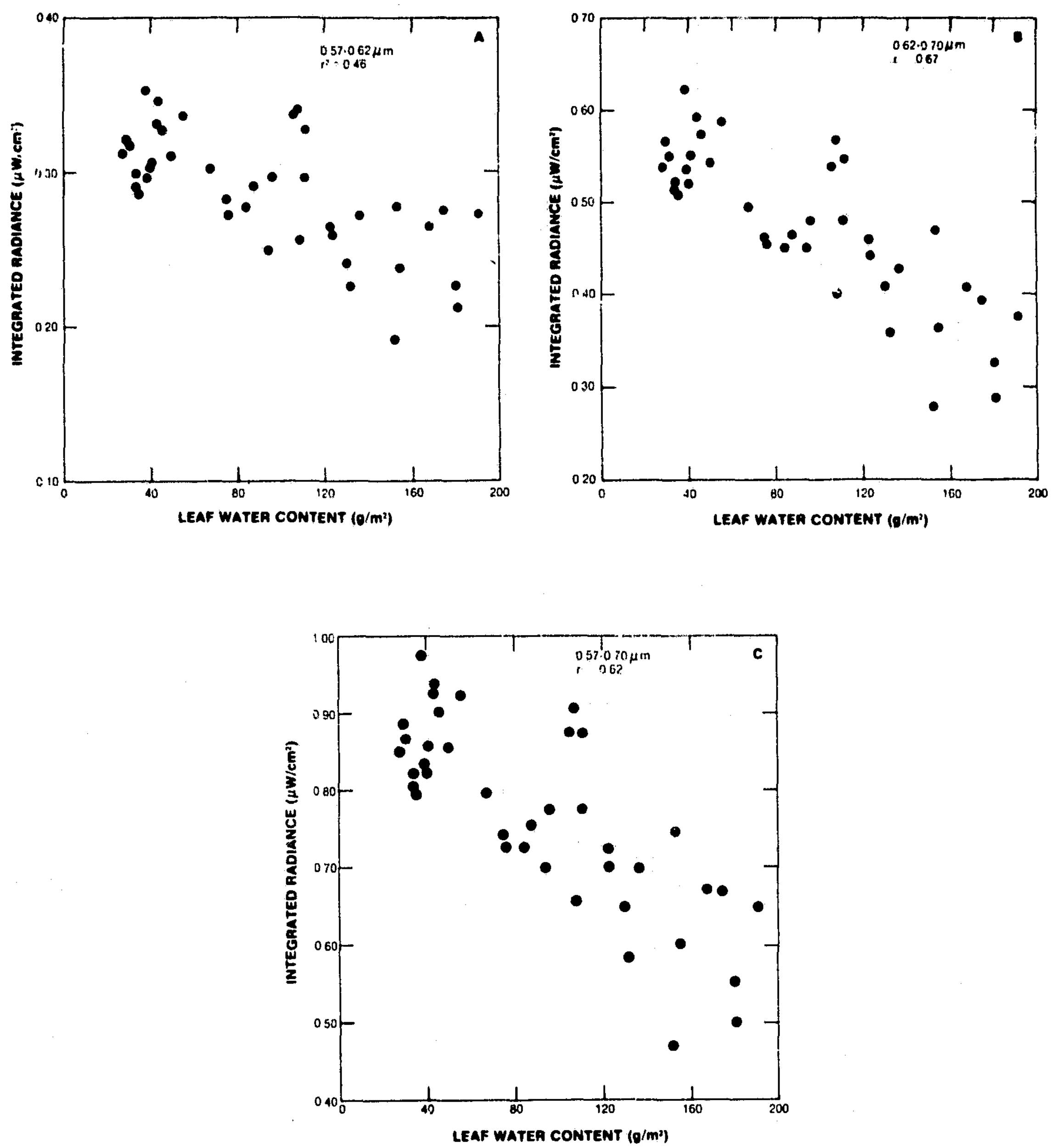

Plot A is 0.57 to 0.62 μm, B is 0.62 to 0.70 μm, and C is 0.57 to 0.70 μm. Note how two different effects occur with Colvocoresses' proposed band 2. This sensor could be improved for more complex vegetational utility by excluding the 0.57 to 0.62 μm region.

Figure 9-2. Integrated Radiance for Three Wavelength Intervals Plotted Against the Leaf Water Content for September Sampling Period Colvocoresses' Band 2

ACRONYMS AND ABBREVIATIONS

AGIS	Automated Geographic Information System
AGU	American Geophysical Union
AMI	Agricultural Management Information
AO	Announcement of Opportunity
APT	Applications Pilot Test
ARC	Appalachian Regional Commission
ASVT	Applications Systems Verification Test
BARC	Beltsville Agriculture Research Center
CCT	Computer Compatible Tape
DCP	Data Collection Platform
DET	Discipline Experiment Teams
DSN	Deep Space Network
EPA	Environmental Protection Agency
ESRI	Environmental Systems Research Institute
GEM	Goddard Earth Model
HO	Haystack Observatory
IAU	International Astronomical Union
IBIS	Image Based Information System
IR	Infrared
JPL	Jet Propulsion Laboratory
LAI	Leaf Area Index
LAS	Landsat-D Assessment System
MLA	Multispectral Linear Array
Moho	Mohorovičić Discontinuity
MRS	Multispectral Resource Sampler
MSDS	Multispectral Scanner and Data System
MSS	Multispectral Scanner
NGS	National Geodetic Survey
NRAO	National Radio Astronomy Observatory
OSTDS	Office of Space Tracking and Data Systems
OVRO	Owens Valley Radio Observatory
PPME	Pacific Plate Motion Experiment
RBV	Return Beam Vidicon
SAFE	San Andreas Fault Experiment
SCD	Spectral Crop Development
SLR	Satellite Laser Ranging
SST	Satellite-to-Satellite Tracking
TM	Thematic Mapper
USDA	U.S. Department of Agriculture
USGS	U.S. Geological Survey
VHRS	Very High Resolution Spectrometer
VLBI	Very Long Baseline Interferometer